Contractor Report 4324

...r Modeling of Joint ...ed Structures

...8864

(NASA-CR-4324) NONLINEAR MODELING OF JOINT DOMINATED STRUCTURES Final Report (Boeing Aerospace Co.) 213 p CSCL 22B

Unclas
H1/18 0302585

NASA Contractor Report 4324

Nonlinear Modeling of Joint Dominated Structures

J. M. Chapman
Boeing Aerospace
Engineering Technology Organization
Seattle, Washington

Prepared for
Langley Research Center
under Contract NAS1-18864

National Aeronautics and
Space Administration
Office of Management
Scientific and Technical
Information Division

1990

Nonlinear Modeling of Joint Dominated Structures

Summary

The objective of our Controls Structures Interaction (CSI) Guest Investigator Program investigation is to develop and verify an accurate structural model of the non-linear joint-dominated Mini-Mast truss. Our approach is to characterize the structural behavior of the Mini-Mast joints and struts using a test configuration that can directly measure the struts' overall stiffness and damping properties, incorporate this data into the structural model using the residual force technique, and then compare the predicted response with empirical data taken by NASA at the Langley Research Center (LaRC) during the modal survey test of the Mini-Mast.

In our investigation, a new testing technique, referred to as "link" testing, was developed and used to test prototype struts of the Mini-Mast. Data from these tests showed the structural behavior of the Mini-Mast longerons and diagonals to be quite complex, though linear for low load and excitation levels. Appreciable nonlinearities including free-play and hysteresis were also demonstrated. Since static and dynamic tests performed on the Mini-Mast also exhibited behavior consistent with joints having free-play and hysteresis, nonlinear models of the Mini-Mast were constructed and analyzed.

The Residual Force Technique was used to analyze the nonlinear structural model of the Mini-Mast having joint free-play and hysteresis. The motivation to do so was based partly on the link tests and also on the the observed behavior of the 18 bay Mini-Mast truss in static torsion tests. Results from these analytical studies show that the dynamic torsional response of the Mini-Mast is greatly affected by gaps as small as one milli-inch. Comparison of the predicted response of the analytical model to the empirical results taken from the Mini-Mast show good agreement although additional improvement may be obtained with additional testing and system identification. Nevertheless, an improved nonlinear model of the Mini-Mast is obtained and is used to explain several amplitude dependent phenomena demonstrated by the Eigen Realization Algorithm (ERA) program.

Motivation for using the residual force technique and link testing is discussed in Section 1.0. The link testing performed for the Mini-Mast struts is discussed in Section 2.0. Investigation of the Mini-Mast using the residual force technique is given in Section 3.0. Documentation of the techniques and computer codes used in the nonlinear Mini-Mast model is given in Section 4.0. Concluding remarks are given in Section 5.0.

THIS PAGE INTENTIONALLY LEFT BLANK

1.0 INTRODUCTION & BACKGROUND

The Residual Force Technique, developed earlier by Boeing under a NASA Marshall Space Flight Center contract NAS8-36420 (Ref.1), can perform the transient analyses of large, flexible, and joint-dominated structures when the deformation of such structures is governed primarily by axial contraction or elongation in the structural members. The technique permits substantial size reduction in the number of degrees of freedom describing the nonlinear joints and beams within the Mini-Mast and can account for such nonlinear joint phenomena as free-play and hysteresis. In general, joints can have arbitrary force versus displacement and velocity functional descriptions generally referred to as force-state maps (Ref. 2).

One essential feature of the residual force technique is to replace the arbitrary force-state state maps describing the nonlinear joints and beams with residual force-state maps describing their collective behavior over all the truss "links" or struts. The main advantage of this replacement is that the incrementally small relative displacements and velocities across a joint are not monitored directly thereby avoiding numerical difficulties. Instead, very small and soft nonlinear residual forces are defined giving a numerically attractive form for the equations of motion. Moreover, the nonlinearities are all contained on the "right hand side" of the equations of motion permitting modal reduction techniques to be applied to the linear left hand side. The equations of motion of a joint dominated truss may therefore be analyzed using only a few global modes with the link nonlinearities restricted to their effect on these modes alone. Figures 1-1, 1-2, and 1-3 give an outline of the residual force technique along with the modeling assumptions and advantages of the link concept. A full discussion of the residual force technique is given in Appendix C for convenience.

The testing technique developed here is specifically designed to directly measure the axial behavior of the truss struts in a test configuration as close to the actual Mini-Mast configuration as possible. Since the structural properties so determined characterize the strut or link behavior within the Mini-Mast truss, the testing technique is referred to as "link" testing. There are many advantages to this link testing. First, direct tests on the truss links can validate the analytical assumption that the links are governed primarily by axial elongation and contraction. Second, link testing could identify behavior that could not be predicted from joint tests alone. And third, link testing could identify a fatal design flaw early on in the design of a deployable truss. Link testing should therefore prove to be a valuable tool for NASA in ascertaining both the structural integrity of a deployable truss and its predictability.

PRECEDING PAGE BLANK NOT FILMED

One advantage of link testing over individual joint testing is that the stiffness and damping properties of the overall strut are determined directly. Joint tests are usually performed to measure the axial stiffness and damping of a joint in a test jig that restrains lateral motion. Such lateral restraints do not exist in the truss structure and, as a result, strut behavior may not be predictable from individual joint tests alone. In general, link testing will be necessary for those struts that exhibit large lateral bending under applied axial loads as is the case for the Mini-Mast struts.

Residual Force Technique Modeling Assumptions

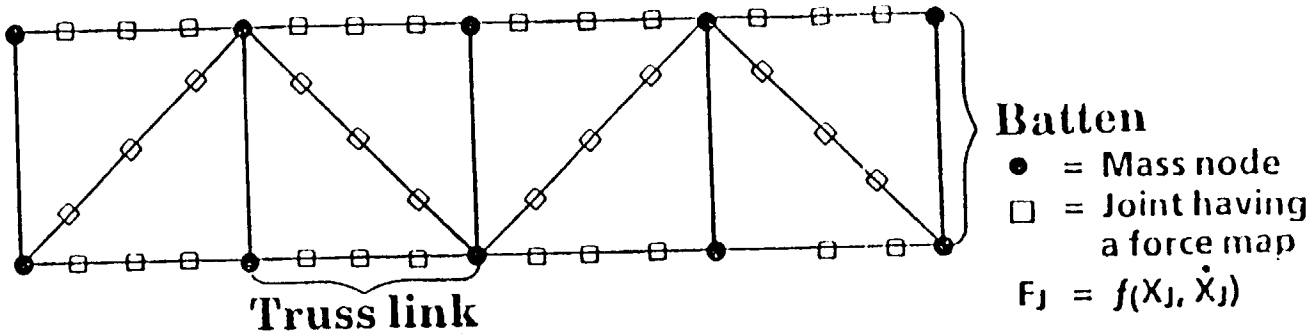

Assumptions:

- Battens do not have pinned joints (otherwise joint rotation modes would exist)
- Truss links are axial load carrying members only
- Joints are described by arbitrary force maps
- Inertial effects can be lumped at the mass nodes

Claim:

- The ability or inability to analyze the above truss is determined by the ability or inability to analyze the nonlinear "truss links" with an efficient, stable numerical integrator

Figure 1-1. Residual Force Technique Modeling Assumptions

Residual Force Technique

Equations of motion using link concept

$$M\ddot{x} + Kx = C\,F_R + F_{External}$$

x = displacements at mass freedoms only

$x_L = C^T x$ = deflections across a link

F_R = residual forces in links = $f(x_L, \dot{F}_R)$

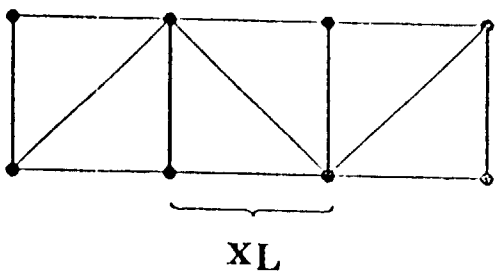

Modal representation

$$\ddot{Q} + \omega^2 Q = \Phi_L{}^T F_R + \Phi^T F_{External} \qquad F_R = f_R(Q,\dot{Q})$$

$$x_L = \Phi_L Q$$

$$\dot{x}_L = \Phi_L \dot{Q}$$

Figure 1-2. Residual Force Equations of Motion

Residual Force Technique

Advantages of link concept

- Substantial size reduction obtained even before modal extraction
- Numerical instabilities avoided by lumping small joint masses at mass nodes
- Link tests can be performed to validate analytical assumptions
- Stable integration achieved by transforming the force maps of the joints to residual force maps of the links

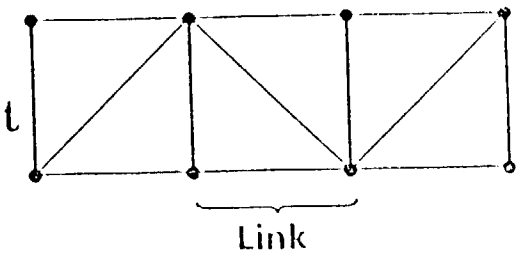

$F_{Joint} = f_J(x_J, \dot{x}_J) \longrightarrow F_R = f_R(x_L, \dot{F}_R)$

x_J = relative displacement in joint

f_J = force map

x_L = relative displacement of link

F_R = residual force in link

Figure 1-3. Residual Force Advantages

2.0 LINK TESTING

Two prototypes of Mini-Mast struts or links were tested, longerons and diagonals. Both longerons and diagonals have hinges at each end which are not perpendicular to the axis of force through the link. All longerons tested were identical, but there were two types of diagonals due to the two different orientations of the collapsible center hinge with respect to its end fittings. The different orientations of the diagonal center hinges are necessary to accommodate folding of the diagonals in the stowed Mini-Mast configuration. The prototypes differed from the actual Mini-Mast hardware in several important ways. First, the tubing diameters for both the diagonals and longerons were smaller. Second, the torsion spring of the prototype center hinge was appreciably weaker. And third, the tolerances of the actual Mini-Mast hardware appeared to be greater than the the prototypes.

The link testing configuration and measurement system designed for the Mini-Mast struts is shown in Figure 2.1. This configuration was generally adequate for the Mini-Mast struts for low frequencies but exhibited deficiencies at frequencies above the first bending frequency of the strut. The reasons for these deficiencies and the proposed modifications to the link testing apparatus and instrumentation are addressed in Section 2.9.

CSA Engineering, Inc. on subcontract to Boeing performed the link testing. In a brief summary of the results, the behavior of the prototype links were found to be quite complex, though linear at low force levels and frequencies. Free-play and Coulomb friction were exhibited by both the diagonals and the longerons at their endfitting connections to the Mini-Mast cornerbodies. The extensional stiffness of the prototype diagonals showed 300 percent unit to unit variations and were also greatly affected by their first bending mode near 12 Hz. Strong axial-bending coupling was also exhibited for the diagonal links. This coupling, however, could be affected by the low bending stiffness of the prototype diagonals and their weak center hinge torsional spring. The axial-bending coupling also appeared to be a function of joint misalignments and/or eccentricities. Moreover, sagging due to gravity of the heavy diagonal center hinge also was shown to have an effect of the diagonal stiffness. Although no tests were performed on the actual Mini-Mast diagonal hardware, it is the opinion of the principal investigator that the stiffer Mini-Mast diagonals would not exhibit the axial-bending coupling exhibited by the soft prototypes.

The test articles and assembly are discussed in sections 2.1 and 2.2, respectively. Data acquisition, reduction and interpretation are discussed in sections 2.3 and 2.4. Test results are given in sections 2.5 thru 2.7. Conclusions and recommendations are given in sections 2.8 and 2.9, respectively.

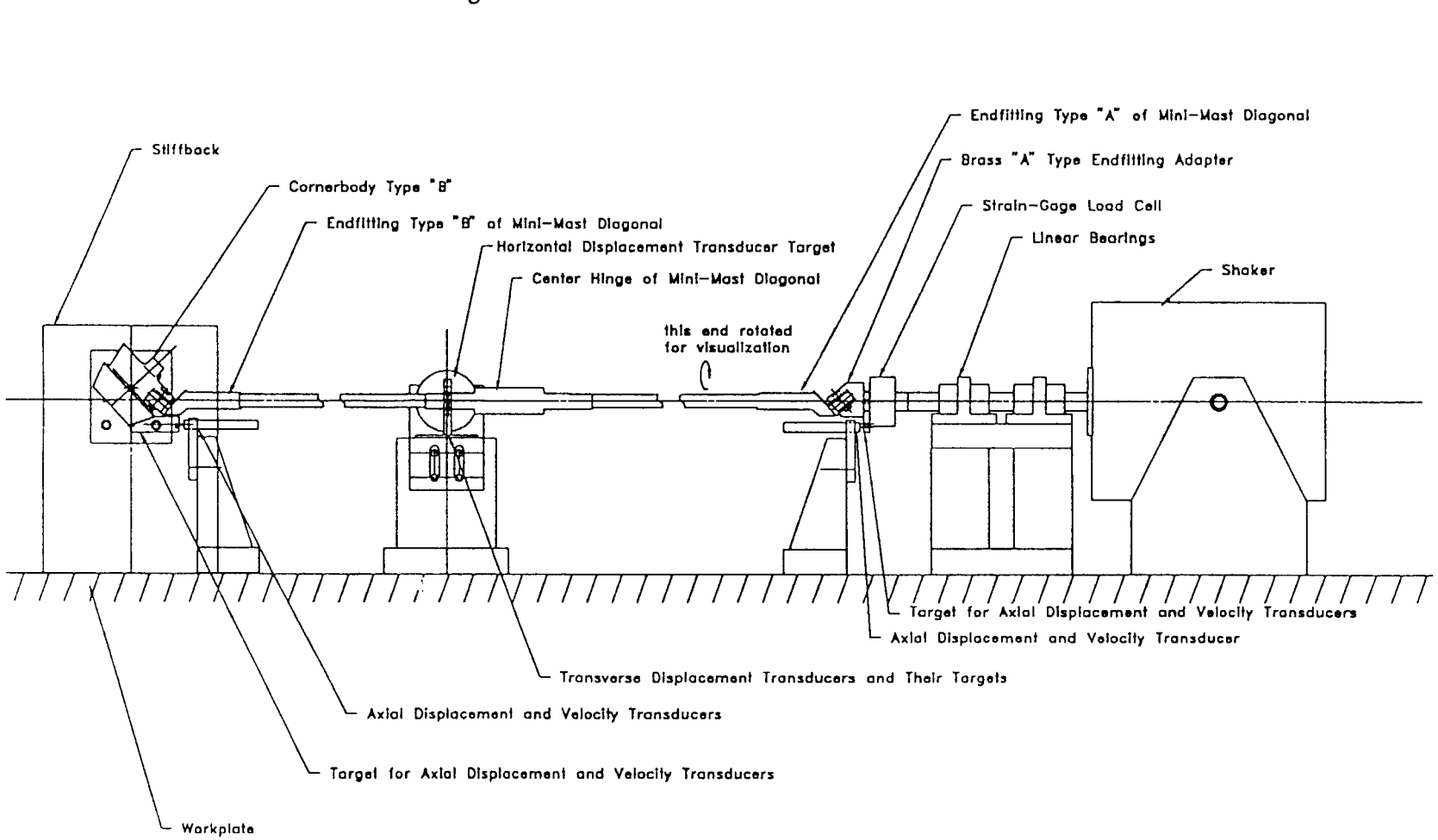

Figure 2-1. Mini-Mast Diagonal Test Assembly

ORIGINAL PAGE
BLACK AND WHITE PHOTOGRAPH

Diagonal Type N

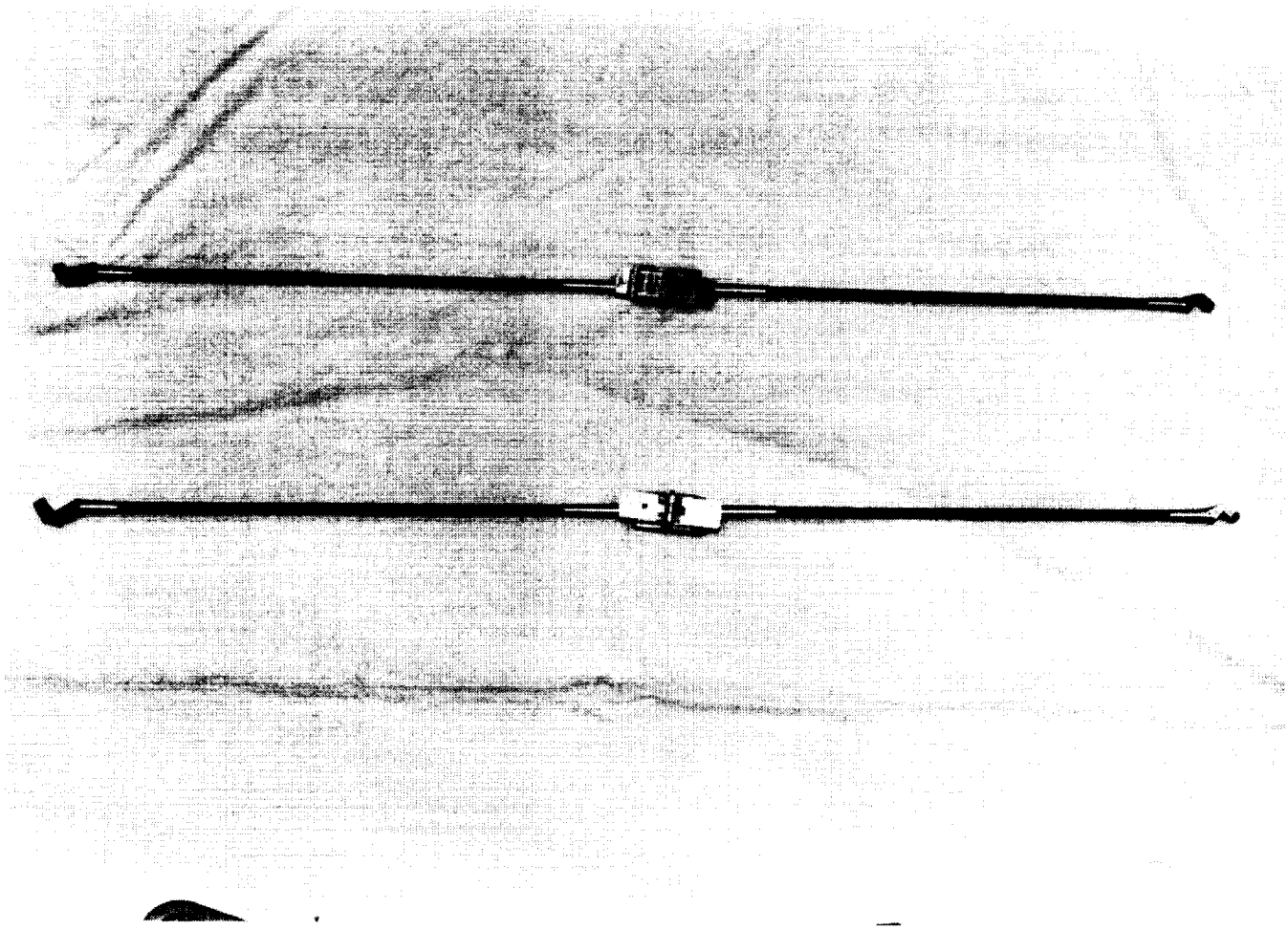

Diagonal Type M

Figure 2-2. Mini-Mast Diagonal Types M and N

2.1 Test Articles

Two prototypes of Mini-Mast links were tested, longerons and diagonals. Both longerons and diagonals have hinges at each end which are not perpendicular to the axis of force through the link. Further complications arise with the diagonals since 4/5 of their mass is lumped in a collapsible hinge at the center. All longerons are identical but there are two types of diagonals. Figure 2-2 shows each of the diagonal types and labels them as types M and N for further discussions in this report. They differ from one another in that their endfittings and center hinges have different orientations about the link axis. Unlike the longerons, diagonals also have dissimilar endfittings at either end. Shown in Figure 2-3 are the two types of endfittings. In this report they will be referred to as Types A and B.

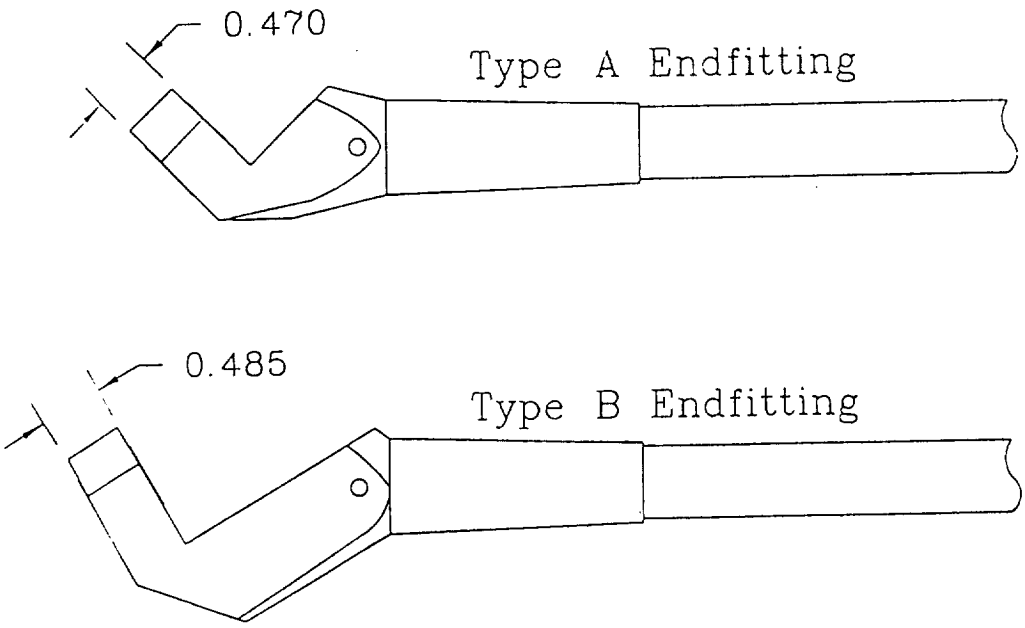

Figure 2-3. Endfitting types A and B for diagonals

The Mini-Mast truss is constructed with inter-link connectors called cornerbodies. Figure 2-4 shows the two type of cornerbodies. A cornerbody labeled Type A accommodates two A style diagonal endfittings above and two longeron endfittings below. Type B cornerbodies differ only in that they accommodate diagonal Type B fittings rather than Type A.

ORIGINAL PAGE
BLACK AND WHITE PHOTOGRAPH

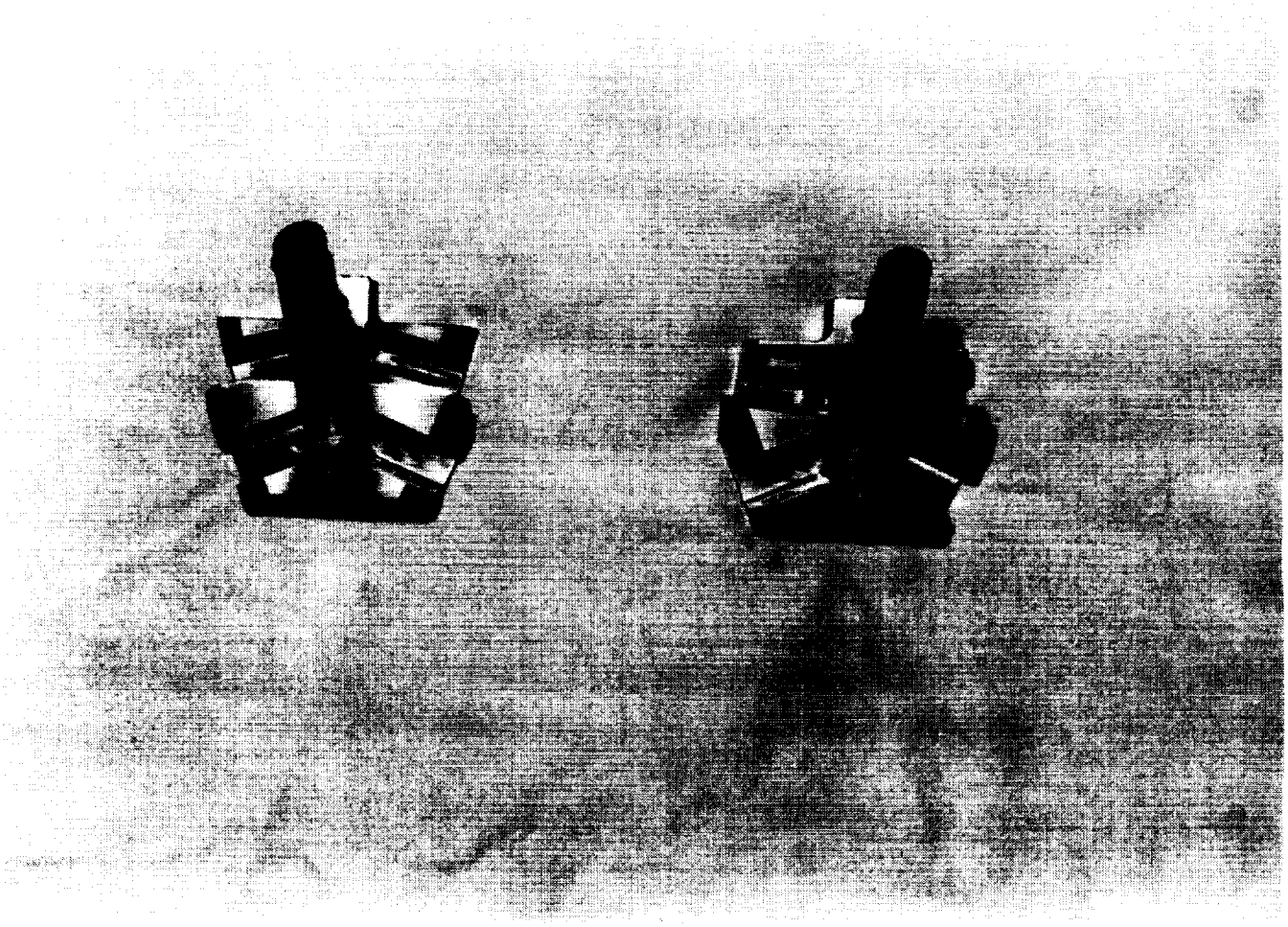

Figure 2-4. Cornerbodies Used in Mini-Mast Truss

All Mini-Mast cornerbodies and links were uniquely numbered by CSA. Three diagonals were received and were arbitrarily numbered from one to three. These numbers correspond to those in the tables of this report. Endfittings from diagonal number 1 were referred to as 1A or 1B depending on whether they were endfitting Type A or B, respectively. Cornerbodies were numbered similarly. For example, Cornerbody 1A refers to the first connector that accommodates Type A diagonal endfittings. Brass block adaptors were made by CSA and referred to as Type 0 connectors. Their purpose is discussed in section 2.2. The above conventions were established so each substantial Mini-Mast part could be easily recorded and uniquely recognized.

The dummy tube used for initial test checkout was a batton from the second generation CSI truss from NASA LaRC. It was an aluminum tube with a 0.039 wall thickness. A 30 inch segment of the tube was used as the test section. Its stiffness was predicted to be 24,055 pounds per inch, and was expected to be similar to those of the Mini-Mast articles.

2.2 Test Assembly

Boeing and CSA had previously developed the apparatus and tested the dynamic force deflection properties of truss links (Ref. 1). Fixturing for these tests was similar though custom designed for the Mini-Mast links which were tested horizontally on a rigid workplate as shown in Figure 2.1. The plate functioned as a stiff support for fixturing as well as for an alignment reference for the test assembly. Relative axial displacement and velocity between the link ends was sensed using targets mounted to the cornerbodies. Transducers near the center hinge measured lateral displacements. Linear bearings were placed at the driving end to direct force accurately and maintain orientation of the brass endfitting adaptor.

Special clevises were constructed to adapt the endfittings to a load cell. Hardened brass was used since its elastic modulus is close to that of titanium, and the metal sections were constructed to be similar to that of the cornerbodies. Critical dimensions and tolerances (such as clearances at endfittings) were measured from the titanium cornerbodies.

Seven transducers were used simultaneously in the joint test fixturing. Four displacement sensors were of the noncontacting eddy-current type. Two Kaman KD4200-1SU probes were used for axial displacement sensing. They were summed to create one differential displacement channel across the test section. Trans-Tek Model 0100-00000 linear velocity transducers measured axial velocity across the test section in a similar configuration. Two Kaman KD2300-8C probes sensed transverse displacement of the center hinges vertically and horizontally. Finally, a Kulite

TC-2000 strain gage load cell was used to measure force imposed on the link. Figure 2.1 shows the locations of these transducers within the test assembly.

2.3 Data Acquisition

Sinusoidal excitation was used for hysteresis loops and force state maps. Hysteresis loops were constructed by plotting force against displacement. These plots were made with constant amplitude sinusoidal force input while the force state maps were constructed with amplitude modulated sine input. Force-state data was acquired by applying a linear ramped sinusoidal carrier excitation to the specimen. Both velocity and displacement were treated as dependent variables. External profiles against the velocity-displacement plane of these plots were determined by the response of the test article.

Frequency response functions of bending compliance were measured for some truss links. Measurements for these tests were triggered by the impact of an instrumented force hammer against the center of the link. Lateral displacement and force signals were digitized, Fourier transformed and effectively divided to obtain these plots.

Interest developed in the lateral deflection properties of the diagonals to enable a better understanding of the large discrepancies in their axial stiffness. Static lateral stiffness tests were performed by hanging weights from the center hinge and reading the displacements from the vertical displacement transducer.

Diagonals were found to sag considerably in their test orientation. Transverse displacements due to gravity were measured with a height gage. The sag of a diagonal due to gravity was estimated by measuring the difference in composite tubing height between the center hinge and the average of its ends.

2.4 Data Reduction and Interpretation

Transducers were configured to respond along the following polarity conventions. Positive forces correspond to compressive and negative to tensile. All displacement were positive for movement away from the transducer, and negative towards it. Axial deflections plotted in hysteresis loops and force state maps were effectively differenced by factoring the transducers out of the test section. Therefore, extension of the test section is seen as a positive signal and shrinkage

as negative. Velocity transducers were configured so that compressive rates across the test section were positive and tensile rates were negative.

Hysteresis loops were used to calculate both stiffness and damping. If a loop is an undeformed ellipse (a very narrow ellipse appears as a line) then a single linear spring constant can be calculated. Figure 2-5 shows how the stiffness was calculated from the slope of the major axis. Loss factor, a measure of the ratio of dissipated energy divided by the stored energy per cycle was calculated as shown in Figure 2-6. Area inside the loop, the dissipated energy per cycle, is directly proportional to its damping.

Force-state maps were created with a three dimensional mapping routine. Simultaneous data output of the three channels (displacement, velocity, and force) were processed through software which averaged the force bins of equal velocity and displacement. Force-state maps are plots of these averaged force values against velocity and displacement.

2.5 Dummy Test Results

Dummy tube test were performed to verify the test method. Extensional stiffness of the dummy tube was calculated as 24,100 pounds per inch. Measurement results yielded a stiffness of 23,100 pounds per inch. These results were considered suitable since they only differ by 4 percent. Damping of the aluminum tube was below the resolution of the test technique; i.e, for loss factors less than 0.006. This was also expected since the loss factor for drawn aluminum tubing is below this value. Force state maps of the specimen show no evidence of nonlinearity.

2.6 Longeron Test Results

Longeron tests also yielded reasonable and expected results. Stiffness at low excitation levels were consistent within 20 percent. Average longeron stiffness at 10 pounds zero to peak and 1 Hz was 68,500 pounds per inch. Table 2-1 contains summarized results of the longeron tests. Loss factors for low level (less than 10 pounds 0-to-peak) longeron measurements were less than 0.15. Actual damping at this excitation level is most likely a fraction of the above test value since small displacements created from the low excitation levels and the high stiffness of the test article limited the resolution of the damping measurements.

Each longeron assembly demonstrated a unique nonlinear response at higher force and/or frequency levels. Nonlinearities were large enough to be readily perceived in the force-state maps

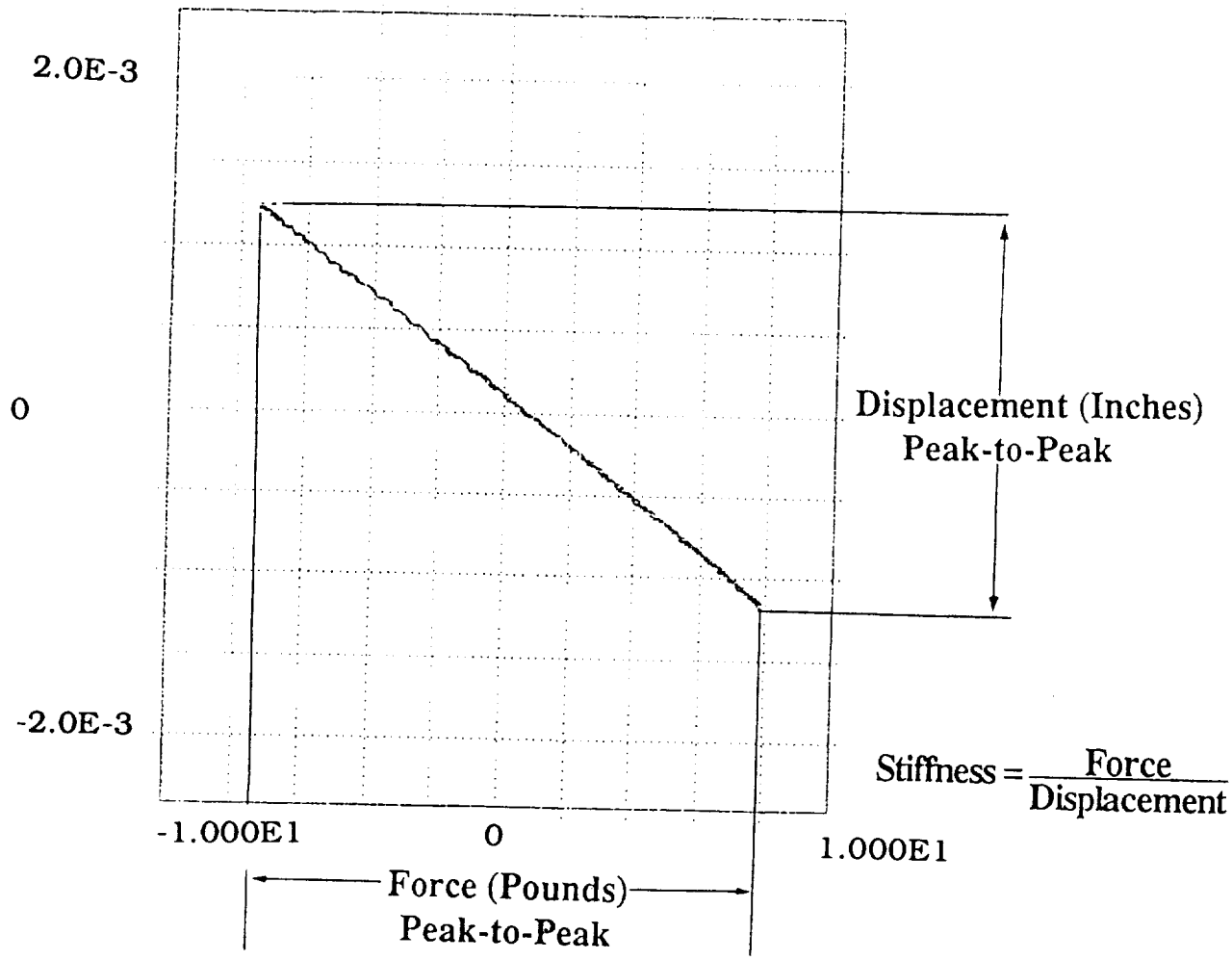

Diagonal test 3, excitation at 1 Hz

Figure 2-5. Stiffness Extraction From a Hysteresis Loop

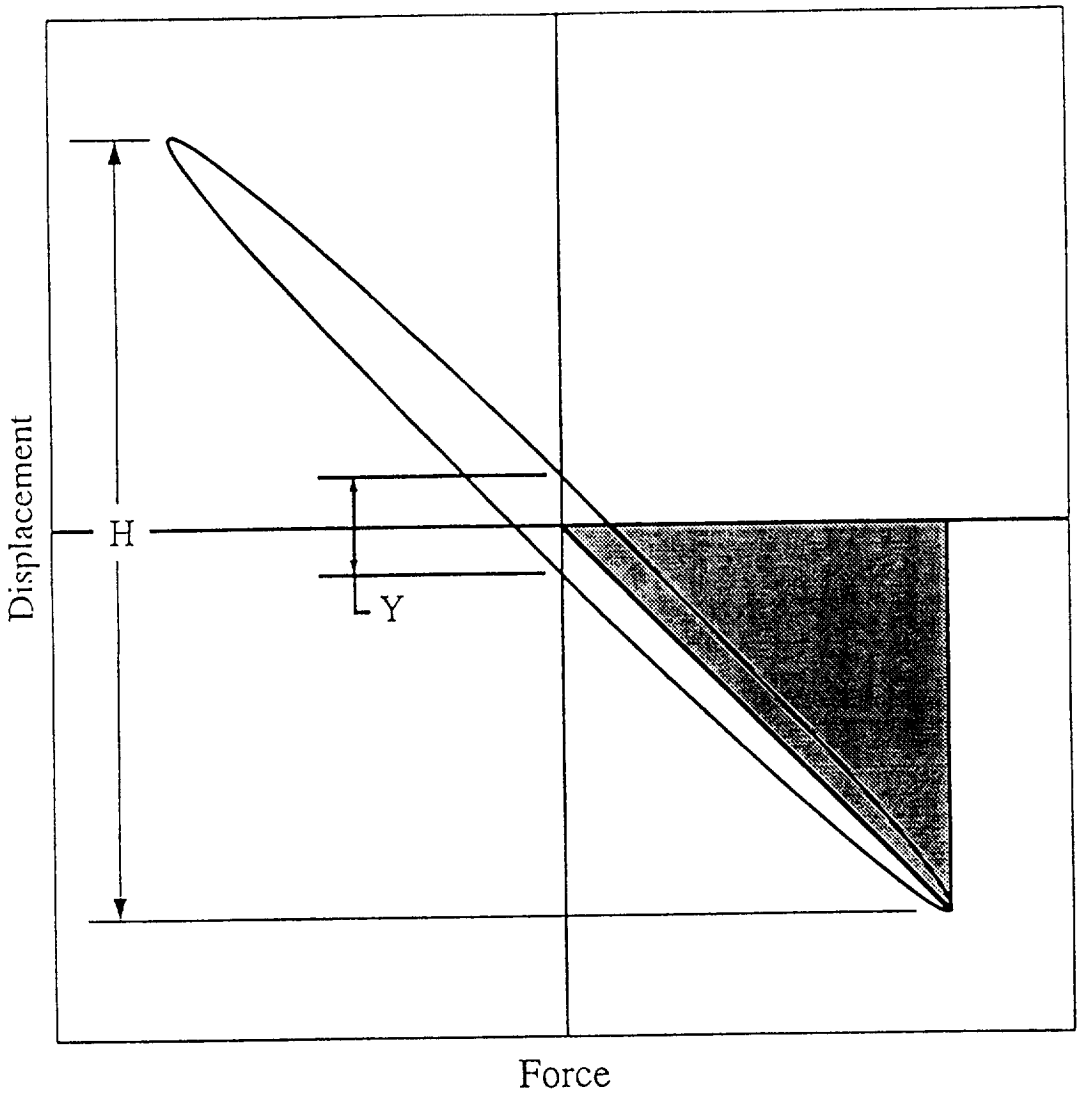

$$\text{Loss Factor} \equiv \frac{\text{Energy dissipated per cycle}}{\text{Maximum energy stored per radian}}$$

$$= \frac{(\text{Area of ellipse})}{2\pi(\text{Area of shaded triangle})} = \frac{Y}{H} \; *$$

* Reduced Equation valid for linear loops only

Figure 2-6. Loss Factor Calculation From a Hysteresis Loop

Force Levels (0-to-peak)	1 Hz			10 Hz			20 Hz		
	<10 lb	<20 lb	<50 lb	<10 lb	<20 lb	<50 lb	<10 lb	<20 lb	<50 lb
Longeron Test 2									
Stiffness (lb/in)	71,300	67,800	69,100		66,000	66,000	70,000	67,800	58,500
Loss Factor	≤0.15	≤0.03	0.09		≤0.03	0.07	≤0.15	≤0.03	0.08
Longeron Test 3									
Stiffness (lb/in)	73,500	60,000	*	75,600	75,900	*	65,700	57,100	*
Loss Factor	≤0.15	0.20		0.13	<0.20		0.11	<0.20	
Longeron Test 4									
Stiffness (lb/in)	58,900	52,600	49,500	56,400		51,600	56,300	56,100	46,300
Loss Factor	≤0.15	≤0.02	≤0.04	≤0.15		≤0.04	≤0.15	≤0.06	0.10
Longeron Test 5									
Stiffness (lb/in)	70,400	64,700	*	65,800	64,000	*	69,800	62,900	*
Loss Factor	≤0.15	≤0.02		≤0.15	≤0.02		≤0.15	0.02	

*Appreciable nonlinearity in hysteresis loop.

Table 2-1. Results of Longeron Tests

Longeron Tests
Test Set-Up Summary

Test No.	Longeron No.	Titanum Cornerbody No.	Endfitting No. at Titanium Cornerbody	Endfitting No. at Brass Connector
Longeron #2	3-4	2A	4	3
Longeron #3	1-2	1B	1	2
Longeron #4	1-2	2B	1	1
Longeron #5	3-4	1A	3	4

Table 2-1(b). Longeron Test Set-Up Summary

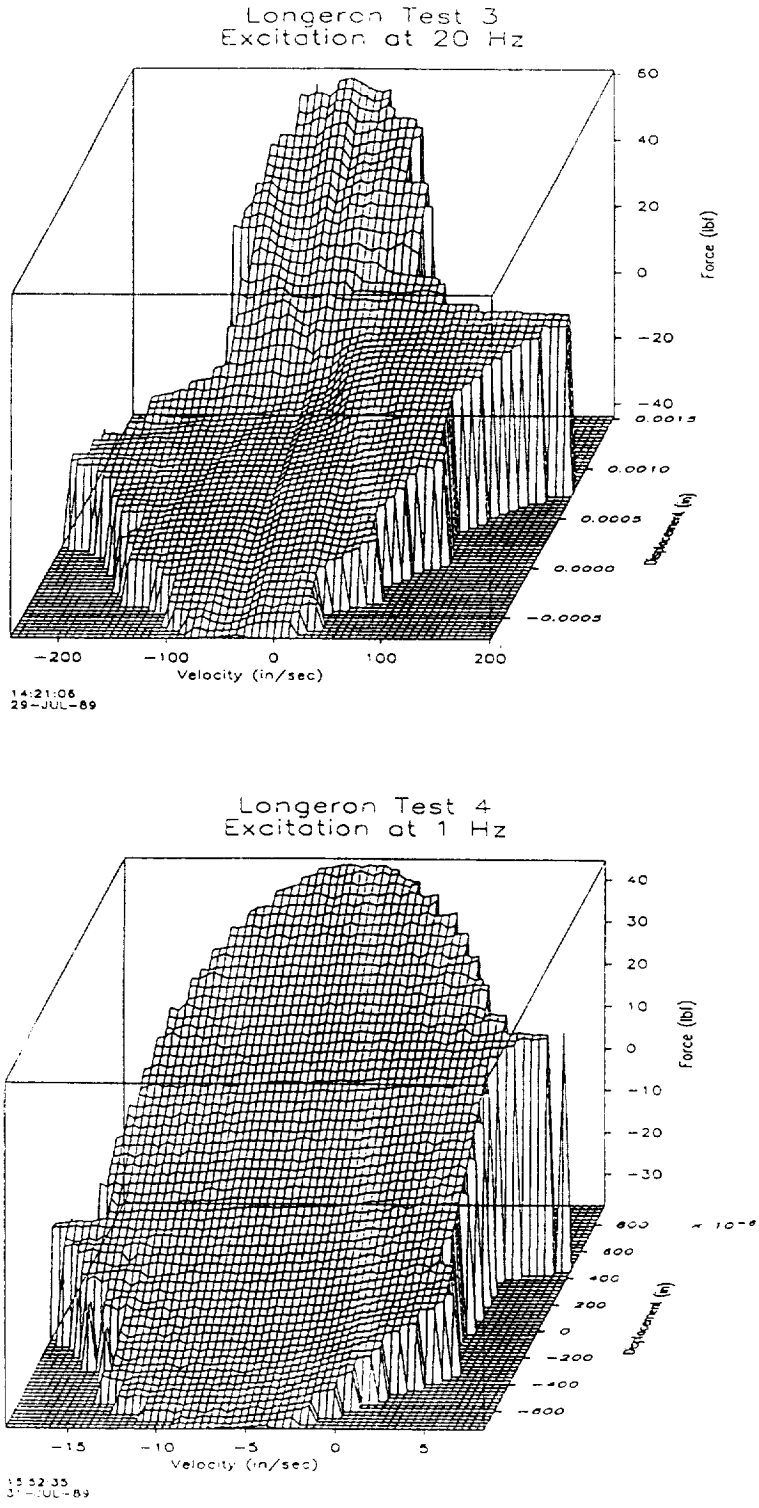

Figure 2-7. Force-State Maps From Longerons

ORIGINAL PAGE IS
OF POOR QUALITY

in two of the four assemblies. The hysteresis loops show the nonlinearities for the other assemblies. Figure 2-7 contains force state maps of the most linear and nonlinear longeron configurations. Compressive stiffness for the longeron in test 3 varied nearly two to one from the tensile. Appendix B contains the hysteresis loops and force state maps for the longerons for the test conditions.

2.7 Diagonal Test Results

The stiffness and damping behavior of the diagonals turned out to be very complex. Knowledge gained by early testing of the diagonals redirected the focus of the following tests. Table 2.2 summarizes the test sequence. Diagonal tests 2 and 3 were performed similar to the longeron tests. These diagonal tests yielded linear stiffnesses that varied nearly by 300 percent from one another as shown in Table 2-3. These results de-emphasized the force state map constructions and began a search for the cause of the stiffness mismatch. Data acquisition at 10 Hz and above was eliminated since the first bending modes were at 12 Hz and stiffness measurements are not valid when the test fixturing or articles have resonance in the test band. Lateral frequency response, static bending tests, and other transverse measurements supplemented the axial tests as diagnostics tests for the peculiar behavior of the diagonals. Attempts were made to measure axial stiffness immediately across local interfaces, yet the fixturing was inadequate for these measurements because diagonal bending introduced errors in the sensed axial displacement.

Mini-Mast link tests documented in this report are numbered from 2 to 11. Test numbers denote a specific assembly of articles. However, the assembly may not be unique to one test number. Numbered tests that are appended by letters specify different fixturing arrangements around an identical assembly of cornerbodies and link. For example, 8D and 8E both were on diagonal 1, cornerbodies 0A and 2B. They differ only by lateral displacement constraints (flexures) imposed on the latter test to eliminate bending of the test article.

Diagonal tests were repeatable for a given assembly and test condition yet the results are not completely understood. In most cases, these links responded linearly with stiffness values from 4600 to 18,500 pounds per inch for the N and M type diagonals respectively. Appreciable nonlinearities were also found to exist due to opening of the center hinge. This behavior is probably eliminated from the diagonals of actual Mini-Mast truss since the center hinge restraining spring is much stiffer.

	Dummy Tube Test	Longeron Tests No. 2–5	Diagonal Tests												
			2	3	4	5	6	7	8D	8E	8F	8G	9A	10A	11
Measurement Along Axis of Specimen															
• Hysteresis Loops[1]															
Force-Frequency Grid[2]	√	√	√	√											
10 lb peak – 1 Hz					√	√	√	√	√	√	√	√	√	√	√
20 lb peak – 1 Hz					√	√	√	√							
40 lb peak – 1 Hz					√	√	√	√							
Maximum possible lb – 1 Hz					√	√		√							
10 lb peak – 5 Hz									√			√	√	√	√
20 lb peak – 5 Hz									√						
• Force-State Maps															
1 Hz	√	√	√	√	√										
10 Hz	√	√	√	√											
20 Hz	√	√	√	√											
• Random Excitation[3]															
5 pounds rms	√	√													
25 pounds rms	√														

[1] Hysteresis loop measurements also include simultaneous lateral displacement time histories of the center hinge in vertical and horizontal directions.

[2] Force-frequency grid consists of all possible combinations between 1, 10, and 20 Hz and 10, 20, 40, and maximum possible pounds force (0-peak). Dummy tube grid excepted, it was combinations of 1, 10, and 20 Hz and 2, 20, 50, and 75 pound (0-peak).

[3] Frequency Response functions between transverse displacement and axial force on the diagonals

Table 2-2. Test Sequence on Links

	Dummy Tube Test	Longeron Tests No. 2–5	Diagonal Tests											
			2	3	4	5	6	7	8D	8E	8F	8G	9A	10A	11
Transverse Measurements															
• Lateral Impact at Center Hinge[4]															
Horizontal Direction	√			√									√	√	√
Vertical Direction													√	√	√
• Static Stiffness Test[5]															
Horizontal Direction							√							√	√
Vertical Direction							√								
• Free Sag at Center Hinge[6]									√				√	√	√

[4] Frequency response measurements of lateral displacement and force. Broadband force input provided by impact of instrumented hammer near center hinge.

[5] Static stiffness test performed by hanging weights on the center hinge. Stiffness was obtained by dividing incremental force by deflection.

[6] This is the vertical displacement of center hinge due to gravity. Displacement value resulted from difference between the composite tubing height (top edge) near center hinge and the average of composite tubing height (top edge) near endfitting. Measurement does not compensate for undeformed eccentricity of the link, however, tubing was confirmed to be within diametrically consistent ±0.001 inches.

Table 2-2. Test sequence on Links (Continued)

The large discrepancies in diagonal stiffness seemed to exist between the single M style diagonal and the two N diagonal tested. Section 2.1 discusses the differences between the two links being simply the orientation of the center hinge. Orientation of the center hinge should not affect the axial stiffness, however. As shown in Table 2-3, diagonal types M and N responded with stiffnesses of around 15,000 and 5,000 pounds per inch, respectively. Additional tests performed to explain this discrepancy are discussed below, but these did not completely resolve the issue.

Diagonal test results were repeatable within 20 percent. Section 2.8 offers an explanation for this scatter in the repeatability, and Appendix A contains a comprehensive collection of hysteresis loops for comparison. Lateral displacement orbit plots also found in Appendix A are from the same measurement as the immediately preceding hysteresis loop.

Differences in bending stiffness as a function of axis orientation were recorded between diagonal types M and N. Figure 2-8 contains orbit plots of transverse displacements plotted against each other. They show that transverse deflections of Test 2 responded at a ratio of nearly four to one, vertical against horizontal. The displacement ratio in Test 3 was about one to one. Attention was focused on bending stiffness in these orthogonal directions once these differences were observed. Lateral impact and static bending tests were performed on later assemblies. Plots for lateral impact tests are displayed in Appendix A. Resonant frequencies varied by less than 0.6 Hz in each case. Static stiffness measurements were performed on configurations of tests 6, 10, and 11 in the vertical direction. In each case, stiffnesses were about 30 pounds per inch plus or minus one.

Diagonals did occasionally exhibit some nonlinear characteristics even though the force state maps indicated a linear response. The greater detail offered by hysteresis loops and less time averaging during their data acquisition enabled detection of the deviations. Two distinct nonlinearities were observed during diagonal testing. The first is shown in the hysteresis loop in Figure 2-9. It was recognized as random deviations from the elliptic path of a hysteresis loop and was most likely caused by clearances at the endfitting interfaces. These effects were not generally appreciable for the diagonals. The second nonlinearity for the diagonals is shown in the hysteresis loop in Figure 2-10. This nonlinearity was most likely due to opening of the center hinge. Although this effect was significant for the diagonals tested in the link testing apparatus, it may not be important for the actual Mini-Mast diagonals having very stiff center hinge restraining springs. Section 2-8 discusses the expected causes and ramifications of both of these nonlinearities in further detail.

Test No	Link No[1]	Cornerbody[2] A	Cornerbody[2] B	Center Hinge Orientation Break Dir.[3]	Center Hinge Orientation Pin[4]	Lateral Support[5]	Vertical Displacement[6] (in)	Stiffness klbf/in at 1 Hz 10 lbf	at 1 Hz 20 lbf	at 1 Hz 50 lbf	at 5 Hz 10 lb	at 5 Hz 20 lb	Remarks
2	2	0	1	U	H	none	G	15.0	15.8	16.2			
3	1	0	2	U	V	none	G	5.2	6.0	*			
4	2	2	0	D	V	none	G	8.9	8.8	8.9			
5	2	0	1	U	H	none	G	18.5	18.1	18.2			repeat of test 2
6	1	0	2	U	V	none	G	6.2	5.8	*			repeat of test 3
7	1	0	2	U	V	flexures	2-lbf upward force	9.5	9.3	9.2			
8D	1	0	2	U	V	none	G	6.2			5.8	5.3	repeat of test 3
8E	1	0	2	U	V	flexures	G	8.7					
8F	1	0	2	U	V	flexures	.073 upwards[8]	9.3					
8G	1	0	2	U	V	flexures	.133 upwards[9]	10.1			10.5		
9A	1	0	1	U	V	none	G	6.1					
10A	2	0	1	U	H	none	G	14.6			15.8		repeat of test 2
11	3	0	1	U	V	none	G	4.6			*		

Notes:

1 Link numbers assigned by CSA – different from BAC numbers. See text for further explanation.

2 0 = brass fitting (load cell end), 1 or 2 = actual titanium cornerbody.

3 U (D) means link ends move upwards (downwards) relative to the center when hinge folds.

4 H (V) means center hinge axis is oriented 22 (8) degrees CW of horizontal (vertical) viewed from stiffback end of link.

5 See text for description of flexures.

6 G = Displaced downwards by sag due to gravity (unmeasured).

7 Displaced upward approximately halfway from gravity-loaded position to straight.

8 Displaced upward to straight.

* Appreciable nonlinearity in hysteresis loop. It is postulated to be from opening of center hinge.

Table 2-3. Stiffness Results From the Diagonal Test

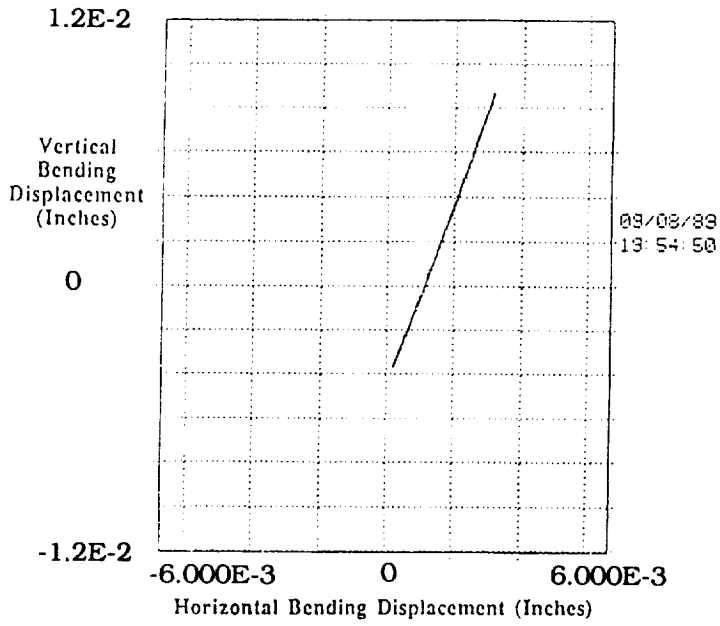

Diagonal test 2, excitation at 1 Hz

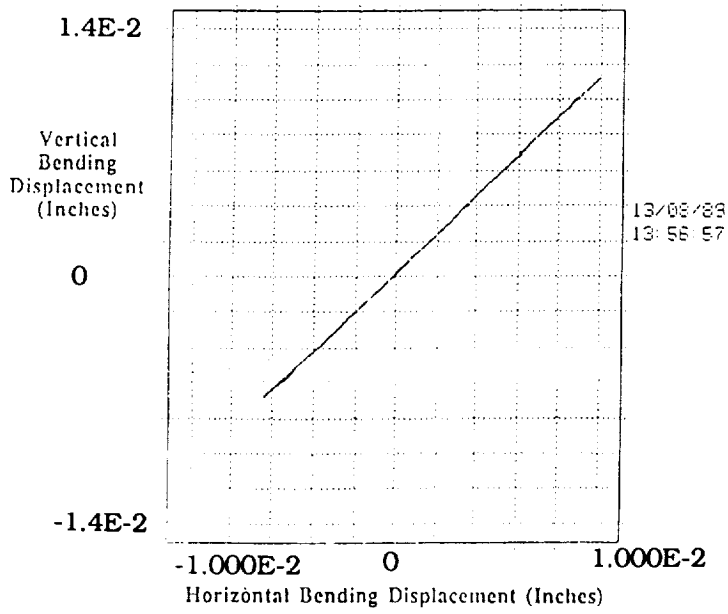

Diagonal test 3, excitation at 1 Hz

Figure 2-8. Transverse Displacement Orbits of Diagonals

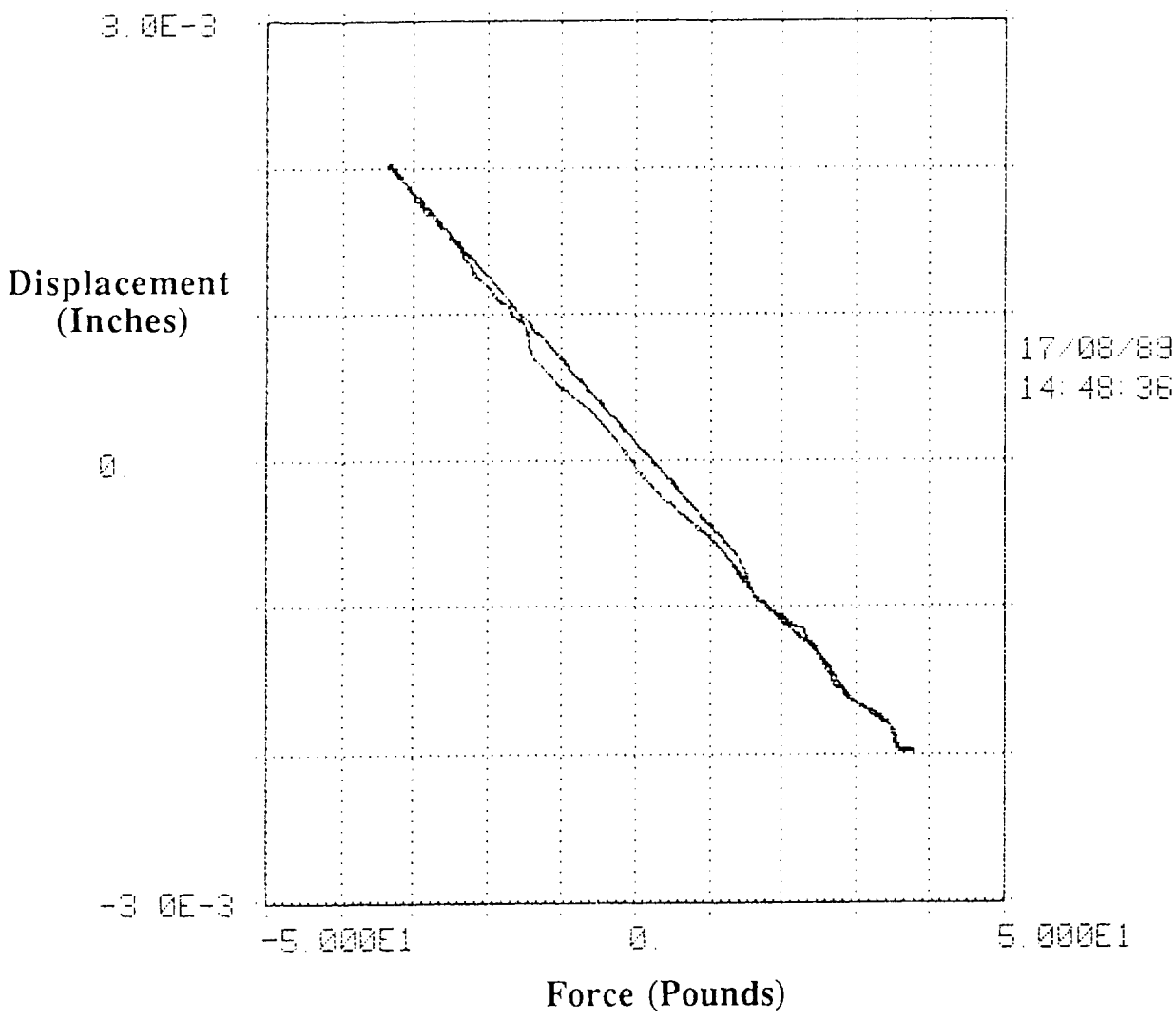

Figure 2-9. Hysteresis Loop of a Diagonal Exhibiting Slight Nonlinearity

Diagonals responded with light damping. The maximum loss factor seen from a linearly responding assembly was 0.04. Loss factor results are shown in Table 2-4. Instrumentation and test technique determined the smallest resolvable loss factor at 0.007. Damping may have been less than this resolution limit. In cases where the center hinge opened and a nonlinear hysteresis loop was created, loss factors as high as 0.07 were recorded. Figures 2-10 and 11 are examples of maximum damping for the nonlinear and linear cases, respectively. Note again that the link tests used diagonal having no center hinge locks. Therefore, higher damping values that resulted from energy dissipation during opening and closing of the hinges may not be seen in the Mini-Mast test article.

Diagnostic tests were performed in an attempt to understand the large stiffness discrepancies exhibited by the diagonals. Tests 7 and 8 were performed with the lateral deflections of the center hinge constrained. This constraint could also eliminate the sag of the center hinge imposed by gravity. The stiffness of the diagonals for constrained lateral deflections increased by 61 percent. It should also be noted that no nonlinear effects were observed for the laterally constrained diagonals even though forces as high as 50 pounds 0-to-peak were applied.

Other miscellaneous diagnostic tests were performed on the diagonals in an attempt to better understand their response. Static lateral stiffness measurements were performed on diagonal test configurations 6, 10, and 11. In each case, transverse vertical stiffness results were 30 pounds per inch plus or minus one pound per inch. Out of round measurements were also performed. Results of these measurements are shown in Table 2-5. In general, center hinges were displaced downward between 0.125 to 0.220 inches with respect to its endfittings. These values may be exaggerated due to inherent out of round of each diagonal since this test measured the total deflection due to gravity and undeformed eccentricity of the link. Center hinges weighed about 2.0 pounds each and a diagonal would be expected to sag only about 0.067 inches (at 30 pounds per inch lateral stiffness). Undeflected out-of-round tolerances were not measured.

Test No	Link No[1]	Cornerbody[2] A	Cornerbody[2] B	Center Hinge Orientation Break Dir.[3]	Center Hinge Orientation Pin[4]	Lateral Support[5]	Vertical Displacement[6] (in)	Loss Factor at 1 Hz 10 lbf	Loss Factor at 1 Hz 20 lbf	Loss Factor at 1 Hz 50 lbf	Loss Factor at 5 Hz 10 lb	Loss Factor at 5 Hz 20 lb	Remarks
2	2	0	1	U	H	none	G	≤0.04	≤0.02	0.03			
3	1	0	2	U	V	none	G	≤0.04	≤0.02	0.07			
4	2	2	0	D	V	none	G	≤0.04	≤0.02	≤0.007			
5	2	0	1	U	H	none	G	≤0.04	0.04	0.02			repeat of test 2
6	1	0	2	U	V	none	G	≤0.04	≤0.02	0.02			repeat of test 3
7	1	0	2	U	V	flexures	2-lbf upward force	≤0.04	≤0.02	0.03			
8D	1	0	2	U	V	none	G	≤0.04			≤0.04	≤0.02	repeat of test 3
8E	1	0	2	U	V	flexures	G	≤0.04					
8F	1	0	2	U	V	flexures	.073 upwards[8]	≤0.04					
8G	1	0	2	U	V	flexures	.133 upwards[9]	≤0.04			≤0.04		
9A	1	0	1	U	V	none	G	≤0.04					
10A	2	0	1	U	H	none	G	≤0.04			≤0.04		repeat of test 2
11	3	0	1	U	V	none	G	≤0.04			≤0.04		

Notes:

1 Link numbers assigned by CSA – different from BAC numbers. See text for further explanation.

2 0 = brass fitting (load cell end), 1 or 2 = actual titanium cornerbody.

3 U (D) means link ends move upwards (downwards) relative to the center when hinge folds.

4 H (V) means center hinge axis is oriented 22 (8) degrees CW of horizontal (vertical) viewed from stiffback end of link.

5 See text for description of flexures.

6 G = Displaced downwards by sag due to gravity (unmeasured).

7 Displaced upward approximately halfway from gravity-loaded position to straight.

8 Displaced upward to straight.

Table 2-4. Loss Factor Results From the Diagonals

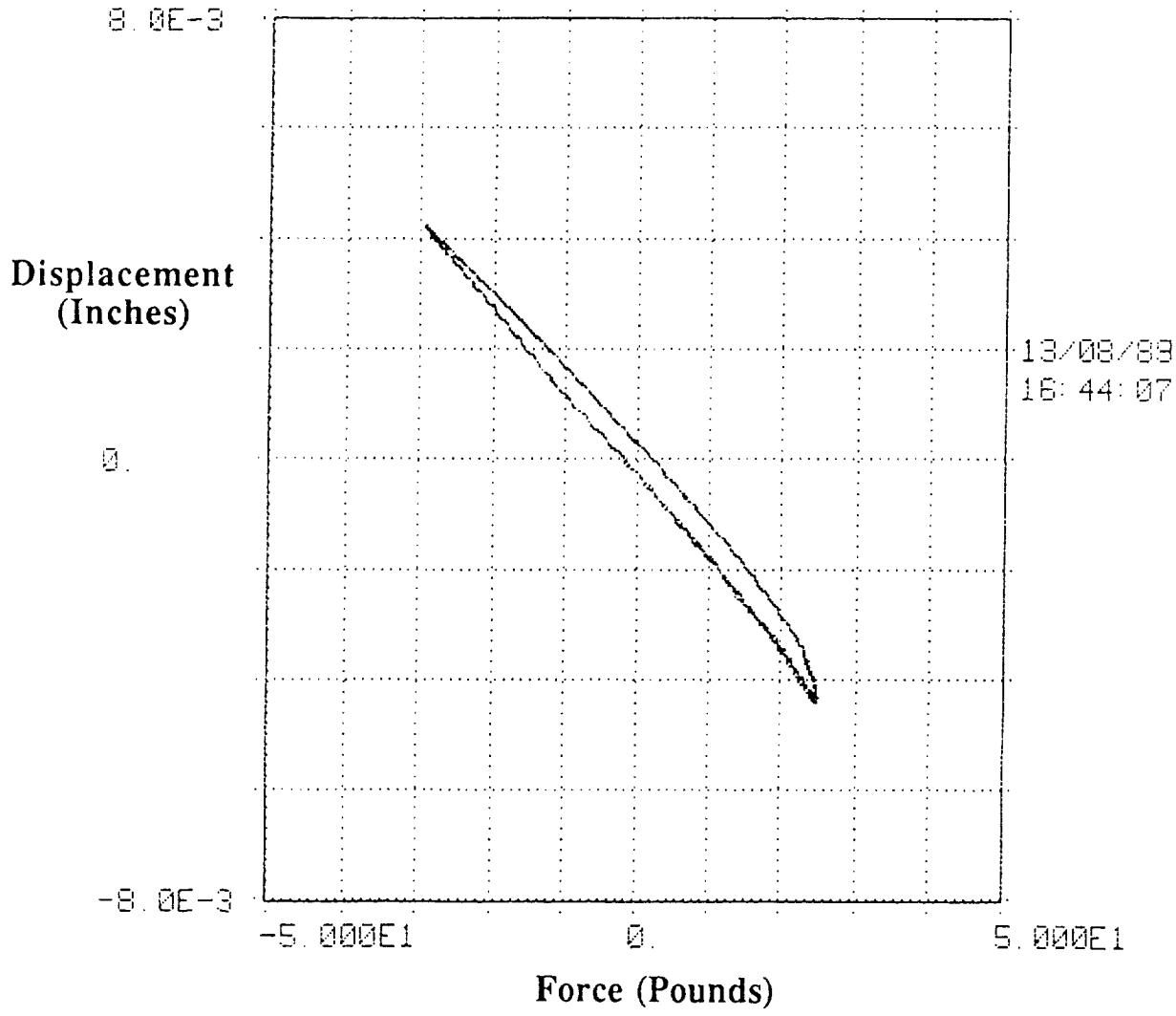

Figure 2-10. Hysteresis Loop Showing Nonlinearity of a Diagonal

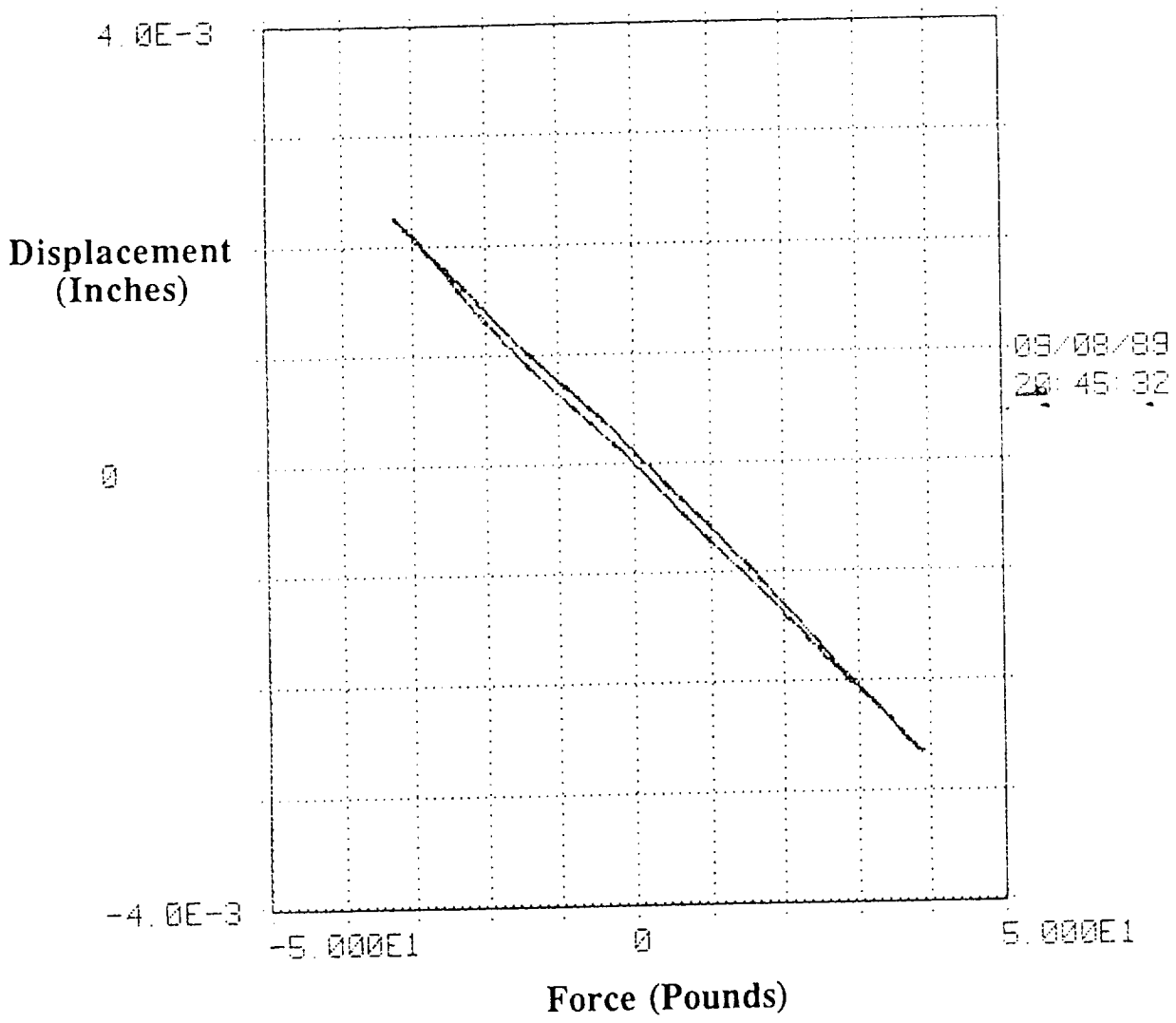

Figure 2-11. Linear Hysteresis Loop From a Diagonal

	Sag at Center of Link (Inches)
Test Series 8	0.123
Test Series 9	0.100
Test Series 10	0.217
Test Series 11	0.157

Table 2.5. Eccentricities of Diagonals Under a Gravity Field.

2.8 Link Test Conclusions

Link testing of the Mini-Mast prototype struts showed that the structural behavior of the longerons and diagonals to be quite complex, though linear for low load and excitation levels. This is not surprising since structures having complicated mechanical hinges that are exposed to alternating loads generally display complex stiffness and damping characteristics. The Mini-Mast longerons and diagonals have hinges at each end which are not perpendicular to the axis of force through the link. This permits the endfitting to slide along the pin connecting the endfitting to the cornerbody. Since the endfitting fits in the cornerbody using a tongue and clevis concept, the endfitting will slide along its pin until the endfitting tongue contacts the wall of the clevis. The manner in which this contact area varies with load can have a large effect on stiffness.

Additional complexities exist for the diagonals. First, the diagonals have a collapsible hinge located midway along its span. This hinge comprises 4/5 of the diagonal's total mass and because of the diagonal's low bending stiffness, gives rise to a first bending frequency between 11.8 to 12.4 Hz when the diagonal is supported at its ends. Force deflection properties were significantly affected by the inertia of this mode near or above the resonant frequency. Force state mapping assumes the force to be a function only of displacement and velocity and not of acceleration. As a result, data acquisition at or above the resonant frequency was discontinued.

A second complexity for the diagonals is due to the off-axis misalignment induced during assembly of the diagonal's two endfittings, two graphite-epoxy tubes, and the center hinge. The misalignment of the center hinge with respect to its endfittings was measured and reported in Section 2.7. This off-axis misalignment will most likely cause the diagonal to bend under an applied axial load and to give an apparent decreased axial stiffness. This conjecture seems to be supported by the lateral restraint tests (also discussed in Section 2.7) in which the axial stiffness of the laterally restrained diagonals increased by 61%. The source of the large 300% variations between the different diagonals may also be attributable to center hinge off-axis eccentricity but the effect is still not fully understood. Only three diagonals were tested and additional specimens need to be tested to support a general conclusion. Furthermore, the actual Mini-Mast diagonals are much stiffer in bending and the above anomalies may not be present.

Both the longerons and diagonals behaved linearly for low load and excitation levels, and became increasingly nonlinear for higher loads and excitation levels. Two types of nonlinearities were observed. In the first, a transition from a linear to nonlinear response was observed to occur about a breakaway excitation level. It is likely that this type of nonlinearity is the result of the endfittings interacting with the cornerbodies. Links appear to be linear at low load since breakaway friction had not been exceeded and the endfittings did not slide along their pins. Larger excitation levels and frequencies worked to exceed these friction forces and slipping occurred. This conjecture is also supported by the results that damping increased when the nonlinearities began occurring, and that the links came to rest at different locations once the excitation ceased. The character of the "breakaway" nonlinearity also varied significantly between link assemblies. Variations in amount of clearances between the endfitting and the cornerbody were also observed to appreciably affect both the breakaway levels and nonlinear magnitudes. Furthermore, repeated assembly and disassemble introduced wear and/or changed the clearances making responses differ measurably.

It is also conjectured that the 20 percent variations in link stiffness that were observed for different assemblies of the same test article was due to the varying clearances between the endfittings and cornerbodies. Although the hinges were designed with very little clearance, surface contact between the endfitting tongue and the cornerbody clevis may dominate their response.

The second type of nonlinearity observed was in the testing of the diagonals under compressive load. The hysteresis loop shown in Figure 2-10 indicates a sharp decrease in stiffness in the compressive range. This behavior is most likely due to the center hinge and suggests that the hinge is beginning to open. It seems plausible that the low bending frequency and large off-axis

eccentricity of the center hinge can lead to premature opening of the center hinge. If so, closer manufacturing tolerances or an improved design would be warranted. The consequences of a premature opening of a diagonal center hinge could be catastrophic for a truss during in-space operation.

To better understand the effects of the individual components of the diagonal links, attempts were made to take measurements across smaller lengths of the diagonal link assembly. Bending of the diagonals, however, caused the off axis displacement transducers to move axially and thus corrupt the axial displacement measurements. Although this testing of each individual joint would have been the most effective troubleshooting method, fixturing redesign and additional instrumentation costs were not within budget.

In conclusion, link tests of the Mini-Mast prototype longerons and diagonals showed that their structural behavior to be quite complex, though linear for low load and excitation levels. Marked unit to unit variations in stiffness and appreciable nonlinearities including free-play with Coulomb friction were also demonstrated. The tests were inconclusive, however, in identifying the source of the unit to unit variations and other anomalies and the need for additional testing of actual Mini-Mast hardware was demonstrated.

2.9 Link Test Recommendations

Testing of the prototype diagonals has yielded a great deal of new information but has also produced inconsistencies and new questions. With the experience described above as a basis, a number of recommendations can now be made relative to improving the test procedure and apparatus. Some are intended to remedy problems encountered during actual tests and some are simply improvements that, while not essential, may be worthwhile if additional tests on actual Mini-Mast hardware are to be done. Recommendations are given below along with the rationale for each.

2.9.1 Improved Simulation of In-Service Conditions

2.9.1.1 Titanium Endfitting Adapters

The brass endfitting adapters were fabricated out of necessity: only a limited number of actual titanium cornerbodies were available at the beginning of the test program. None could be sacrificed to make the load cell adapters. Since then, additional parts have become available which

could be used for that purpose. This could improve the simulation since fits and tolerances on the simulated body parts were based on measurements of actual cornerbodies.

2.9.2 Improved Statistical Basis

2.9.2.1 Statistical Degrees of Freedom

It appears that some amount of random stiffness variation may be inherent in the design of the diagonal links. This is not unusual in situations where load-bearing structures contain unbonded surfaces such as bolted connections or hinge-pins. If so, some recourse to statistical methods is warranted: one must determine empirically the statistics of the stiffness distribution and use them to determine confidence bounds on the overall Mini-Mast properties. The main requirement for doing so is simply a larger number of tests of nominally identical assemblies. While cost constraints will always force this number to be small in statistical terms, it may be worthwhile to test more than the three assemblies done so far.

2.9.2.2 Reduced Re-use of Test Assemblies

In some cases, stiffness properties of an assembly may actually have changed during the test series simply because of unavoidable repeated use. For example, the titanium-coated, press-fit hinge pins were in short supply. While they were carefully cold-fitted and removed with a special puller, it was found that repeated assembly cycles produced a noticeable reduction in removal force. This indicates a loosening of the interference fit and possible change in stiffness. A more plentiful supply of new parts could improve the validity of tests.

2.9.3 Simulation of Gravity Effects

Link eccentricity was found to affect axial stiffness significantly. Part of the eccentricity is due to weight-induced sag, an effect that will vary with the orientation of the link axis relative to vertical (47.3 degrees in the deployed Mini-Mast). Ideally, one would simulate in-service conditions by off-loading about 32% of the hinge weight, but without adding significant transverse stiffness. Off-loading should be done through a spring which is soft compared to the 30 lbf/inch transverse stiffness of the link. Such an arrangement could easily be built and would probably be worthwhile if further tests are performed.

2.9.4 Enhanced Instrumentation

The displacement sensors of Figure 2-12 are necessarily displaced from the axis of the link. Bending of the link can produce rotation of the sensor flag and thus an apparent axial displacement. The amplitude of this effort component depends on the displacement of the sensor from the link axis and the amount of bending rotation. Bending error can be suppressed by using paired sensors, one on either side of the link axis with their outputs summed (Figure 2-12). This was not done on tests to date for cost reasons. It was expected that, as long as the sensor flags were located close to the link axis, the effect would be minor.

Diagnostic tests verified that bending error is quite small for end-to-end stiffness measurements of the entire link. However, the effect is sufficient to preclude a secondary goal of the tests: measurement of individual joint stiffnesses. Spacing the sensors across a single joint, particularly the midspan hinge, produces much lower axial deflection (signal) but the bending deflection (noise) either stays the same or increases. The resulting poor signal-to-noise ratio produces inaccurate stiffness values, a fact that became painfully evident when the measured overall link compliance appeared to be LESS than the sum of measured joint compliances. It is therefore suggested that any additional tests should use paired sensors (four total) to eliminate bending error.

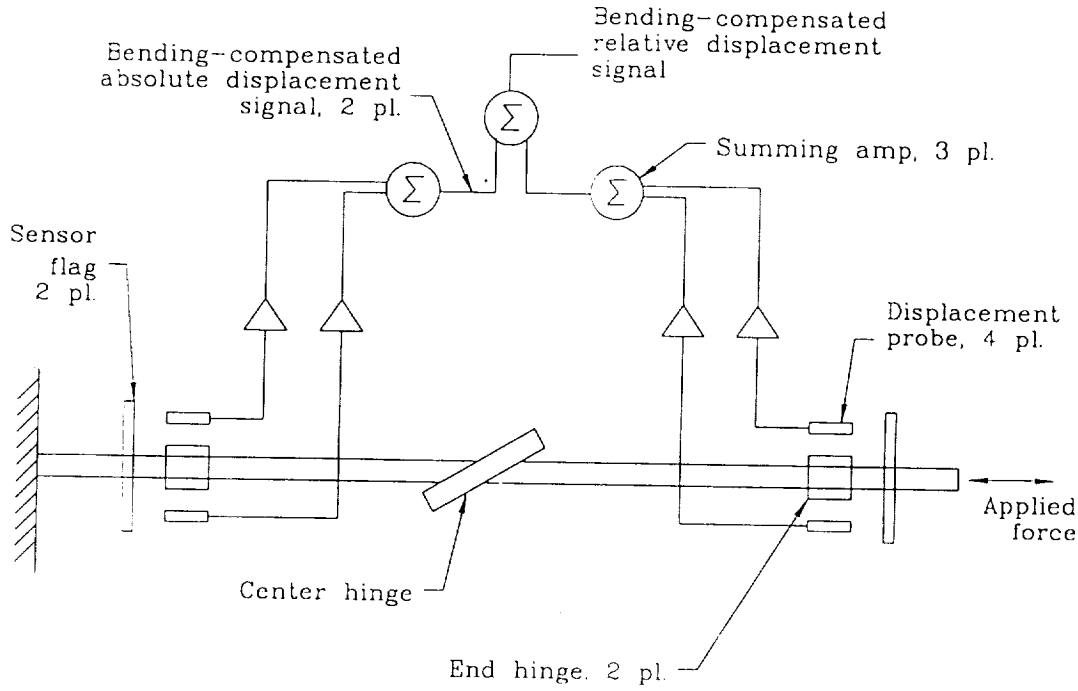

Figure 2-12. Four Sensor System to Eliminate Bending Error

2.9.5 Miscellaneous

Some miscellaneous minor areas for possible improvement include the following:

1. Improved registration of the pushrod guide relative to the stiffback.

2 Analog differentiation of the displacement signal rather than direct velocity sensing for force-state mapping.

3. Revised load cell fixturing to reduce moment sensitivity.

3.0 INVESTIGATION OF THE MINI-MAST TRUSS WITH JOINT FREE-PLAY

In this section, free-play and Coulomb friction in the diagonal links will be incorporated in a transient analysis of the Mini-Mast using the Residual Force Technique. The motivation to do so is based not only on the observed behavior of the proto-type link tests but also on the the observed behavior of the 18 bay Mini-Mast truss in torsion. Parametric analyses of the Mini-Mast using varying amounts of free-play and joint friction are performed to qualitatively examine the nonlinear effects of joint hysteresis on the transient response of the Mini-Mast in torsion. Results from the empirical torsional response of the Mini-Mast are then used to define the values for the free-play and Coulomb friction in the diagonals. An improved nonlinear model of the Mini-Mast is thereby obtained and is used to explain the paradoxical increased modal damping with decreasing amplitude that the ERA program has demonstrated.

Joint free-play with varying amounts of Coulomb friction was demonstrated in the static hysteresis tests performed on the Mini-Mast. In particular, significant nonlinearity was demonstrated for the torsional response as reported by Lawrence W. Taylor, Jr. in the paper "Nonlinear and Distributed Parameter Models of the Mini-Mast," at the 3rd NASA/DOD Controls-Structures Interaction Technology Conference, Jan. 30, 1989. In this paper, the total free-play in the tip rotation of the Mini-Mast is 0.2 degrees. Since the torsional behavior of the Mini-Mast is governed primarily by the diagonal links, the total free-play in the tip rotation can be ascribed to the free-play in the Mini-Mast diagonals. The free-play in the diagonals is calculated to be 0.002 inches using the formula :

$$d = R/2 * \cos B * A / 18$$

where $R = .7\ m$

$\cos B = .7515$

$A = 0.2\ degrees$

and $d = diagonal\ free\text{-}play$

A nominal amount of 5.0 Newtons (N) of Coulomb friction in the diagonal joints may also be calculated using the slip distribution function defined in Taylor's paper.

In section 3.1, parametric analyses of the Mini-Mast are performed to determine the torsional response of the Mini-Mast to varying amounts of free-play and Coulomb friction in the diagonal members. Section 3.2 derives the equations necessary to perform system identification of a modal response governed by modal damping, free-play and hysteresis. Section 3.3 examines the empirical response of the Mini-Mast after torsional excitation and shows the damping behavior of

the Mini-Mast cannot be ascribed to modal damping alone. Conclusions and recommendations are given in Section 3.4.

3.1 Parametric analyses of the Mini-Mast

The effect of including free-play and Coulomb friction in the Mini-Mast links are described in this section. The transient response is determined using the residual force technique and integrated using a technique developed by the author in Ref. 3. The modal equations of motion governing the transient response are shown in Figure 1-2. Integration of these equations of motion is accomplished using a solution technique that is exact when the excitation and nonlinear forces can be taken as linear over the integration time step. This seems to require that the nonlinear force must be known at the next time step in order to calculate the response. There are two methods that can be used to calculate the unknown nonlinear forces. First, when the nonlinear forces are few in number, an implicit nonlinear set of equations can be derived that contains the nonlinear forces as the unknowns. Since this set is the same order as the number of unknown forces, powerful numerical techniques may be used to solve for the unknown forces exactly. The solution to the full set of modal equations can then also be said to be exact, so long as the nonlinear forces can be taken as linearly varying over the time step. The second approach to solving nonlinear modal equations of motion uses a predictor corrector method; i.e., the nonlinear forces at the next time step are predicted based on the past behavior, and then corrected repeatedly by calculating the modal response and the resulting nonlinear forces. This method is useful when the number of nonlinear forces are large as is the case for the Mini-Mast where nonlinear residual forces are defined for each strut throughout the entire truss. The integration technique is summarized in Appendix D for convenience.

The linear transient response of the Mini-Mast when a constant torque of 376 Newton-meters (N-m) is suddenly released is shown in Figure 3-1. The transient response of the Mini-Mast for links having .001 inches of free-play both with and without Coulomb friction are shown in Figures 3-2 thru 3-6. The nonlinear response is calculated using only one torsion and the first two bending modes of the cantilevered structure to give a general indication of the nonlinear effects. Modal damping values of 1.964 and 1.194 percent were taken for the first and second bending mode, respectively. A damping value of 1.660 is taken for the torsion mode. A total of five modes are analyzed since each bending mode has two structural modes.

Figure 3-2 shows the tip response of the Mini-Mast when the diagonals have 0.001 inch free-play. Two observations are readily apparent when this response is compared to Figure 3-1. First,

the structure having gaps is softer and has an initial angular tip deflection that is larger than the linear structure. And second, the frequency of oscillation of the structure having diagonal free-play continues to decrease as the amplitude decays. Both of the above effects are to be expected for a truss having free-play in the diagonal elements. A third observation not readily apparent from Figures 3-1 and 3-2 is the energy transfer from the torsion mode to the higher bending modes.

Figure 3-3 shows the tip response of the Mini-Mast when the diagonals have 0.001 inch free-play and Coulomb friction of 1.0 Newton in each diagonal. Comparison of this response to the linear response in Figure 3-1 again shows the higher initial tip response and decreasing frequency of oscillation as the amplitude decays. The effect of including one Newton of Coulomb friction in each gap can be seen by comparing Figures 3-2 and 3-3. First, increased decay is seen in the structure having Coulomb friction in the diagonal gaps. And second, the frequency of oscillation is amplitude dependent implying that for any single oscillation of the tip in Figure 3-3 that has the same amplitude as an oscillation in Figure 3-2 the periods will be identical. These observations appear reasonable when the Coulomb friction forces are small and do not cause the diagonal gaps to lock up.

Figure 3-4 shows the tip response of the Mini-Mast when the diagonals have 0.001 inch free-play and Coulomb friction of 5.0 Newtons in each diagonal. Comparing this figure to the previous three figures again shows the increased damping due to friction and the amplitude and frequency effects of the gaps. Also shown in Figure 3-4 is the non-zero offset that results at the end of decay. The small oscillations that occur after 3.5 seconds is due to linear decay of the truss since the gaps in the diagonals are locked up due to Coulomb friction.

Figure 3-5 shows the tip response of the Mini-Mast when the diagonals have 0.001 inch free-play and Coulomb friction of 50.0 Newtons in each diagonal. This figure shows the response to decay linearly when the gap elements are sliding and shows exponential decay after the gaps lock-up. Since all diagonals have identical values for the Coulomb friction force, the transition of the tip response from linear to exponential decay occurs nearly instantaneously when the tip amplitude reaches a certain threshold.

A more realistic situation to analyze when the Mini-Mast diagonals have free-play and Coulomb friction is when the Coulomb friction force values have some probability distribution throughout the truss. Figure 3-6 shows the tip response of Mini-Mast when the Coulomb friction force values are calculated using the absolute value of a Gaussian distribution centered about zero and having 10.0 Newton standard deviation. This distribution is taken for analysis only and should not be

taken as representing the empirical response of the Mini-Mast. The tip response of the Mini-Mast shown in Figure 3-6 now exhibits gradual transition from the nonlinear to exponential decay. In addition, as the amplitude decreases, the decreasing frequency effect of the gaps appears to be compensated by the increasing frequency effect of gaps locked-up due to friction.

3.2 Analytical Response of an Oscillator Having Small Nonlinearities.

In this section, the analytical behavior of a single degree of freedom oscillator having small nonlinearities is derived using the method of multiple scales. An energy expression is then derived that describes the decay rate of an oscillator with a slowly varying amplitude. This expression is applied to an oscillator having free-play and Coulomb friction so that the amplitude dependence upon these parameters can be analytically determined.

Consider

$$\ddot{x} + \omega^2 x = -\varepsilon f(x, \dot{x}) \quad \varepsilon << 1 \tag{1}$$

where x = amplitude
$\ddot{x}$ = acceleration
ω = radian frequency
and $f(x, \dot{x})$ = nonlinear function of x and $\dot{x}$.

We seek a perturbation solution that is valid to order ε for times on the order of $1/\varepsilon$.

The solution is obtained using the method of multiple scales. In brief, the solution is:

$$x = A \sin(\omega t + \vartheta) \tag{2}$$

where A and ϑ are functions of the slow variable $t = \varepsilon t$ governed by the equations:

$$\omega A' + \frac{1}{2\pi} \int_0^{2\pi} f(A \sin\theta, \omega A \cos\theta) \cos\theta \, d\theta = 0 \tag{3}$$

and

$$\omega A \vartheta' - \frac{1}{2\pi} \int_0^{2\pi} f(A \sin\theta, \omega A \cos\theta) \sin\theta \, d\theta = 0 \tag{4}$$

Define

$$E = \frac{1}{2}\dot{x}^2 + \frac{1}{2}\omega^2 x^2 = \frac{1}{2}\omega^2 A^2 \qquad 5)$$

then equation 3 can be rewritten as:

$$\frac{dE}{dt} + \frac{1}{T}\int_0^T \varepsilon f \cdot \dot{x}\, dt = 0 \qquad 6a)$$

where

$$T = \frac{2\pi}{\omega} \qquad 6b)$$

Equation 6 is useful since the time rate of change in the amplitude can be determined from an energy conservation relation.

Now consider an oscillator having free-play and hysteresis. The governing differential equation for the energy obtained from equation 6 is:

$$\frac{dE}{dt} + 2\xi\omega E = -\frac{\delta}{\pi}\omega f_c/m \qquad 7)$$

where E = energy of the oscillator = $1/2\ \omega^2 A^2$
ξ = modal damping
δ = total freeplay in the oscillator
f_c = Coulomb friction within the gap
and m = mass of the oscillator

The time variation of the amplitude for an oscillator having free-play and hysteresis is easily obtained from the above equation. This equation will be used in the next section to identify the Coulomb and modal damping values for the Mini-Mast in torsion.

3.3 Empirical response of the Mini-Mast

The empirical transient response of the Mini-Mast after torsional excitation was determined by NASA/LaRC. Figures 3-7 and 3-8 show the amplitudes of the response measured by KAMAN

displacement transducers 51 and 15, respectively, when the truss was subject to torsional excitation of 4.2 Hertz (Hz) at bay 9 and then allowed to decay freely. KAMAN 15 is located at bay 10 and KAMAN 51 at the tip or bay 18. See the Mini-Mast CSI Testbed Users' Guide (Ref. 5) for complete details. The ERA program was used on this data by NASA to identify the torsional mode frequency and damping and the values are reported to be 4.2 Hz with 1.66% modal damping. In addition, the modal frequency and damping values were both shown to increase as the amplitude decreases.

Figures 3-9 and 3-10 show the amplitudes of KAMANs 15 and 51 during the free decay portion and are compared to the exponential decay of a 4.2 Hertz (Hz) damped sinusoid with 1.66% modal damping. Note that the exponential decays of the damped sinusoids are good approximations of the empirical response during the initial decay but under predicts the damping at low amplitudes. In particular, modal damping values of 2.58% and 2.47% depict the decay rates of Kamans 51 and 15, respectively, in the time period 35 to 37.5 seconds. This apparent increasing values for modal damping with decreasing amplitude is also demonstrated in Ref. 5 using the ERA program.

Figure 3-10 shows an apparent piecewise linear behavior in the empirical response at the tip of the Mini-Mast. One hypothesis to explain this nonlinear behavior is to permit the Mini-Mast joints to have free-play with varying amounts of Coulomb friction so that as the structure decays, an increasing larger number of joints lockup and the energy dissipation becomes increasingly smaller. The noticeable change in slope of the KAMAN 51 amplitude at 35 seconds then suggests that a group of joints locked up simultaneously. The amplitude decay of KAMAN 51 then remains remarkably linear until the amplitude becomes less than 0.02 inches. The behavior of KAMAN 15 in Figure 3-3 also exhibits the change in slope near 35 seconds although the change is not nearly as noticeable. The above hypothesis also supports the ERA results that depict an increasing frequency of oscillation as the amplitude decays.

The joint free-play with hysteresis hypothesis, however, seems to contradict the ERA results that show increased damping with decreasing amplitude. This apparent contradiction arises because ERA can calculate damping values assuming exponential decay only. An improved representation of the Mini-Mast torsional decay should therefore consider damping due to joint slippage in addition to the usual modal damping.

In Section 3.2, Equation 7, the time rate of change of the square of the amplitude is shown to be proportional to the gap size and Coulomb friction value. The effect of modal damping on the

decay rate is also shown. This equation demonstrates that modal damping will dominate frictional damping during large amplitude oscillations but will become increasingly unimportant as the amplitude decays. If the total gap size in the diagonals is taken as 0.002 inches as in the static hysteresis tests (Ref. 6), then variations in the torsional response of the Mini-Mast with modal damping and Coulomb friction may be calculated using the Residual Force Technique.

In Figures 3-11 through 3-14, the Residual Force Technique is used to calculate the amplitude envelope of the Mini-Mast tip rotation when the diagonals have a total of .002 inches of free-play and varying amounts of Coulomb friction. The envelopes are calculated for the free decay of the Mini-Mast structure after the sudden release of an applied torque at the tip. The free decay calculated this way is compared to the free decay of the empirical results shown in Figures 3-7 through 3-10. The comparisons performed in this manner are legitimate so long as the initial amplitudes are identical. In Figure 3-11, the modal damping of the torsional mode is taken as 1.66% and the Coulomb friction value in the diagonal links is taken as 5.0 N. The envelope without Coulomb friction is also shown for comparison. Note that Figure 3-11 shows the increased importance of frictional damping as the amplitude decays.

Comparison of the response in Figure 3-11 to the response of Kaman 51 in Figure 3-10 shows good agreement after the first three seconds of free-decay. To improve the comparison, the modal damping value was reduced from 1.66% to 1.5%. Figures 3-12 through 3-14 show the amplitude envelopes for Coulomb friction values of 20, 10 and 5 N, respectively. Comparison of the envelopes in these figures to the envelope in Figure 3-10 clearly shows that the best overall description of the Mini-Mast damping is given by the response having 5 N of Coulomb friction . This nominal value of Coulomb friction at 5 N is plausible since this is also the value that can be obtained from the static hysteresis tests as described by L. Taylor in Ref. 6. Further improvements to the nonlinear Mini-Mast model can be obtained through a comprehensive system identification that permits a distribution in Coulomb force values as in Taylor's paper.

3.4 Conclusions

An improved nonlinear model of the Mini-Mast has been obtained by permitting the diagonal links to have 0.002 inches of free-play and Coulomb friction with a nominal value of 5 N. These values are consistent with those reported earlier in Ref. 6 for the static hysteresis tests in torsion. Improved transient results can be obtained, however, by including an improved distribution of Coulomb friction values throughout the truss. A distribution in Coulomb force values throughout the truss is required to replicate the observed behavior of the truss to have its frequency of

oscillation *gradually* increase as the amplitude decreases. This distribution of friction values will also cause some diagonals to lock earlier than others causing the structure to become gradually stiffer with decreasing amplitude. This implies that there will be less frictional damping in the structure as the response decays.

Decreased frictional damping as the response decays is not to be confused, however, with the apparent increase in modal damping that the ERA program predicts. Equations were derived in Section 3.2 showing that frictional damping becomes increasingly dominant over modal damping as the structure decays. Any calculations that ignore frictional damping at these low levels of oscillation must necessarily compensate by having increased values for modal damping.

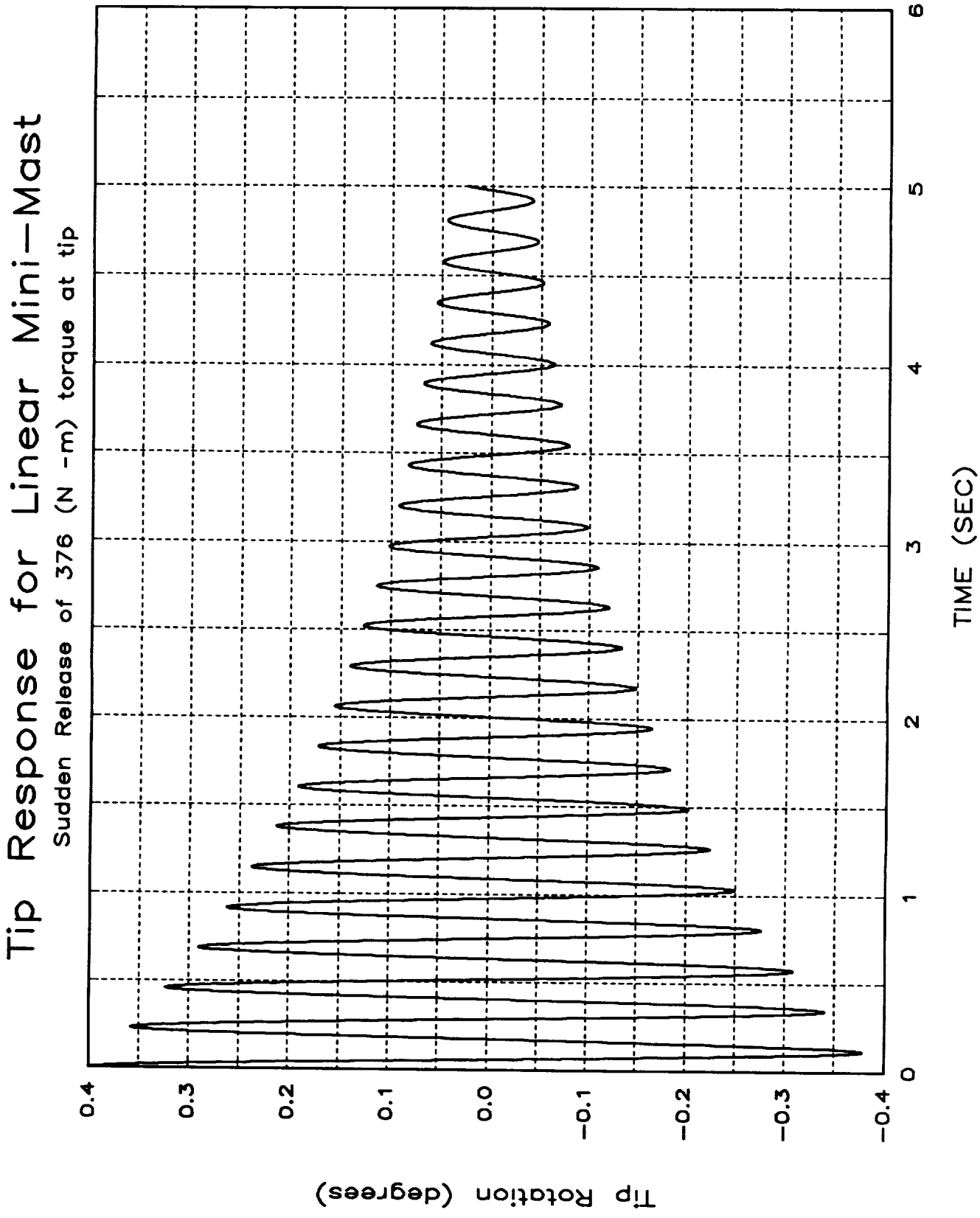
Tip Response for Linear Mini-Mast
Sudden Release of 376 (N -m) torque at tip
Tip Rotation (degrees)
0.4
0.3
0.2
0.1
0.0
-0.1
-0.2
-0.3
-0.4
0
1
2
3
4
5
6
TIME (SEC)

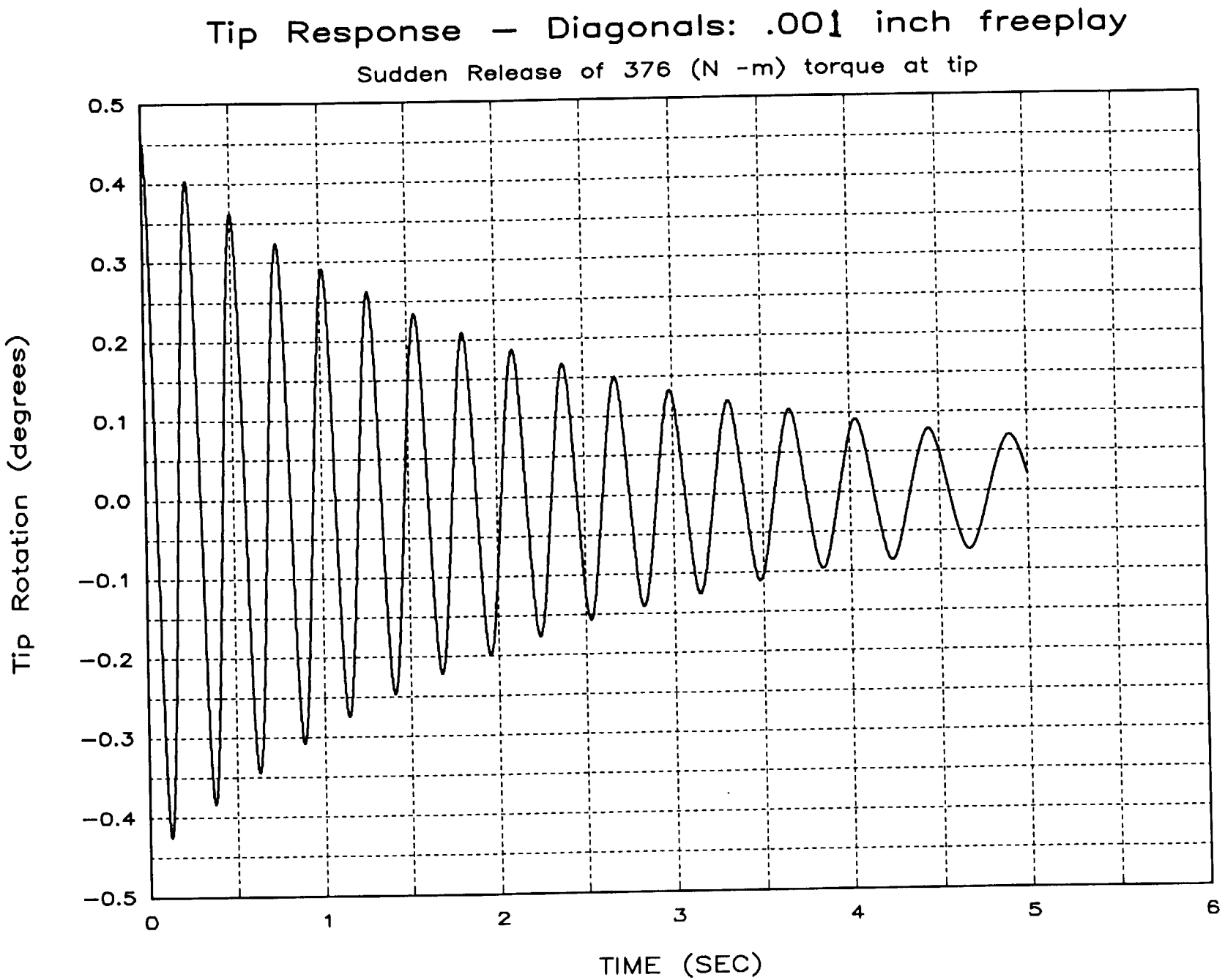
Tip Response — Diagonals: .001 inch freeplay
Sudden Release of 376 (N -m) torque at tip
Tip Rotation (degrees)
0.5
0.4
0.3
0.2
0.1
0.0
−0.1
−0.2
−0.3
−0.4
−0.5
0
1
2
3
4
5
6
TIME (SEC)

Figure 3-2.

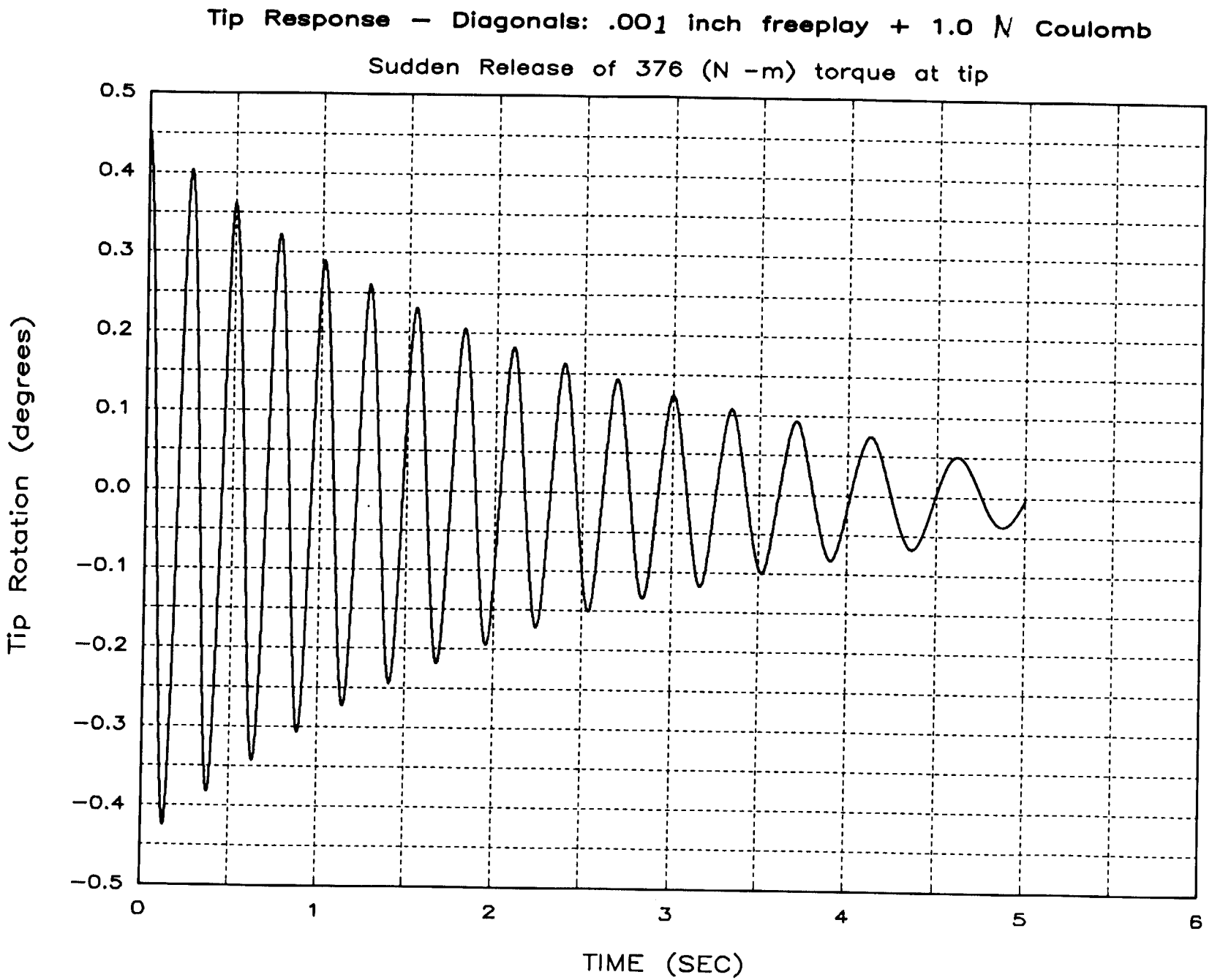
Tip Response — Diagonals: .001 inch freeplay + 1.0 N Coulomb
Sudden Release of 376 (N -m) torque at tip
Tip Rotation (degrees)
0.5
0.4
0.3
0.2
0.1
0.0
−0.1
−0.2
−0.3
−0.4
−0.5
0
1
2
3
4
5
6
TIME (SEC)

Figure 3-3.

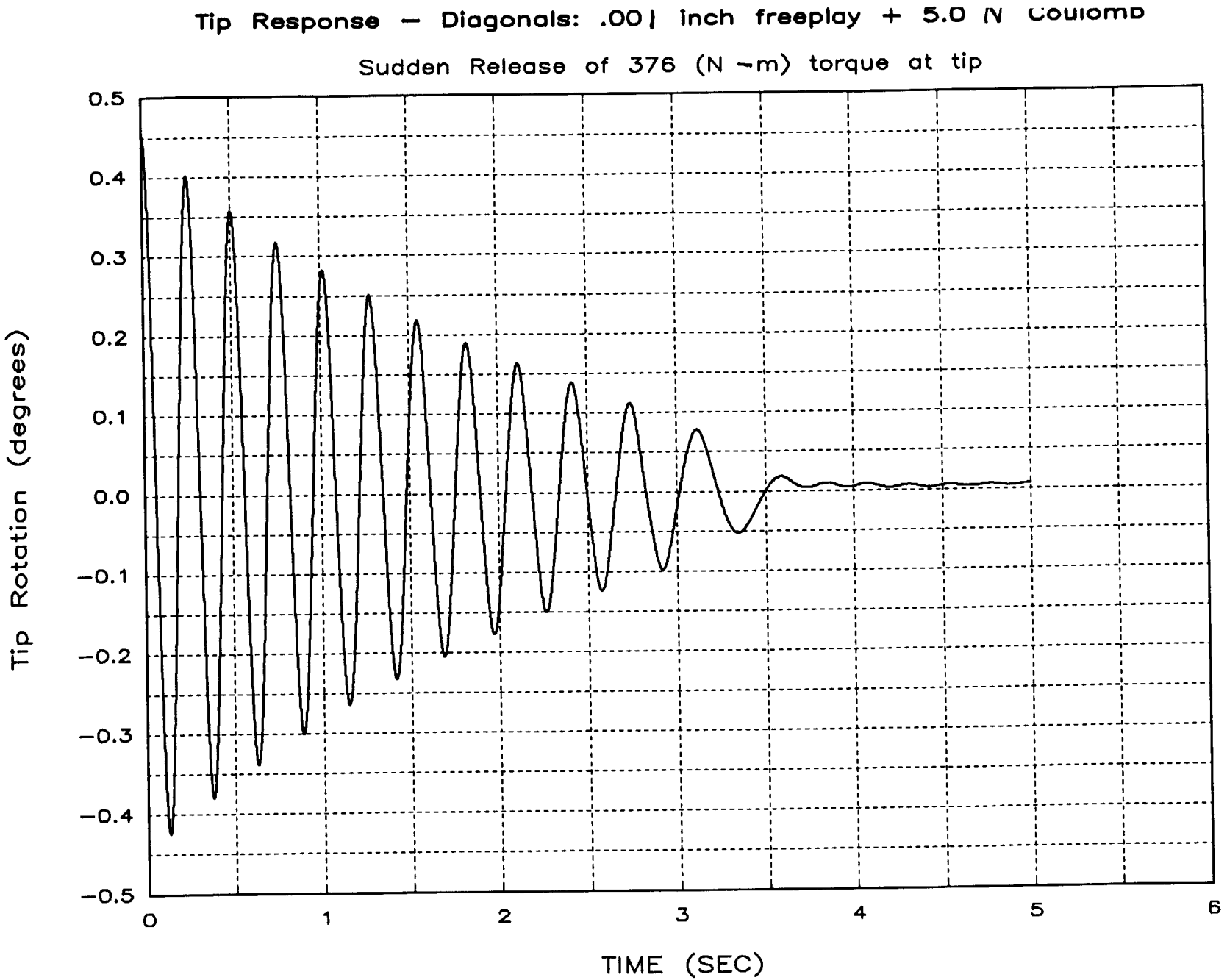
Tip Response — Diagonals: .001 inch freeplay + 5.0 N Coulomb
Sudden Release of 376 (N −m) torque at tip
Tip Rotation (degrees)
0.5
0.4
0.3
0.2
0.1
0.0
−0.1
−0.2
−0.3
−0.4
−0.5
0
1
2
3
4
5
6
TIME (SEC)

Figure 3-4.

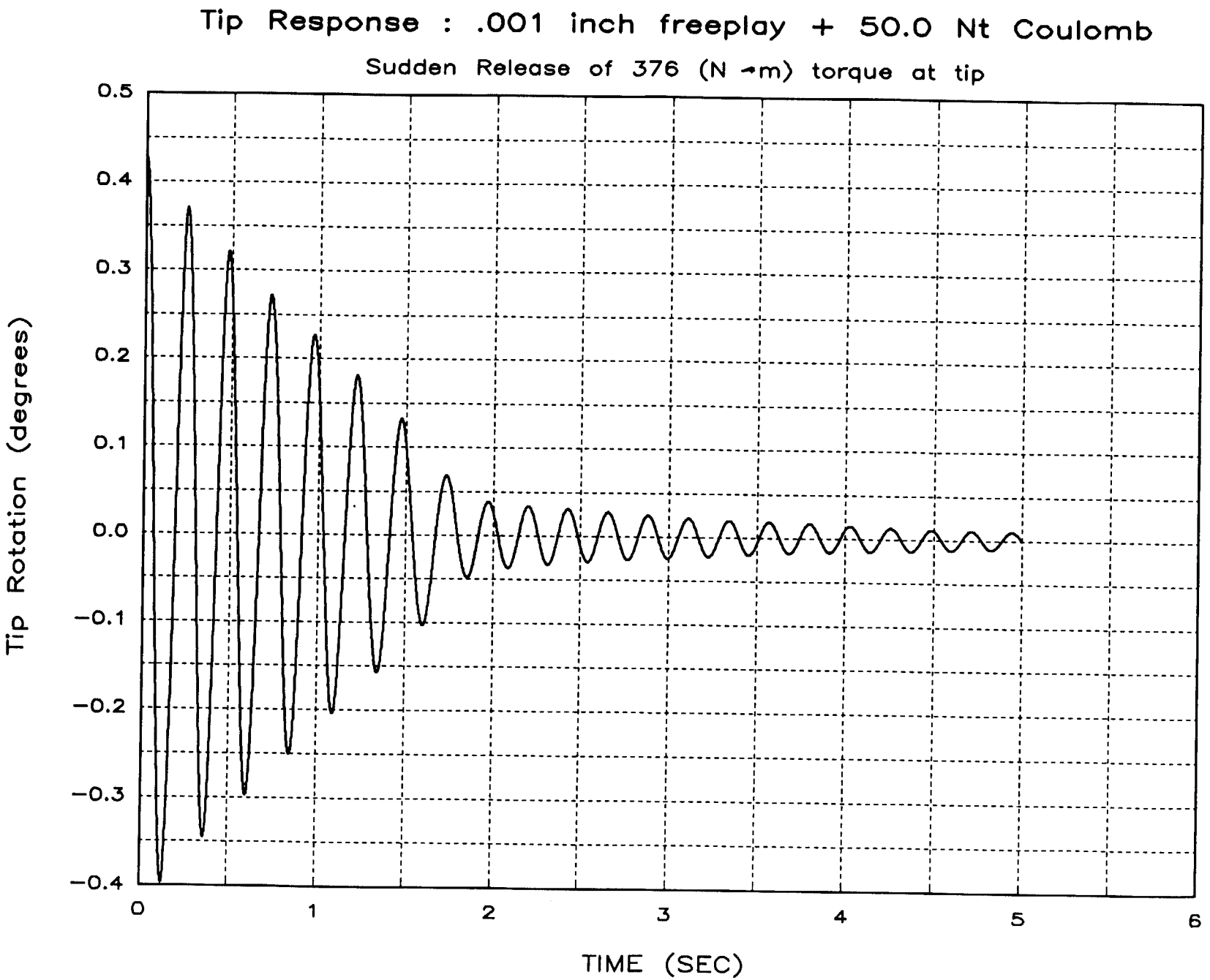
Tip Response : .001 inch freeplay + 50.0 Nt Coulomb
Sudden Release of 376 (N-m) torque at tip
Tip Rotation (degrees)
0.5
0.4
0.3
0.2
0.1
0.0
−0.1
−0.2
−0.3
−0.4
0
1
2
3
4
5
6
TIME (SEC)

Figure 3-5.

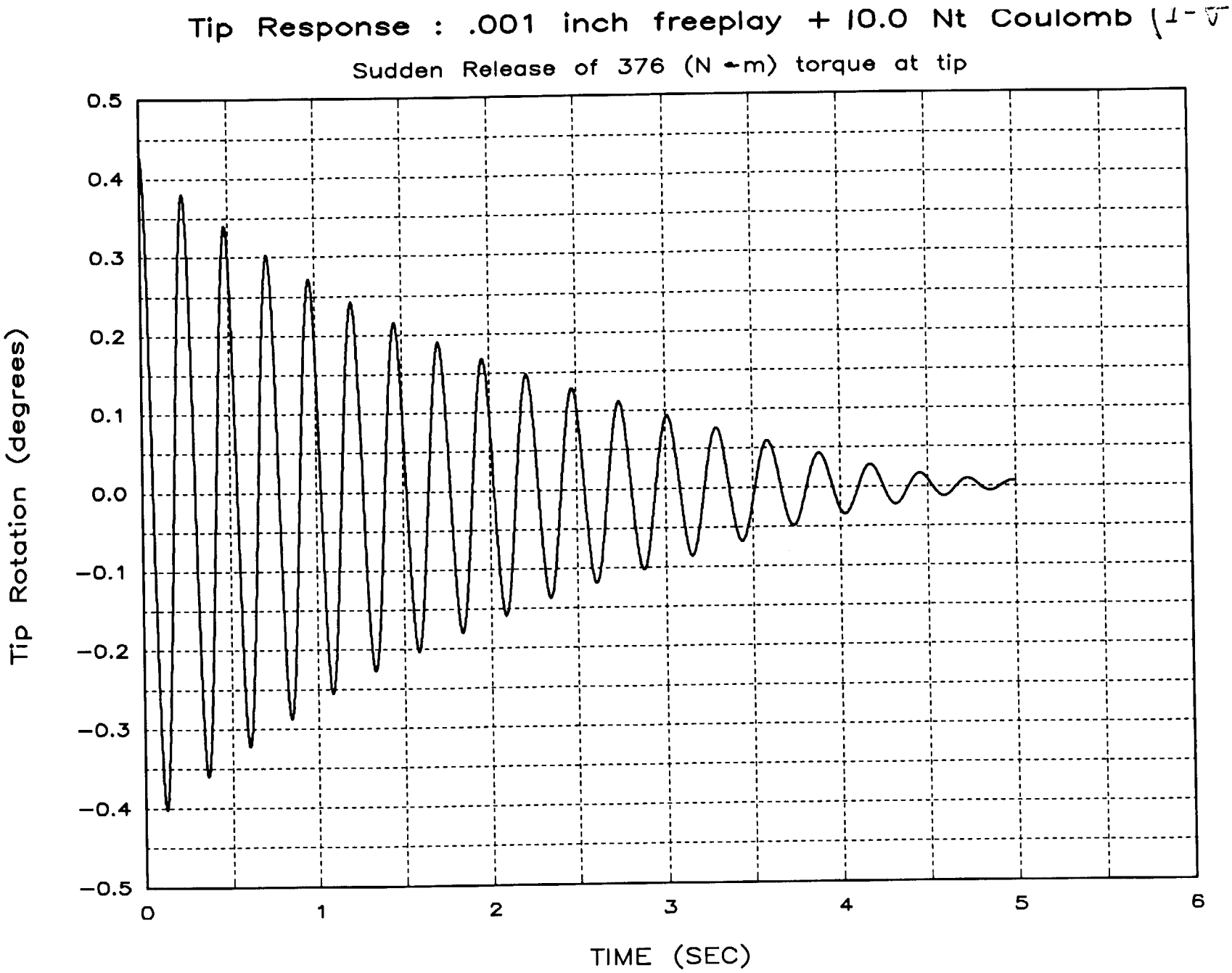
Tip Response : .001 inch freeplay + 10.0 Nt Coulomb (1-5)
Sudden Release of 376 (N-m) torque at tip
Tip Rotation (degrees)
0.5
0.4
0.3
0.2
0.1
0.0
−0.1
−0.2
−0.3
−0.4
−0.5
0
1
2
3
4
5
6
TIME (SEC)

Figure 3-5.

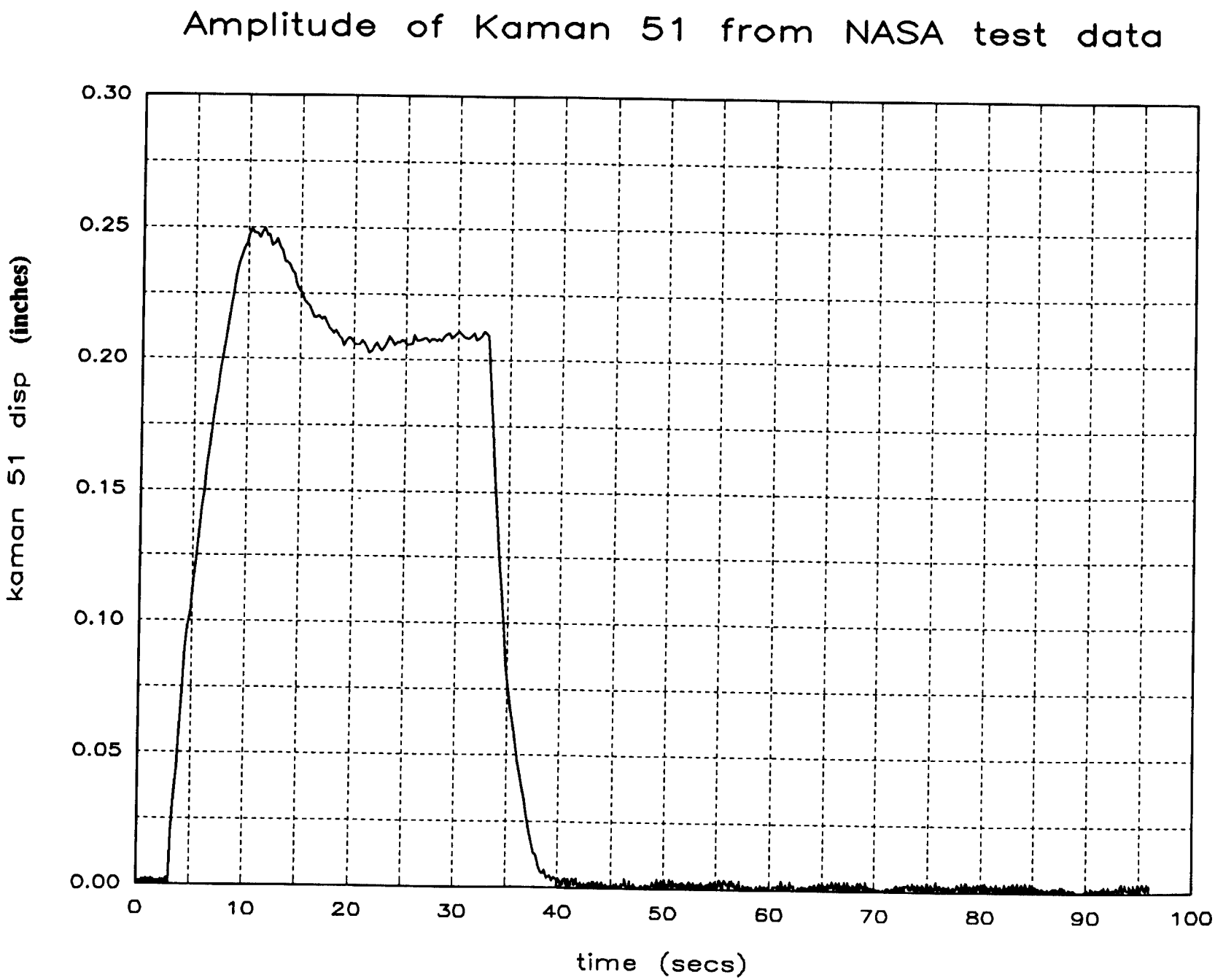
Amplitude of Kaman 51 from NASA test data
kaman 51 disp (inches)
0.30
0.25
0.20
0.15
0.10
0.05
0.00
0
10
20
30
40
50
60
70
80
90
100
time (secs)

Figure 3-7

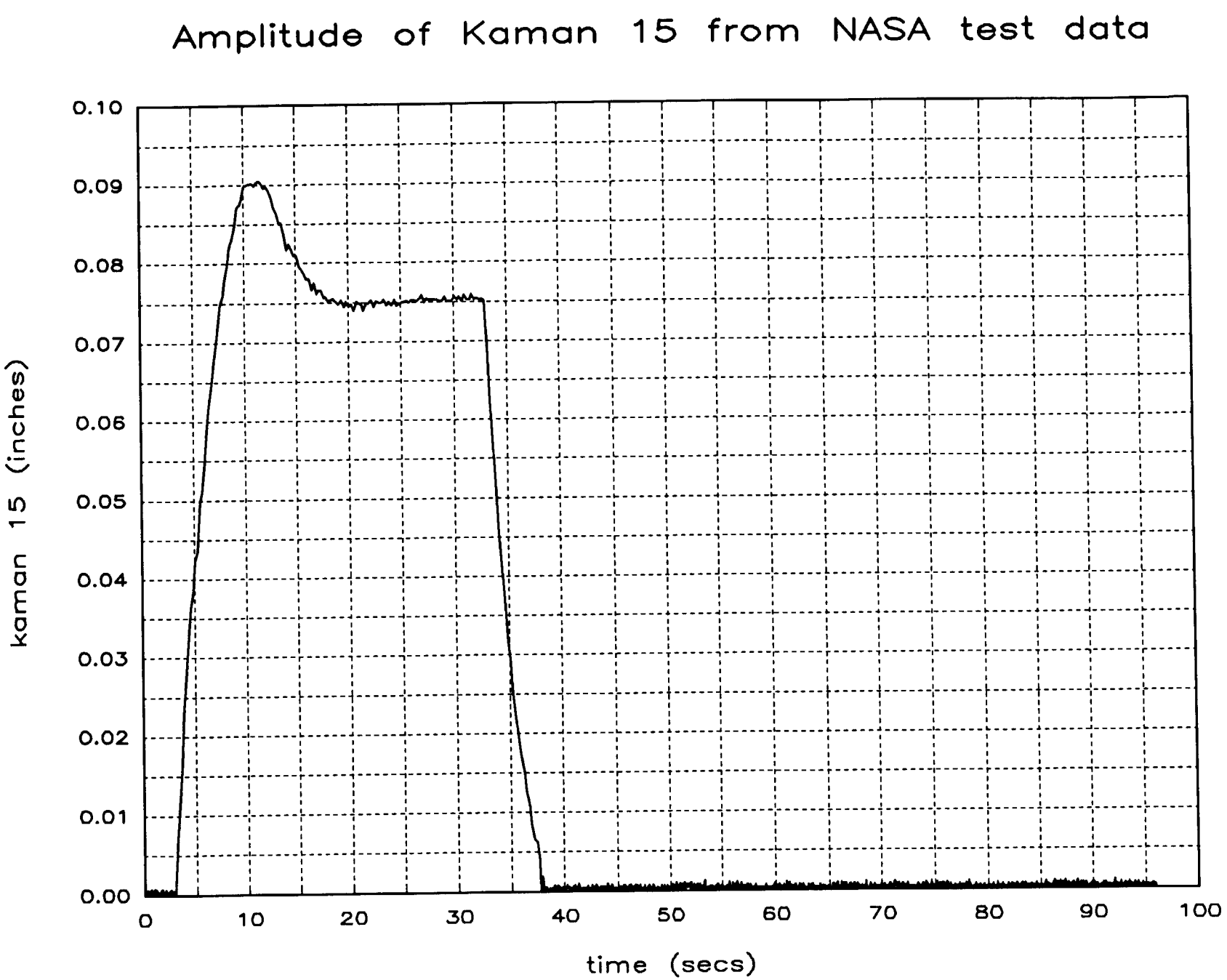
Amplitude of Kaman 15 from NASA test data
kaman 15 (inches)
0.10
0.09
0.08
0.07
0.06
0.05
0.04
0.03
0.02
0.01
0.00
0
10
20
30
40
50
60
70
80
90
100
time (secs)

Figure 3-8

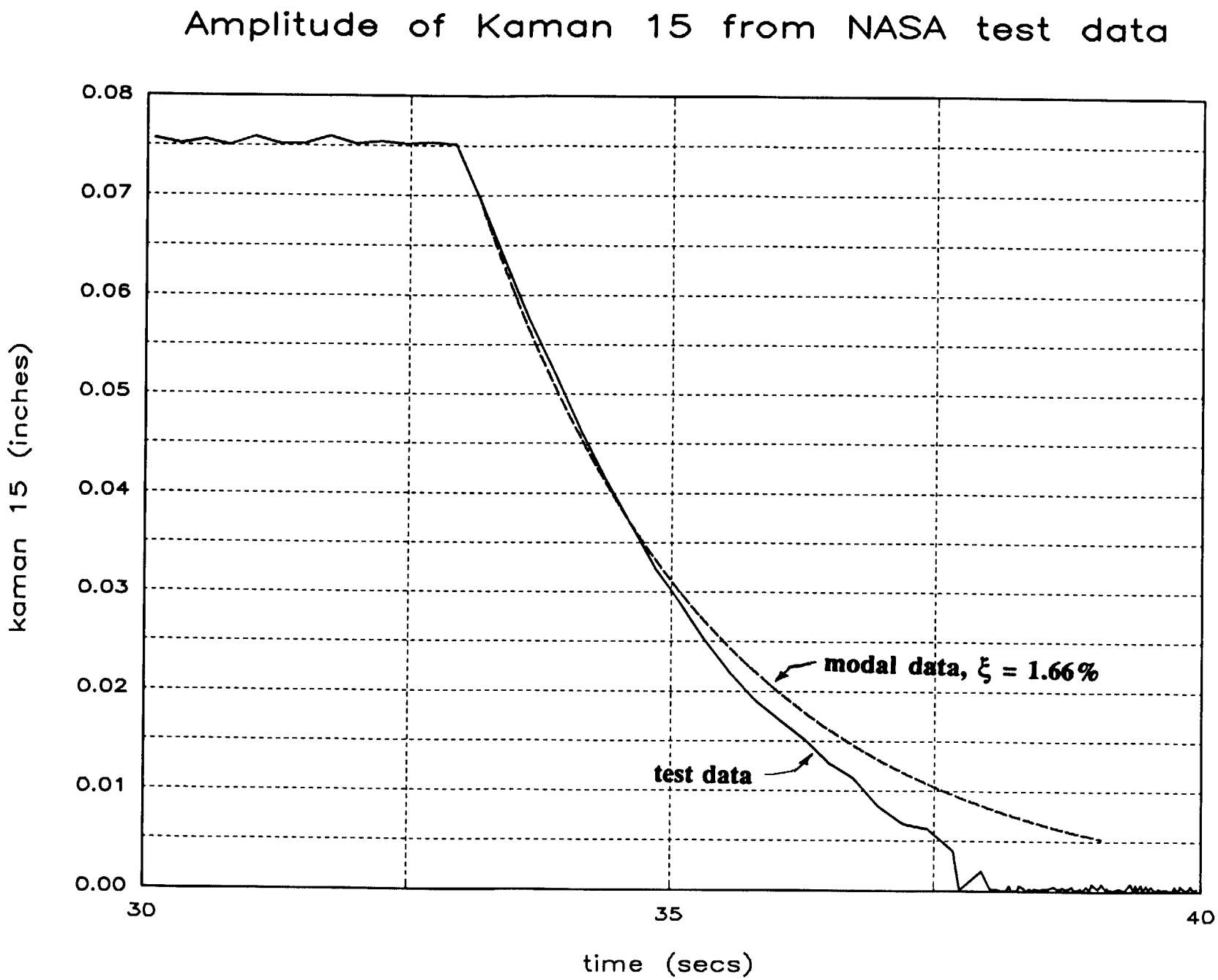
Amplitude of Kaman 15 from NASA test data
0.08
0.07
0.06
0.05
0.04
0.03
0.02
0.01
0.00
kaman 15 (inches)
30
35
40
time (secs)
modal data, ξ = 1.66%
test data

Figure 3-9

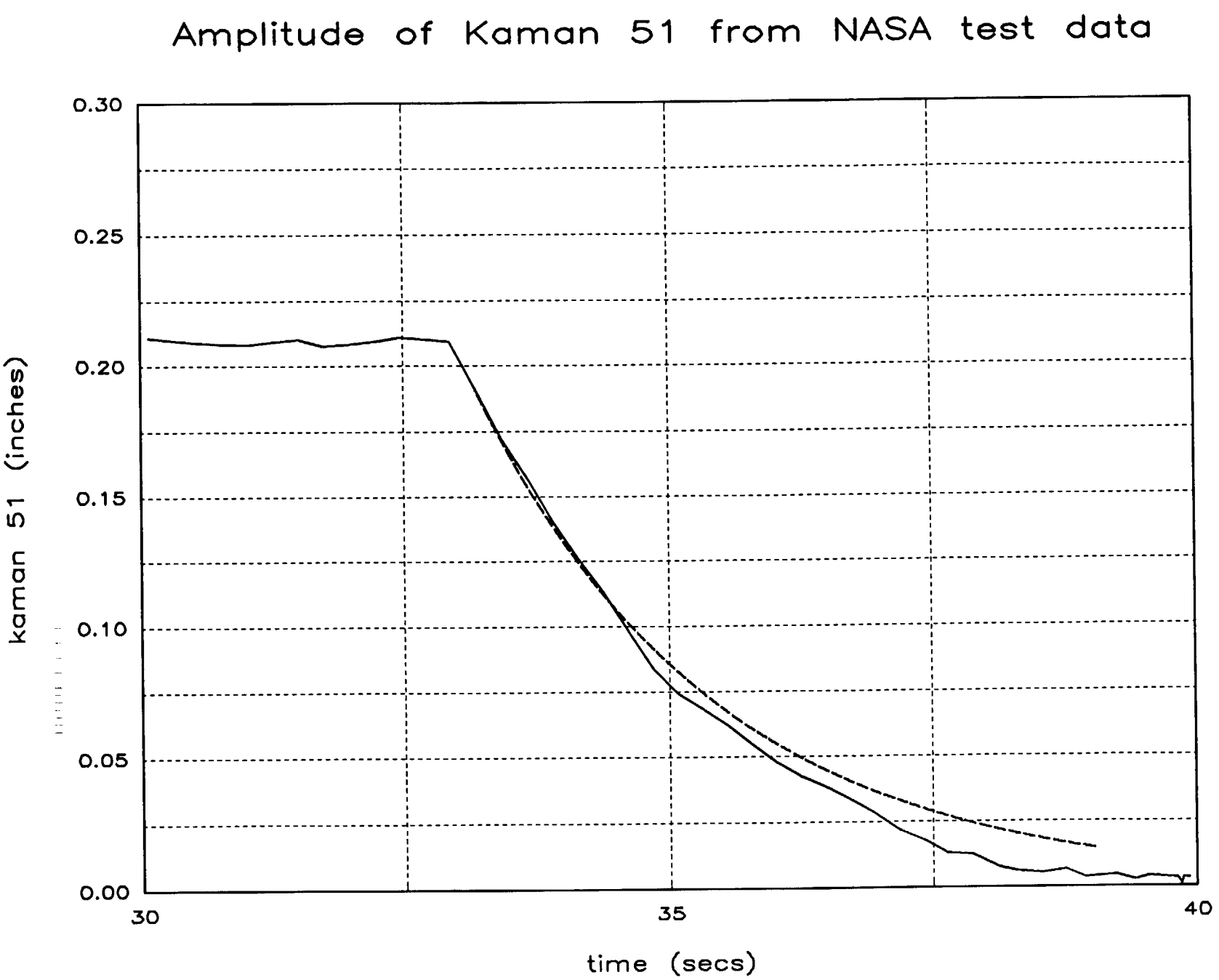
Amplitude of Kaman 51 from NASA test data
0.30
0.25
0.20
0.15
0.10
0.05
0.00
kaman 51 (inches)
30
35
40
time (secs)

Figure 3-10

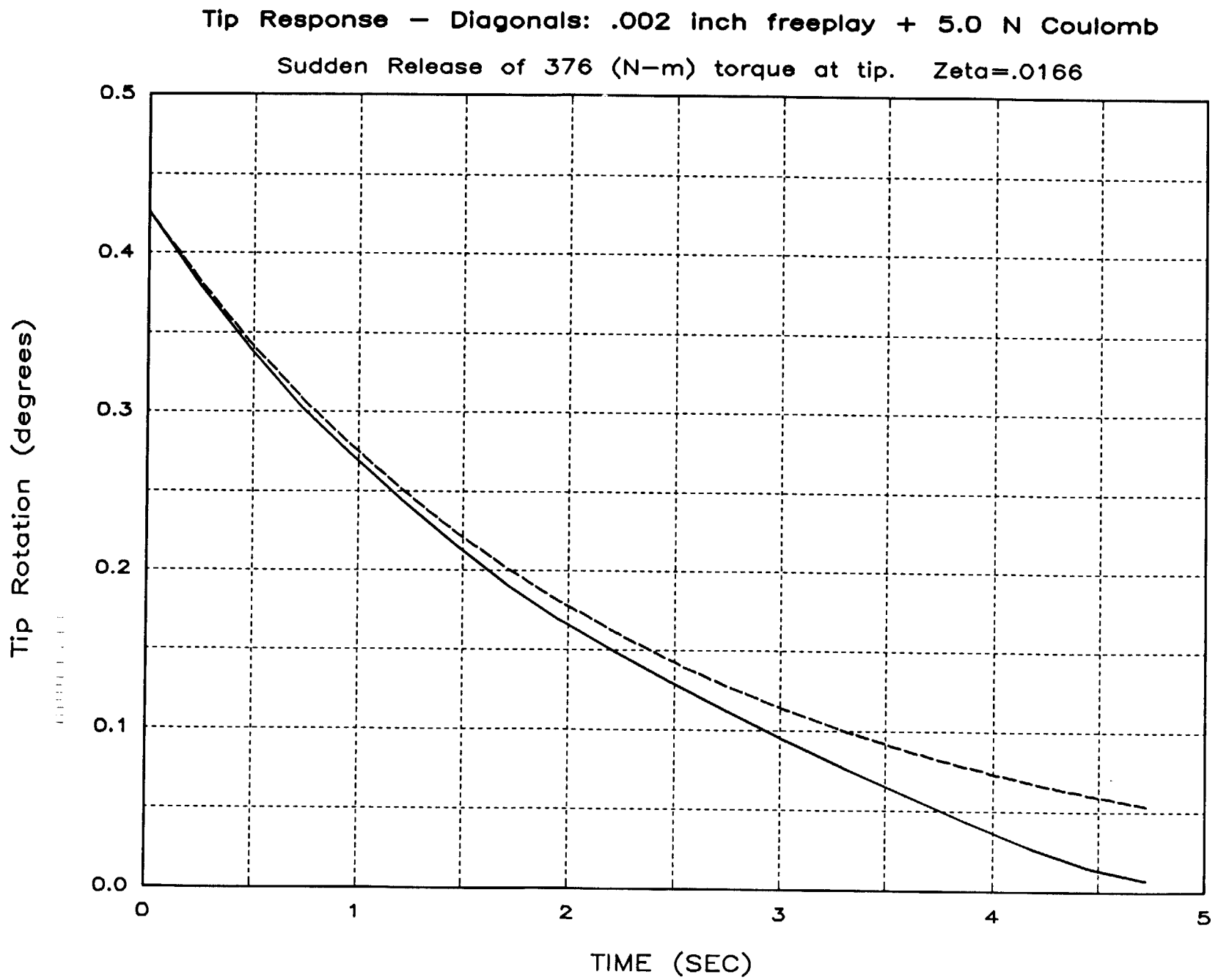
Tip Response – Diagonals: .002 inch freeplay + 5.0 N Coulomb
Sudden Release of 376 (N–m) torque at tip. Zeta=.0166
Tip Rotation (degrees)
0.5
0.4
0.3
0.2
0.1
0.0
0
1
2
3
4
5
TIME (SEC)

Figure 3-11

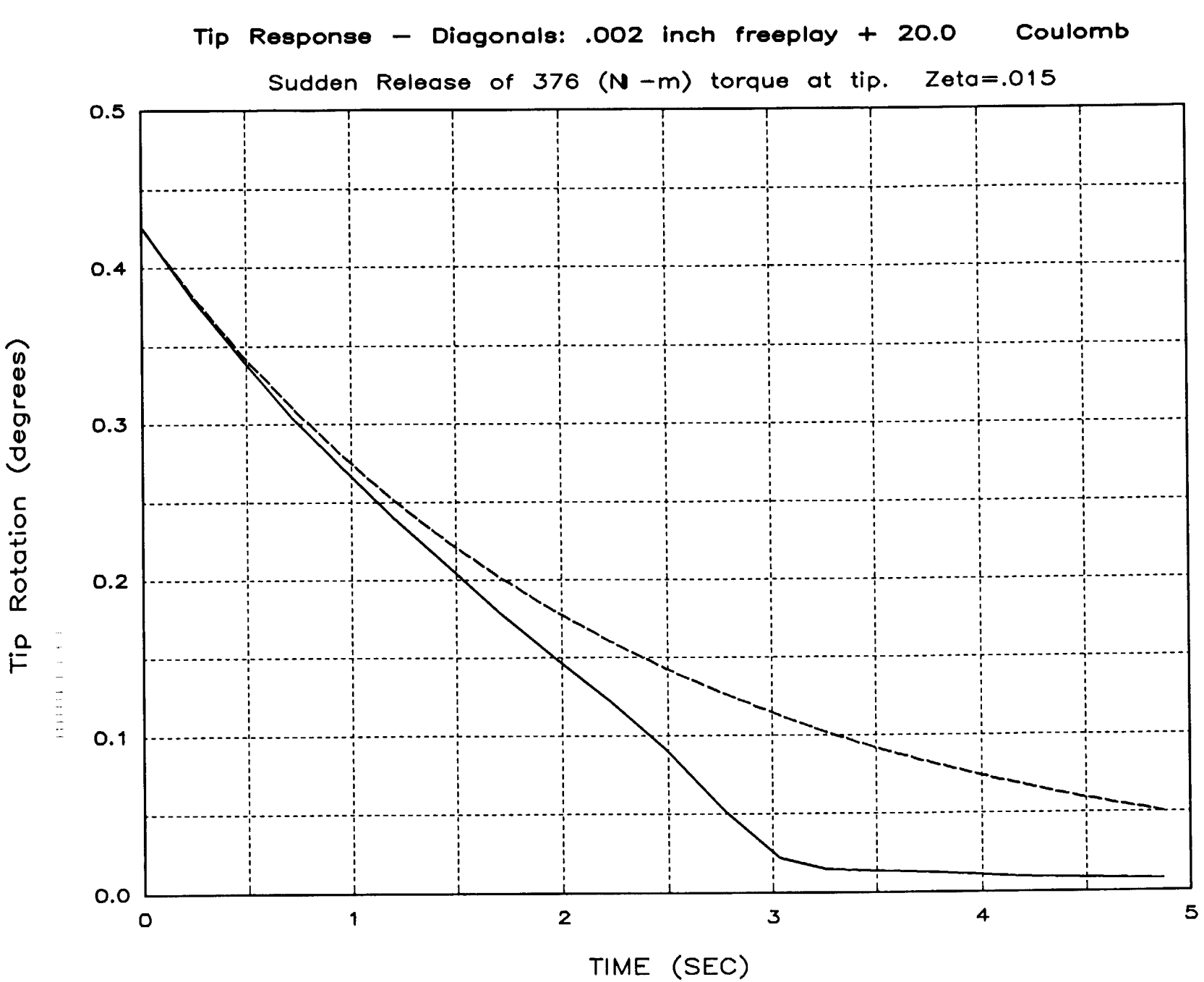
Tip Response — Diagonals: .002 inch freeplay + 20.0 Coulomb
Sudden Release of 376 (N -m) torque at tip. Zeta=.015
Tip Rotation (degrees)
0.5
0.4
0.3
0.2
0.1
0.0
0
1
2
3
4
5
TIME (SEC)

Figure 3-12

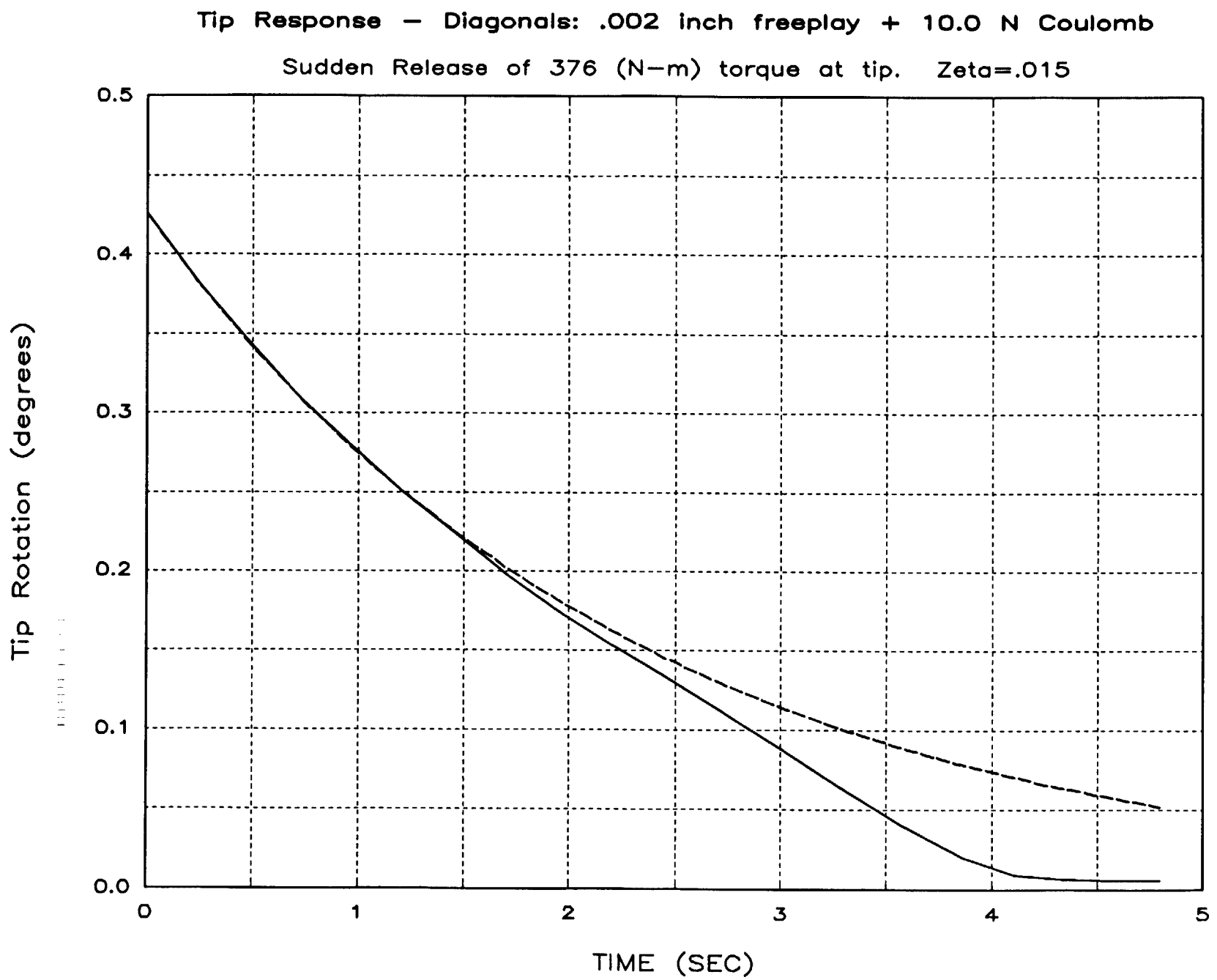
Tip Response — Diagonals: .002 inch freeplay + 10.0 N Coulomb
Sudden Release of 376 (N—m) torque at tip. Zeta=.015
Tip Rotation (degrees)
0.5
0.4
0.3
0.2
0.1
0.0
0
1
2
3
4
5
TIME (SEC)

Figure 3-13

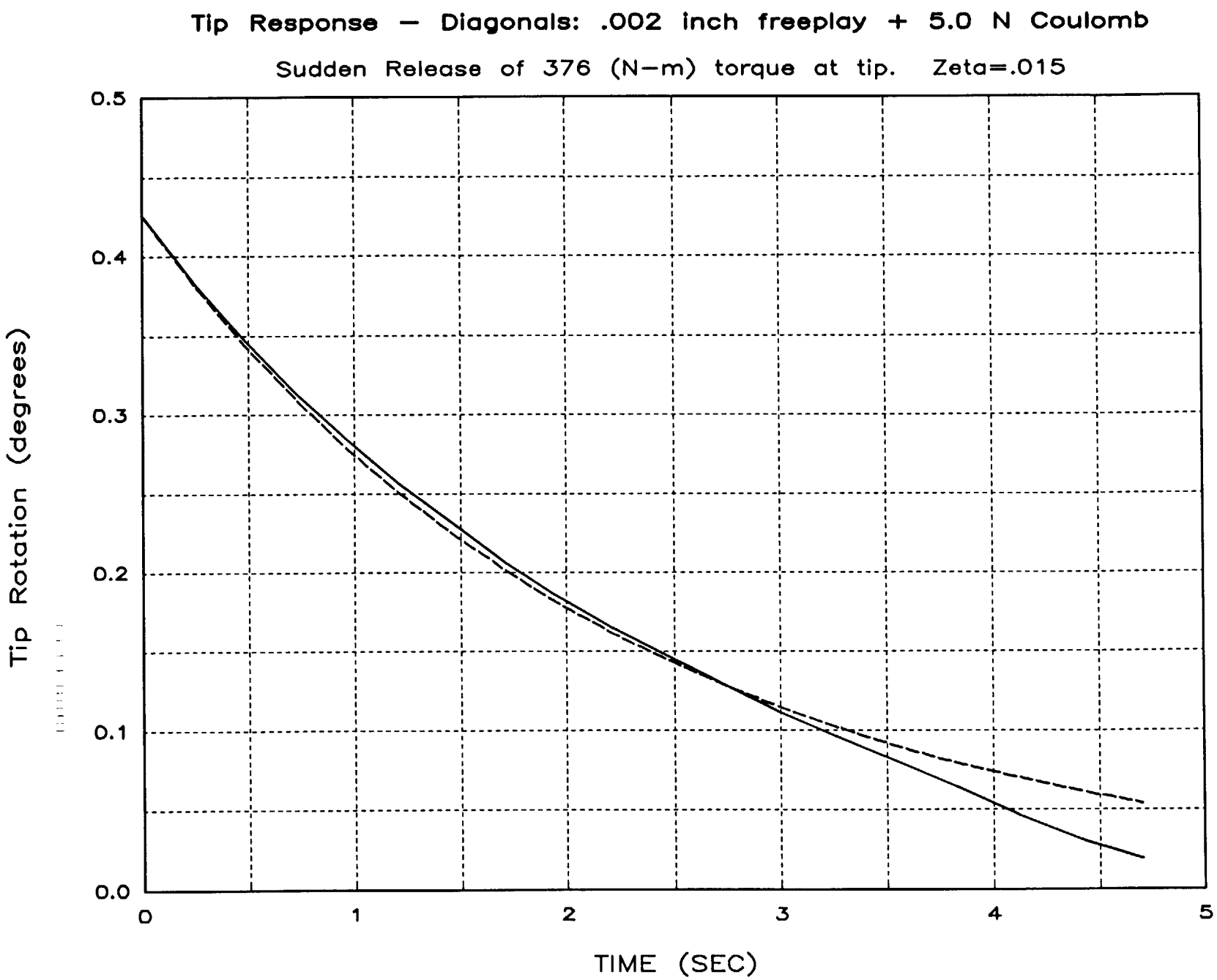
Tip Response — Diagonals: .002 inch freeplay + 5.0 N Coulomb
Sudden Release of 376 (N−m) torque at tip. Zeta=.015
Tip Rotation (degrees)
0.5
0.4
0.3
0.2
0.1
0.0
0
1
2
3
4
5
TIME (SEC)

Figure 3-14

4.0 MINI-MAST MODELING

This section is provided to document the models or input decks used in the nonlinear analysis of the Mini-Mast truss.

The modeling effort is a straight forward task composed of four parts. The first task is to preload the Mini-Mast with the gravitational loads in order to obtain the differential stiffening. This task was previously conducted by NASA personnel and they supplied a model to Boeing. The second task is to conduct a normal modes analysis of the prestiffened structure. Again this analysis was previously conducted by NASA personnel and they supplied a model to Boeing. Only minor changes to the original models were required. These changes are discussed in section 4.1.

The third task is to process NASTRAN Output2 formatted data generated through a DMAP alter and to conduct some preliminary manipulation of this data. Finally in the fourth task the transient analysis of the truss is conducted using the Residual Force Technique (RFT). Tasks 3 and 4 are discussed in section 4.2 and 4.3, respectively.

4.1 NASTRAN Modeling

The Mini-Mast NASTRAN model delivered by NASA /LaRC is a precise model for a truss whose joints and structural members are modeled with beam elements called CBAR's. In addition to axial and torsion supported by CROD elements, the CBAR elements support bending.

The NASTRAN bulk data deck received from LaRC was modified in order to take advantage of existing post-processing programs within the Boeing Company. DYNASTY was developed by the principal investigator to pre- and post-process NASTRAN data and to perform a variety of matrix algebraic operations. This software and documentation are part of the deliverables to NASA.

Existing programs within DYNASTY can determine the coordinates and element connectivity within a NASTRAN model for CROD elements. CROD elements were therefore superimposed on the diagonal CBAR elements in order to determine the grid and element connectivity within the model. The area of the diagonal CROD elements was set to 1.0E-10 times the area of the original CBAR elements. The axial elements provided a mechanism to use existing software to interface

NASTRAN and DYNASTY and to conduct the nonlinear simulation. The area of the CROD elements was scaled up to their proper value during the nonlinear analysis in DYNASTY.

This use of coincident elements was not attractive but it expedited the analysis. The original CBAR elements could have been used but this would have increased the programming effort. The element stiffness matrices must be obtained in element coordinates. NASTRAN transforms the CBAR element stiffness from element coordinates into global coordinate. Further investigation did not provide any way to obtain the CBAR element stiffness from the NASTRAN database in element coordinates.

A listing of the NASTRAN bulk data deck modified to include the coincident CROD elements is given below. Note that a DMAP alter is included so that the generated NASTRAN model data will be stored in OUTPUT2 format and can be post-processed by the DYNASTY software.

```
NASTRAN
ID VIBRATION ANALYSIS
$
$           MiniMast Model with cable
$
TIME 500
$DIAG 8,14
SOL 63
$
$ ALTER FOR DATABASE OUTPUT
ALTER 963 $
DRMS1,OPG1,OQG1,OES1,OEF1/TPHIG,MPHIG,TQG,MQG,TES,MES,TEF,MEF/$
OUTPUT2   TEF,MEF,,,//-1/V,N,IUNIT=25 $   /V,N,TO2=TO2
ALTER 1159$
DBFETCH  /KELM,,,,/MODEL/PEID//DBSET3 $
OUTPUT2   ,,KELM,,//0/IUNIT $
OUTPUT2  GPL,BGPDT,USET,UGVS,LAMA//0/IUNIT $
CEND
$
$     CASE CONTROL
$
$SET 1 =1112 thru 1219
SET 1 =all
DISPLACEMENTS(PLOT)=ALL
ELFORCES(PLOT)=1
TITLE = MINIMAST
SUBTITLE = SOL 63 VIBRATION ANALYSIS
ECHO = SORT
SEKR = ALL
SEMR = ALL

METHOD = 1
temp = 2
```

```
SPC = 1
$
$ BULK DATA DECK FOLLOWS
$
BEGIN BULK
eigrL,1,,,150
param,autospc,yes
PARAM,GRDPNT,0
PARAM,DBDICT,2
PARAM,MAXRATIO,1.0E10
PARAM,COUPMASS,1
GRAV,100,,9.8146,0.,0.,-1.
MAT1   *              1  .124000000E12                .350          MAT1
*MAT1        .102610000E+04   .000000000E+00   .000000000E+00   .000000000E+00 MAT2
*MAT2        .000000000E+00   .000000000E+00   .000000000E+00
.
.
.
$       thermal expansion coefficient added to cable properties
$       as mechanism for applying load during normal modes analysis
mat1,4,5.515e10,,.3,7.8334e3,4.557e-5,100.
GRID   *              1                .000000000E+00  .700000000E+00 GR1
*GR1       -.140000000E-01
GRID   *              2                .606200000E+00 -.350000000E+00 GR2
*GR2       -.140000000E-01
GRID   *              3                -.606200000E+00 -.350000000E+00 GR3
*GR3       -.140000000E-01
spc1,1,12345,331,332,333
CBAR         1      1      7     16    1.00     .00     .00
CBAR         2      1     25     34    1.00     .00     .00
CBAR         3      1     43     52    1.00     .00     .00
CBAR       112      3      8     13    -.87     .50     .00
CBAR       113      3     13     17    -.87     .50     .00
CBAR       114      3     26     31     .87    -.50     .00
.
.
.
prod,10,4,6.195e-6
PBAR   *              1              1  .146107622E-03  .575344413E-08 PB1
*PB1       .575344413E-08   .115068883E-07   .000000000E+00                 PB2
*PB2                                                    PB3
*PB3                                                    PB4
*PB4         .100000000E+01   .100000000E+01   .000000000E+00
$$$$$$$$$$$$$$$$$$$$$$$$$$$$$$$$$$$$$$$$$$$$
$$$$$$   added crods for residual force   $$$
$$$$$$$$$$$$$$$$$$$$$$$$$$$$$$$$$$$$$$$$$$$$
crod       1112     13      8     13
crod       1113     13     13     17
crod       1114     13     26     31
crod       1217     13    303    309
crod       1218     13    318    321
crod       1219     13    321    327
ENDDATA
```

4.2 Nonlinear Model Preparation

Data generated from the NASTRAN run must be processed in preparation to the nonlinear transient analyses. NASTRAN OUTPUT2 data is read and placed into a DYNASTY database. A matrix of modes describing the relative displacement of the diagonal members required for the nonlinear analyses is also generated. The following listing is a copy of the actual code. The liberal use of comment statements throughout the input deck make it self-explanatory. The DYNASTY manual contains documentation on the language syntax and program operations.

```
!!!!!!!!!!!!!!!!!!!!!!!!!!!!!!!!!!!!!!!!!!!!!!!!!!!!!!!!!!!!!!!!!!
!!!!!!!!!!!!!INITIALIZATION !!!!!!!!!!!!!!!!!!!!!!!!!!!!!!!!!!!!!!
!!!!!!!!!!!!!!!!!!!!!!!!!!!!!!!!!!!!!!!!!!!!!!!!!!!!!!!!!!!!!!!!!!
!
!      Section I (Initialization) This section defines the program name,
!      and opens the NASTRAN Output2 file, a scratch file, and the
!      output DYNASTY file.
!

*ZSPACE 500000 ! allocates work space
!
!
*DEFINE !  Define symbols to be used throughout the job.
 NAME= MMNEW ! PROBLEM NAME
*END
!
!
*FILE
   20=[-.NAST]"NAME".NBF,OLD,DB=NASTRAN !  The Nastran file mmnew.nbf is an output2 file
  31=SCRATCH
  25="NAME"INI.DYN,NEW ! DYNASTY database file
*END


!!!!!!!!!!!!!!!!!!!!!!!!!!!!!!!!!!!!!!!!!!!!!!!!!!!!!!!!!!!!!!!!!!
!!!!!!!!!!! INPUT ELEMENT NUMBERS !!!!!!!!!!!!!!!!!!!!!!!!!!!!!!!!
!!!!!!!!!!!!!!!!!!!!!!!!!!!!!!!!!!!!!!!!!!!!!!!!!!!!!!!!!!!!!!!!!!
!
!      Section II (Node Numbering) This subtask is to read the internal
!      and external node numbering from the NASTRAN output.


*NASTEF
% NASOUT=20
 INTERNAL_EID = [31 INTERNAL_EID]
 MEF_RID = [31 MEF_RID]
*END
!!!!!!!!!!!!!!!!!!!!!!!!!!!!!!!!!!!!!!!!!!!!!!!!!!!!!!!!!!!!!!!!!!
!!!!!!!!!! DEFINE NONLINEAR ELEMENT NUMBERS !!!!!!!!!!!!!!!!!!!!
!!!!!!!!!!!!!!!!!!!!!!!!!!!!!!!!!!!!!!!!!!!!!!!!!!!!!!!!!!!!!!!!!!
```

```
!
!       Section III (Element Definition) This subtask defines the nonlinear
!       element numbers.  The numbers are identical to those used in the
!      NASTRAN bulk data deck.
*FETCH NONLINEAR ELEMENT NUMBERS
  [25 NL_EID] = INTERNAL_EID(RID=1112 THRU 1219;)
*END
!!!!!!!!!!!!!!!!!!!!!!!!!!!!!!!!!!!!!!!!!!!!!!!!!!!!!!!!!!!!!!!!!!!!!!!
!!!!!!!!!!!GET ELEMENT FORCE MATRIX !!!!!!!!!!!!!!!!!!!!!!!!!!!!!!!!!!!!
!!!!!!!!!!!!!!!!!!!!!!!!!!!!!!!!!!!!!!!!!!!!!!!!!!!!!!!!!!!!!!!!!!!!!!!
!
!       Section IV (Element Force Matrix) This section gets the linear
!       element forces per unit mode displacement for the elements
!      defined in section III.

*FETCH MODAL ELEMENT FORCES
  [31 DMEF]=[20 MEF(RID = MEF_RID;)](RID=[25 NL_EID];)
*END

!!!!!!!!!!!!!!!!!!!!!!!!!!!!!!!!!!!!!!!!!!!!!!!!!!!!!!!!!!!!!!!!!!!!!!!
!!!!!!!!!!GET  ELEMENT  stiffness!!!!!!!!!!!!!!!!!!!!!!!!!!!!!!!!!!!!!!
!!!!!!!!!!!!!!!!!!!!!!!!!!!!!!!!!!!!!!!!!!!!!!!!!!!!!!!!!!!!!!!!!!!!!!!
!
!       Section V (Element Stiffness) This section gets the element
!       stiffness of the nonlinear elements defined in section III.
!        Notice that the element stiffness are corrected to their true
!       value.  Recall that the Nastran model use 10^-10 of the actual
!      for the superimposed CROD elements.
!
*CALC ELEMENT STIFFNESS
 [31  ESTIF]=(1.e10)[20  KELM]
*END
*CALC ELEMENT STIFFNESS
 [25 ESTIF]=[20 KELM(;CID=INTERNAL_EID<RID>)](1;CID=[25 NL_EID]<RID>)<T>
*END


!!!!!!!!!!!!!!!!!!!!!!!!!!!!!!!!!!!!!!!!!!!!!!!!!!!!!!!!!!!!!!!!!!!!!!!
!!!!!!!!!!!!GET DEGREES OF FREEDOM!!!!!!!!!!!!!!!!!!!!!!!!!!!!!!!!!!!!!
!!!!!!!!!!!!!!!!!!!!!!!!!!!!!!!!!!!!!!!!!!!!!!!!!!!!!!!!!!!!!!!!!!!!!!!
!
!       Section VII (Uset DOF) This setion gets the G-set and the A-set
!       degrees of freedom.
!
! Determine G-Set degrees of freedom
!
*NASSET GSET COORDS
%   NASOUT=20,  SET='G',
   COORD = [25 GSET_COORD]
*END
!
```

```
! Determine A-Set degrees of freedom
!
*NASSET ASET COORDS
%  NASOUT=20,   SET='A'
  COORD = [25 ASET_COORD]
*END


!!!!!!!!!!!!!!!!!!!!!!!!!!!!!!!!!!!!!!!!!!!!!!!!!!!!!!!!!!!!!!!!!!!!
!!!!!!!!!!! CALCULATE THETA !!!!!!!!!!!!!!!!!!!!!!!!!!!!!!!!!!!!!!!!!
!!!!!!!!!!!!!!!!!!!!!!!!!!!!!!!!!!!!!!!!!!!!!!!!!!!!!!!!!!!!!!!!!!!!
!
!      Section VIII (Calculate THETA) This section constructs the generalized
!       coordinate to element coordinate transformation matrix (THETA) for the
!      elements defined in section III.  This is used to transform the modal amplitudes
!       into element deformations and to transform element nonlinear loads into
!      modal nonlinear loads.

*FETCH PHI FOR FORCE
[25 PHIA] =[20 UGVS(RID=GSET_COORD<CID>;)](RID=ASET_COORD<CID>;)
*CALC MODAL ELEMENT DISPLACEMENTS
 [25 THETA] =  [25 ESTIF]<-1,D>* [31 DMEF]
*END

!!!!!!!!!!!!!!!!!!!!!!!!!!!!!!!!!!!!!!!!!!!!!!!!!!!!!!!!!!!!!!!!!!!!
!!!!!!!!!!GET GENERALIZED STIFFNESS !!!!!!!!!!!!!!!!!!!!!!!!!!!!!!
!!!!!!!!!!!!!!!!!!!!!!!!!!!!!!!!!!!!!!!!!!!!!!!!!!!!!!!!!!!!!!!!!!!!
!
!      Section VI (Generalized Stiffness) This section gets the generalized
!       stiffness matrix.
!
*RDLAMA LAMDA
% NASOUT=20
 EIGENVALUES = [25 OMEGS]
 RADIAN_FREQ = [25 RAD_FREQ]
*END

!!!!!!!!!!!!!!!!!!!!!!!!!!!!!!!!!!!!!!!!!!!!!!!!!!!!!!!!!!!!!!!!!!!!
!!!!!!!!!!CREATE DAMPING MATRIX!!!!!!!!!!!!!!!!!!!!!!!!!!!!!!!!!!!!!!
!!!!!!!!!!!!!!!!!!!!!!!!!!!!!!!!!!!!!!!!!!!!!!!!!!!!!!!!!!!!!!!!!!!!

*CALC DAMP
 [25 DAMP]=(.04)RAD_FREQ

*STOP
```

4.3 Nonlinear Transient Analysis of the Minimast

The program in section 4.2 creates a database which contains all the information from the NASTRAN structural model required for the nonlinear analysis. The database is accessed by the following program which actually conducts the nonlinear simulation.

```
*ZSPACE 500000 ! Allocates work space memory.

! Define assigns values to several variables which are frequently changed during the
! analysis.

*DEFINE
 name= gap
 x1 = 12.0
 x2 = 60.0
 nm =13          ! number of modes
 ts=0.0          ! start time
 tf=5.0          ! final time
 dt=.001         !output interval
 ntstep=1        !number of time steps per output interval
 iterat=3        !max number of interations in each time step
 nmem=54         !max number of members
*END

! Open both existing and new databases


*FILE  ! Open database files
 in_file =25,model_small.dyn,old
 outfile =26,"name"_out.dyn,new
 scr     =30,scratch
 qddfile =31,"name"_qdd.dyn,new
 gf_file =32,gforce.dyn,new
 qfile   =33,"name"_q.dyn,new
 tipfile =41,"name"_x.dyn,new
 35 = phi_tip.dyn,old
*END
!
! Executes the subroutine Load.
! Assign the residual force parameters such as gap size,damping strengths, etc.
!
*LOAD("in_file","outfile")
```

```
! Zord is the nonlinear integrator used to determine nonlinear response.
!
!
*ZORD NONLINEAR
% TS="TS"            !START TIME
% TF="TF"            !FINAL TIME
% DT="DT"            !OUTPUT INTERVAL
% NTSTEP="NTSTEP"    !TIME STEPS PER OUTPUT INTERVAL
% ITERAT="ITERAT"    !MAX NUMBER OF INTERATIONS IN EACH TIME STEP
% NM =-"NM"
!
! Input data
!
 OMEGS=["in_file" OMEGS]
 DAMP= ["in_file" DAMP_test]
!
! Calculate generalized force
!
 GFORCE=["gf_file" gforce] = ["in_file" PHIA]([26 FORCE]<RID>;1 thru "nm")<T>
                                                    *[26 FORCE]

!
! Output data
!
 QDD=["qddfile" QDD]
 Q= ["qfile" Q]
!
*END

!postprocess the results of the simulation


*PUTS(MAXMIN,'[EF_MAXMIN]',"OUTFILE","NMEM",2,"NMEM",EFMAX)
*PUTMPC tip rotation
% KIND = 1,MAXSIZE=100,NUMEQ=1
 OUTPUT = ["scr" PLOT_EQ]
*END
101,5  -.481,3281   .24,3291  .416,3292  .24,3301  -.416,3302
*CALC
 ["scr" phi_x]= PLOT_EQ<T> * ["in_file" phia % size=0,-"nm"]
*CALC
 ["tipfile" tip]= Phi_x * ["qfile" q]
!*calc
! ["tipfile" tip]= [35 Phi_tip % size=0,-"nm"] * ["qfile" q]
```

```
*PLOT2D Tip Rotation
% TITLE = 'Tip Response : .001 inch freeplay + random Coulomb ("x1" "x2")',
%       ' Sudden Release of 376 (Nt-m) torque at tip'
% FILE  = 'tip.P2D',
% YTITLE= 'Tip Rotation (degrees)'
% XTITLE= 'TIME (SEC)'
  YDATA= (57.2958) ["tipfile" tip]
*PLOT2D Mode Amplitudes
% TITLE='Modal Response : .001 inch freeplay + random Nt Coulomb ("x1" "x2")',
%       ' Sudden Release of 376 (Nt-m) torque at tip'
% FILE  = 'q.P2D',
% YTITLE= 'MODE 1','MODE 2', 'MODE 3','MODE 4','MODE 5'
% XTITLE= 'TIME (SEC)'
  YDATA= ["qfile" q]
*STOP
*FORTRAN load.FOR
```

A listing of LOAD.FOR follows:

```
      SUBROUTINE LOAD(ntape,nout)
       COMMON/THETA/NR,NC,THETA("NMEM","NM")   !DSET PHI
      COMMON/GAP/GAP("NMEM")                   !LINK GAP
      COMMON/VIS/VIS("NMEM")                    !LINK VISCOUS DAMPING CONSTANT
      COMMON/JVIS/JVIS("NMEM")                  !JOINT VISCOUS DAMPING CONSTANT
      COMMON/COU/COU("NMEM")                    !LINK MAX FRICTION FORCE
      COMMON/ESTIF/ESTIF("NMEM")                !ELEMENT STIFFNESS

     NR = 0
      MID_THETA=0
        CALL GETS(MID_THETA,'[THETA]',ntape,NR,-"NM","NMEM",THETA)
     NC = "NM"
!
!GET  ELEMENT  STIFFNESSES
     MID_ESTIF=0
          CALL GETSV(MID_ESTIF,'[ESTIF]',ntape,NR,ESTIF)
       do 5 i=1,nr
         estif(i)=estif(i) * 1.0e+10
 5     continue
C
C      MEMBER GAPS SIZE
C
       DO 10 I=1,NR
        GAP(I)=(25.4E-6)/4.
10       CONTINUE
       MID_GAP=0
         CALL PUTSV(MID_GAP,'[GAP]',nout,NR,GAP)
C
C      FRICTION FORCE LINK
C
       DO 20 I=1,NR
       COU(I)=20.
20       CONTINUE
      MID_CLMB=0
```

```
C
      DO 30 I=1,NR
        VIS(I)=0.0166*ESTIF(I)
30    CONTINUE
      MID_VISCOUS=0
        CALL PUTSV(MID_VISCOUS,'[VISCOUS]',nout,NR,VIS)
      RETURN
      END

       SUBROUTINE NFORCE(nout,title)
       CHARACTER*(*) title
       CHARACTER*80 ANAME
       parameter (nrnf=5,ncnf=4)
       integer LISTR(NRNF)
       real    ZNF(NRNF,NCNF),TIMES(NCNF)
       COMMON/IFORM/IFORM
!
!      USER SUPPLIED TO GENERATE NODAL FORCE HISTORY
!
      LISTR(1)=3281
      LISTR(2)=3291
      LISTR(3)=3292
      LISTR(4)=3301
      LISTR(5)=3302

      DO 10 IC = 1,NCNF
       DO 10 JC=1,NRNF
       IF (IC.Gt.2) then
        ZNF (JC,IC) = 0.0
       ELSE
C        TORQUE= .01 <---<< bills value
         TORQUE= 376. ! gives .4 degrees under static load
        ARM=.7    !    MOMENT ARM
         APPPNTS=3.   ! NUMBER OF APPLICATION POINTS
         IF (JC.EQ.1) ZNF (JC,IC) =    -1.*TORQUE/ARM/APPPNTS
         IF (JC.EQ.2) ZNF (JC,IC) =      .5*TORQUE/ARM/APPPNTS
         IF (JC.EQ.3) ZNF (JC,IC) =   .886*TORQUE/ARM/APPPNTS
         IF (JC.EQ.4) ZNF (JC,IC) =      .5*TORQUE/ARM/APPPNTS
         IF (JC.EQ.5) ZNF (JC,IC) = -.866*TORQUE/ARM/APPPNTS
       ENDIF
10    CONTINUE
       TIMES(1)=0.0
       TIMES(2)="DT"
       TIMES(3)=2*"DT"
       TIMES(4)=100.

      MID=0
      nr=nrnf
      nc=ncnf
       IFORM=-5
         call PUTSK(MID,title,Nout,NR,NC,NR,ZNF,LISTR,times,1,-1)
C
       RETURN
       END
```

```
      SUBROUTINE RHS(NM,Q,QD,QDD,FGNL)
C
C     CALCULATES THE NONLINEAR RESIDUAL FORCE
C
C
      COMMON/THETA/NR,NC,THETA("NMEM","NM")    !DSET PHI
      COMMON/DELX/DELX("NMEM")                  !ELEMENT ELONGATION
      COMMON/DELXD/DELXD("NMEM")                !ELEMENT ELONGATION
      COMMON/DELXDD/DELXDD("NMEM")              !ELEMENT ELONGATION
      COMMON/EF/EF("NMEM")                      !ELEMENT FORCE
      COMMON/EFmax/EFmax("NMEM"),efmin("nmem")
      COMMON/ESTIF/ESTIF("NMEM")               !ELEMENT STIFFNESS

      COMMON/ITERAT/ITERAT,ERR,NTAPE,ICRHS,IFINAL
      COMMON/TSIZE/DT,TS,TF
      COMMON/NTSTEP/NTSTEP,ISTEP
      REAL Q(NM),QD(NM),QDD(NM),FGNL(NM)
      data efmax/"nmem"*0.0/

      CALL CSAB(THETA,Q,DELX,"NMEM",NM,"NMEM",NR,NM,NM,1)
C     CALL CSAB(THETA,QD,DELXD,"NMEM",NM,"NMEM",NR,NM,NM,1)
C     CALL CSAB(THETA,QDD,DELXDD,"NMEM",NM,"NMEM",NR,NM,NM,1)

      DO 10 I=1,NR
        DELU=DELX(I)
C       DELV=DELXD(I)
C       DELA=DELXDD(I)
C       CALL LINKMAP(I,DELU,DELV,DELA,FORCE)
        CALL LINKGAP(I,DELU,FORCE)
        EF(I)=FORCE
        EFMAX(I)=MAX(FORCE,EFMAX(I))
        EFMIN(I)=MIN(FORCE,EFMIN(I))
10    CONTINUE

      CALL CSATB(THETA,EF,FGNL,"NMEM","NMEM",NM,NR,NC,NR,1)

      RETURN
      END
      SUBROUTINE LINKGAP(I,DELU,FORCE)
      COMMON/GAP/GAP("NMEM")                    !ELEMENT GAPS
      COMMON/ESTIF/ESTIF("NMEM")
      COMMON/GAPF/XO("NMEM"),FO("NMEM")
      DATA XO,FO/"NMEM"*0.0,"NMEM"*0.0/
C
C     I=MEMBER
C
      xf="COULOMB"/estif(I)
      if(xf.le.0) then
        if(abs(delu).le.gap(i))then
          force=delu*estif(i)
      else
          force=gap(i)*estif(i)*sign(1.,delu)
      endif
      return
      endif
C
      fmax=estif(I)*gap(I)
      fmin=-fmax
```

```
C
      delta=delu-x0(I)
      if(delta.gt.xf) then
          FORCE=min(estif(I)*(delu-xf),fmax)
        f0(I)=FORCE
         x0(I)=FORCE/estif(I)
      else if(-delta.gt.xf) then
          FORCE=max(estif(I)*(delu+xf),fmin)
        f0(I)=FORCE
         x0(I)=FORCE/estif(I)
     else
        FORCE=f0(I)
     endif

     RETURN
     END
```

5.0 CONCLUDING REMARKS

A new testing technique, referred to as "link" testing, was developed and used to test the Mini-Mast struts. These tests proved valuable for several reasons. First, they characterized the overall stiffness and damping of the Mini-Mast struts directly. Second, they determined the behavior of the struts that could not be predicted from individual joint and element stiffness tests alone. And third, link testing identified a possibly fatal design concept in the design of the collapsible diagonal. The value of link testing for ascertaining both the structural integrity of a deployable truss and its predictability has therefore been demonstrated.

A structural model of the Mini-Mast with diagonal links having free-play and Coulomb friction was constructed and analyzed. The motivation to do so was based partly on the link tests and also on the the observed behavior of the 18 bay Mini-Mast truss in torsion. Results from these analytical studies show that the torsional response of the Mini-Mast is greatly affected by gaps as small as one milli-inch. Comparison of the predicted response of the analytical model to the empirical results taken from the Mini-Mast show good agreement although additional improvement may be obtained with additional testing and system identification. Nevertheless, an improved nonlinear model of the Mini-Mast is obtained and is used to explain several amplitude dependent phenomena demonstrated by the ERA program.

5.0 REFERENCES

1. Chapman,J.M., Shaw, F.H., and Russell, W.C.," Nonlinear Transient Analyses of Joint Dominated Structures," AIAA paper 87-0892 presented at the 28th Structures, Structural Dynamics and Materials Conference, April 9-10,1987 .

2. Crawley, E.F. and Aubert, A.C., "Identification of Nonlinear Structural Elements by Force State Mapping," AIAA paper 84-0992 presented at the 1984 SDM meeting.

3. Chapman, J.M., "A Friction Methodology for Space Shuttle/Payload Transient Loads Analyses," JPL report JPL D-1347, page 543, given at the Proceedings of the Shuttle Payload Dynamic Environments and Loads Prediction Workshop, Jan. 24-26, 1984

4. Allen, B.R., "Force-Deflection Tests of Links From NASA LaRC Mini-Mast Truss", CSA report 89-11-01, November 1989.

5. NASA Langley Research Center, Mini-Mast CSI Testbed, Users's Guide, March 23, 1989.

6. Taylor Jr., Lawrence W. ,"Nonlinear and Distributed Parameter Models of the Mini-Mast," the 3rd NASA/DOD Controls-Structures Interaction Technology Conference, Jan. 30, 1989.

ORIGINAL PAGE
BLACK AND WHITE PHOTOGRAPH

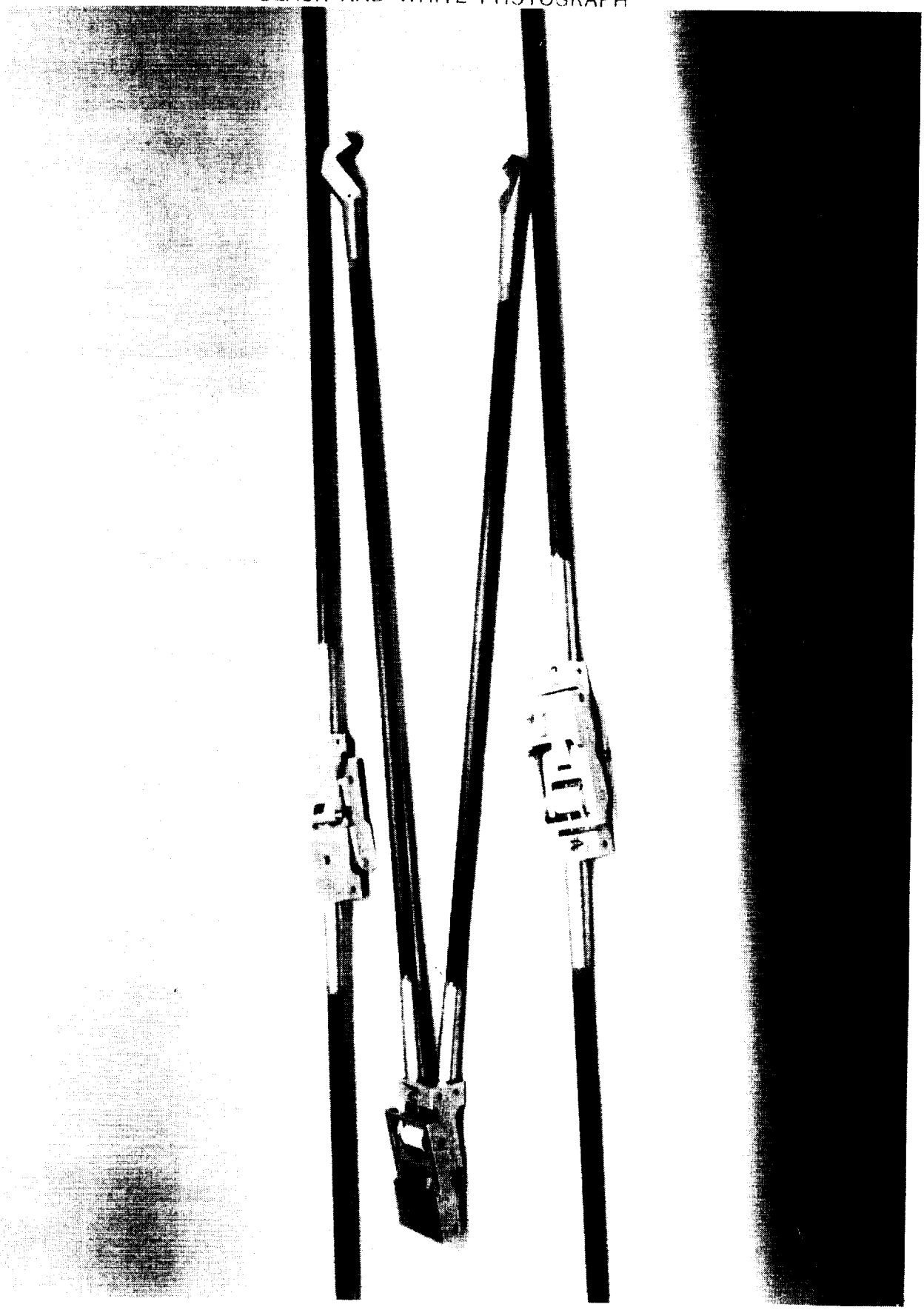

EXCEPTIONAL PAGE
BLACK AND WHITE PHOTOGRAPH

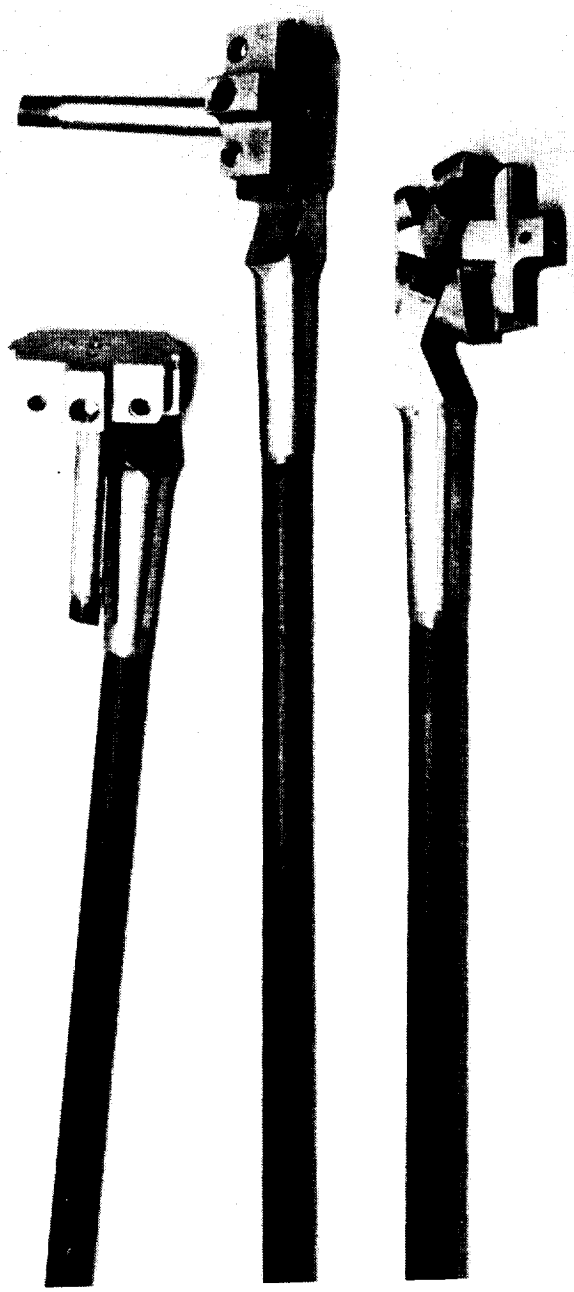

ORIGINAL PAGE
BLACK AND WHITE PHOTOGRAPH

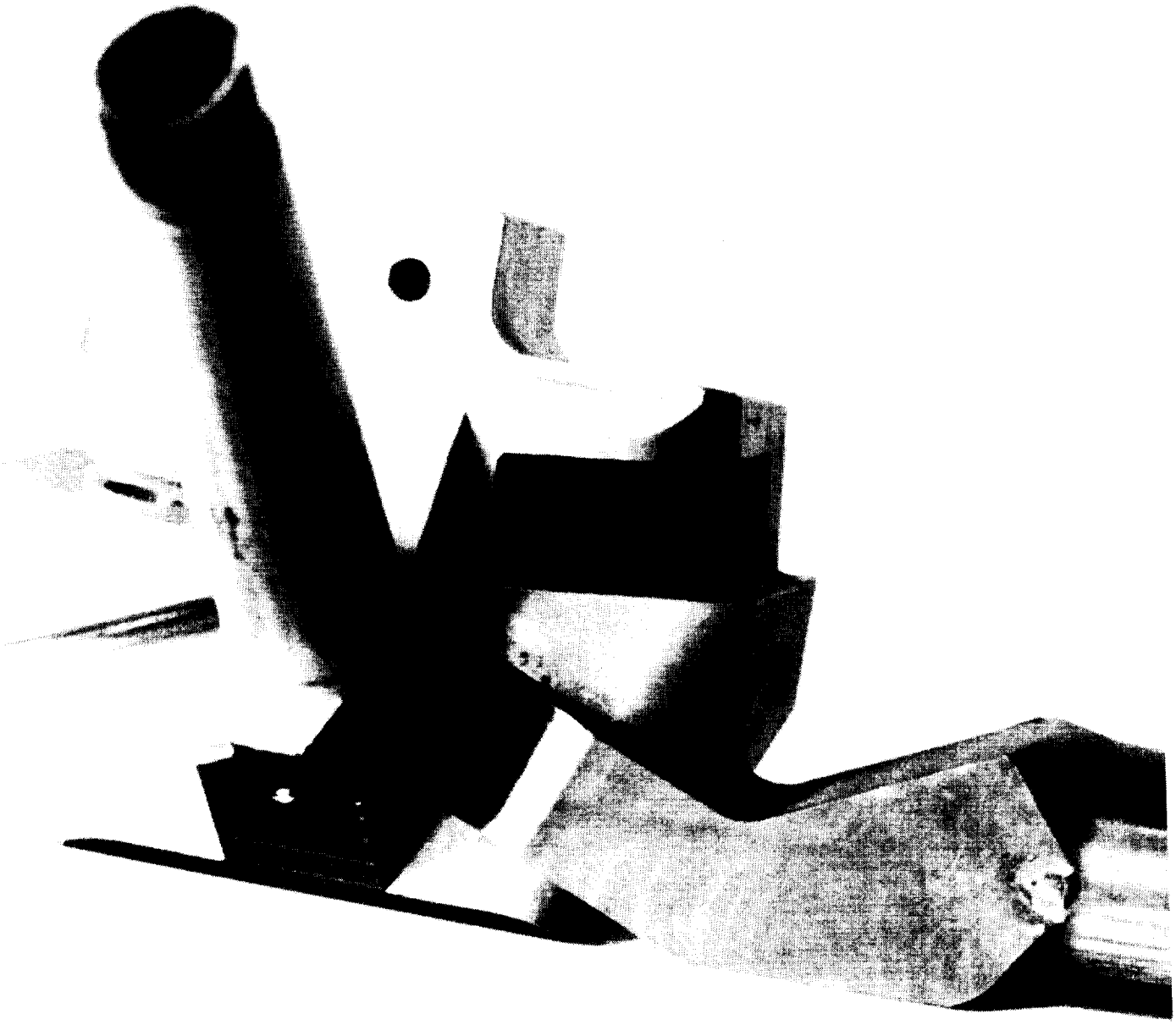

ORIGINAL PAGE
BLACK AND WHITE PHOTOGRAPH

BLACK AND WHITE PHOTOGRAPH

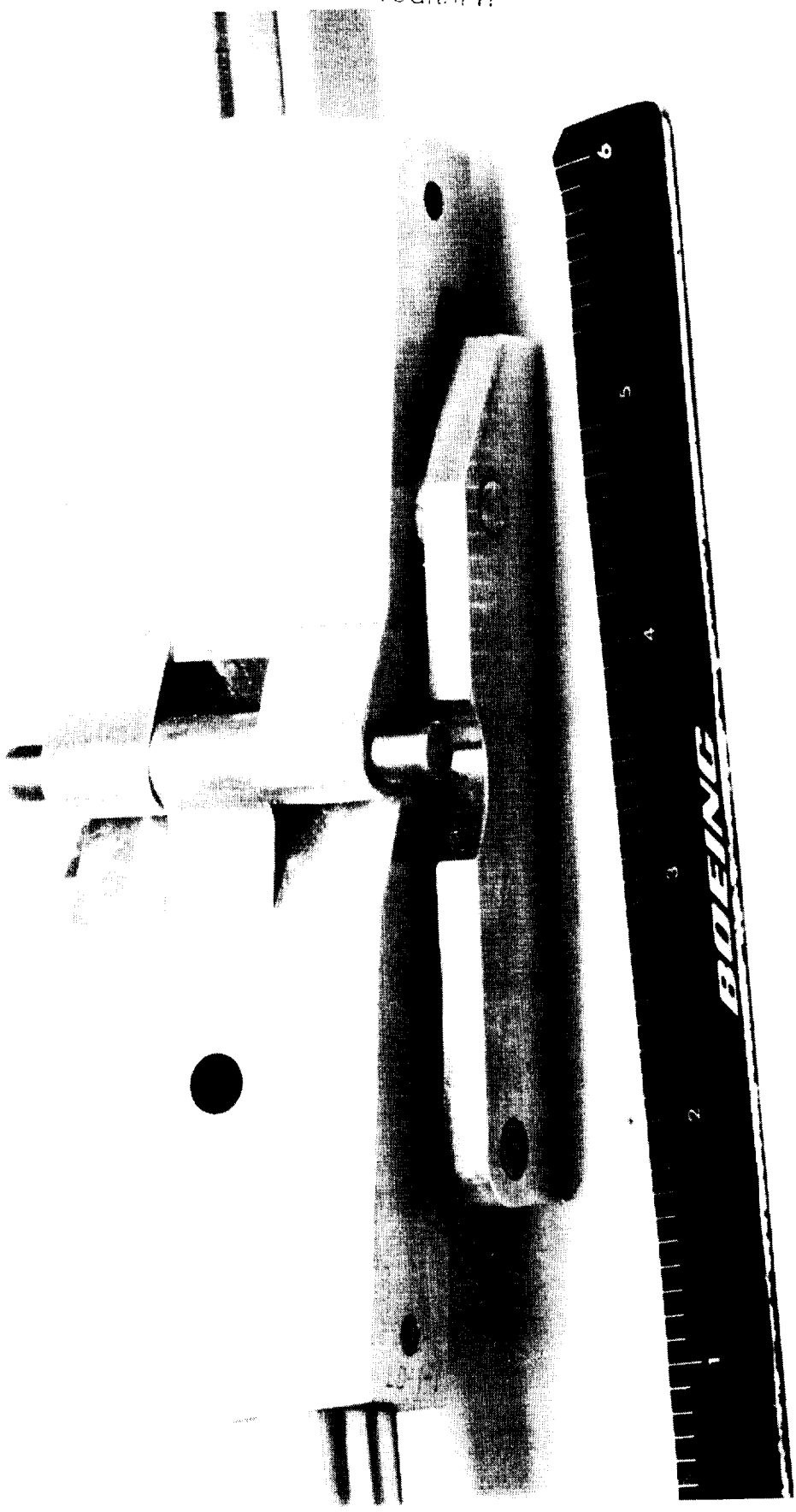

Appendix A

(Taken from Ref. 4 pages 29-91)

PAGE 80 INTENTIONALLY BLANK

PRECEDING PAGE BLANK NOT FILMED

Appendix A
Mini-Mast Diagonal Test Results

PRECEDING PAGE BLANK NOT FILMED

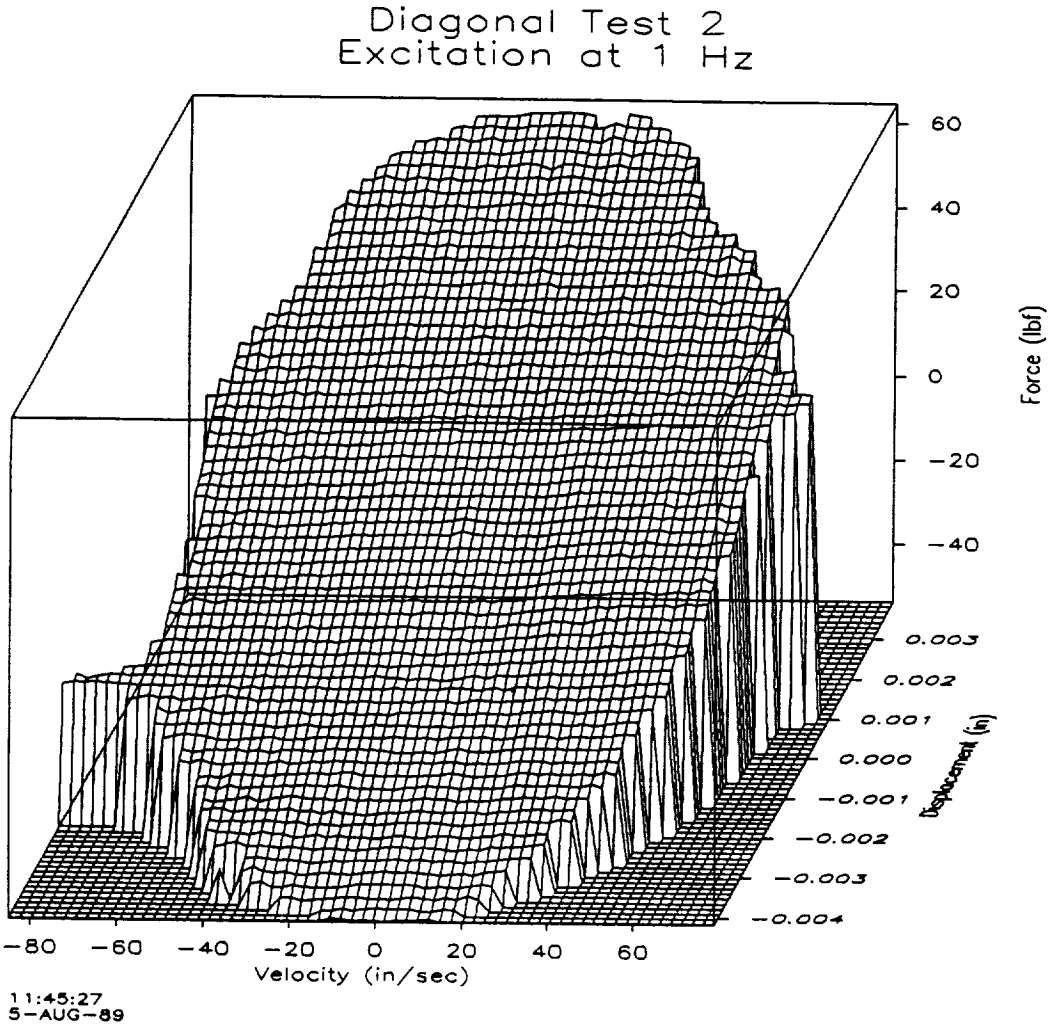
Diagonal Test 2
Excitation at 1 Hz
60
40
20
0
−20
−40
Force (lbf)
0.003
0.002
0.001
0.000
−0.001
−0.002
−0.003
−0.004
Displacement (in)
−80 −60 −40 −20 0 20 40 60
Velocity (in/sec)
11:45:27
5−AUG−89

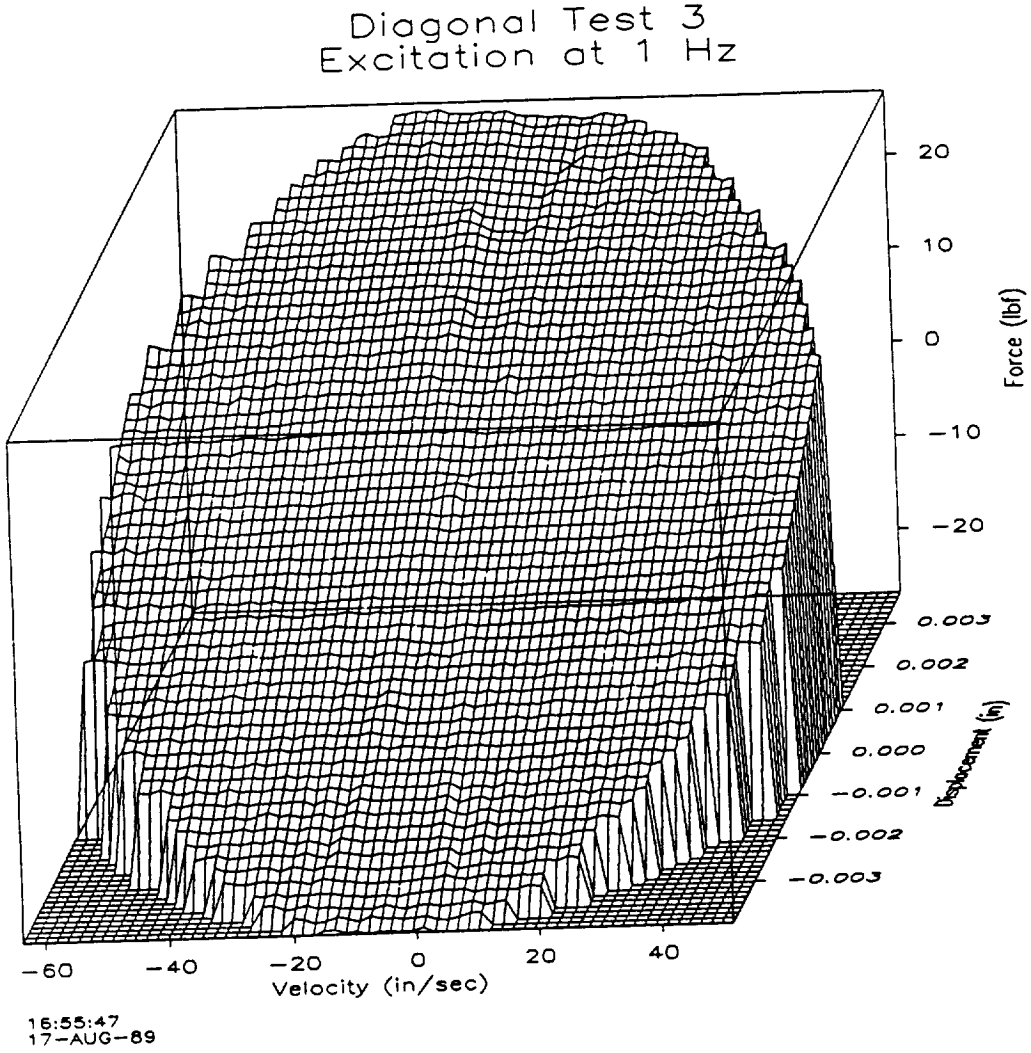
Diagonal Test 3
Excitation at 1 Hz
20
10
0
−10
−20
Force (lbf)
0.003
0.002
0.001
0.000
−0.001
−0.002
−0.003
Displacement (in)
−60
−40
−20
0
20
40
Velocity (in/sec)
16:55:47
17−AUG−89

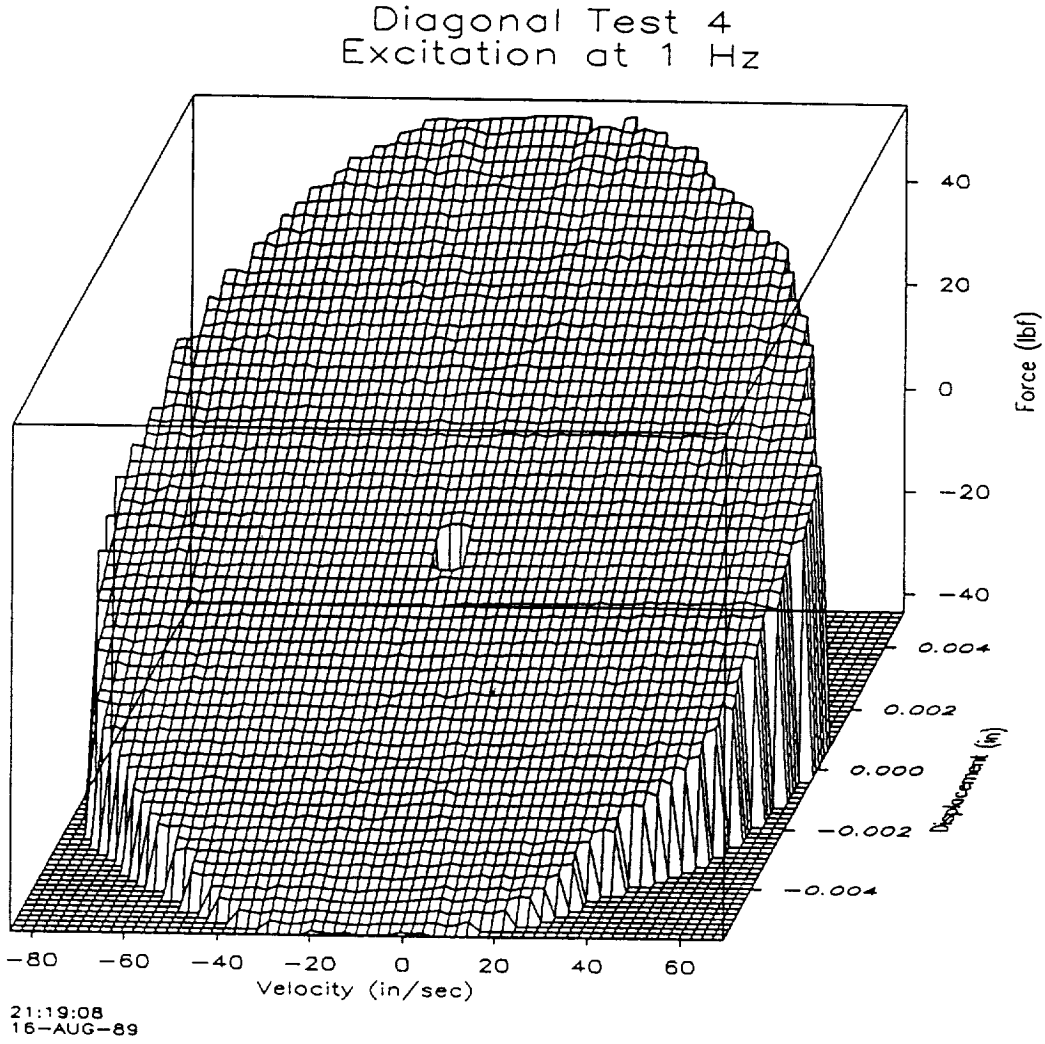
Diagonal Test 4
Excitation at 1 Hz
40
20
0
−20
−40
Force (lbf)
0.004
0.002
0.000
−0.002
−0.004
Displacement (in)
−80
−60
−40
−20
0
20
40
60
Velocity (in/sec)
21:19:08
16−AUG−89

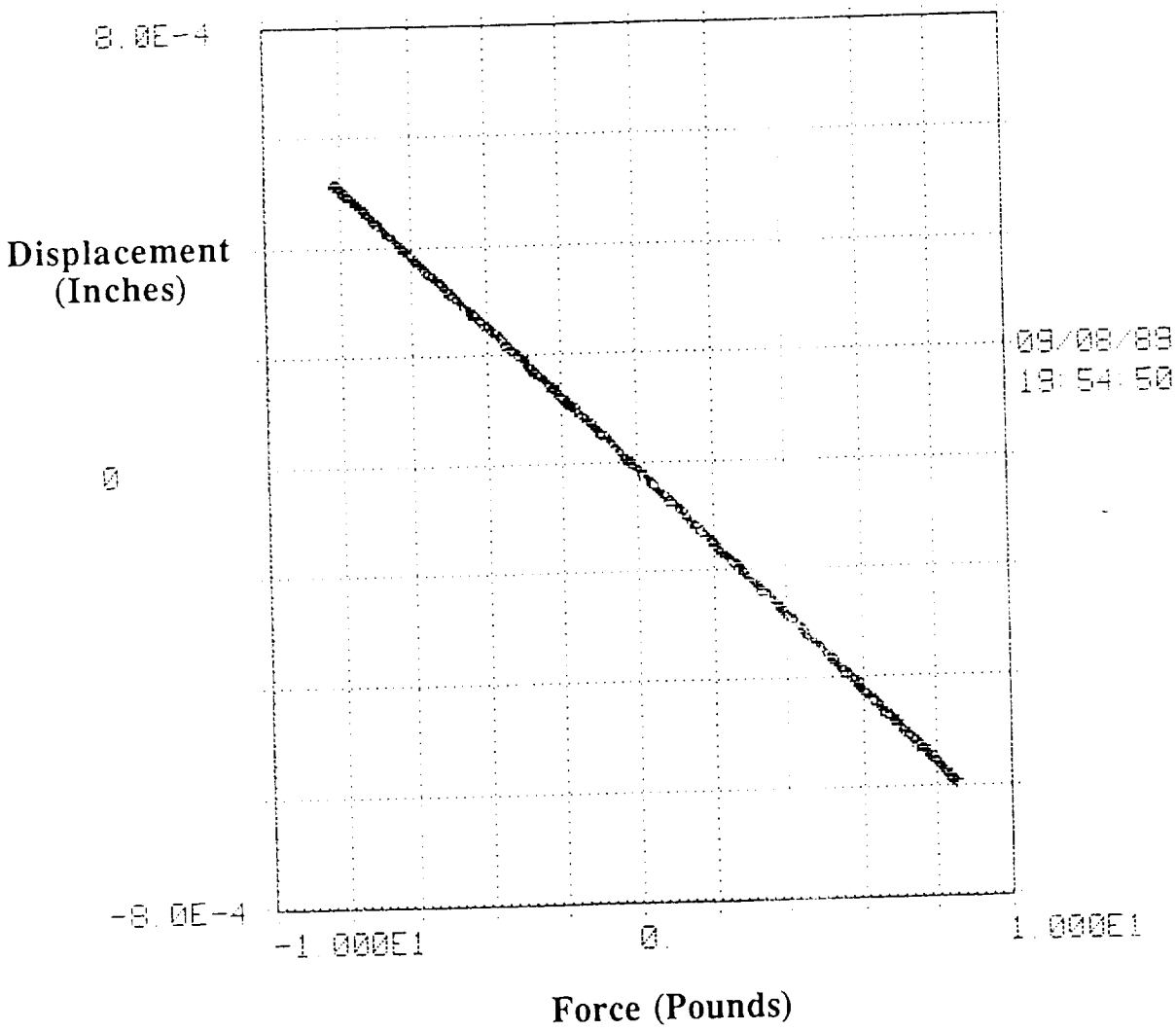

Diagonal test 2, excitation at 1 Hz

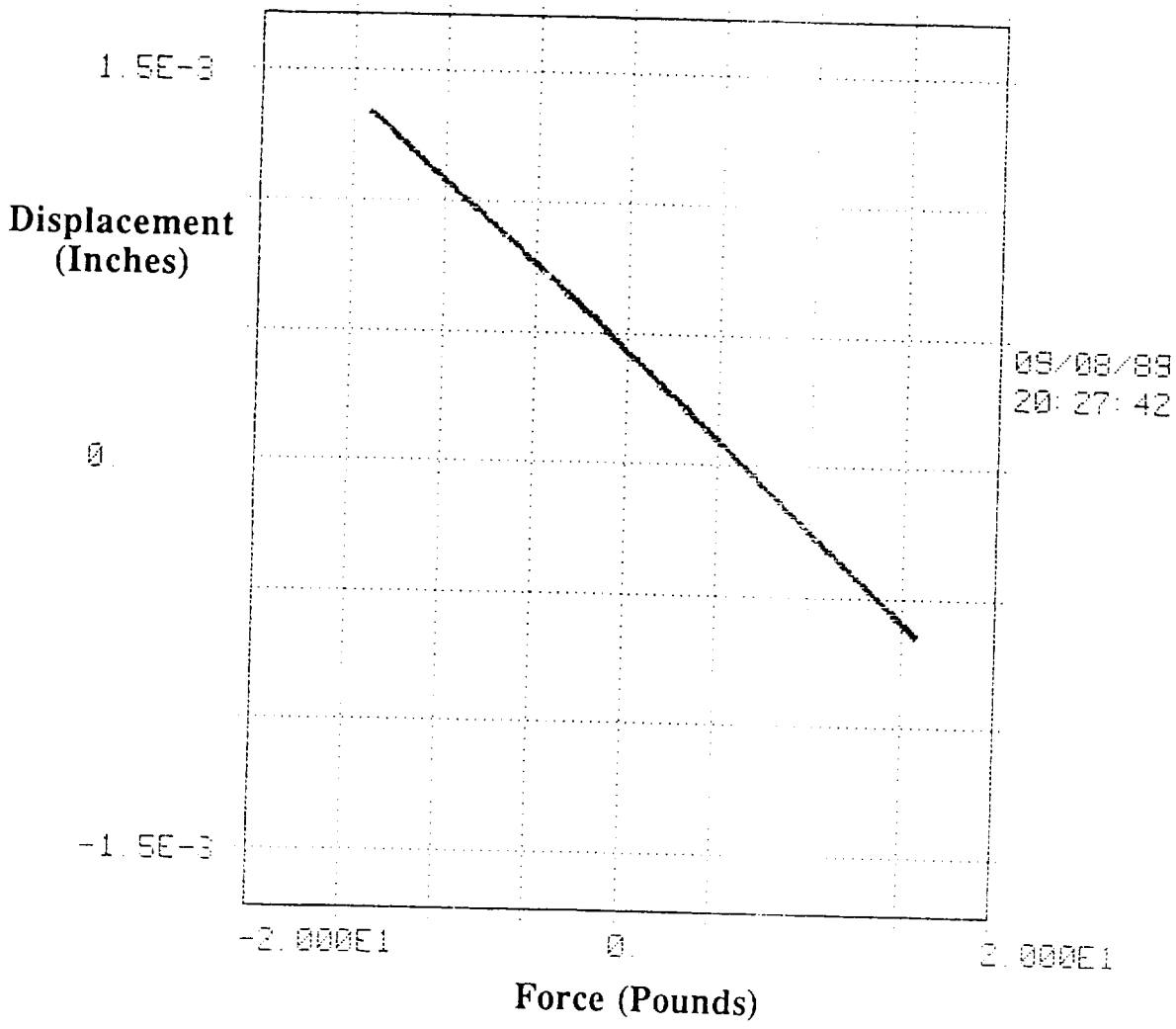

Diagonal test 2, excitation at 1 Hz

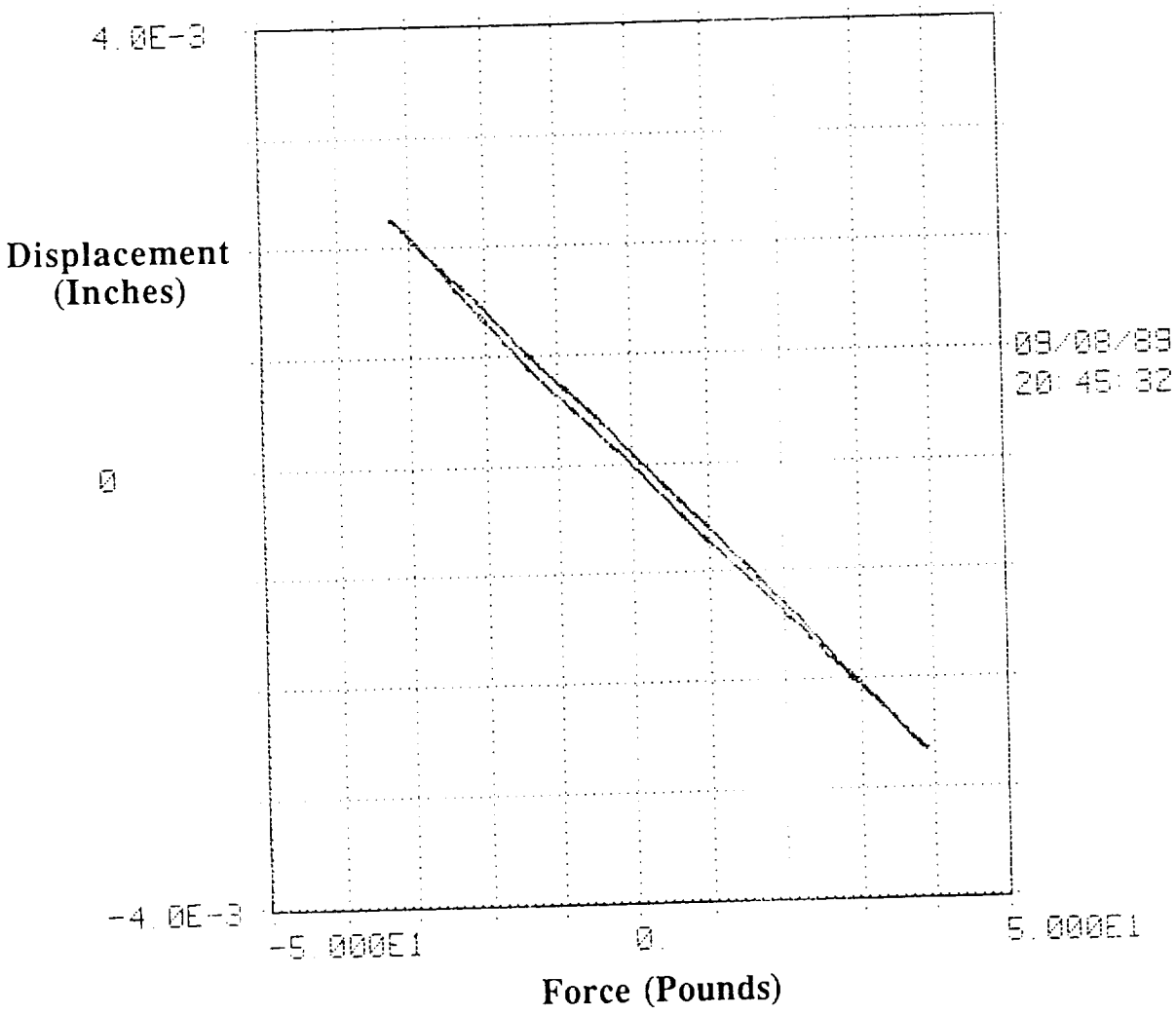

Diagonal test 2, excitation at 1 Hz

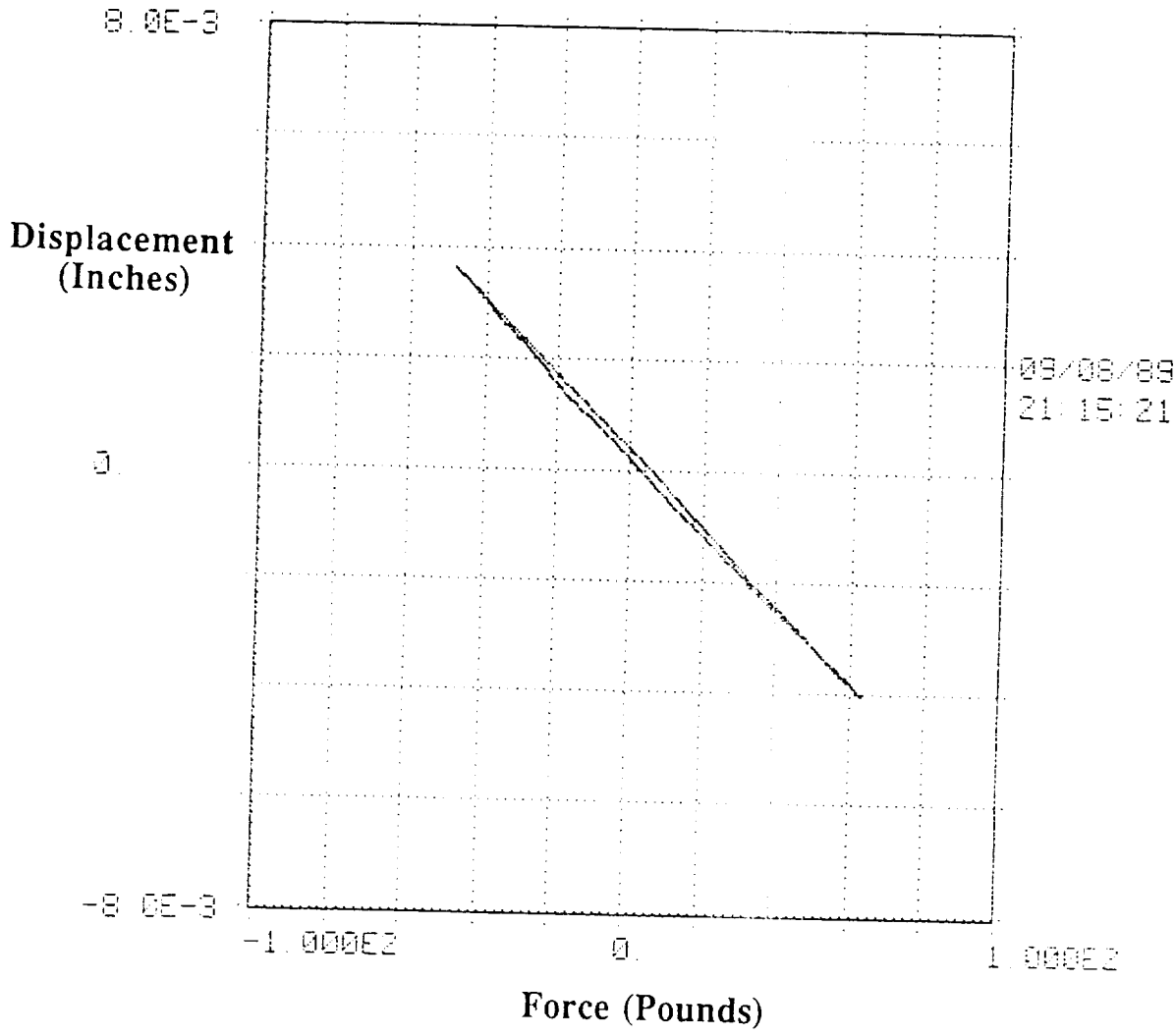

Diagonal test 2, excitation at 1 Hz

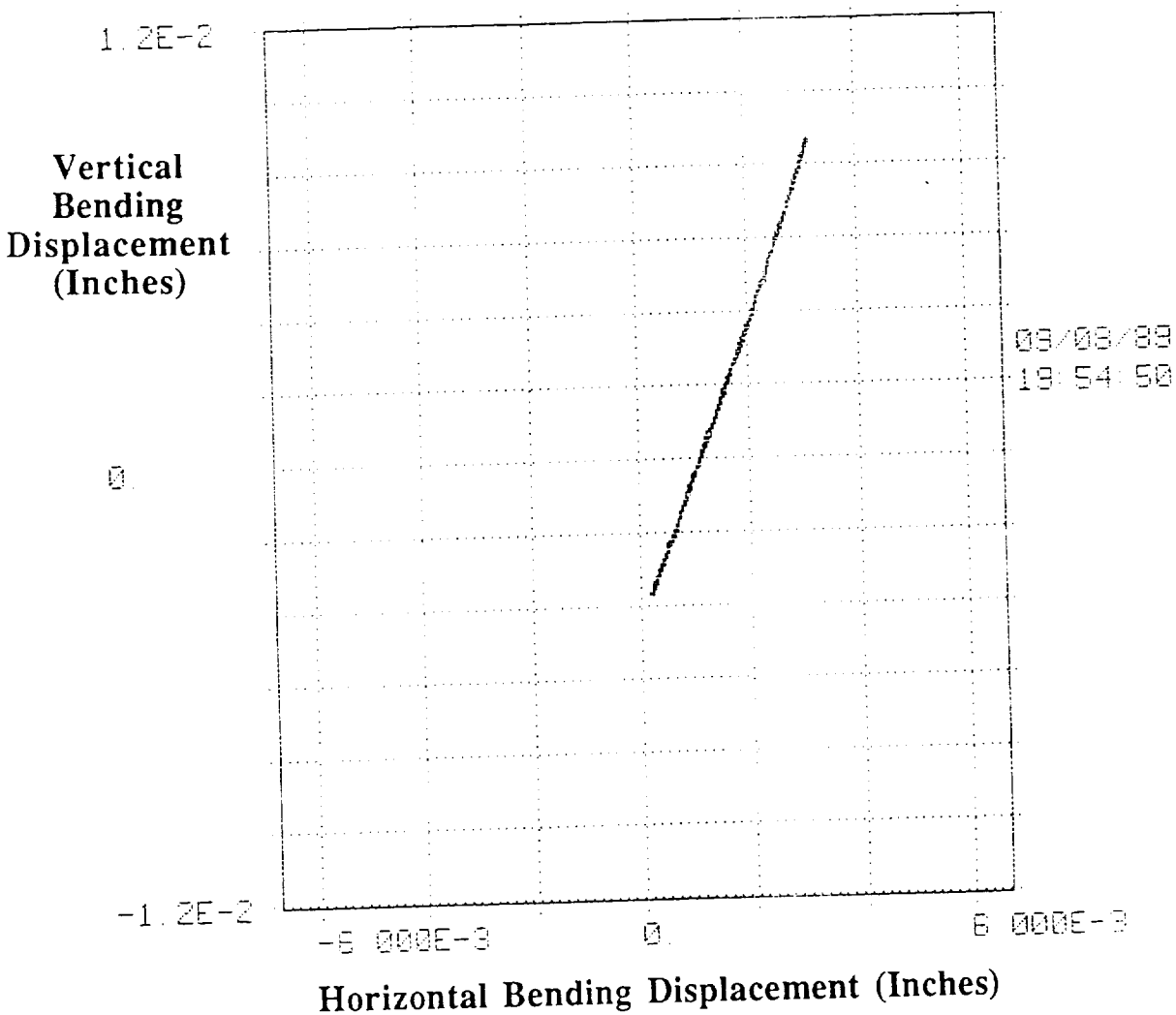

Diagonal test 2, excitation at 1 Hz

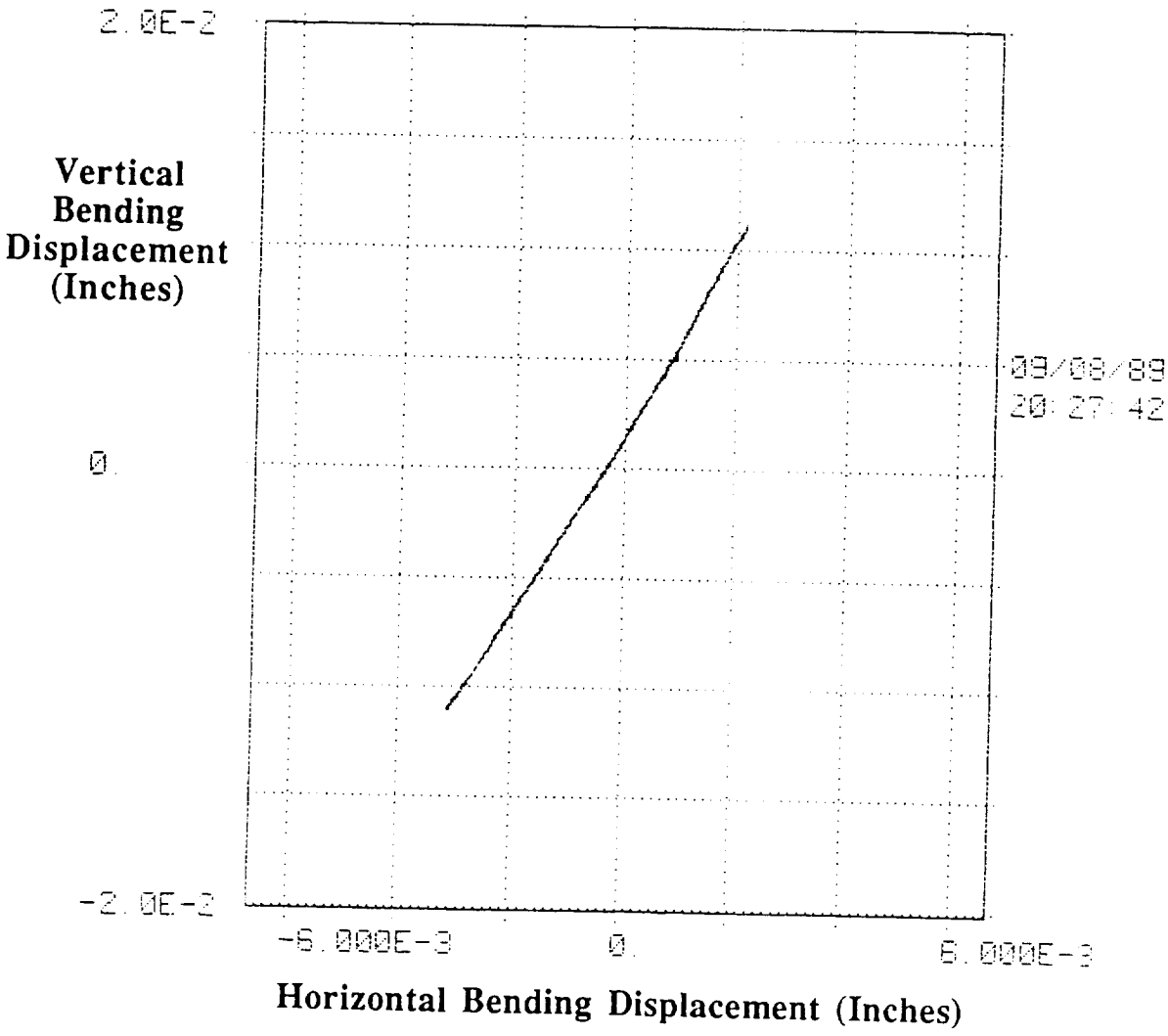

Diagonal test 2, excitation at 1 Hz

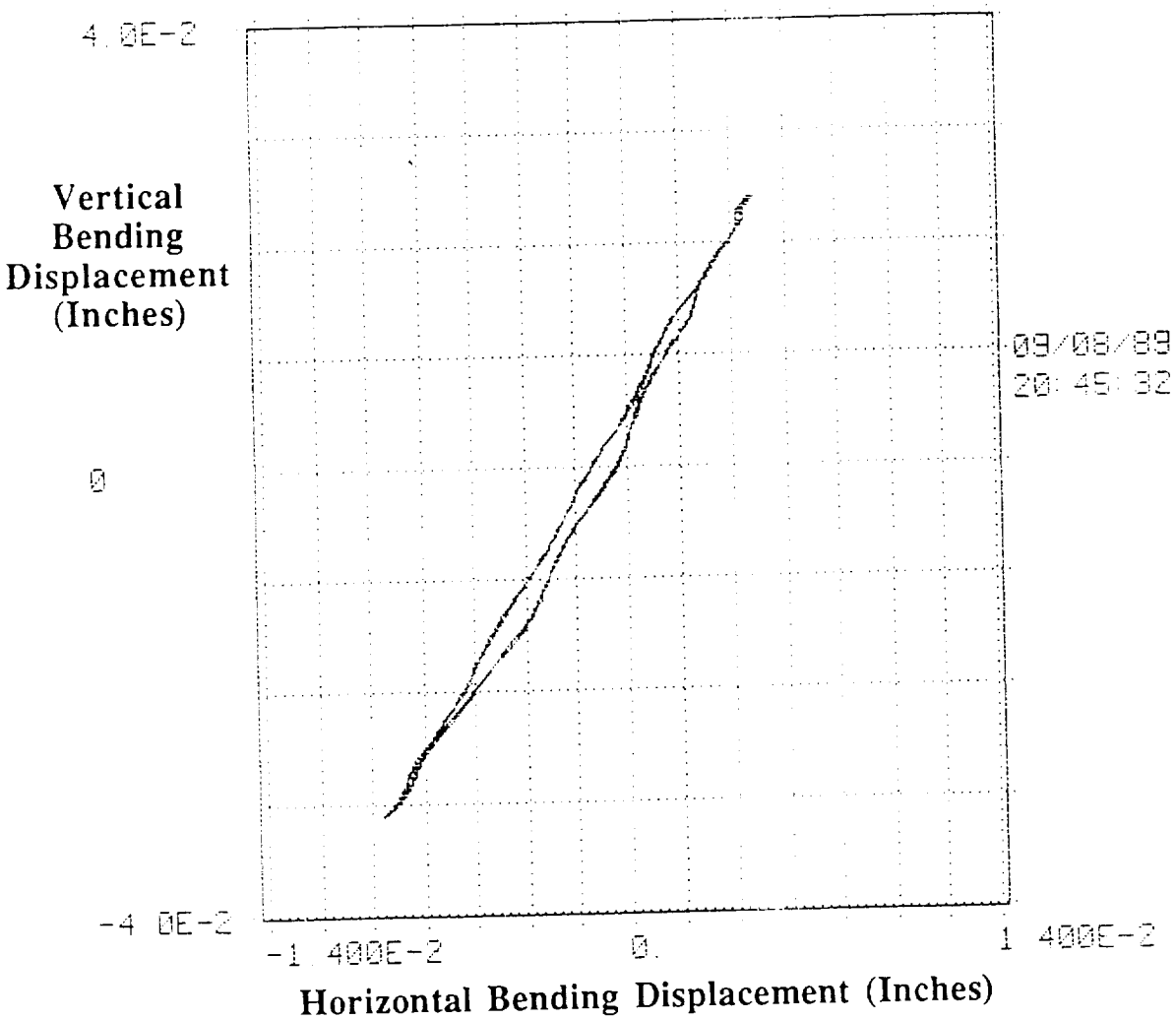

Diagonal test 2, excitation at 1 Hz

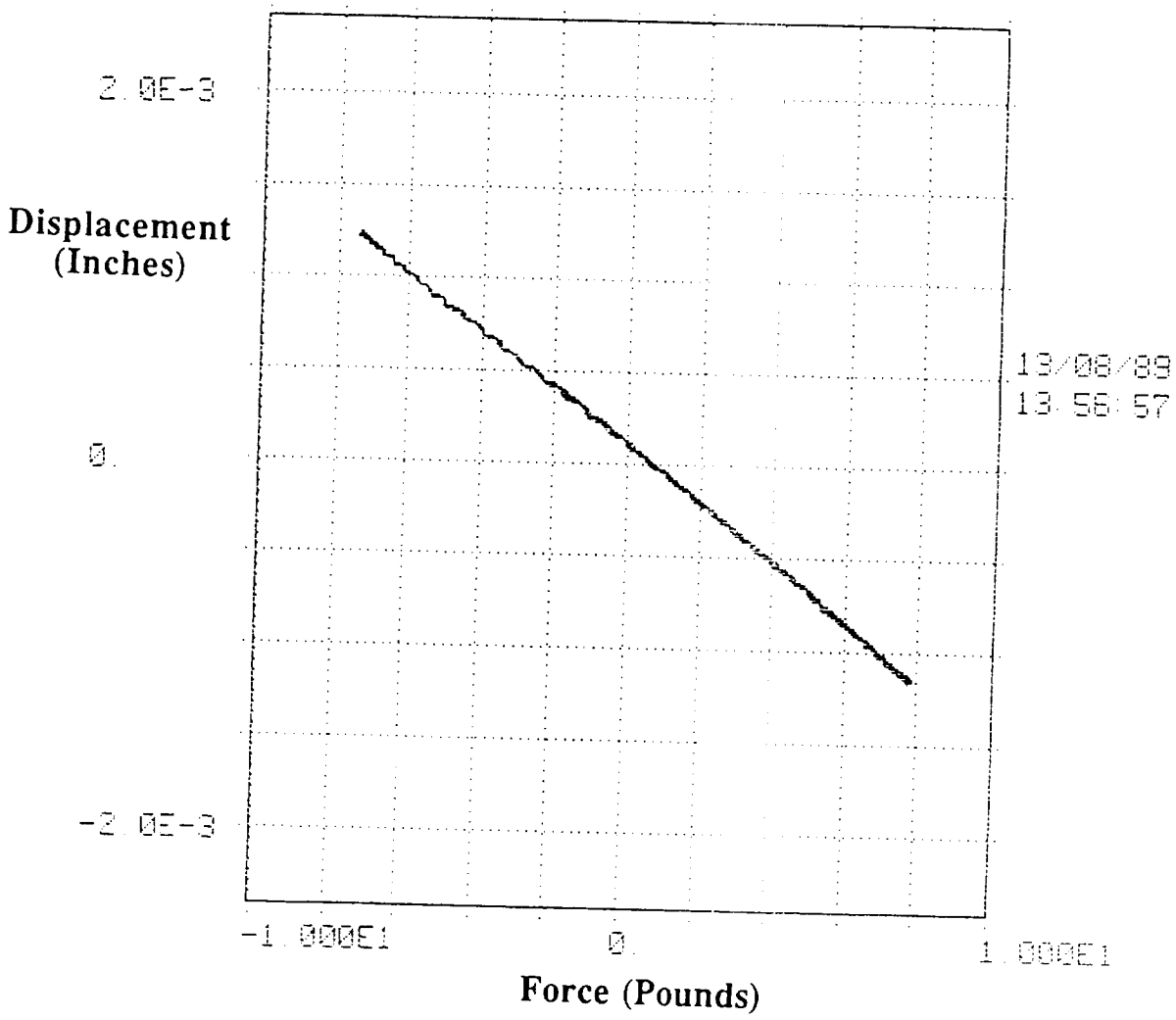

Diagonal test 3, excitation at 1 Hz

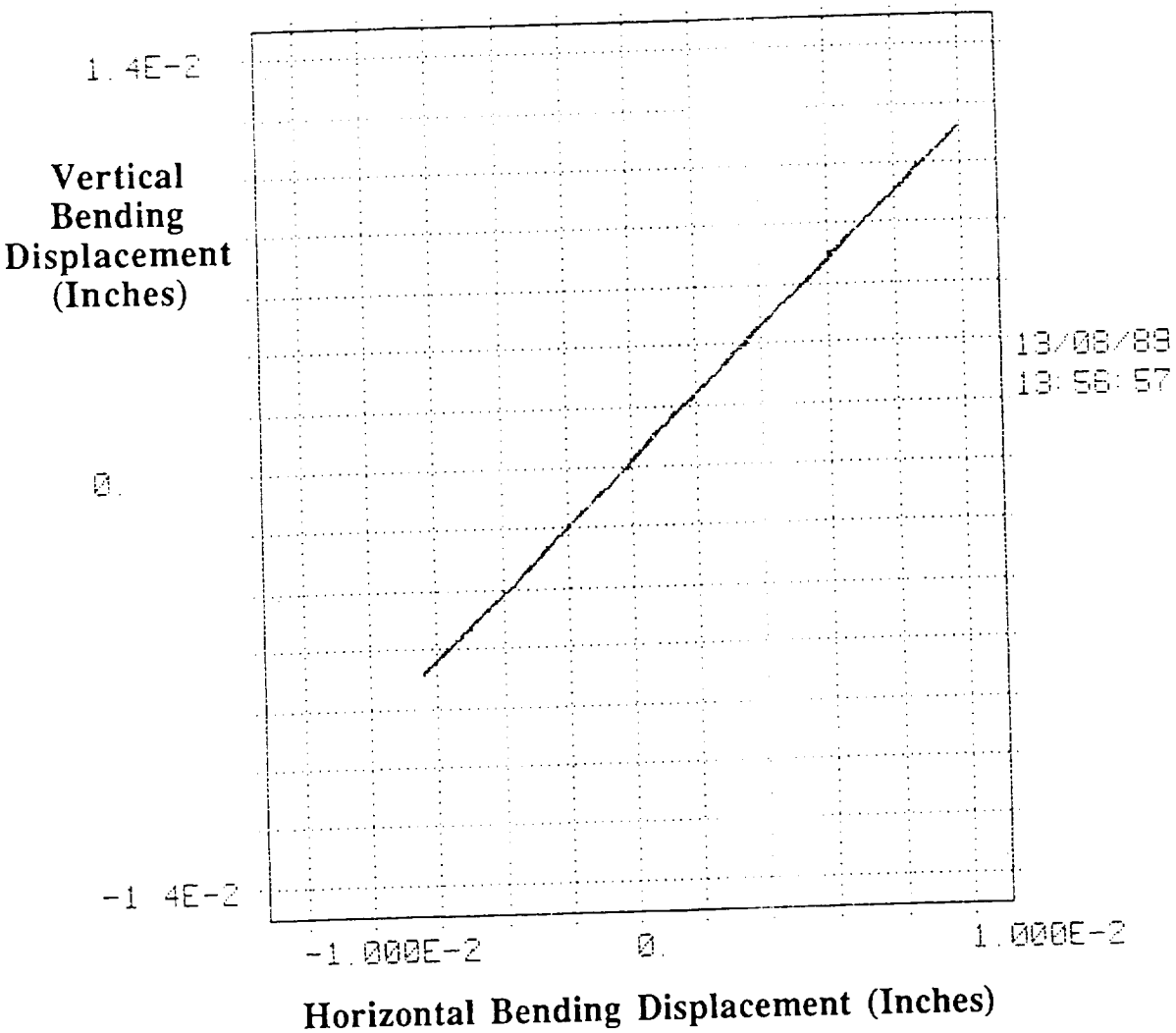

Diagonal test 3, excitation at 1 Hz

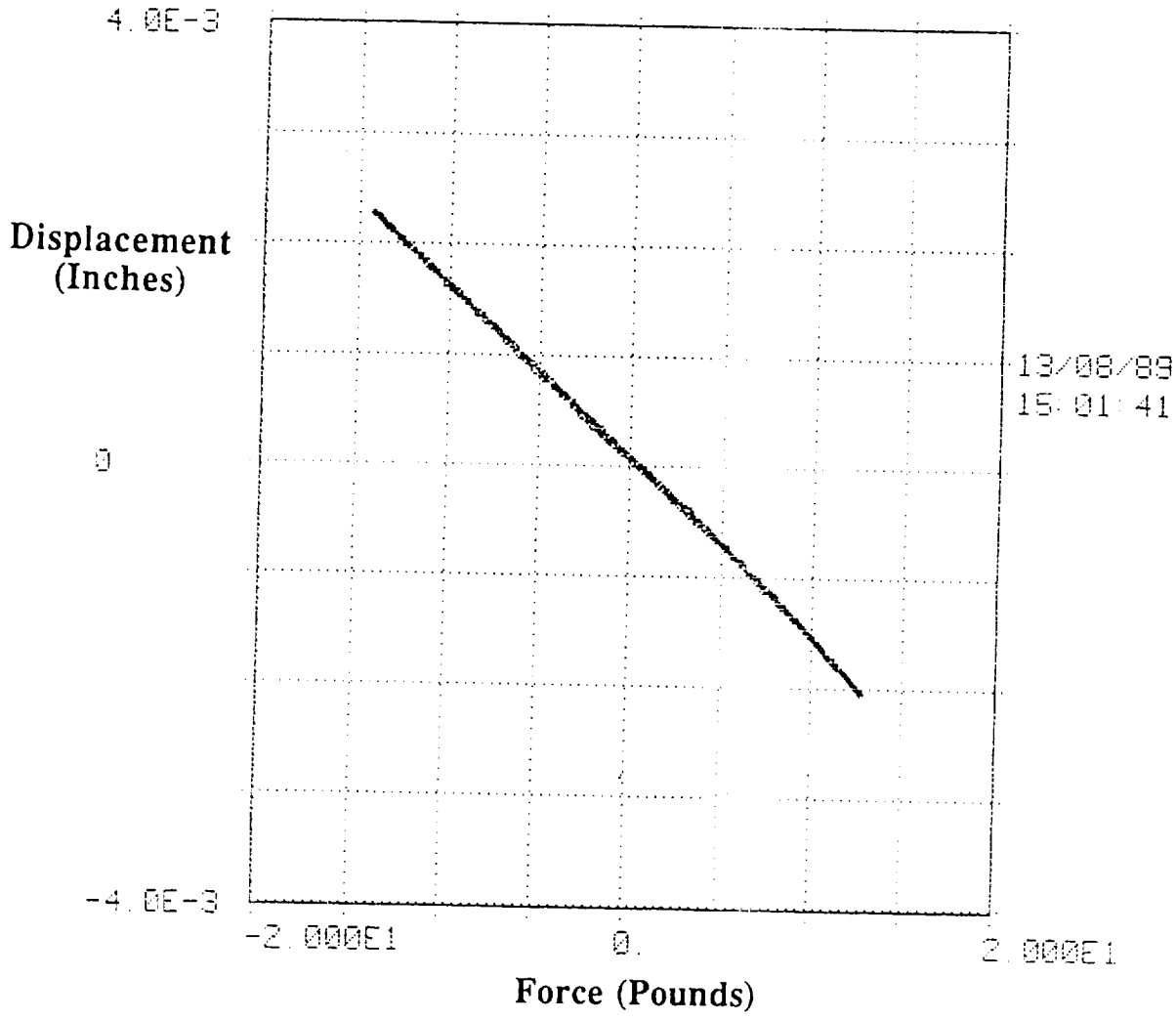

Diagonal test 3, excitation at 1 Hz

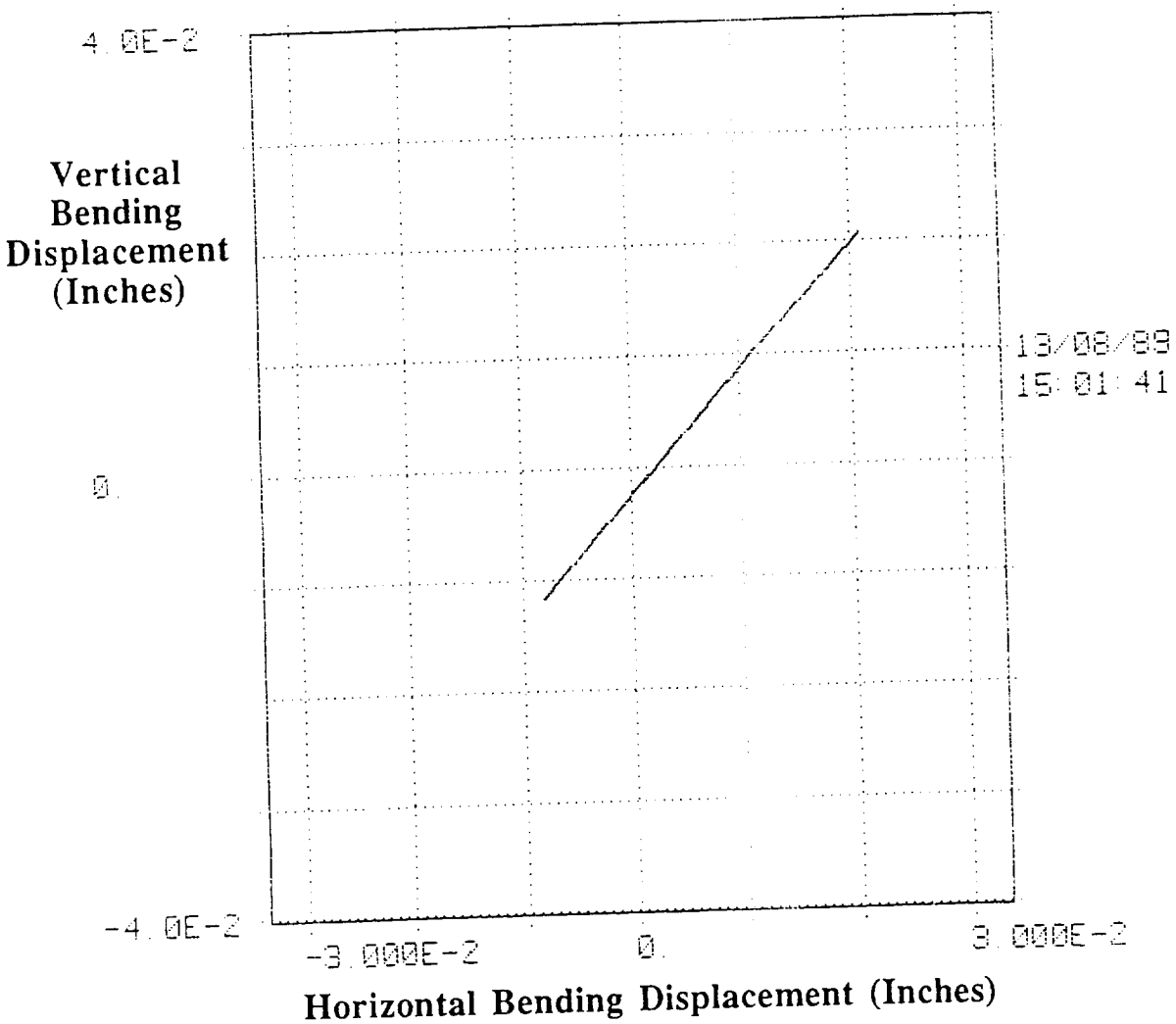

Diagonal test 3, excitation at 1 Hz

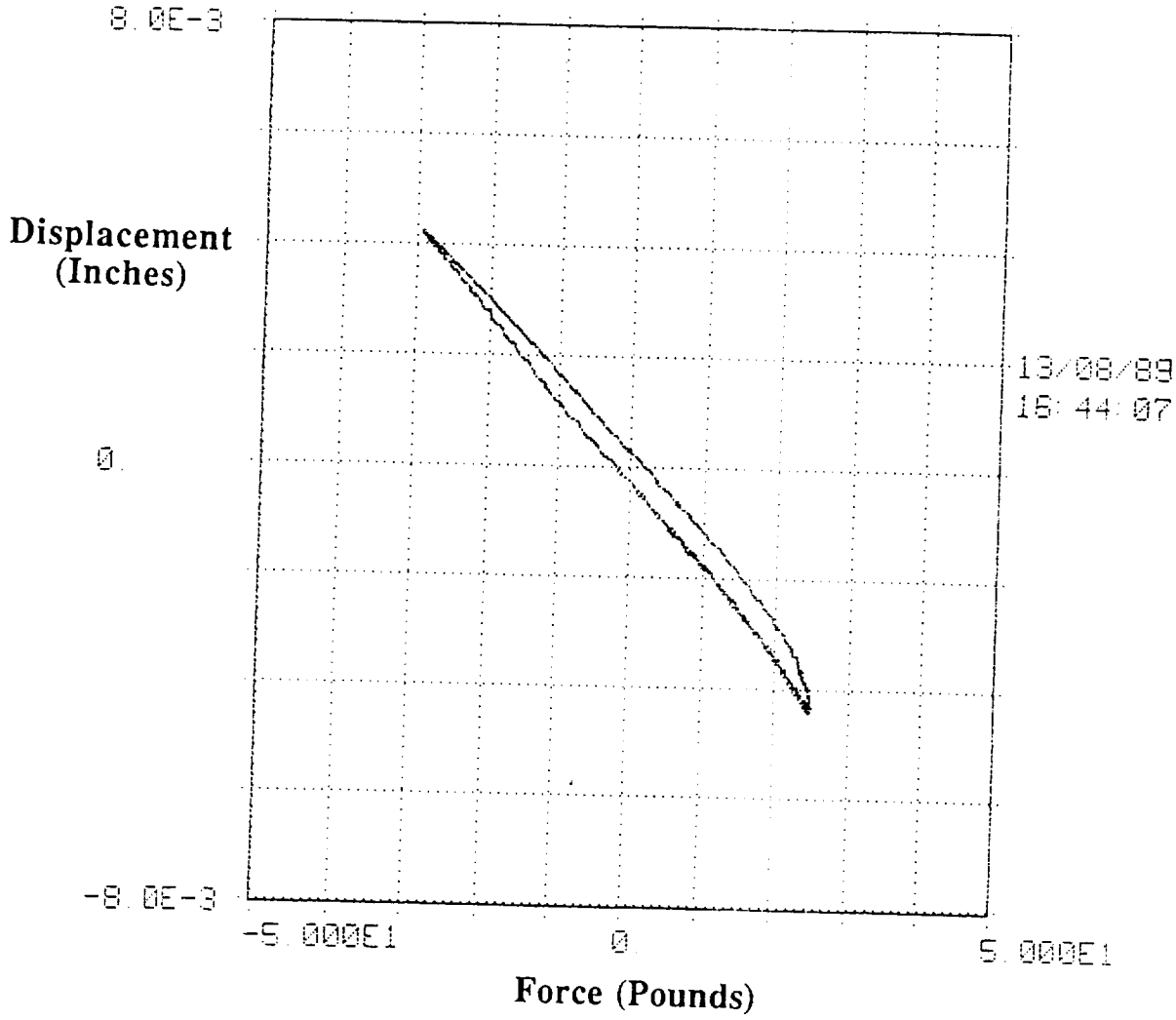

Diagonal test 3, excitation at 1 Hz

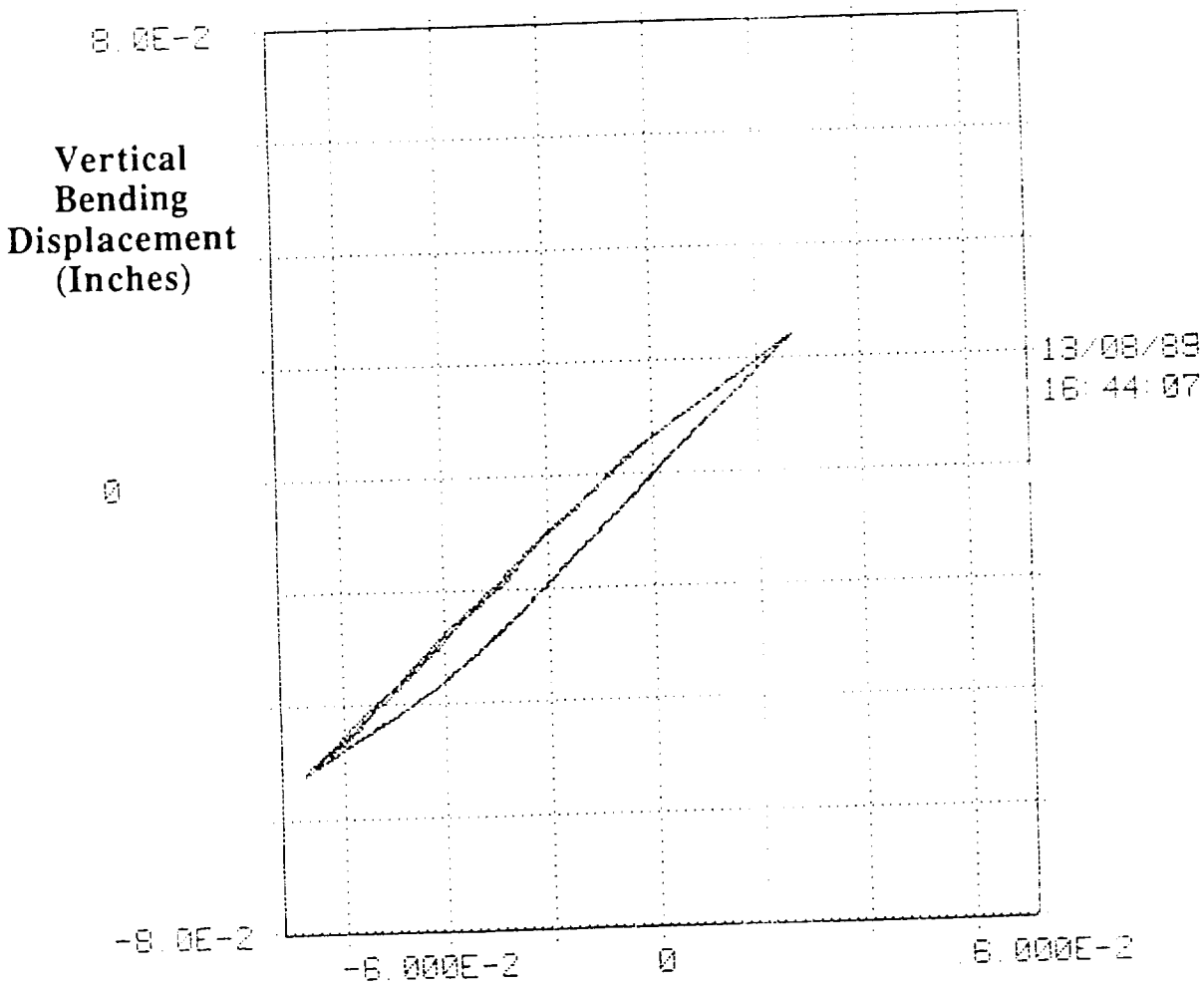

Diagonal test 3, excitation at 1 Hz

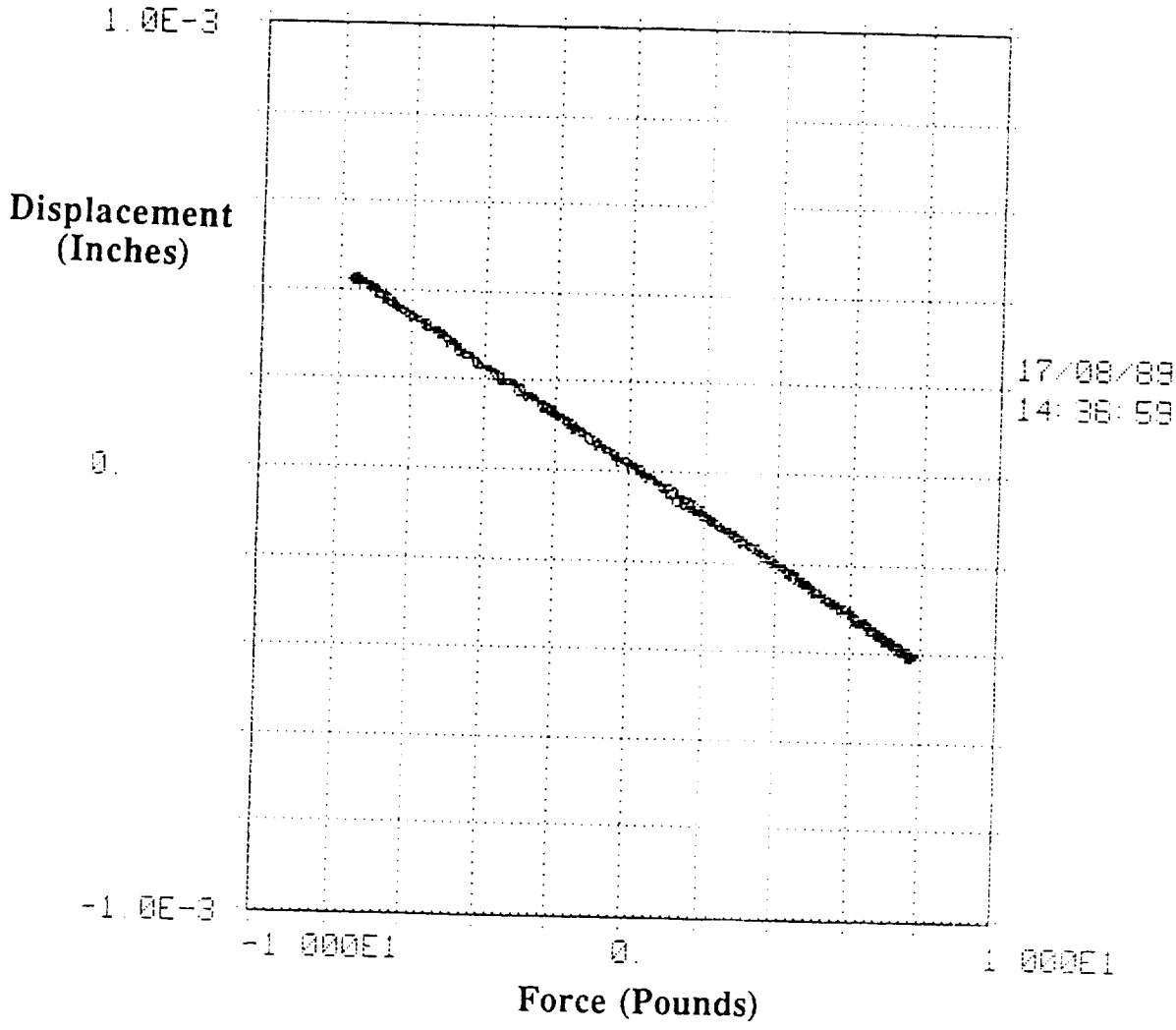

Diagonal test 5, excitation at 1 Hz

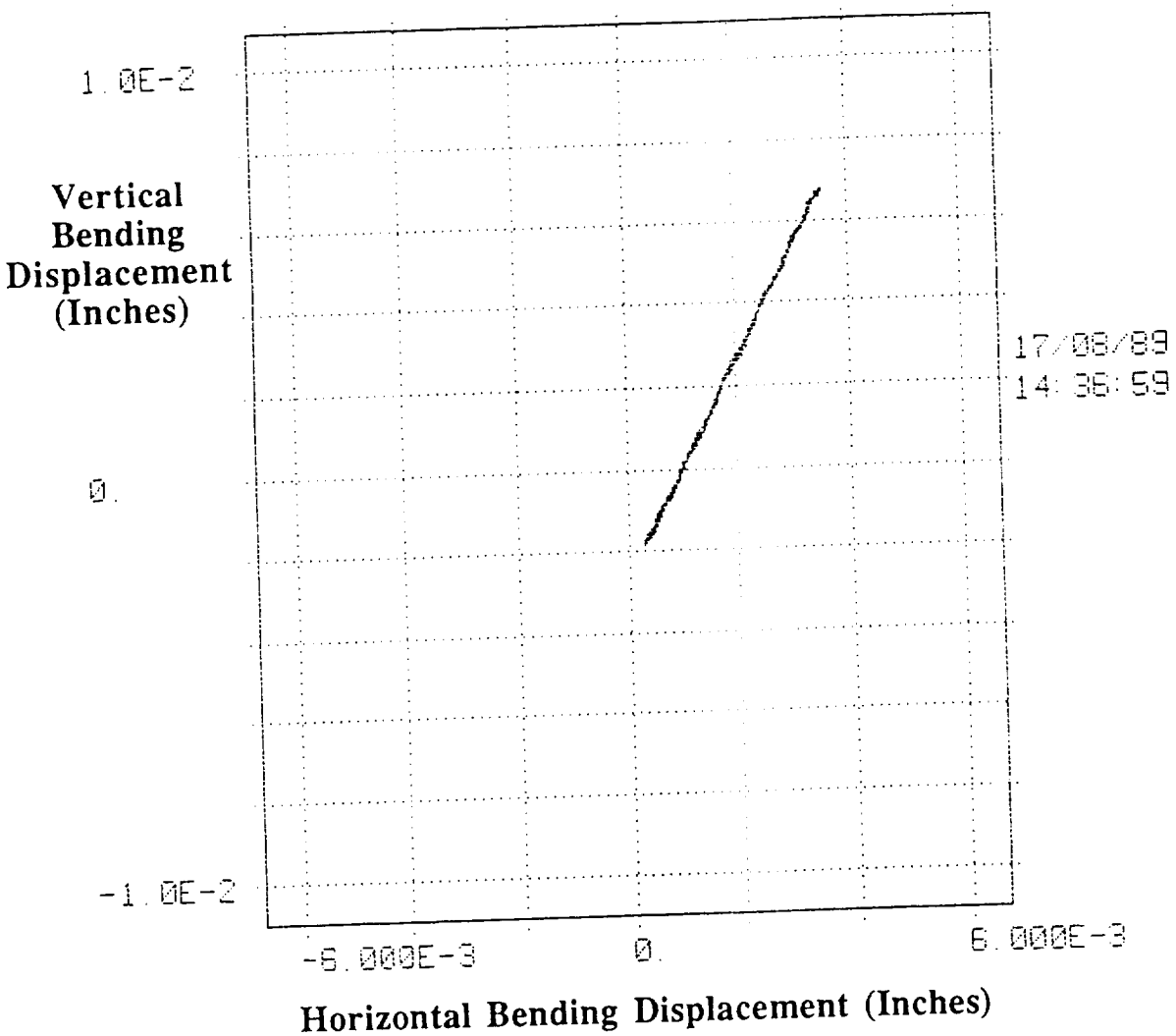

Diagonal test 5, excitation at 1 Hz

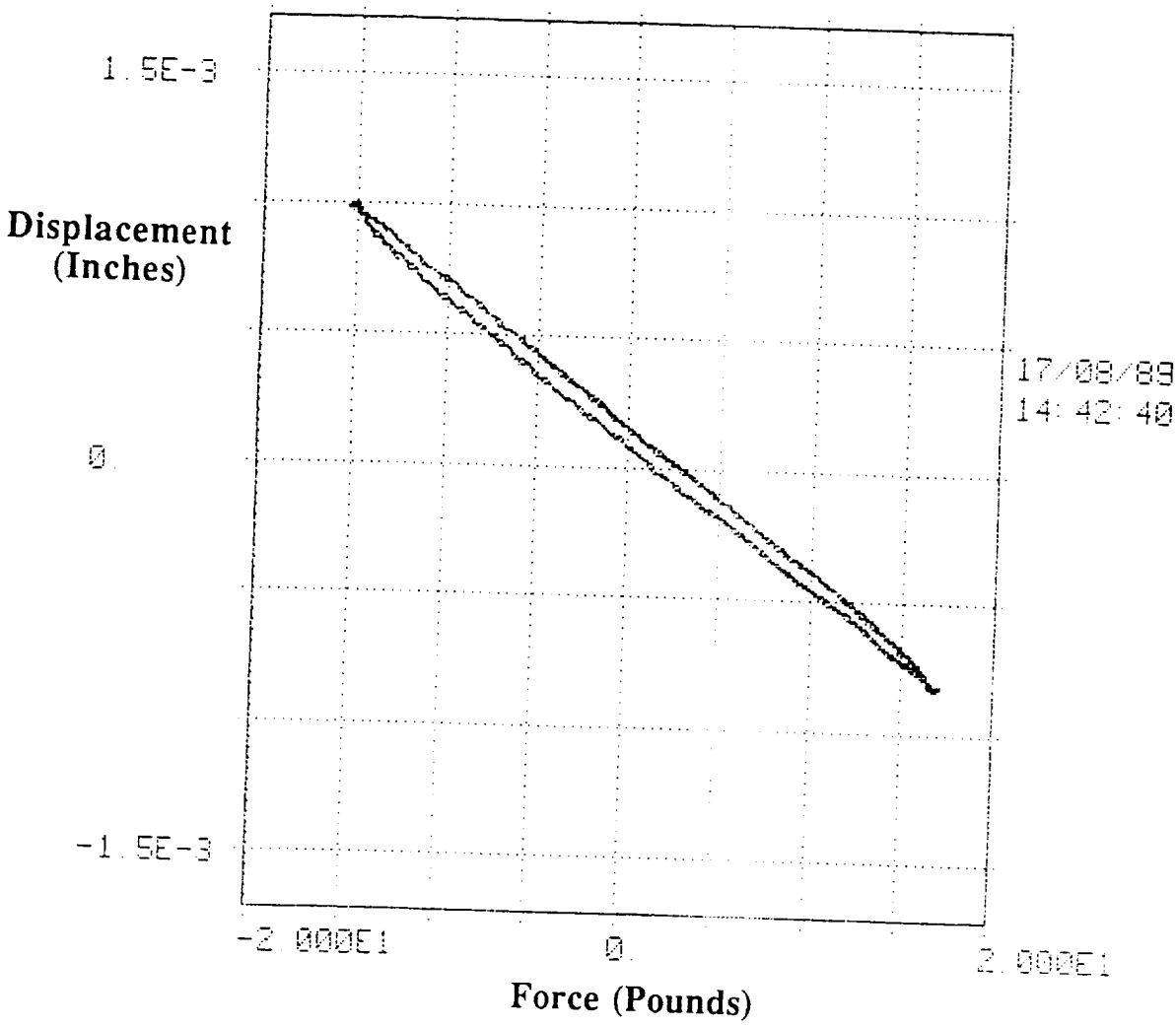

Diagonal test 5, excitation at 1 Hz

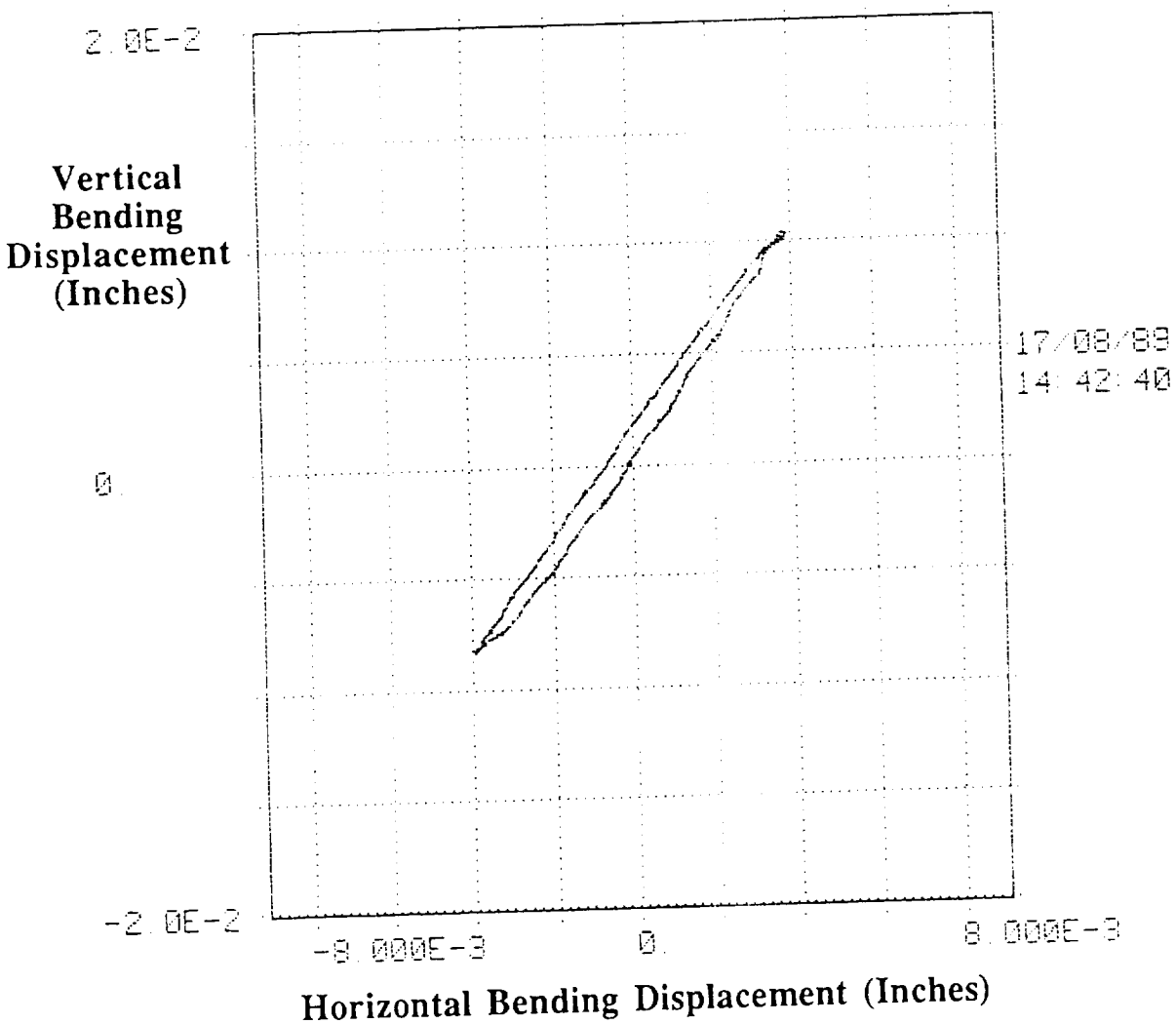

Diagonal test 5, excitation at 1 Hz

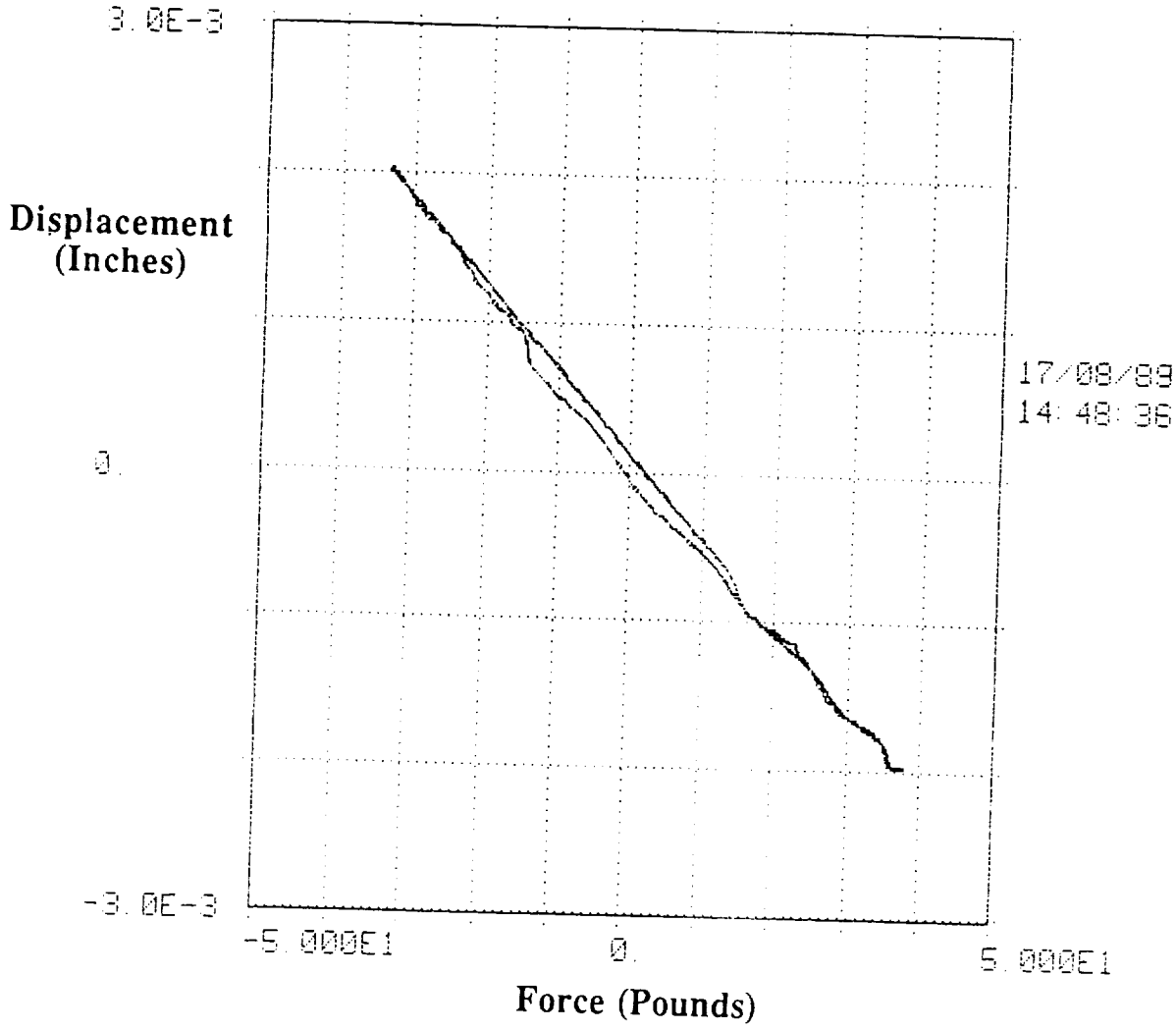

Diagonal test 5, excitation at 1 Hz

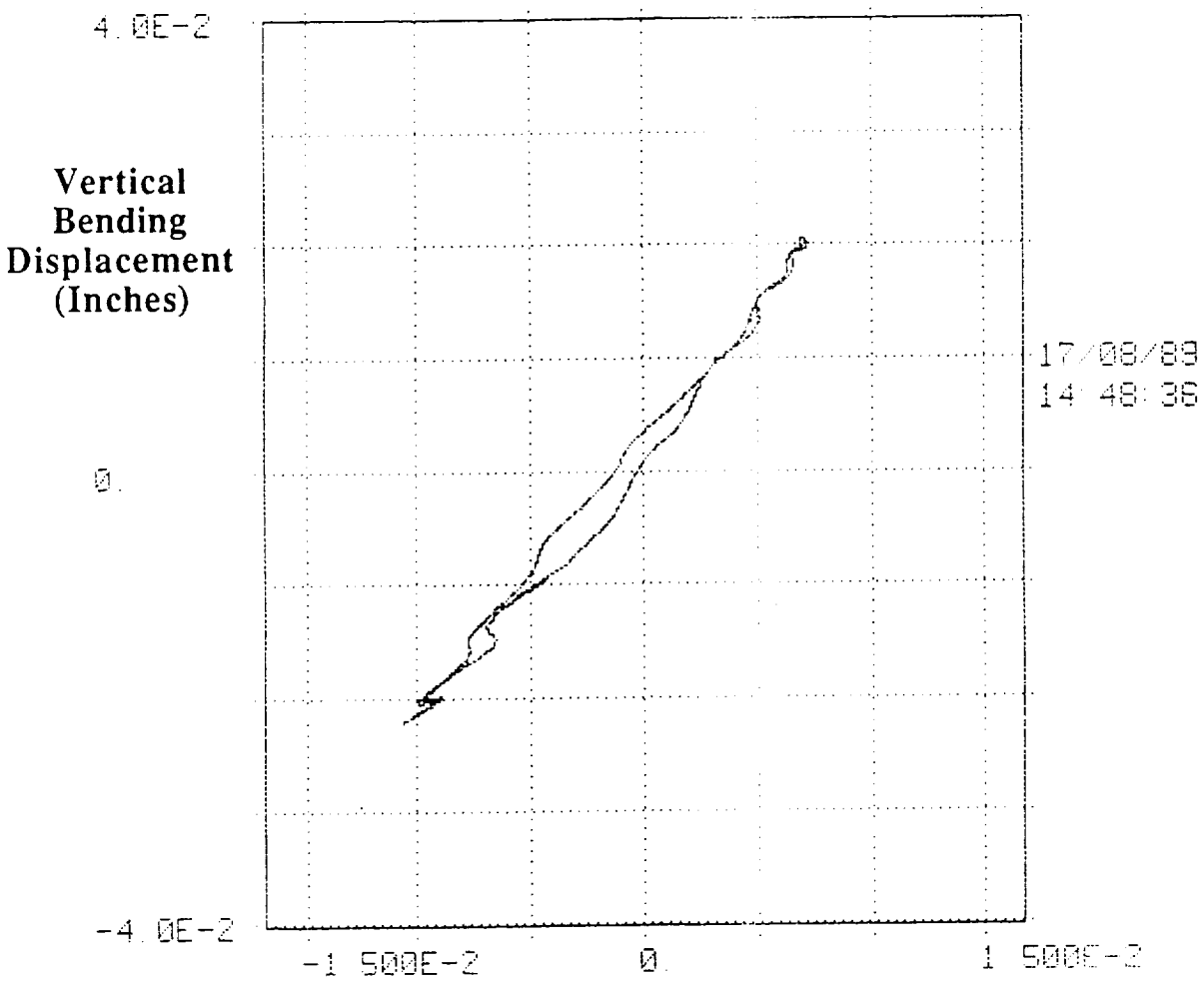

Diagonal test 5, excitation at 1 Hz

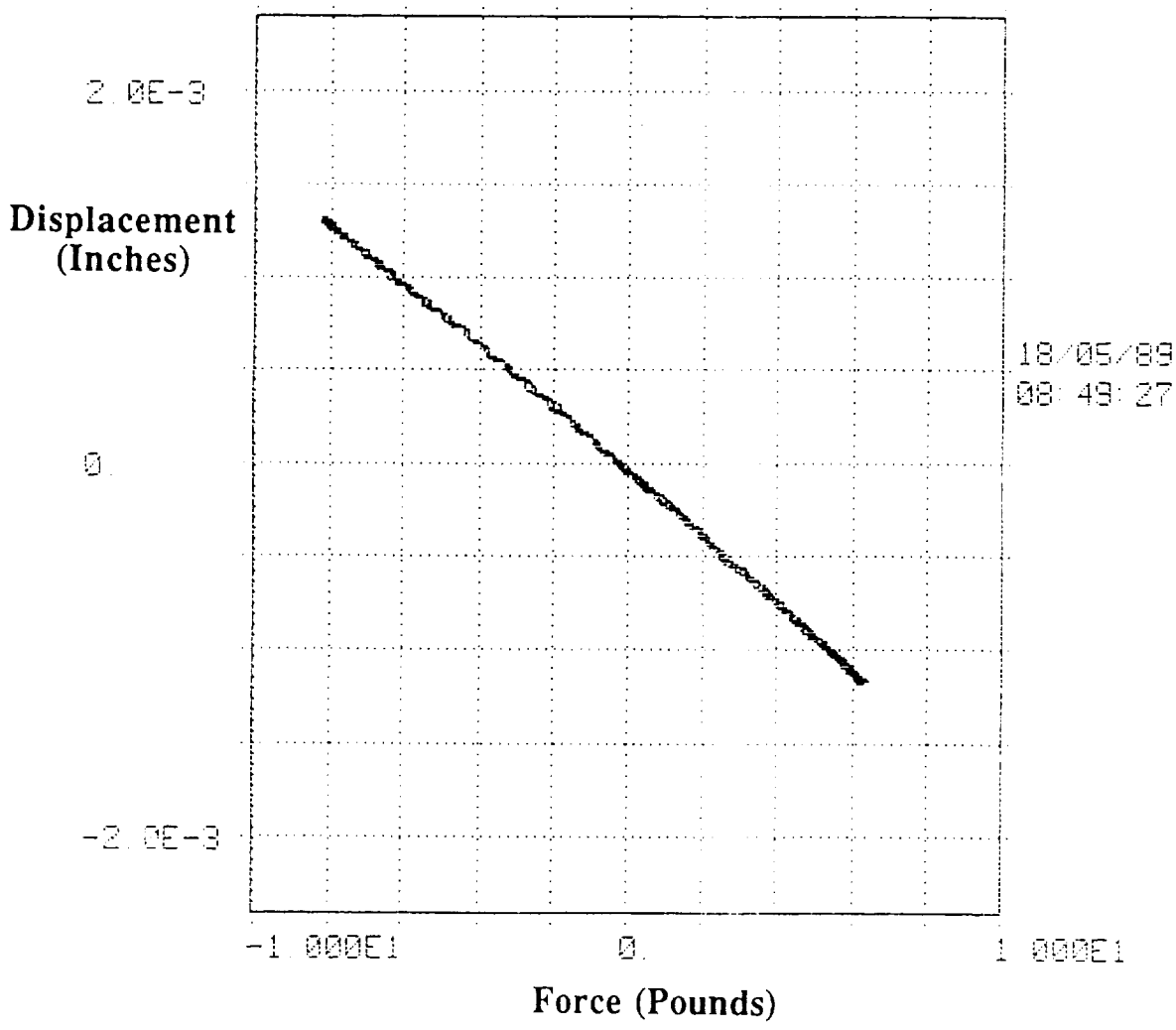

Diagonal test 6, excitation at 1 Hz

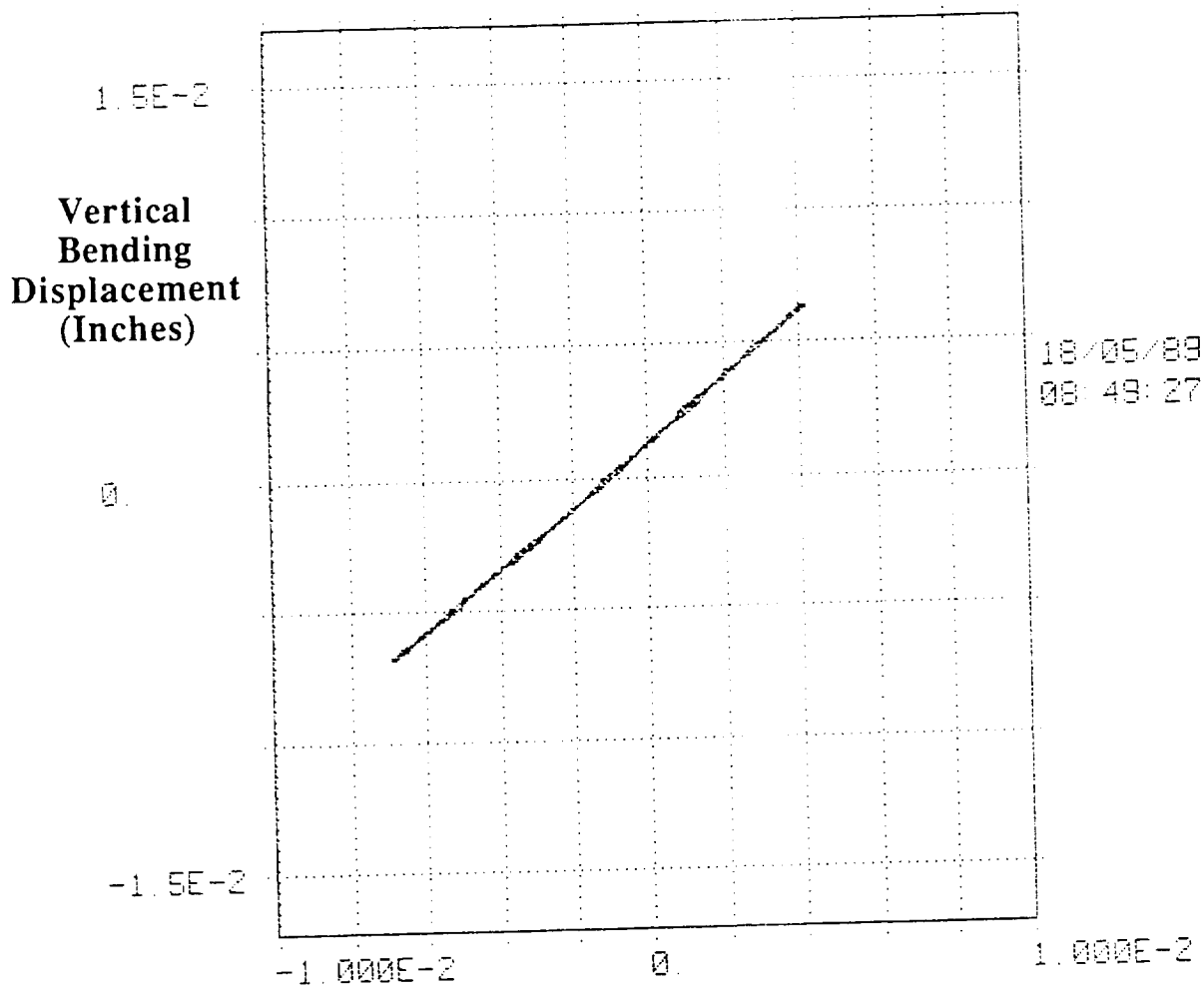

Diagonal test 6, excitation at 1 Hz

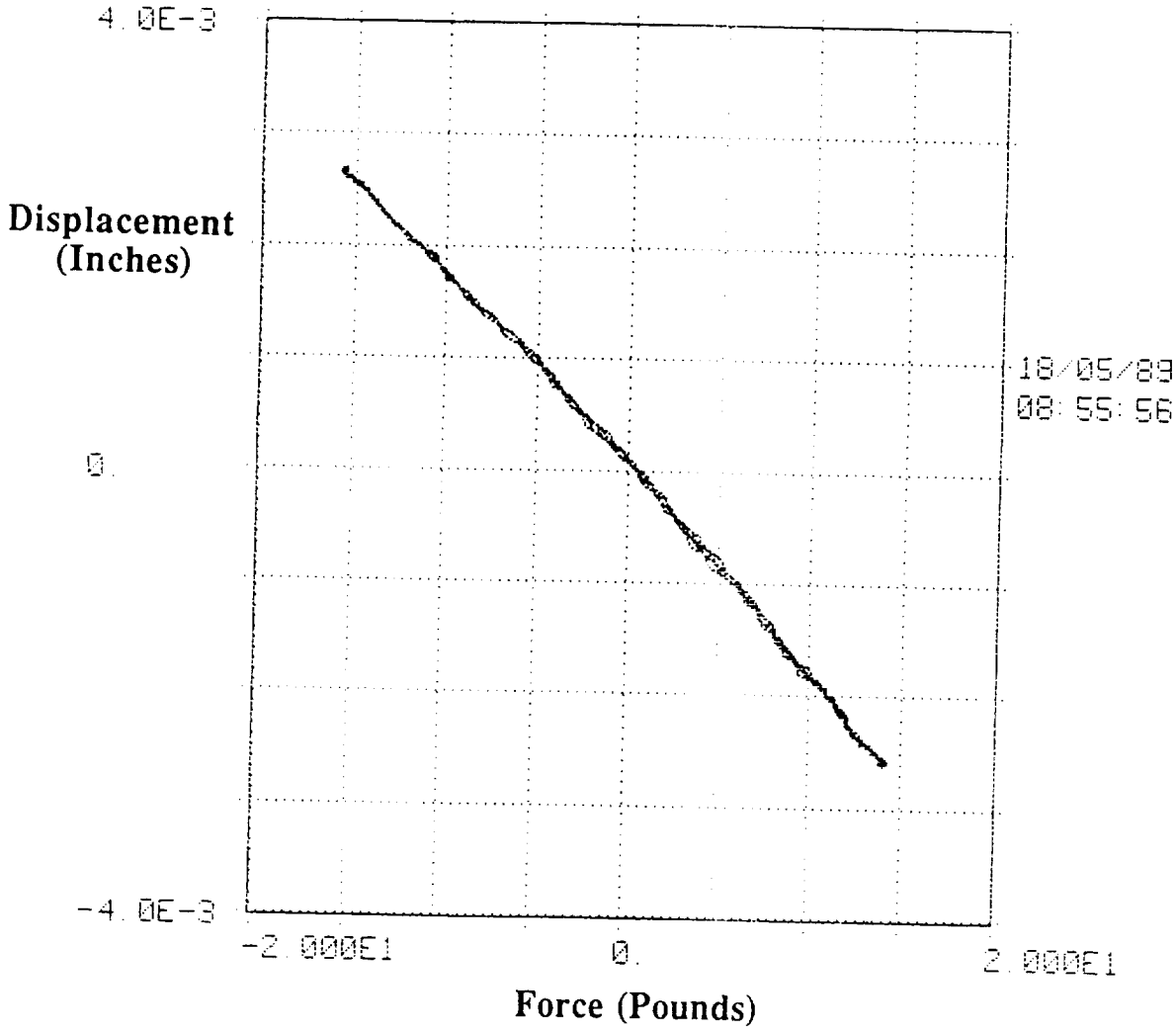

Diagonal test 6, excitation at 1 Hz

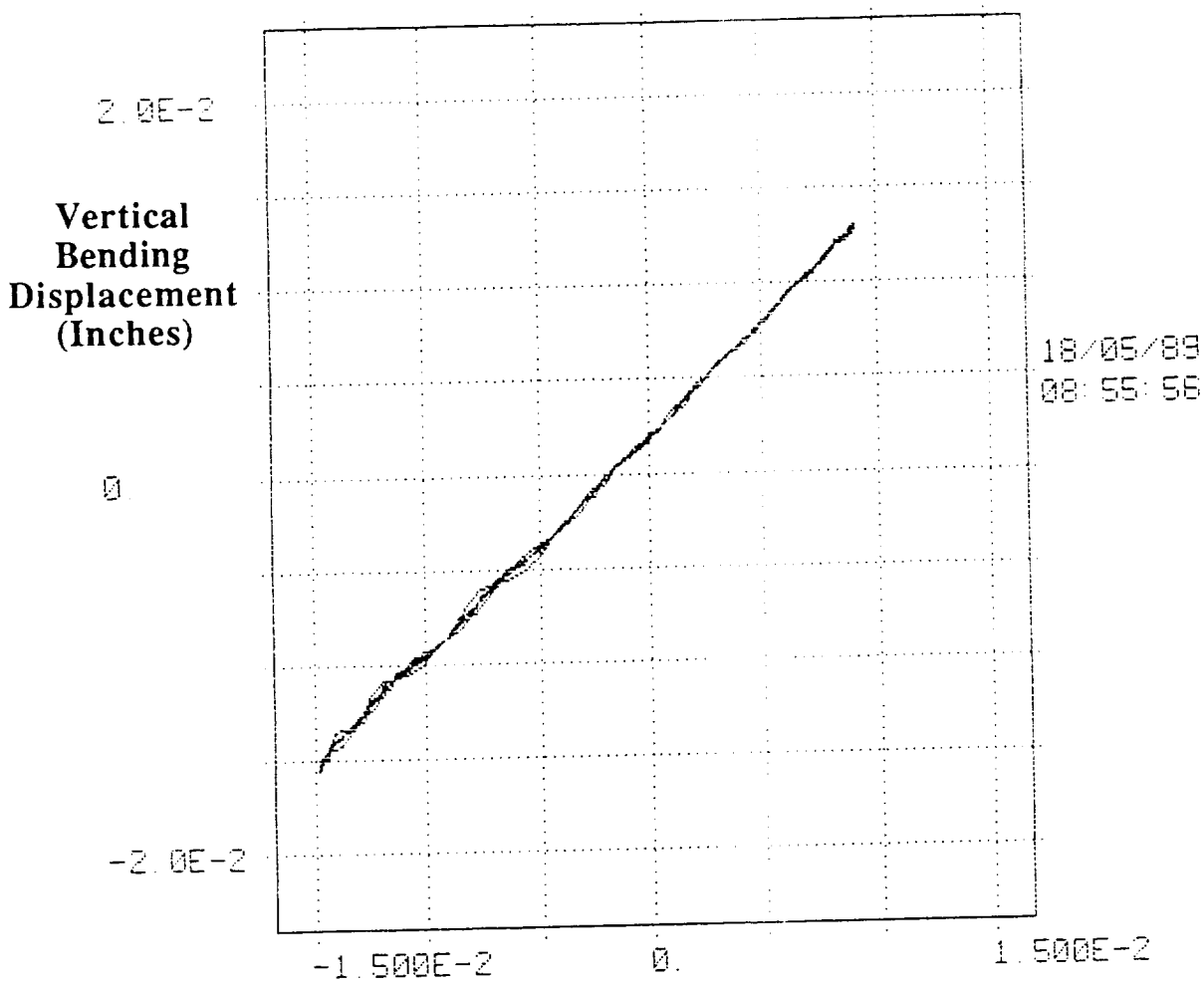

Diagonal test 6, excitation at 1 Hz

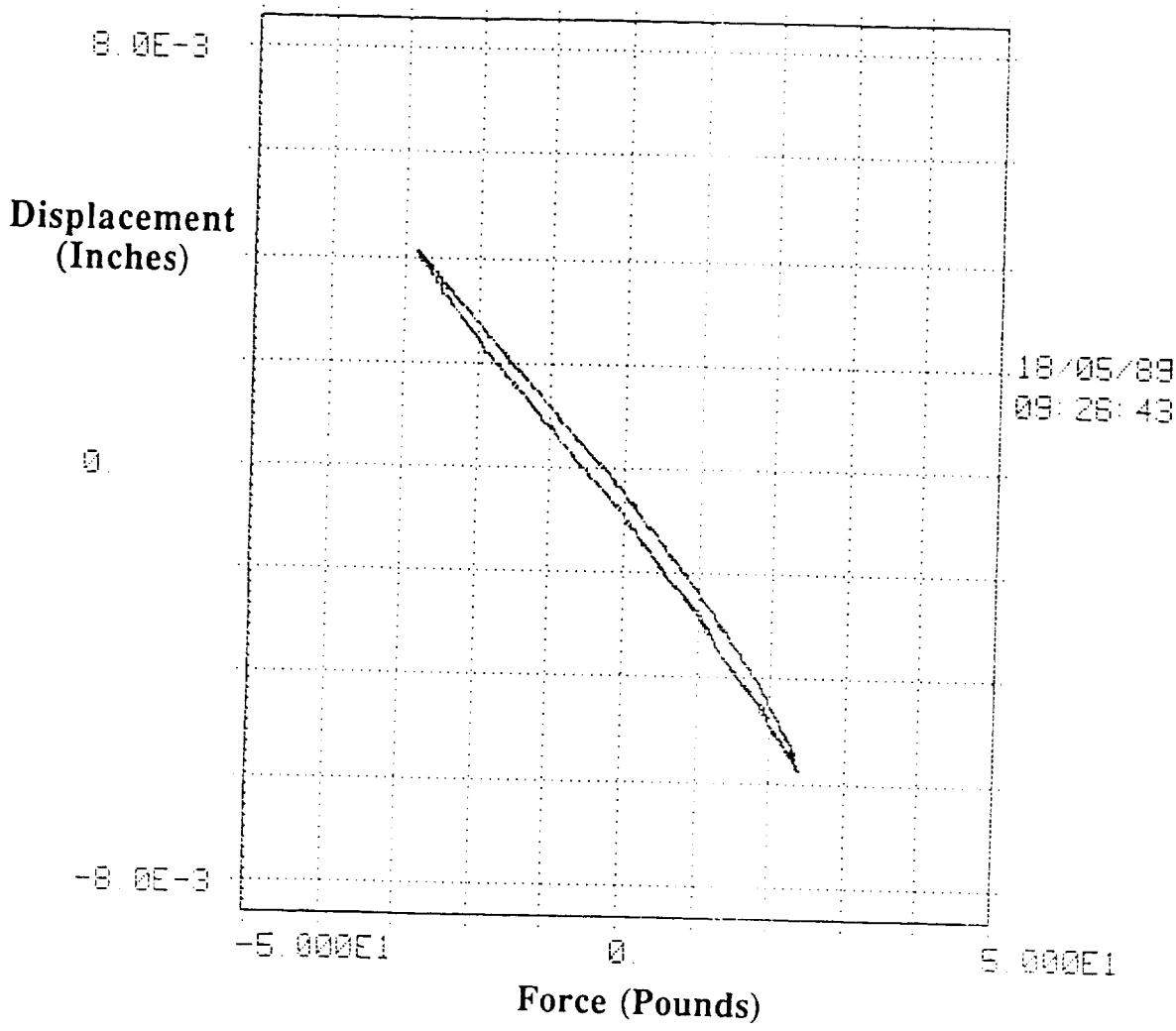

Diagonal test 6, excitation at 1 Hz

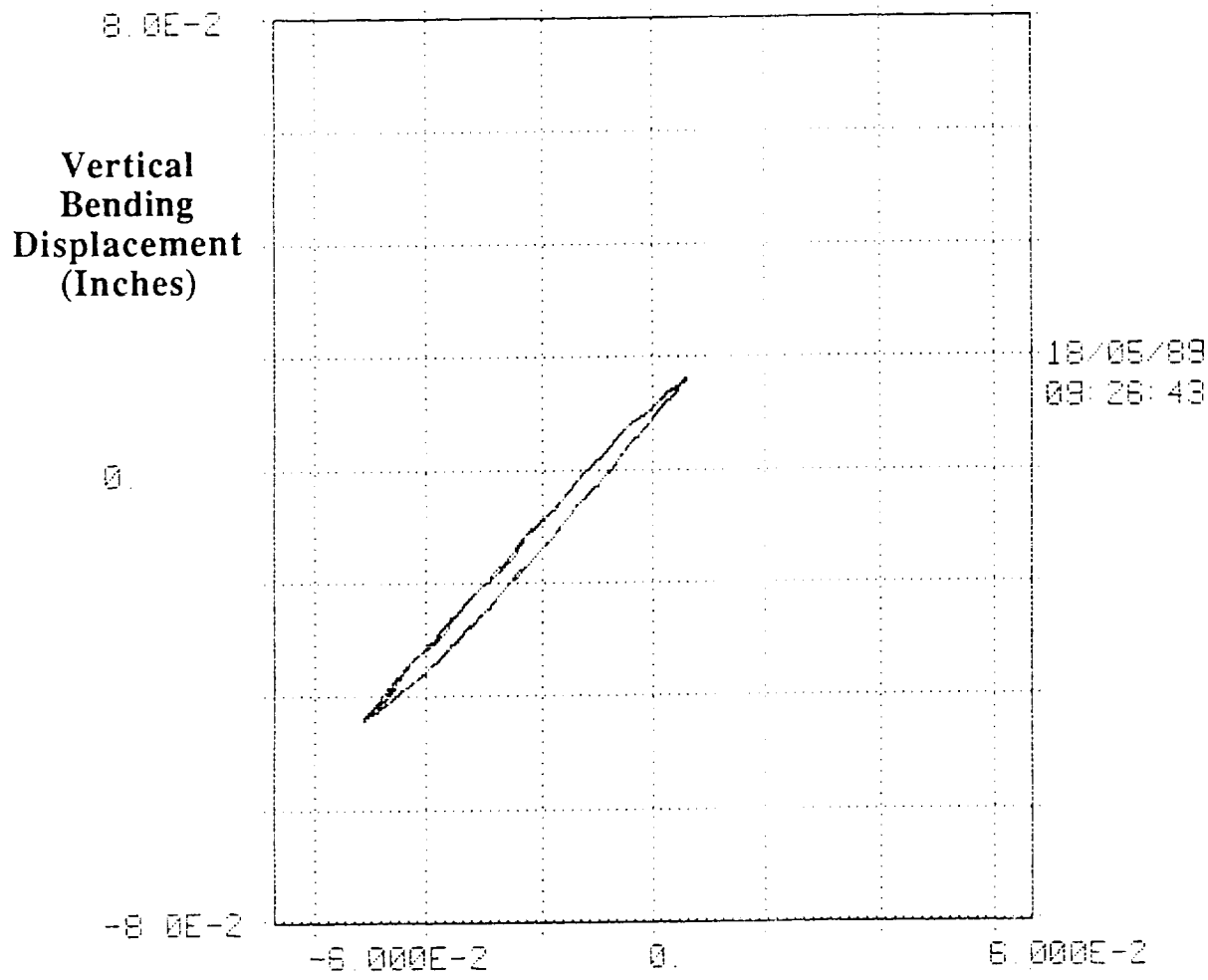

Diagonal test 6, excitation at 1 Hz

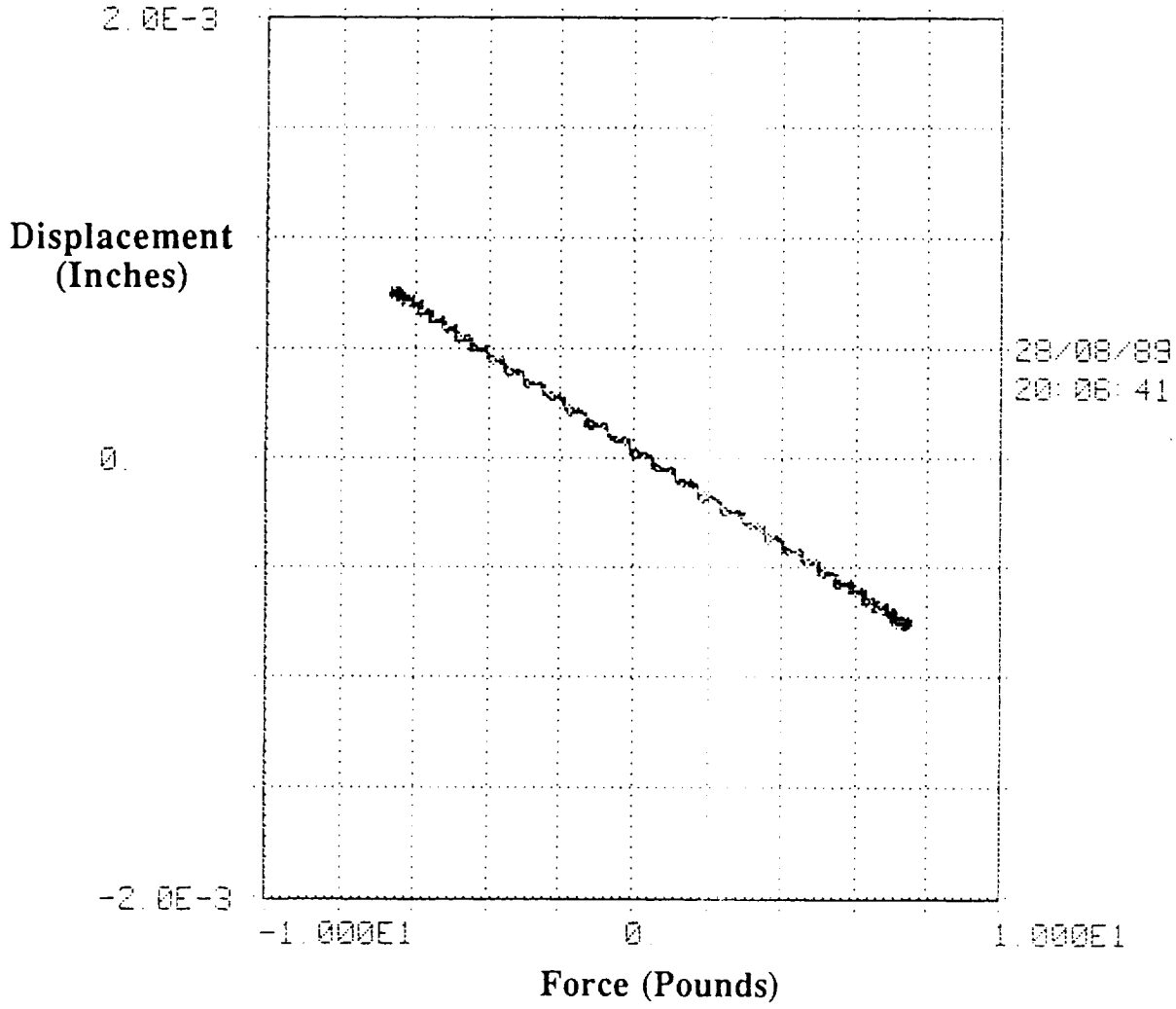

Diagonal test 7, excitation at 1 Hz

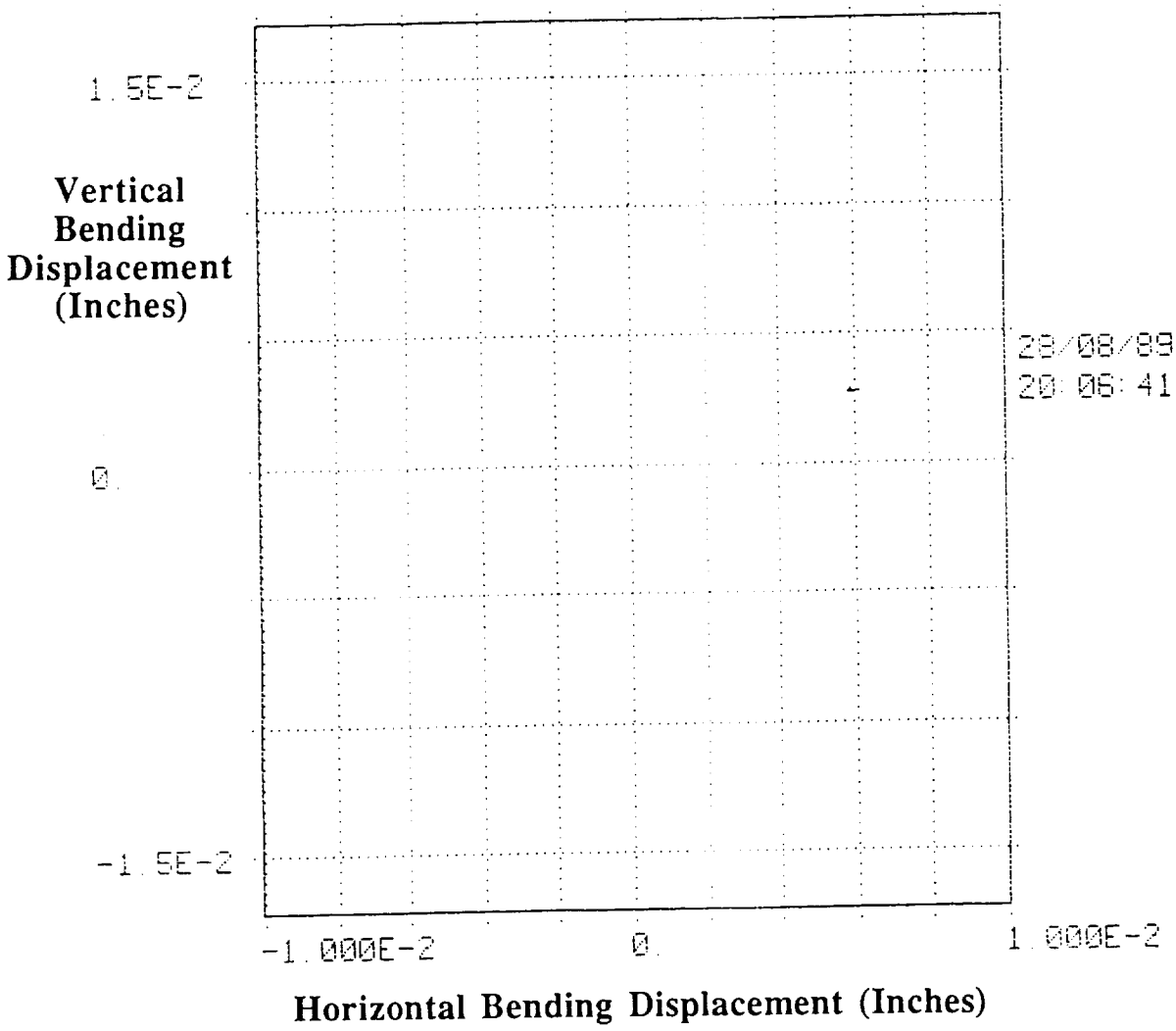

Diagonal test 7, excitation at 1 Hz

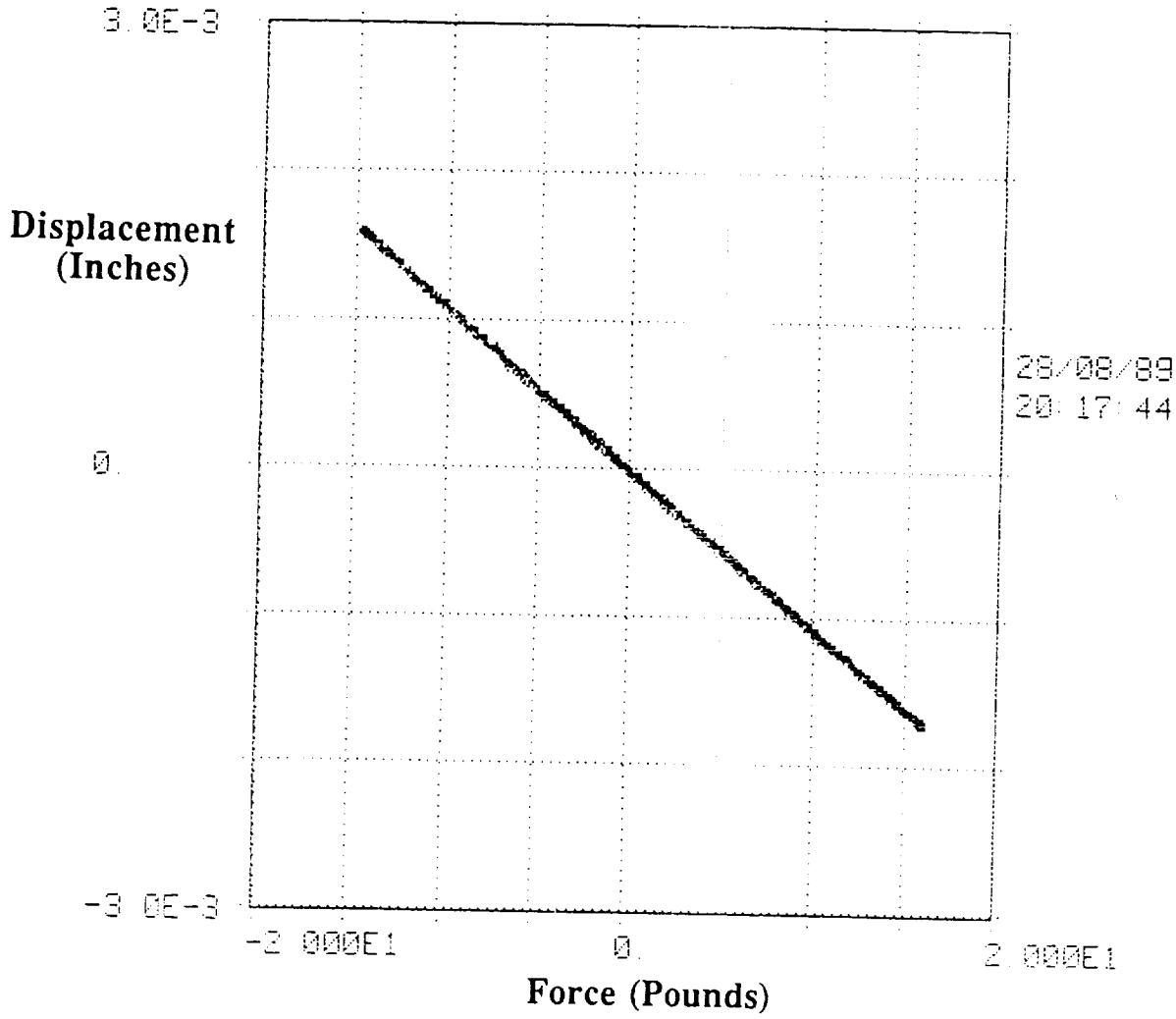

Diagonal test 7, excitation at 1 Hz

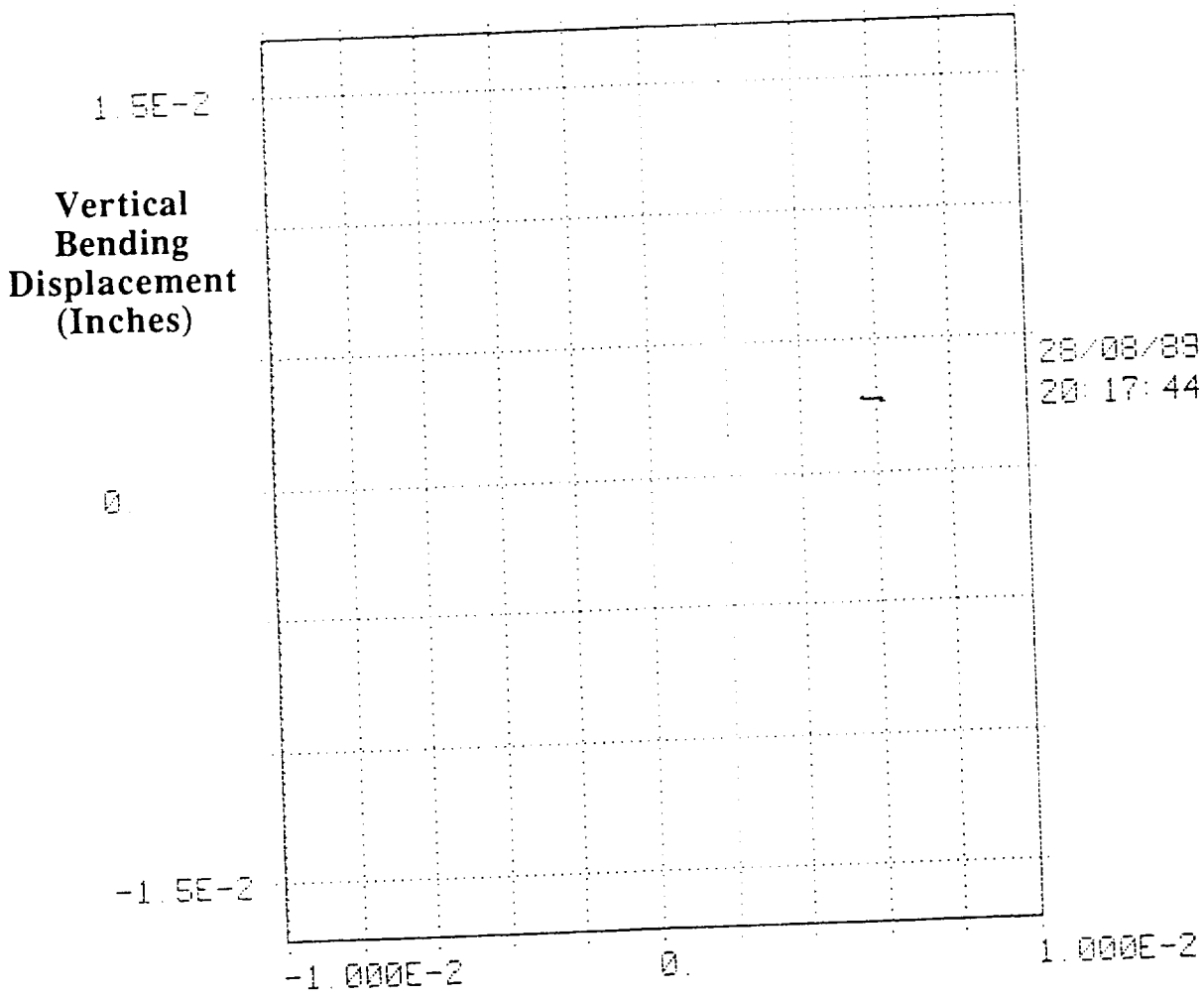

Diagonal test 7, excitation at 1 Hz

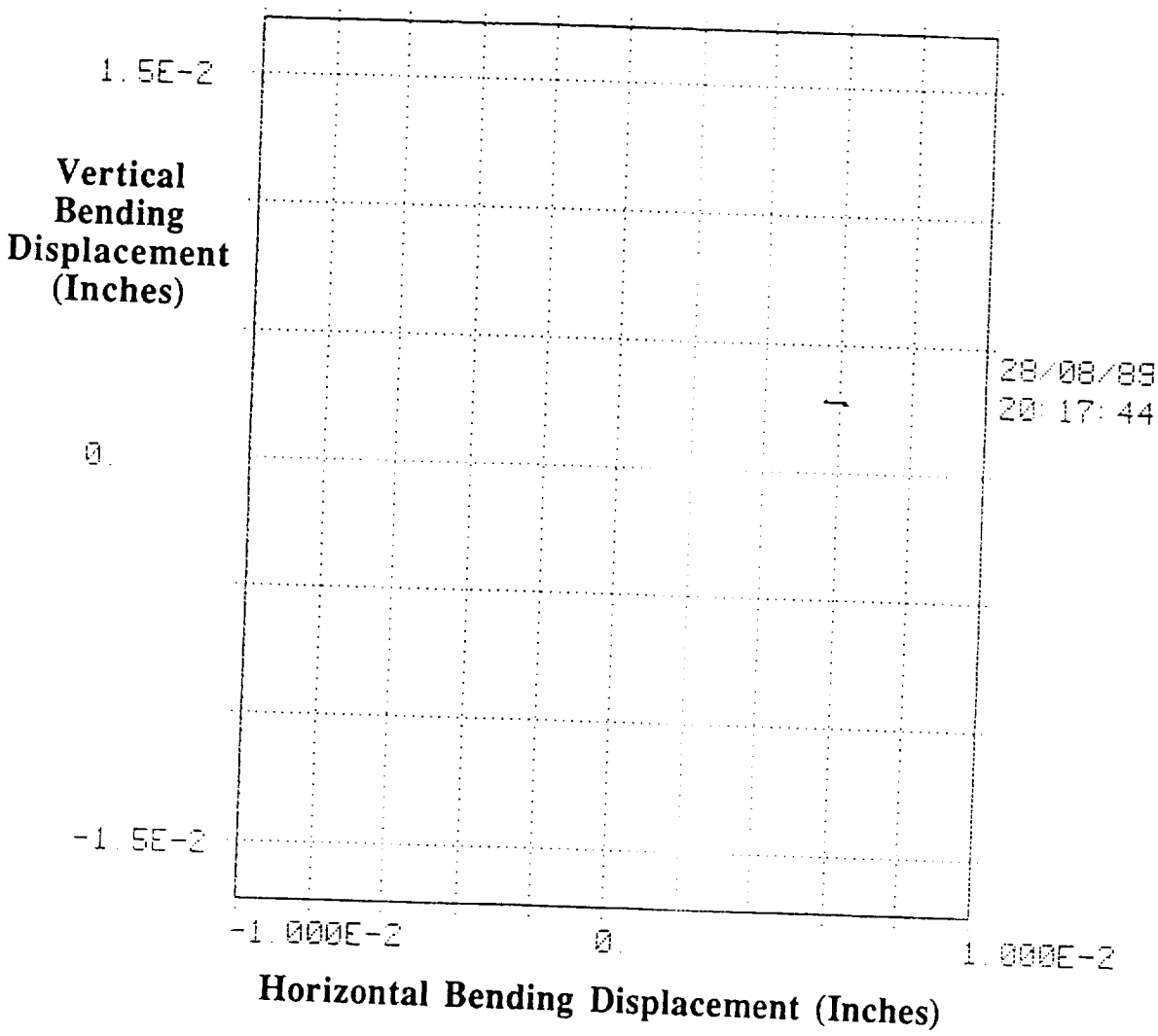

Diagonal test 7, excitation at 1 Hz

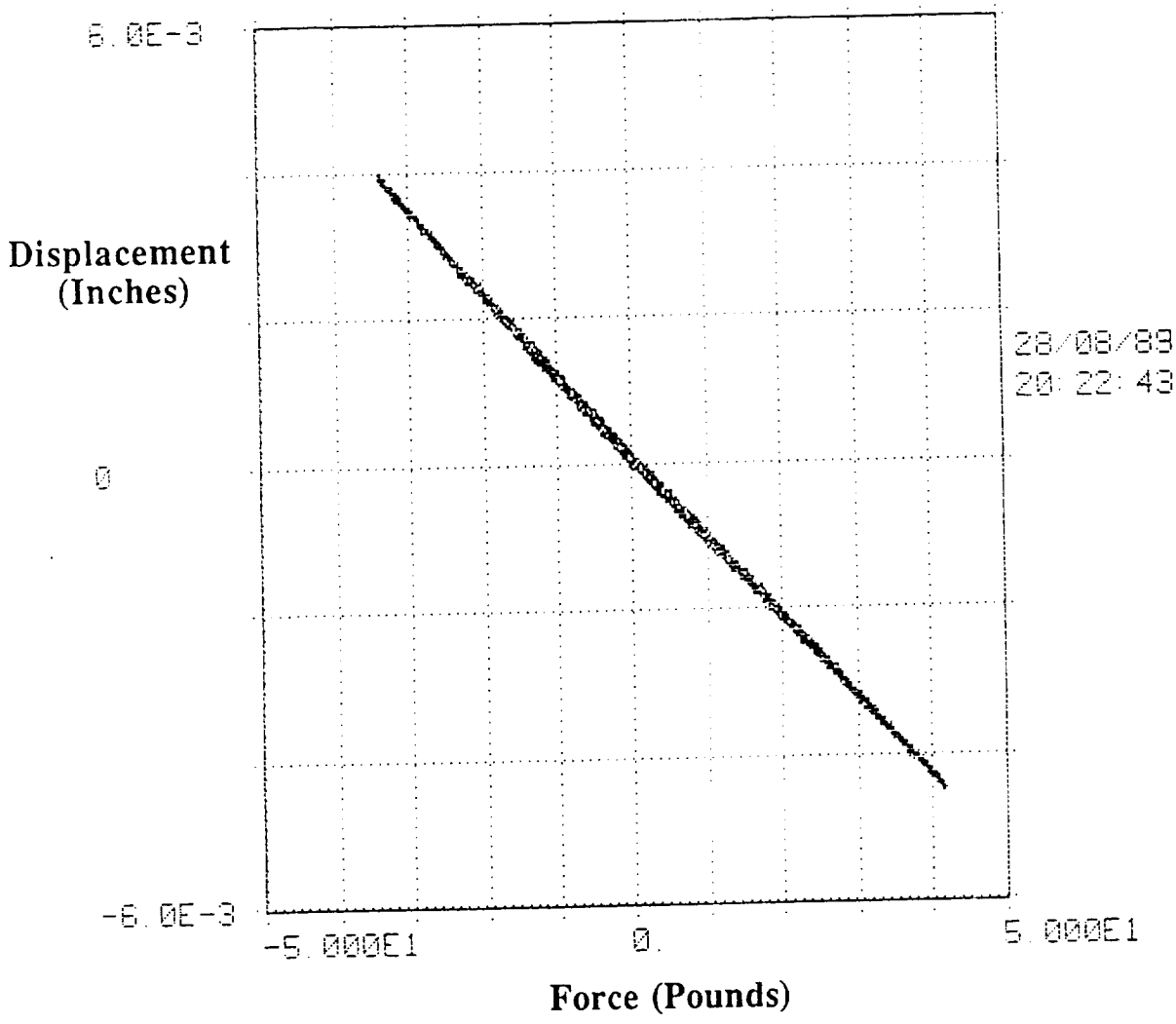

Diagonal test 7, excitation at 1 Hz

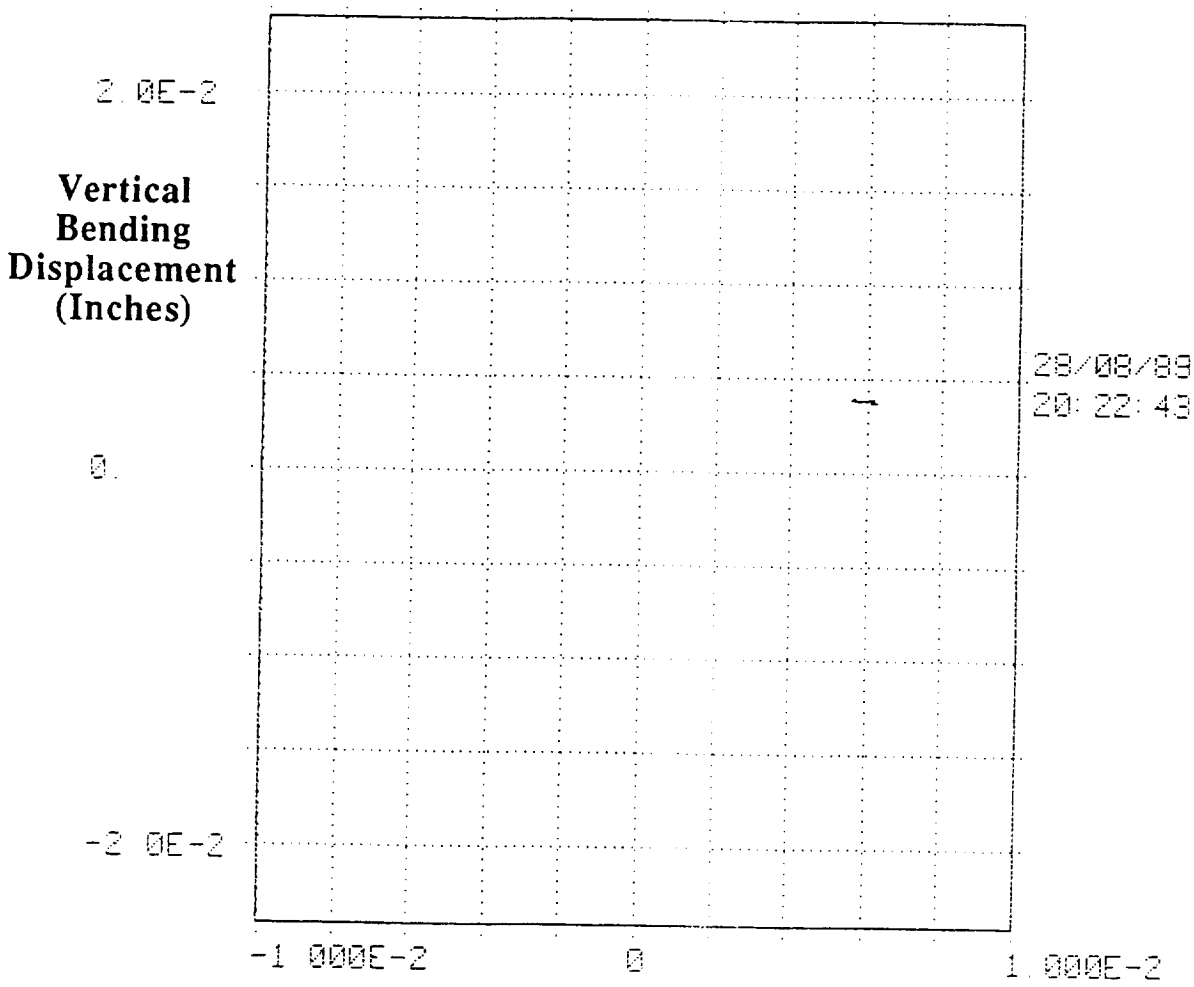

Diagonal test 7, excitation at 1 Hz

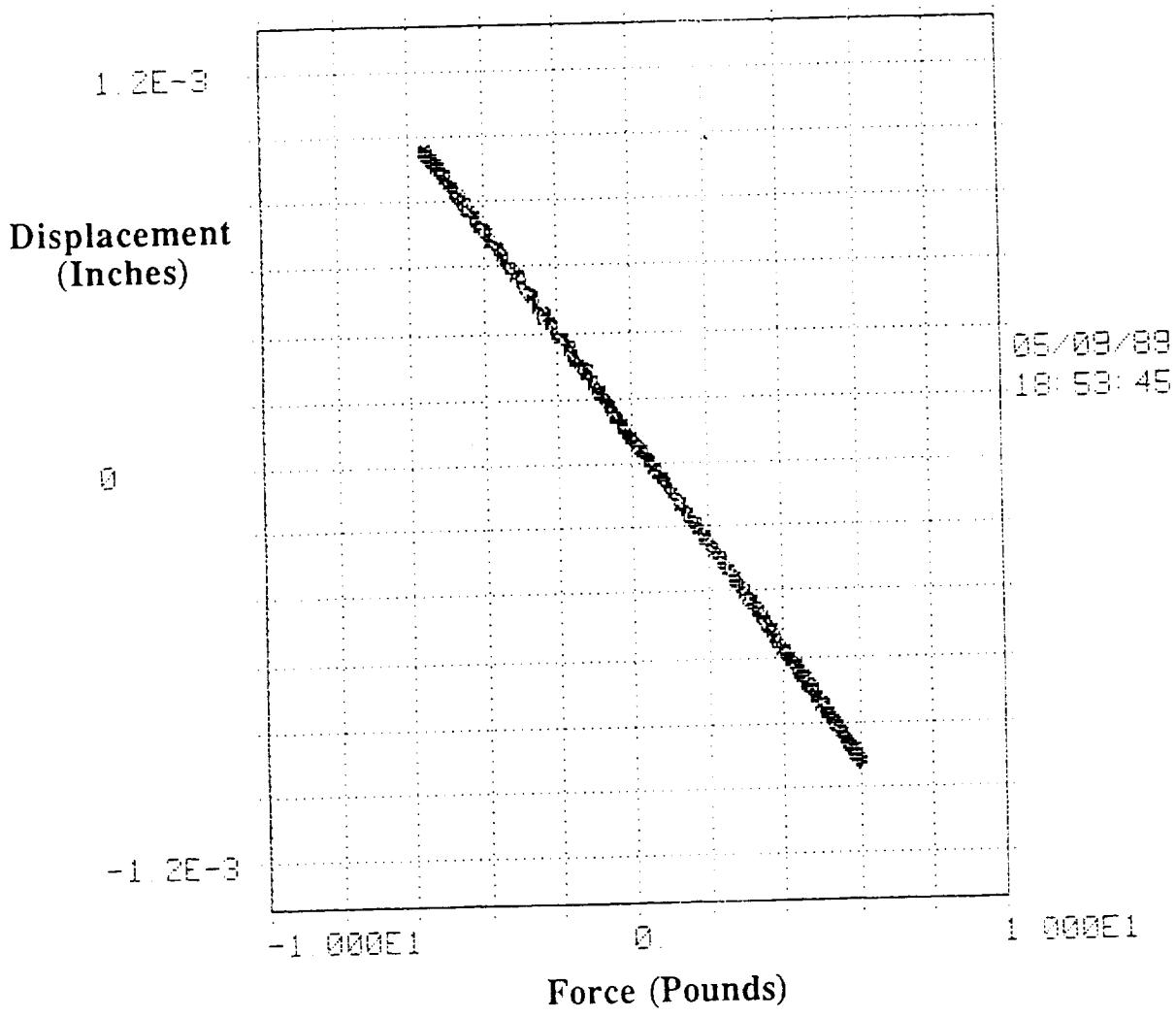

Diagonal test 8D, excitation at 1 Hz

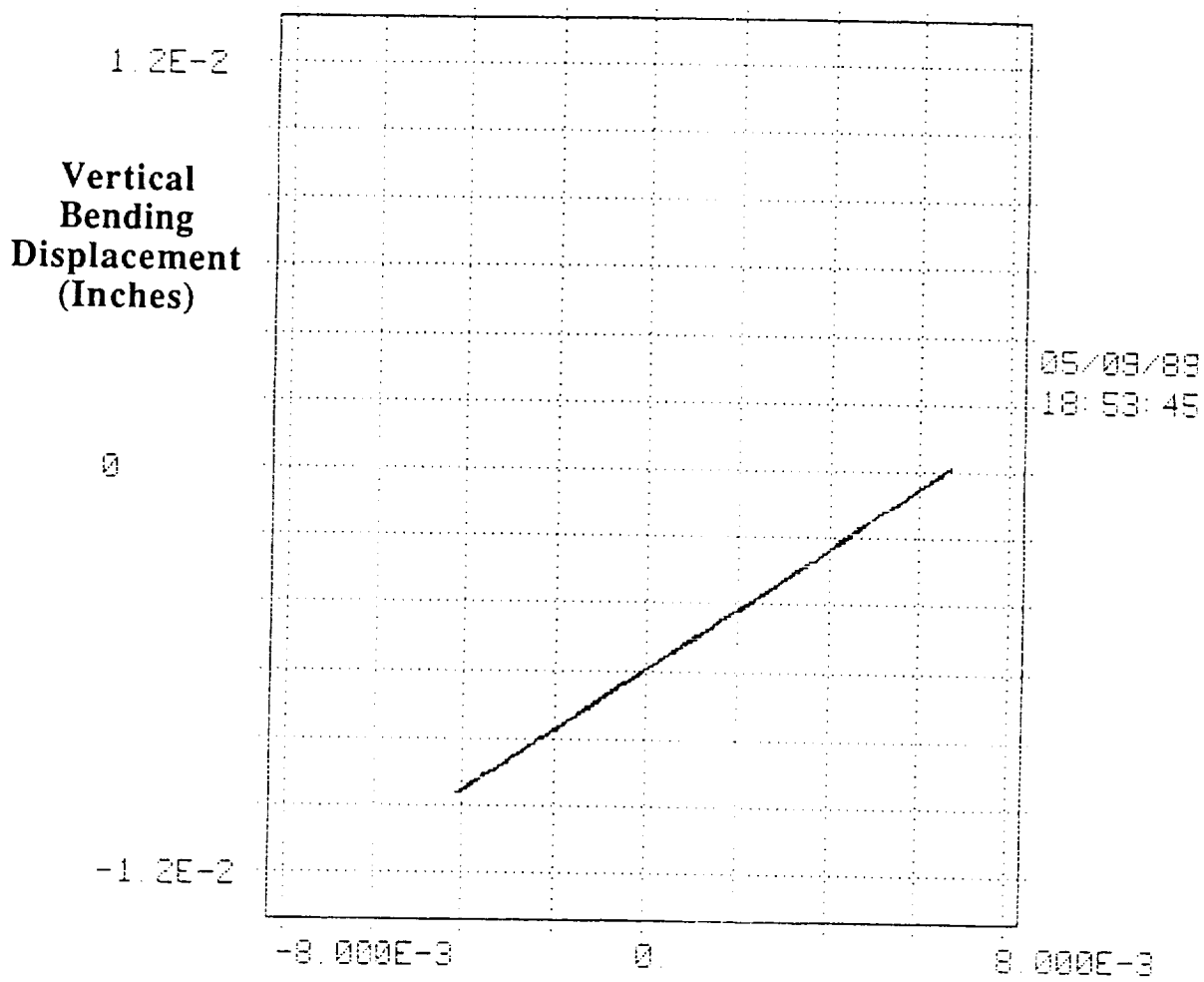

Diagonal test 8D, excitation at 1 Hz

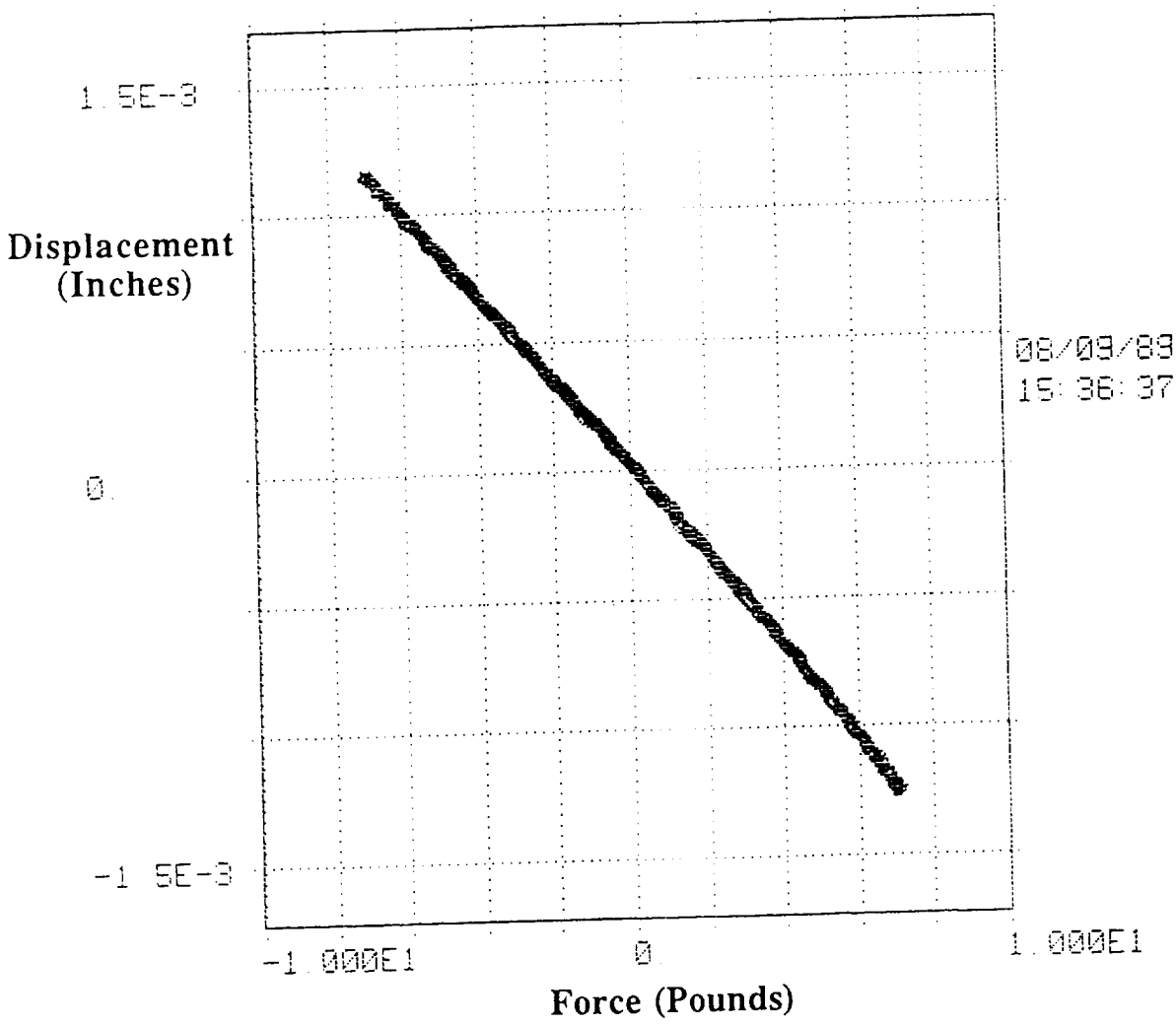

Diagonal test 8D, excitation at 5 Hz

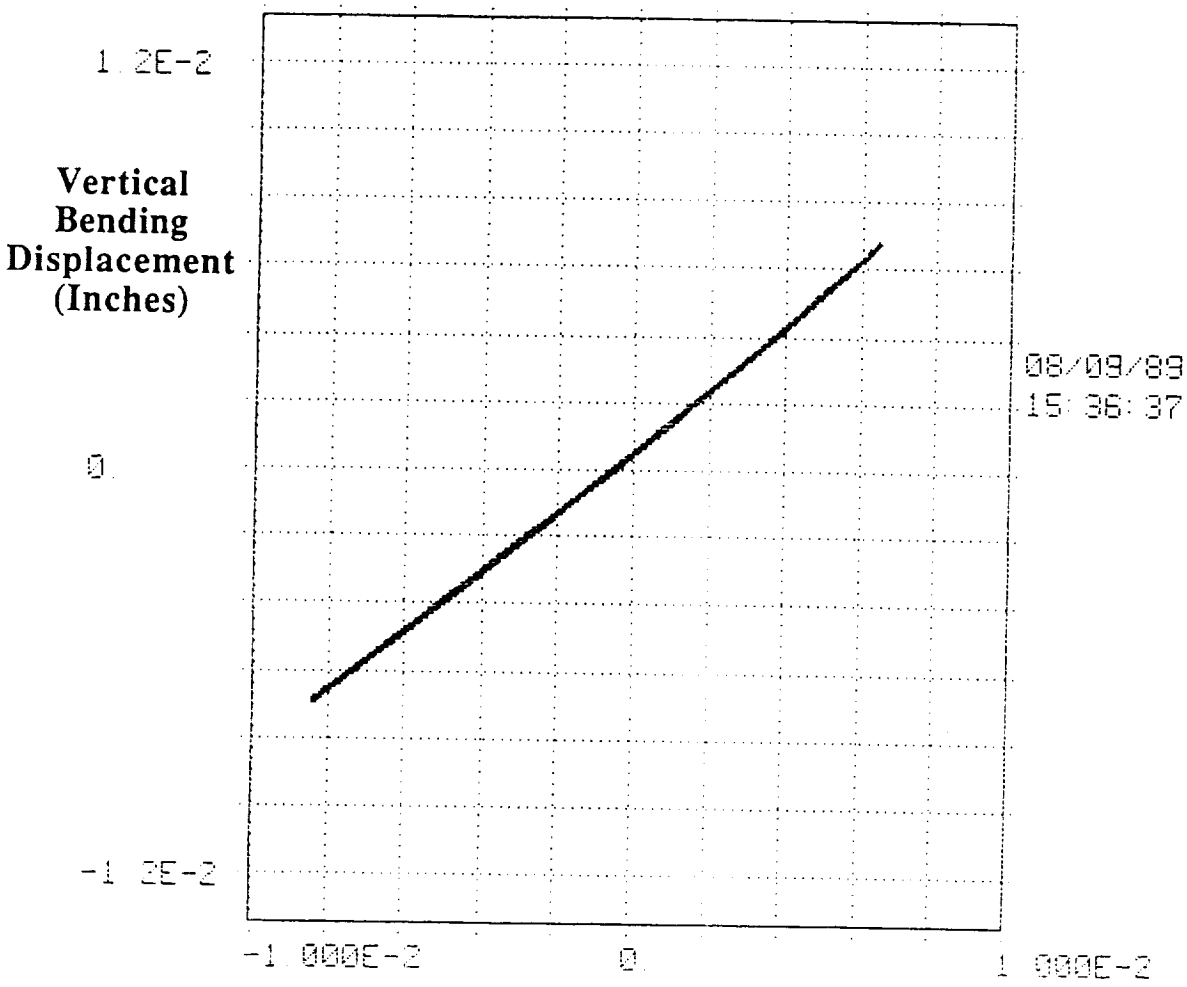

Diagonal test 8D, excitation at 5 Hz

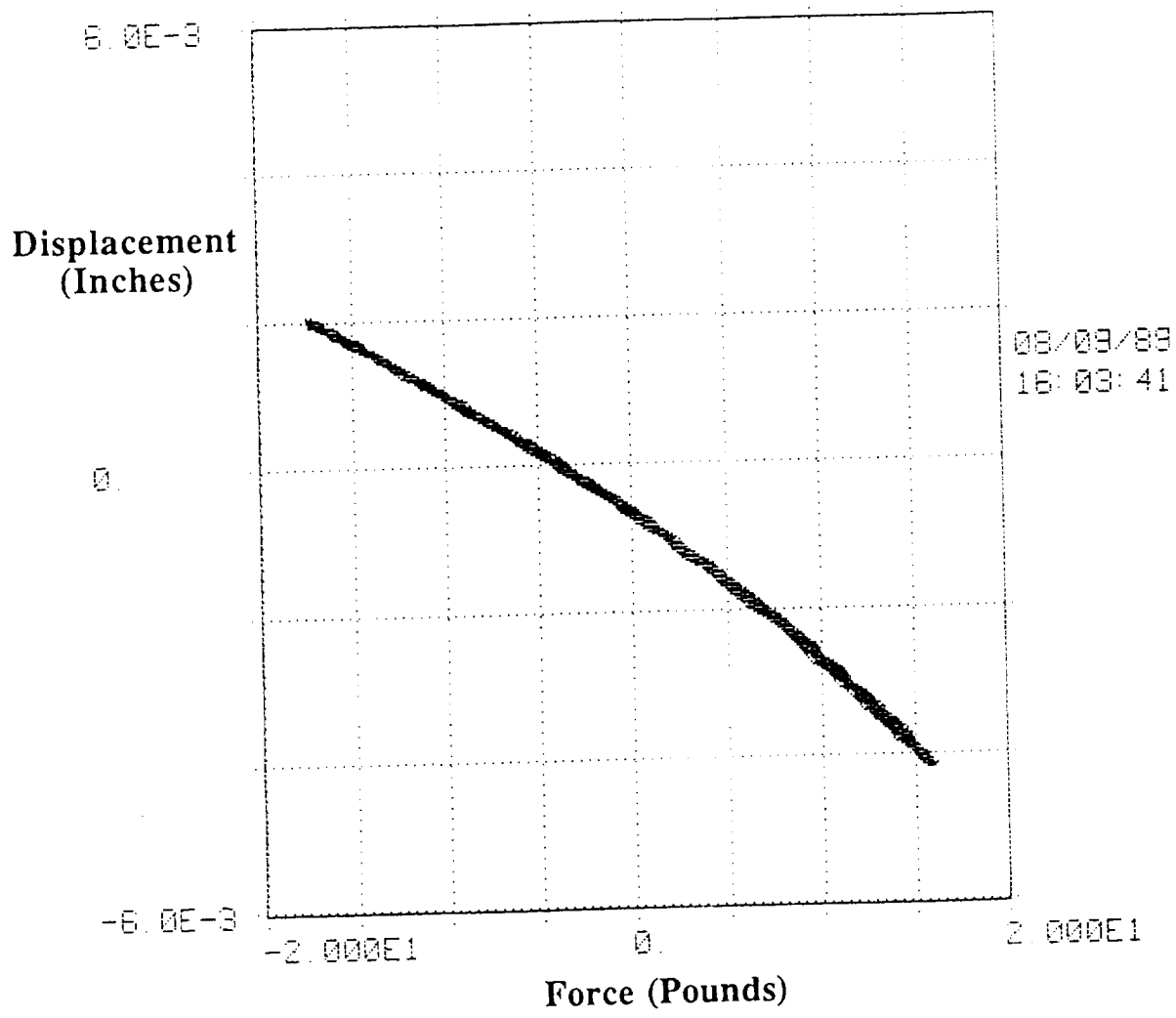

Diagonal test 8D, excitation at 5 Hz

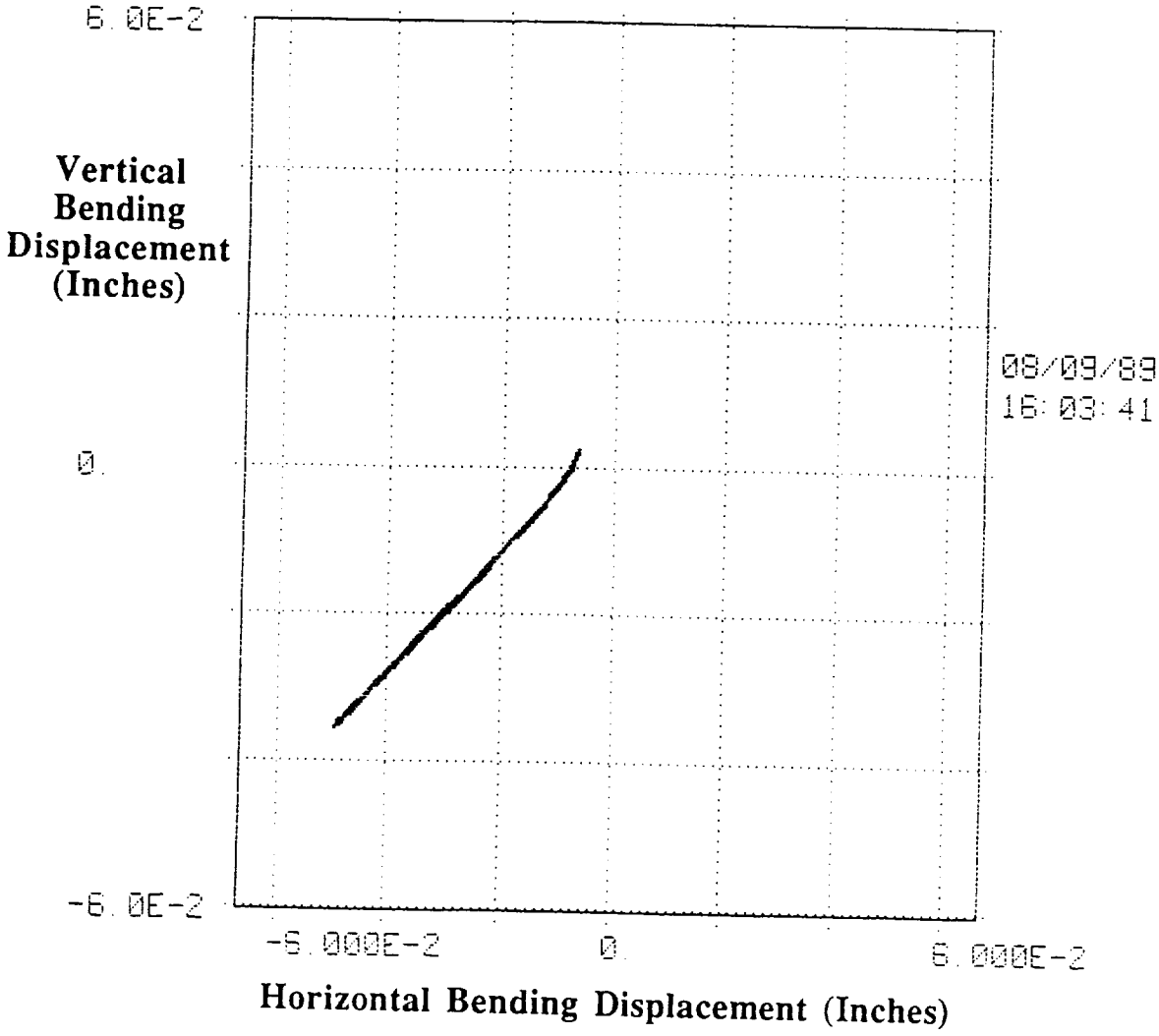

Diagonal test 8D, excitation at 5 Hz

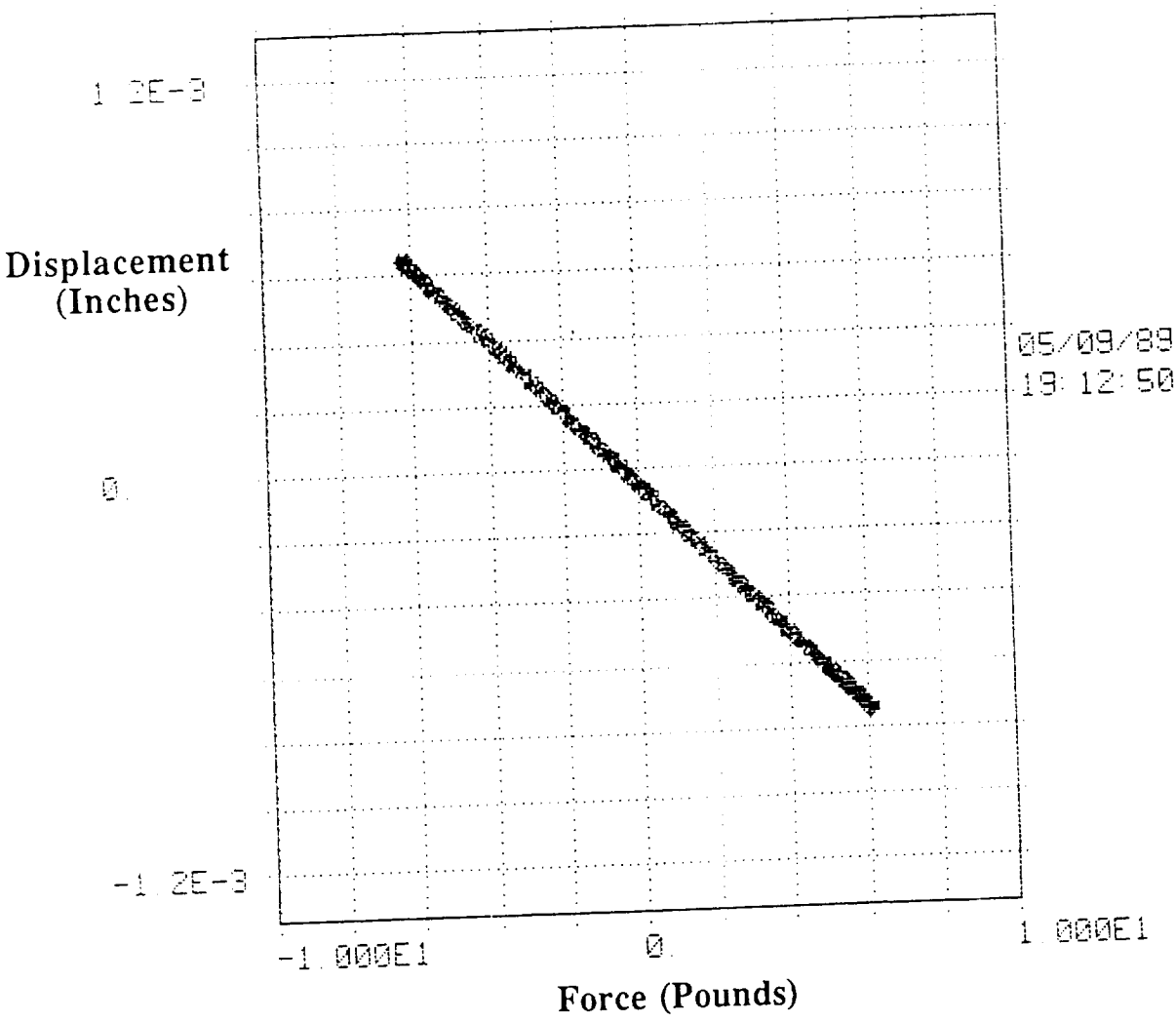

Diagonal test 8E, excitation at 1 Hz

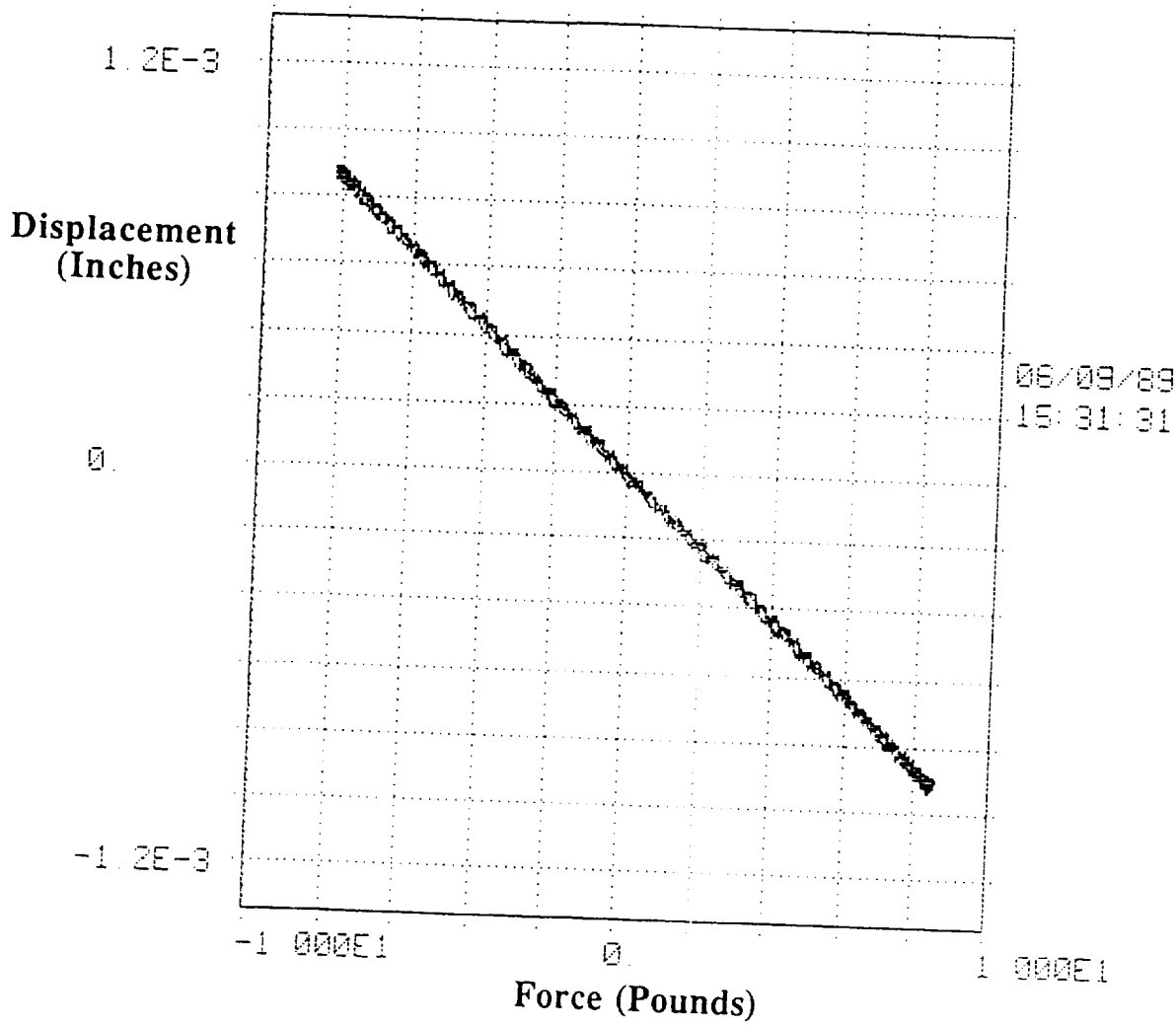

Diagonal test 8F, excitation at 1 Hz

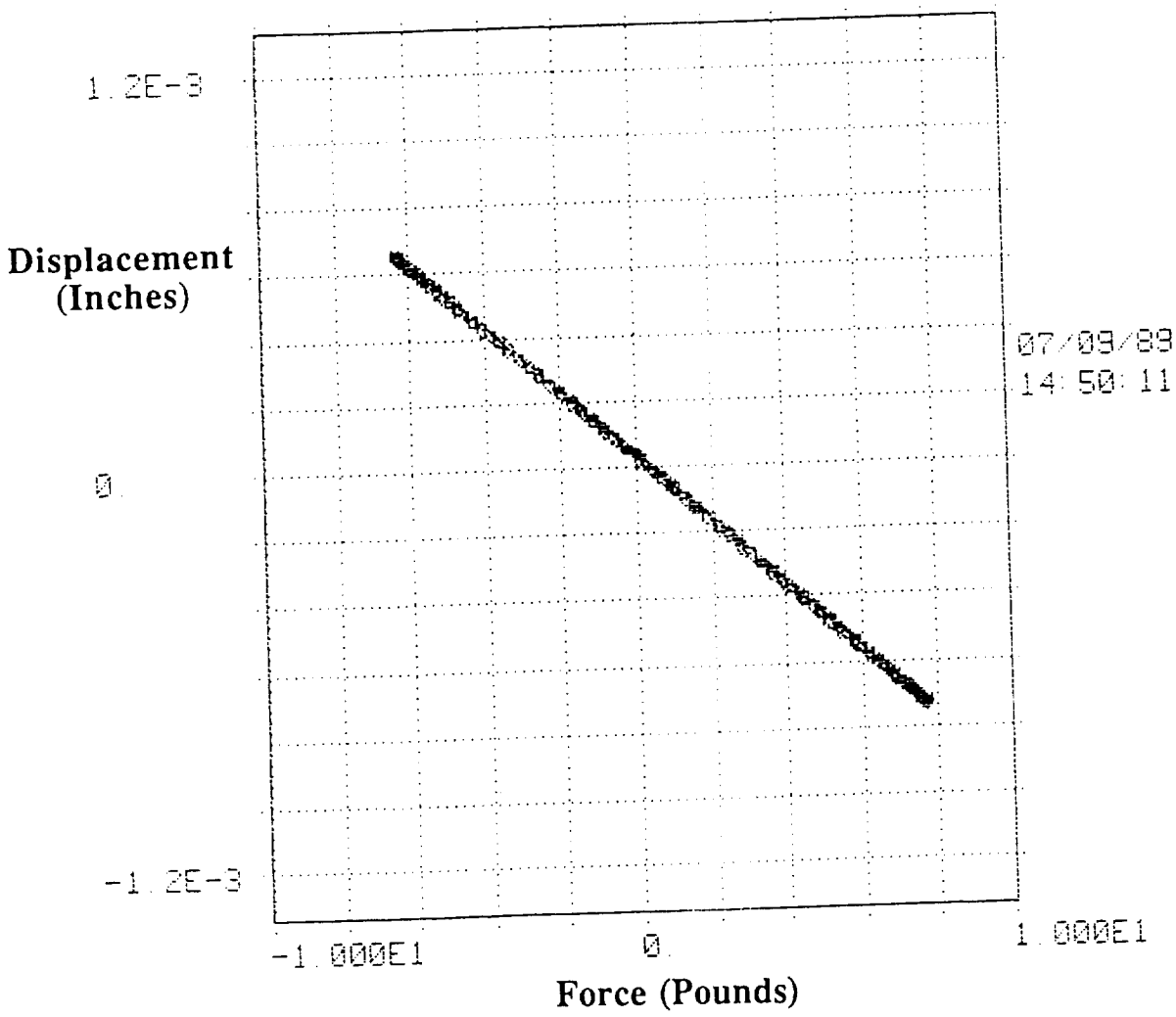

Diagonal test 8G, excitation at 1 Hz

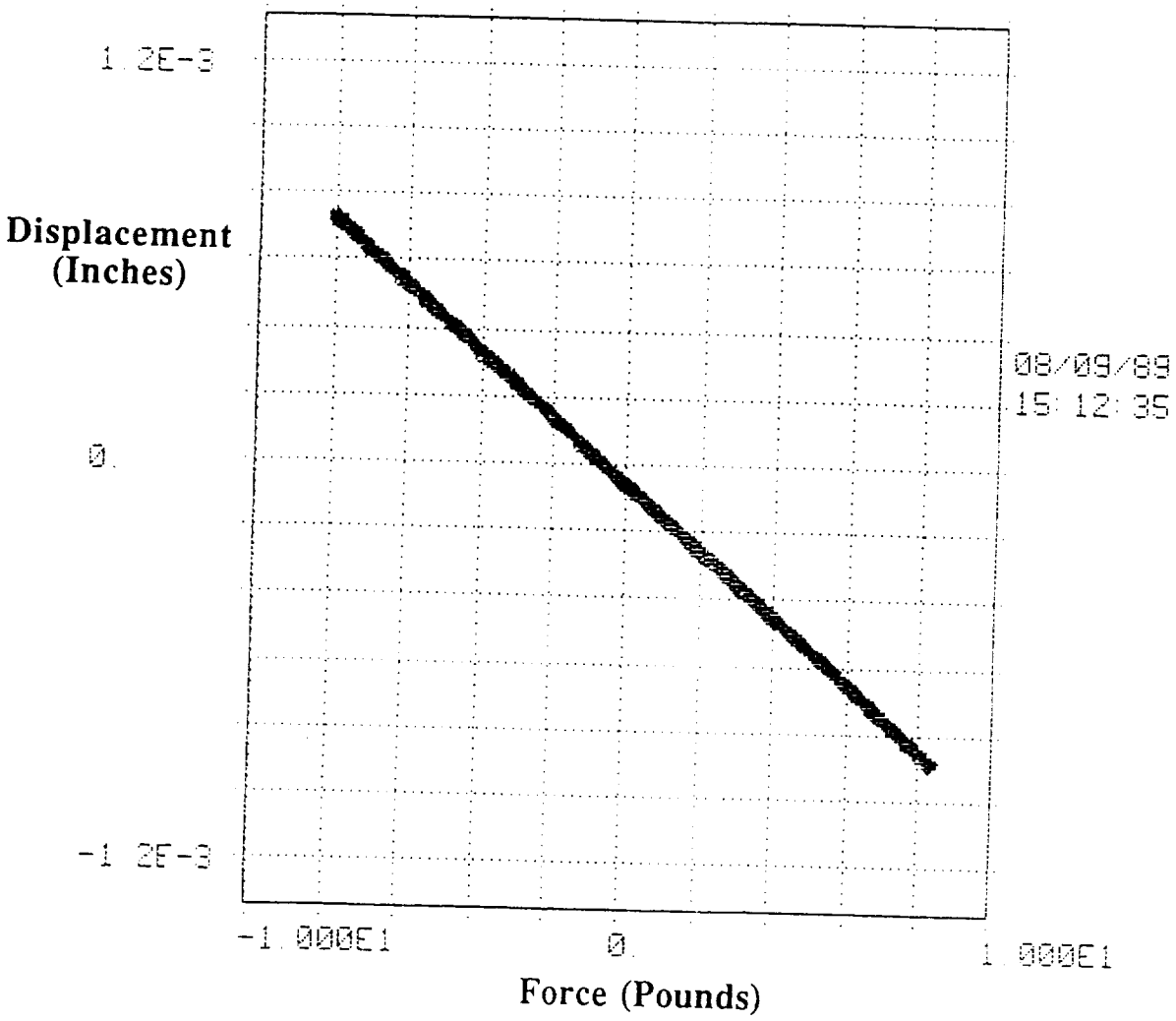

Diagonal test 8G, excitation at 5 Hz

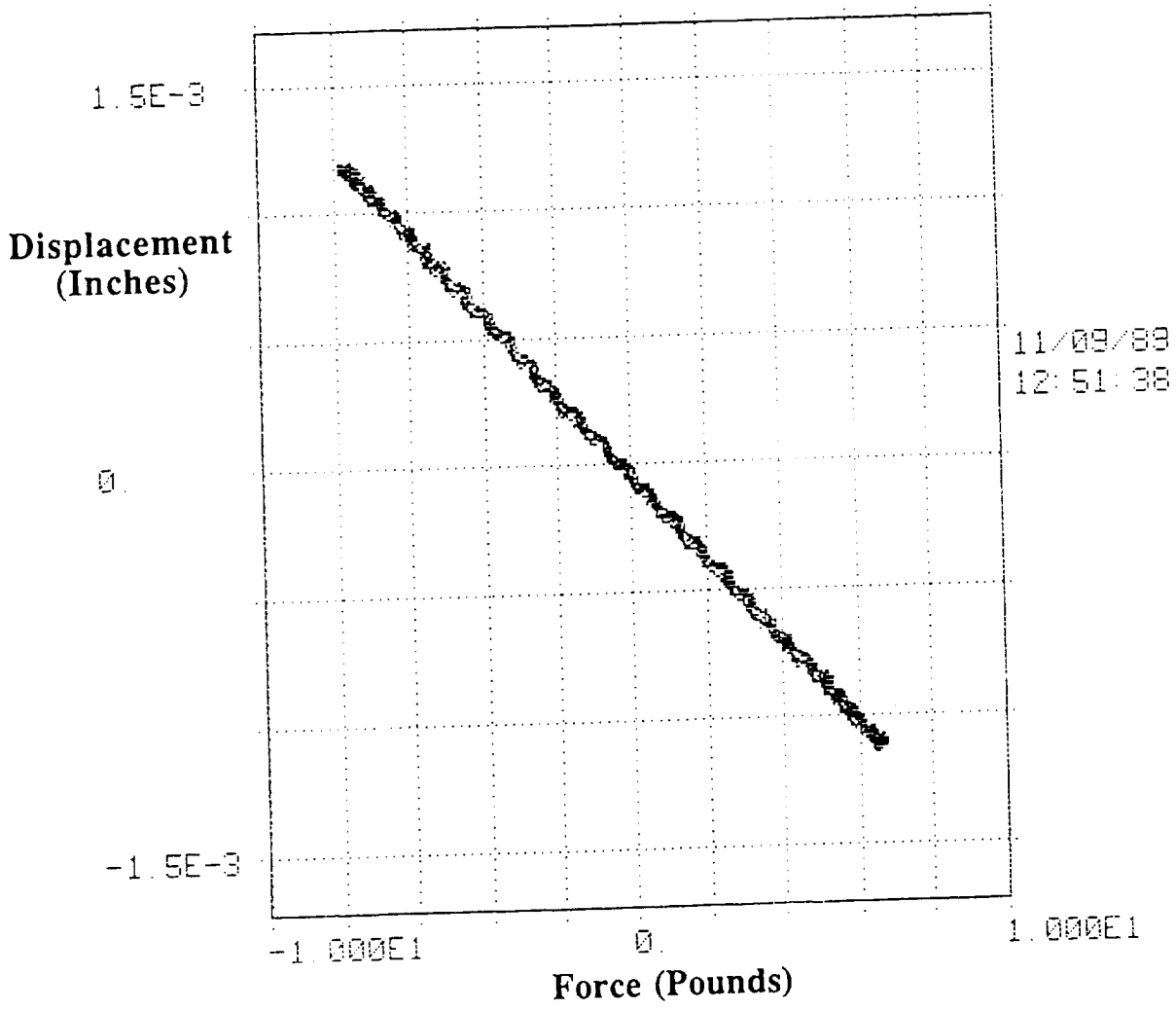

Diagonal test 9A, excitation at 1 Hz

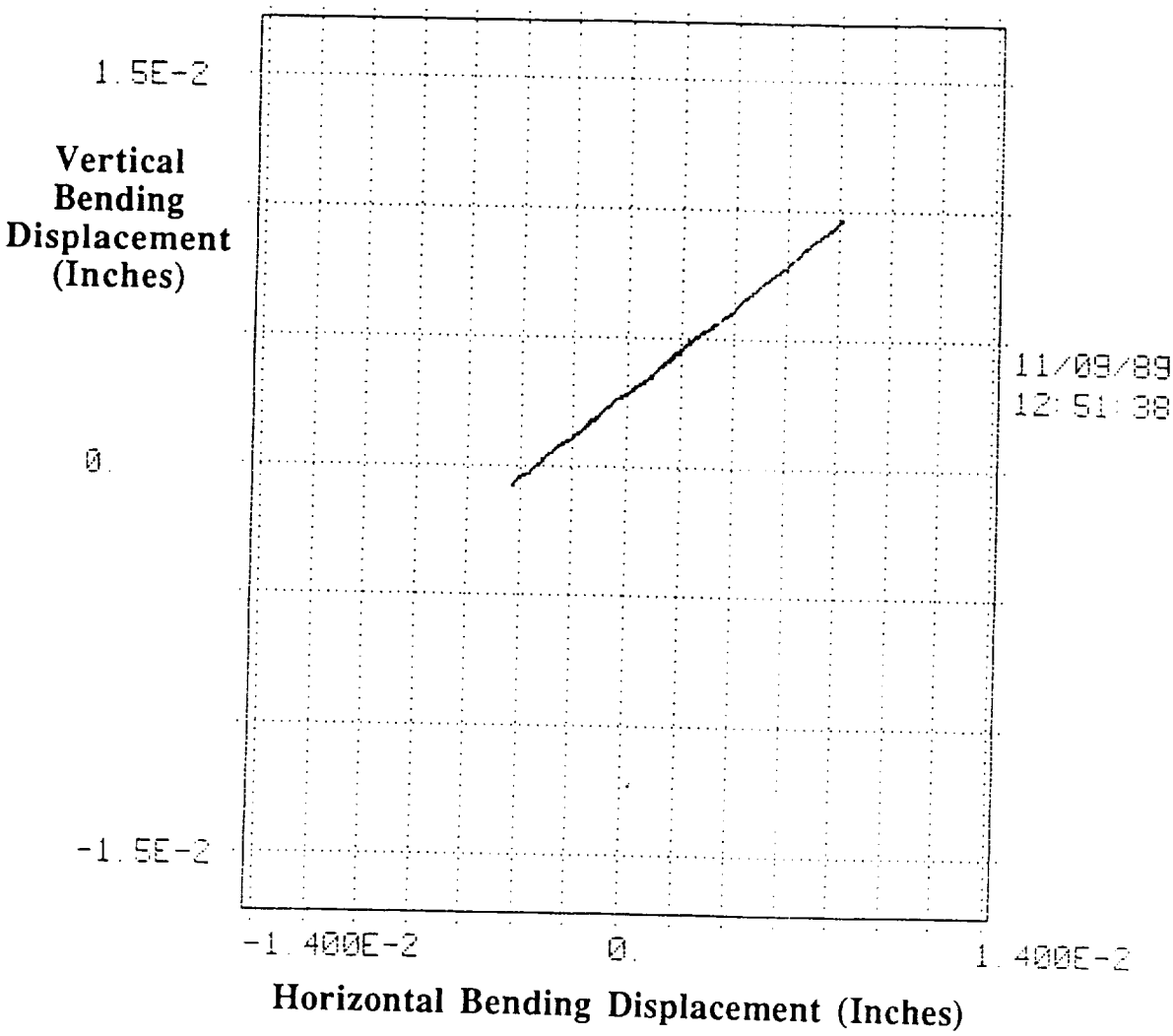

Diagonal test 9A, excitation at 1 Hz

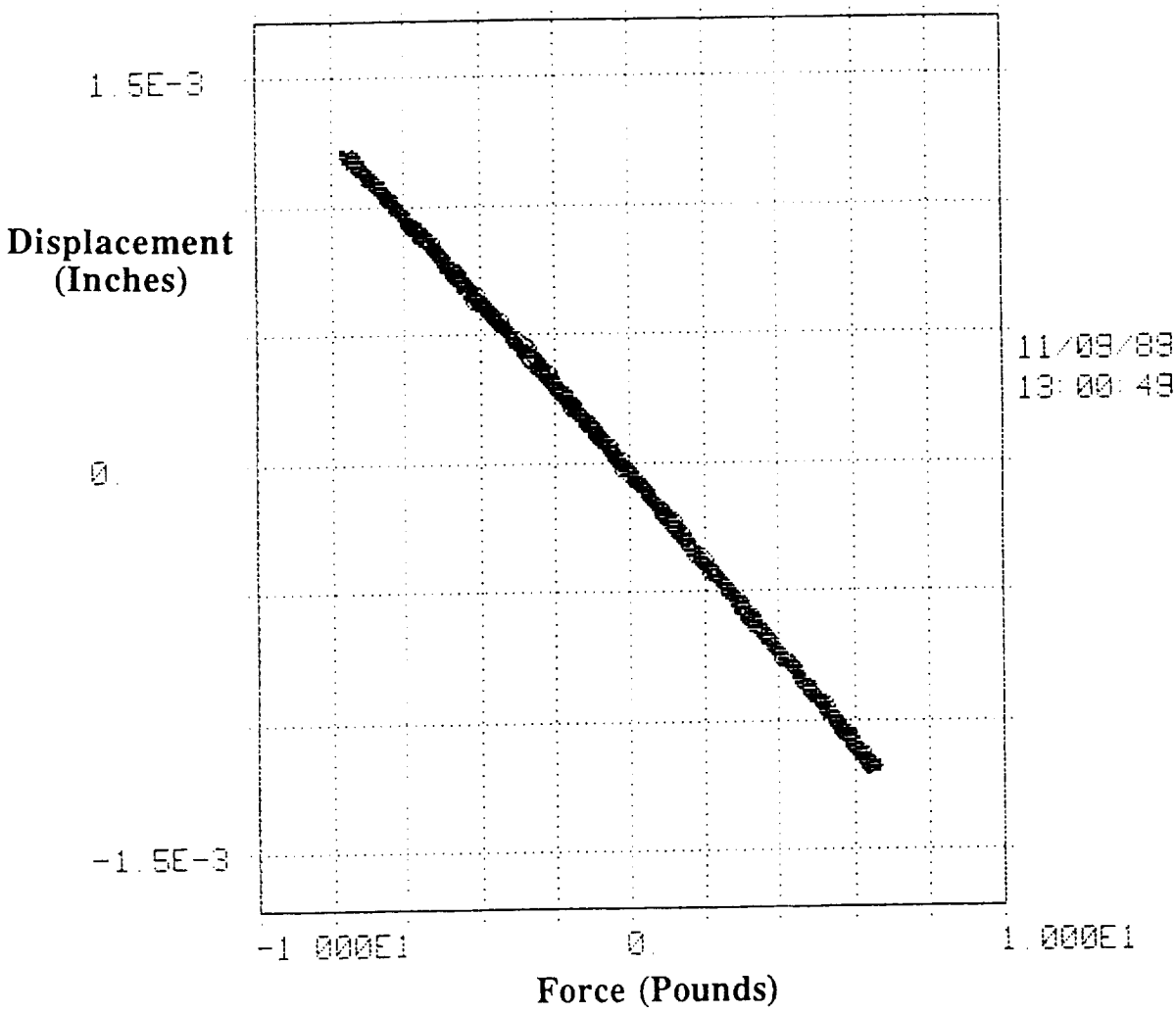

Diagonal test 9A, excitation at 5 Hz

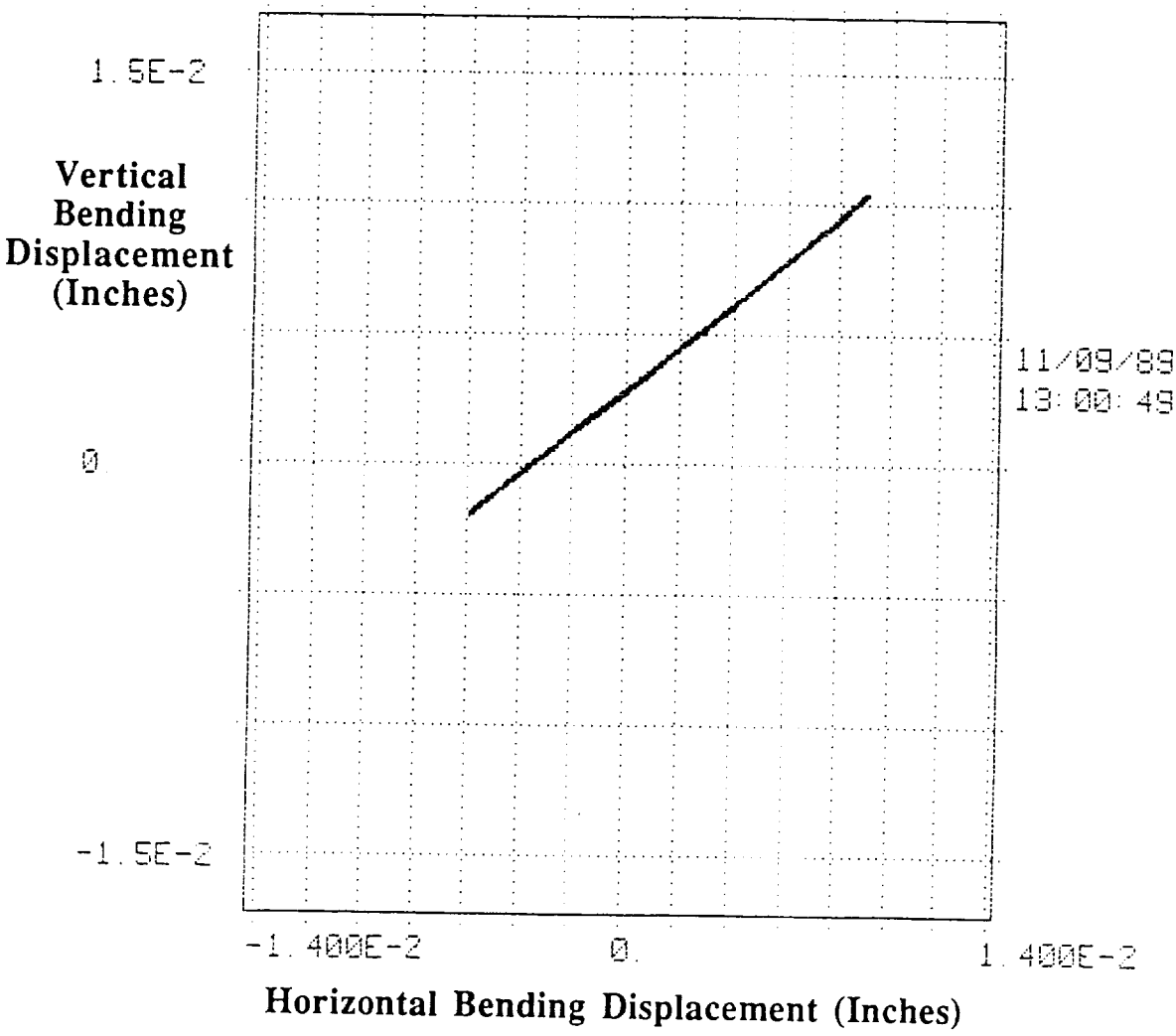

Diagonal test 9A, excitation at 5 Hz

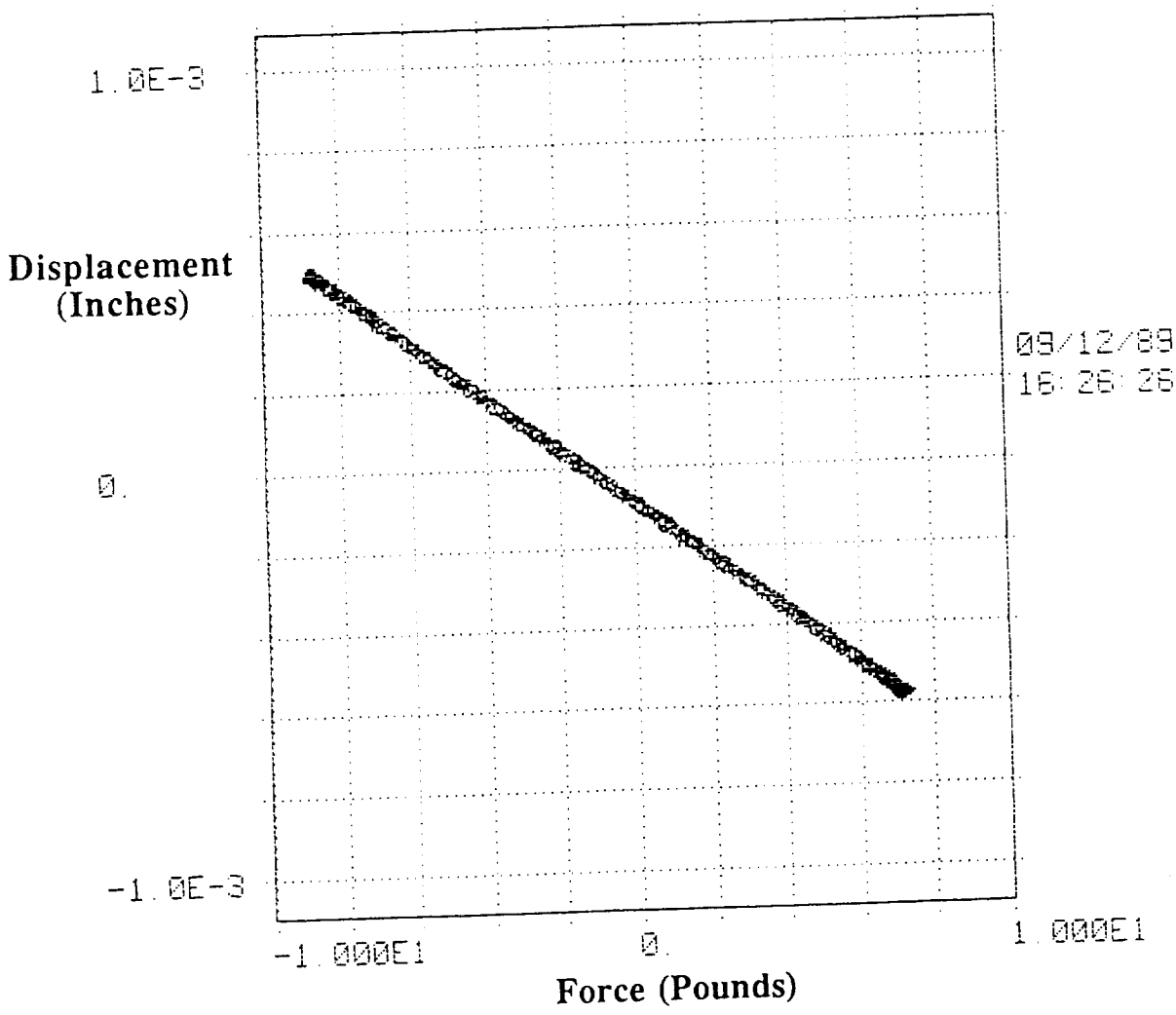

Diagonal test 10A, excitation at 1 Hz

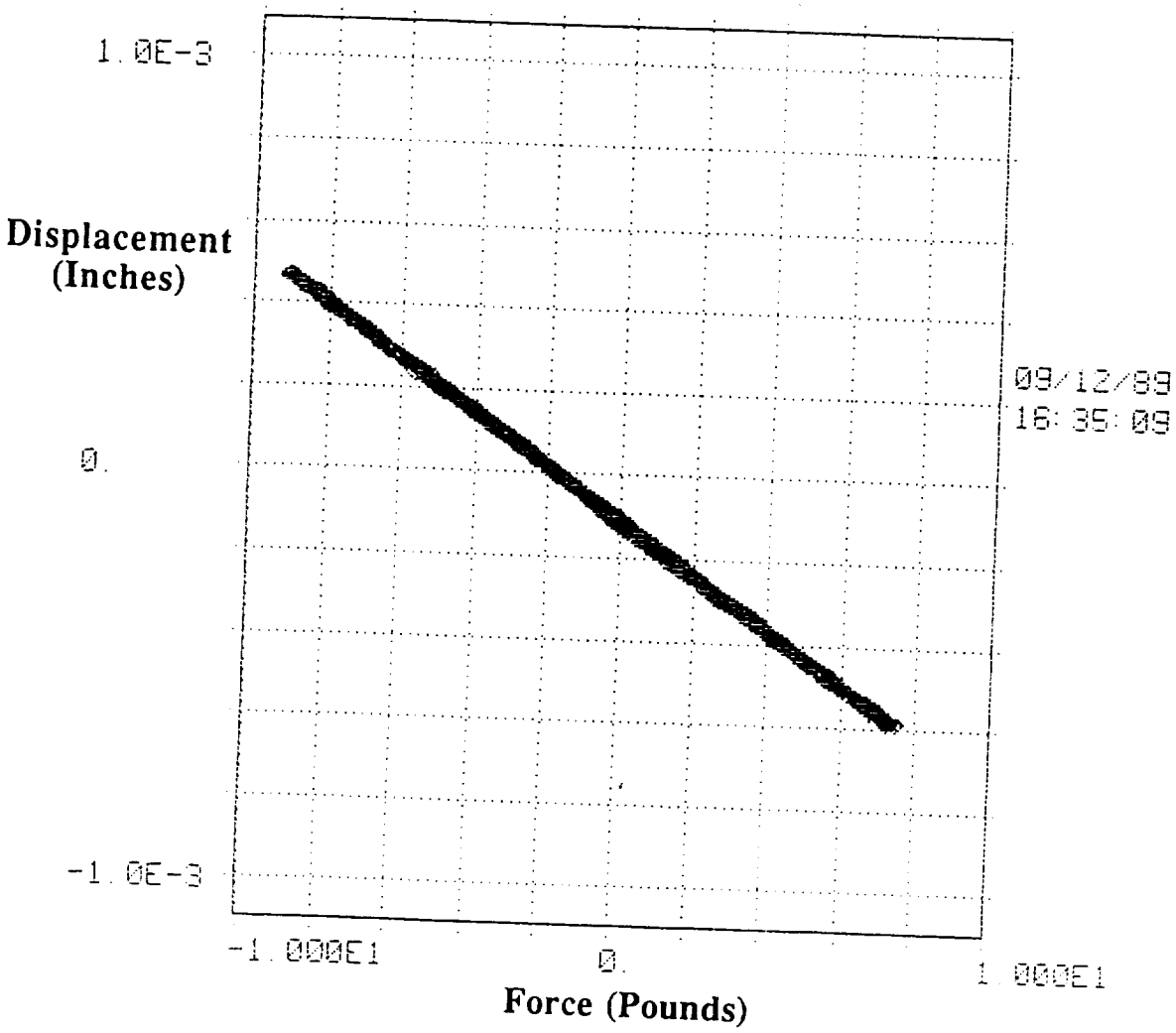

Diagonal test 10A, excitation at 5 Hz

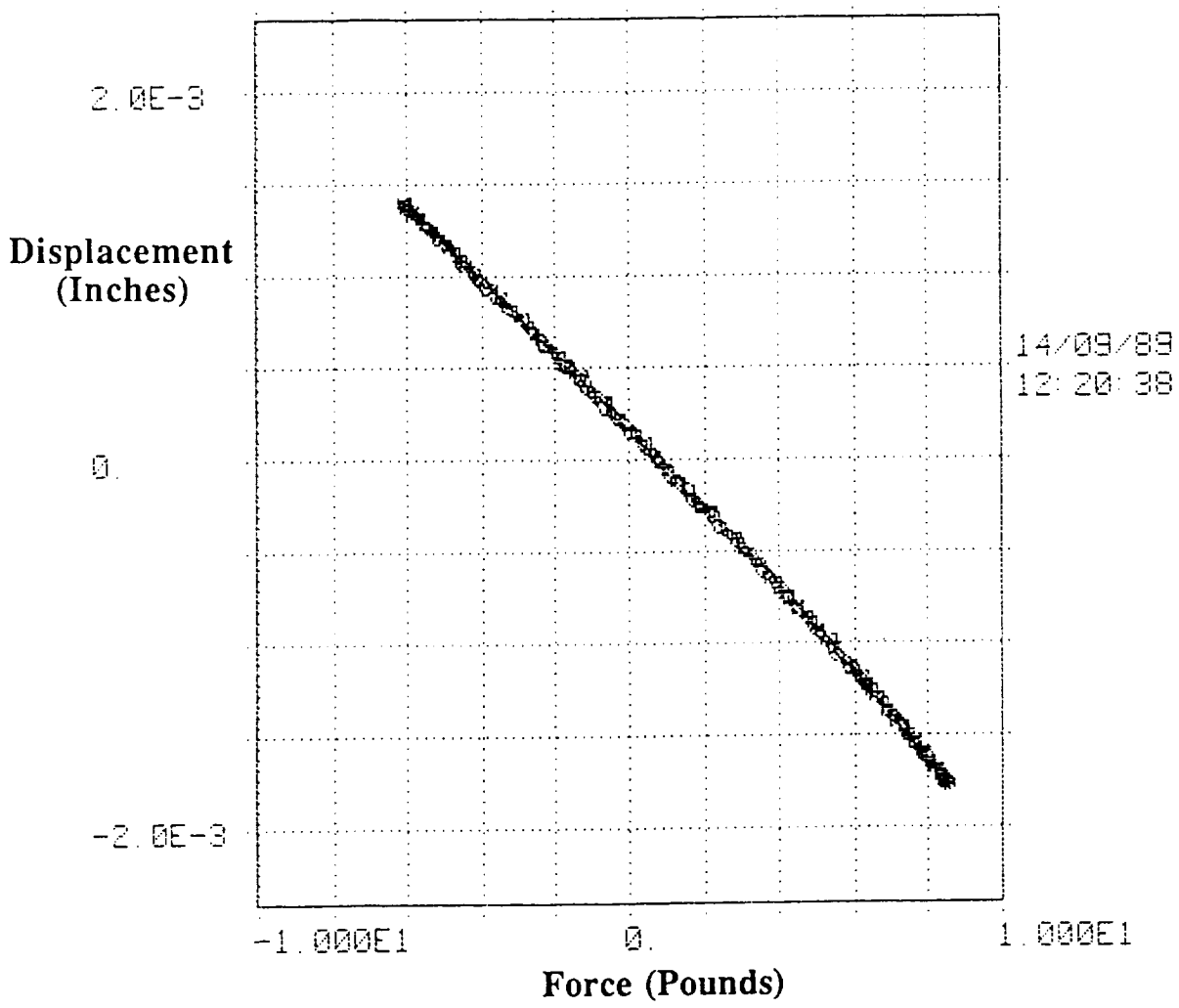

Diagonal test 11, excitation at 1 Hz

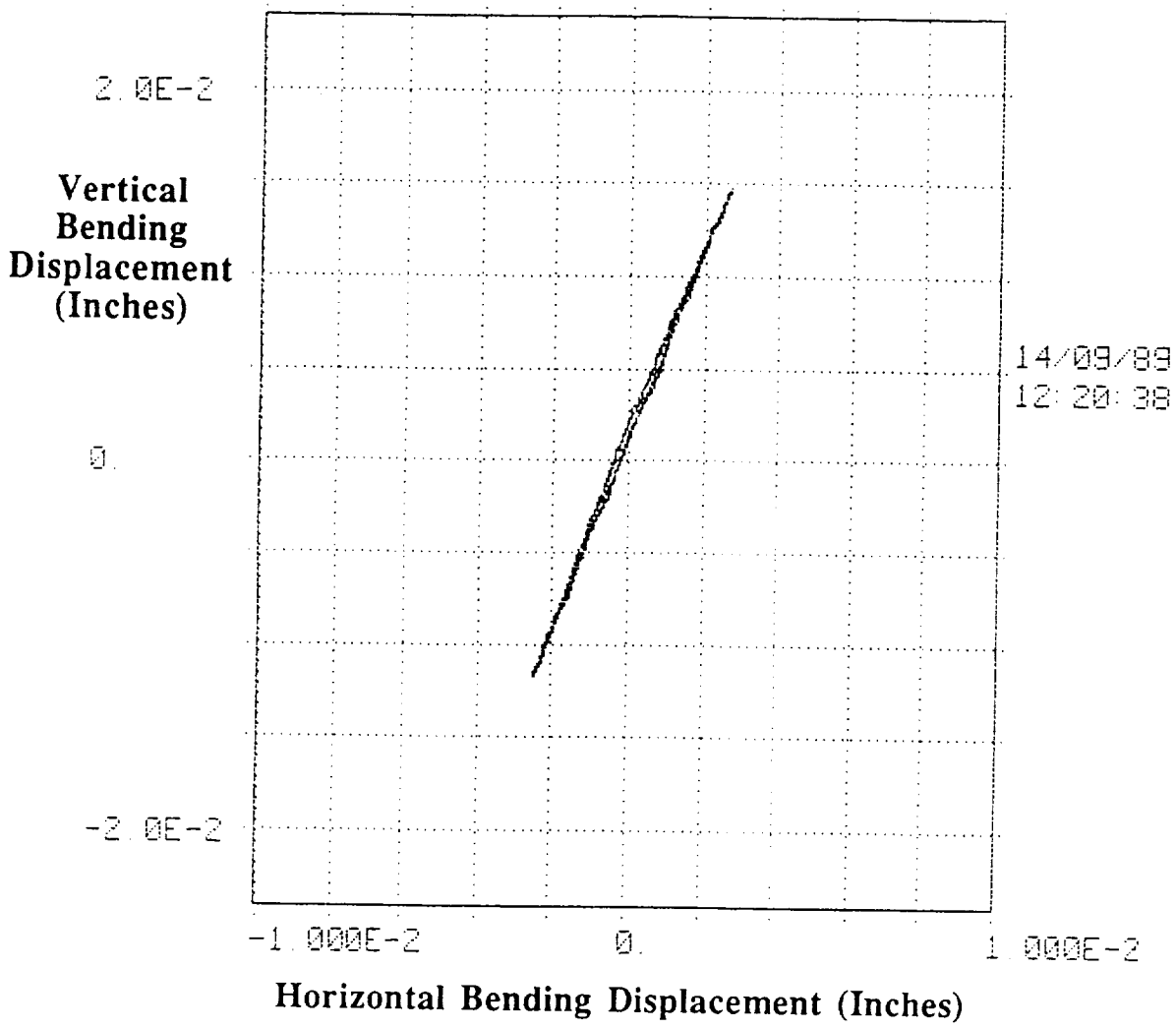

Diagonal test 11, excitation at 1 Hz

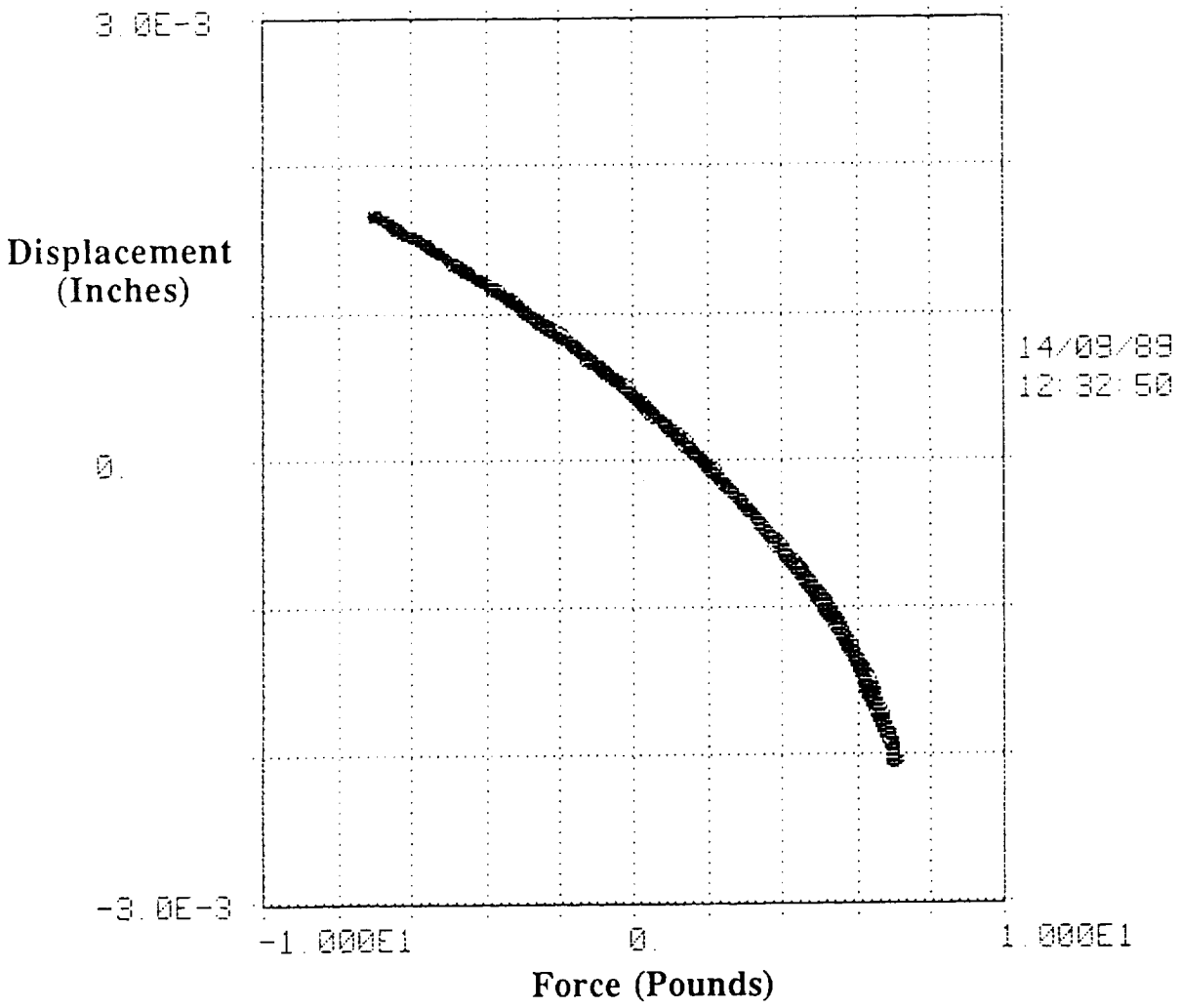

Diagonal test 11, excitation at 5 Hz

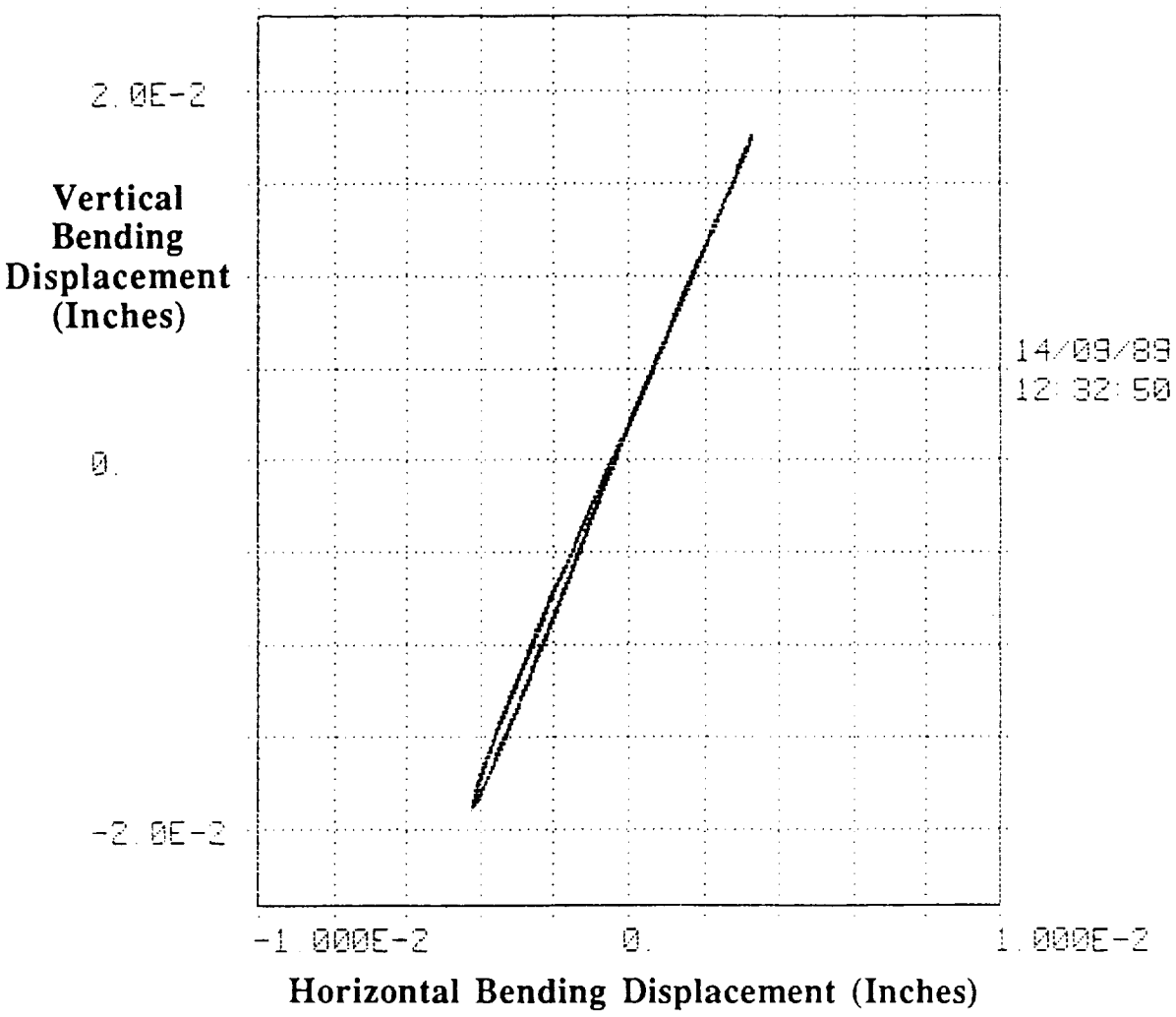

Diagonal test 11, excitation at 5 Hz

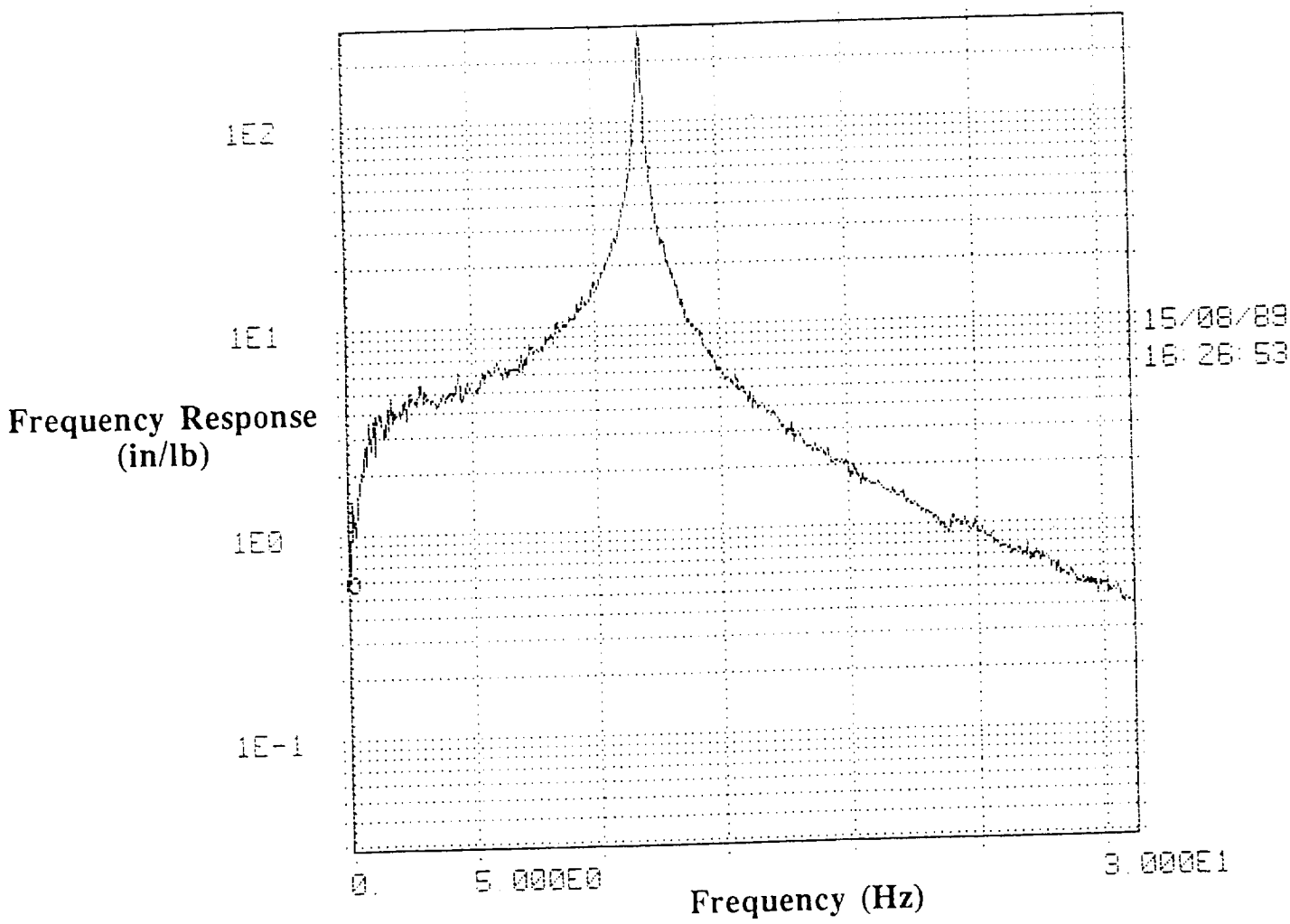

Diagonal test 3, horizontal direction

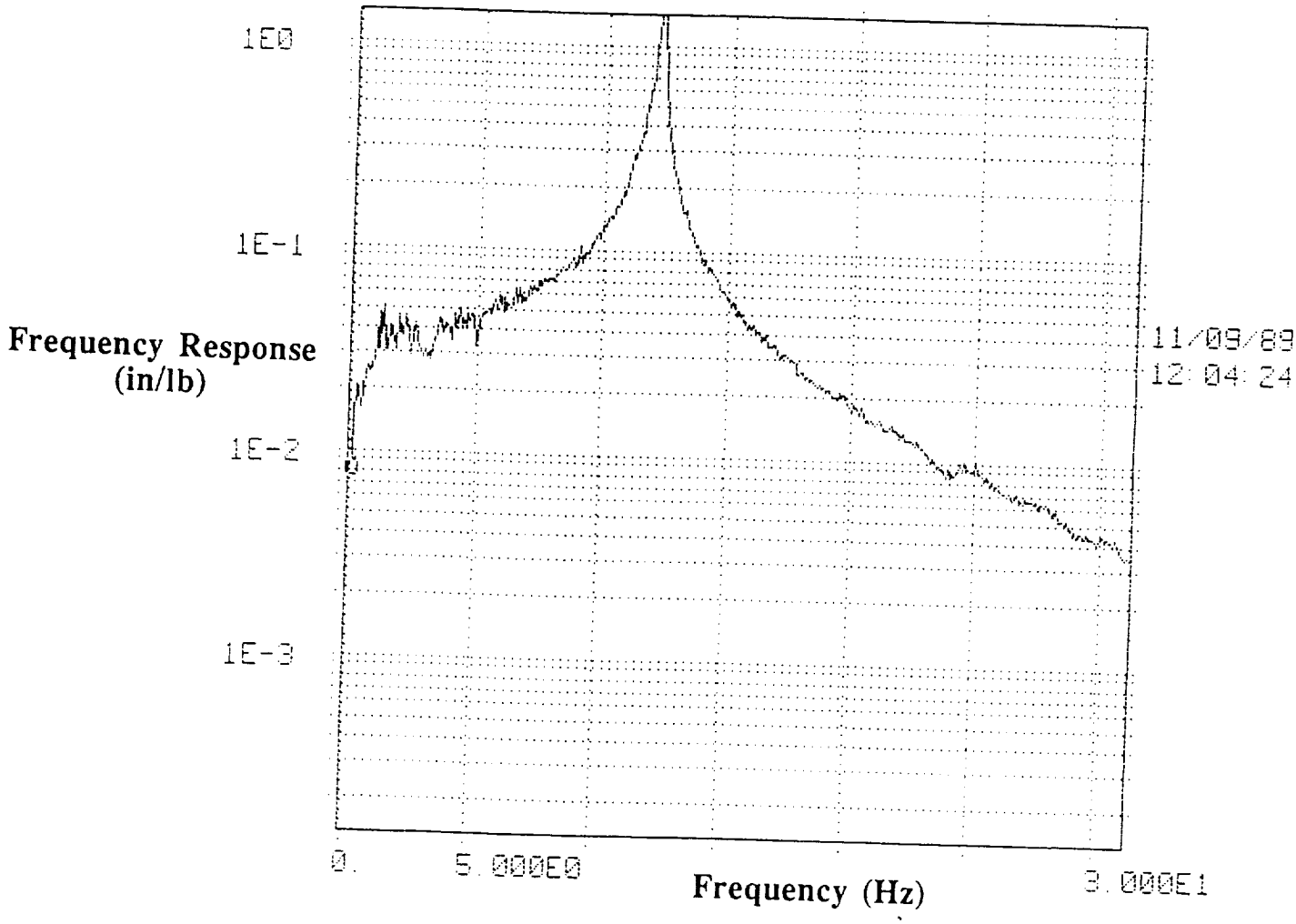

Diagonal test 9, horizontal direction

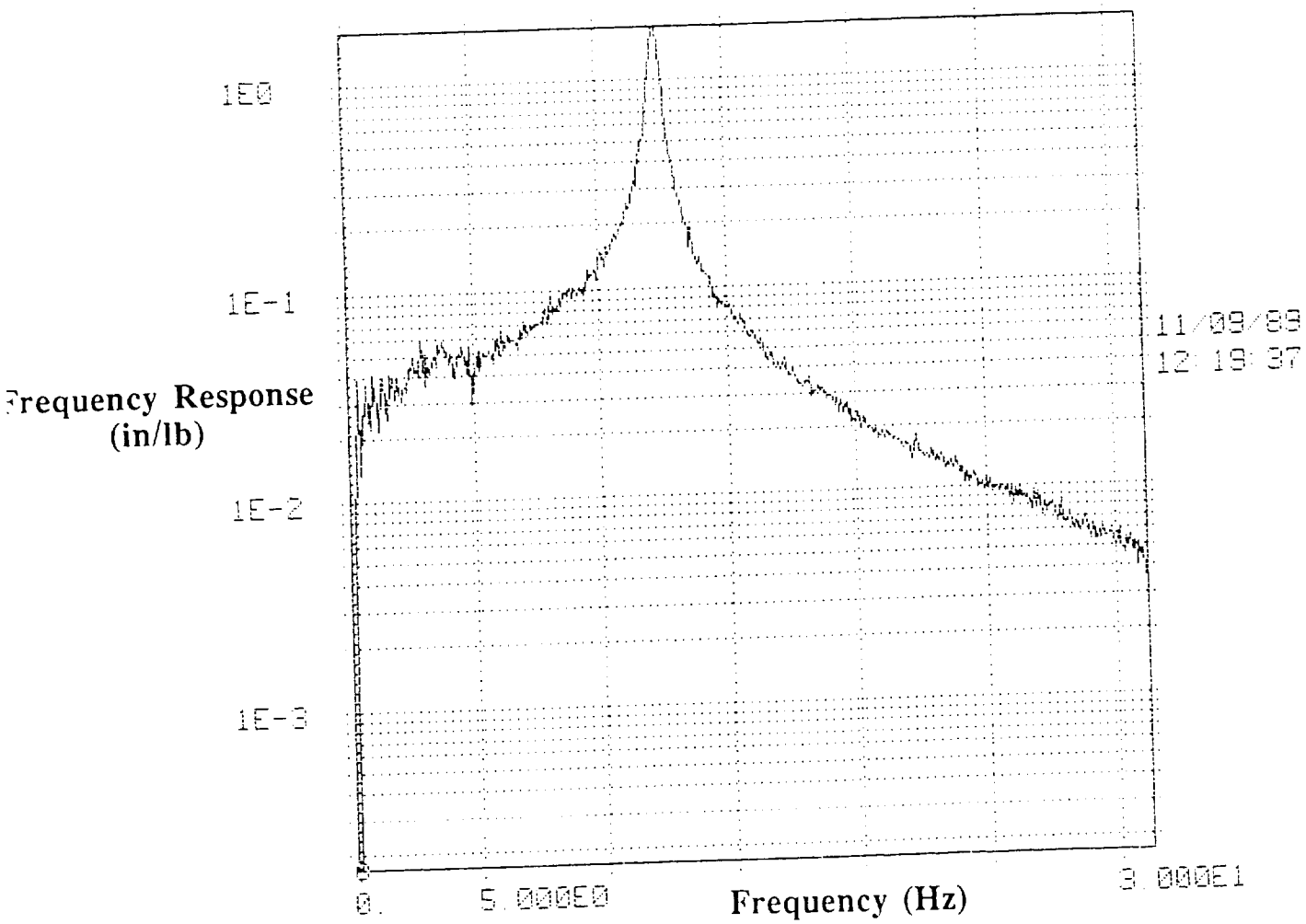

Diagonal test 9, vertical direction

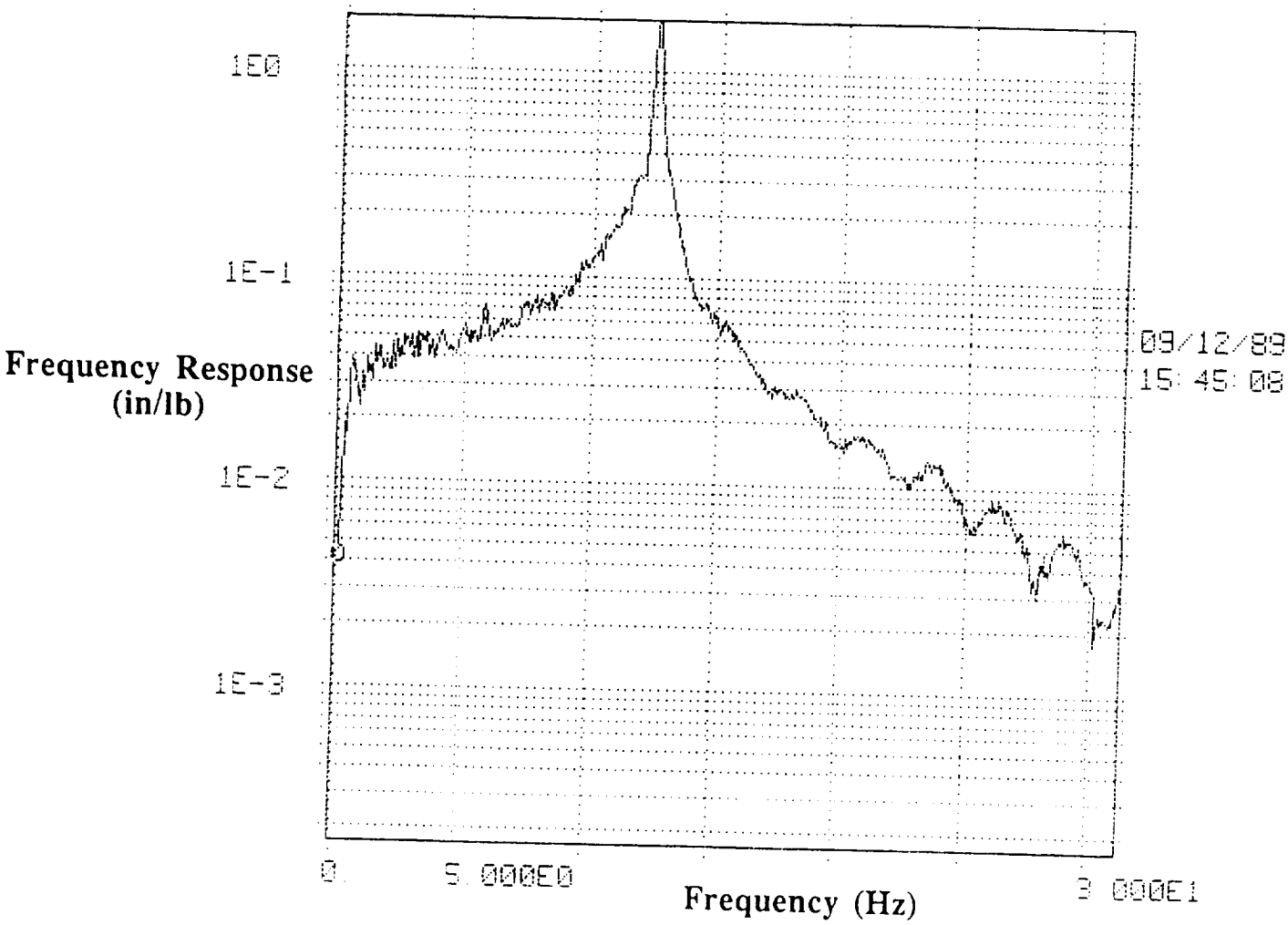

Diagonal test 10, horizontal direction

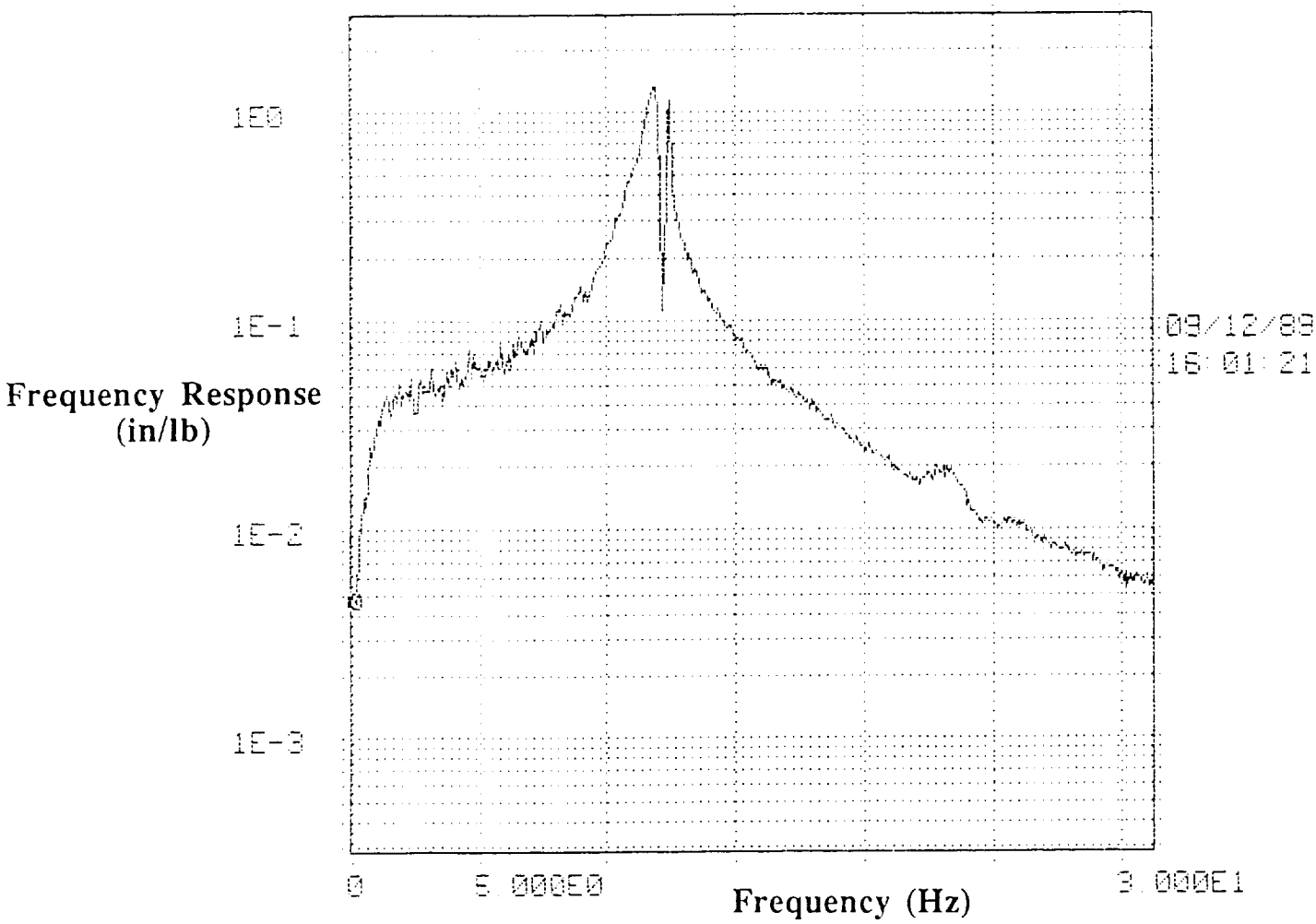

Diagonal test 10, vertical direction

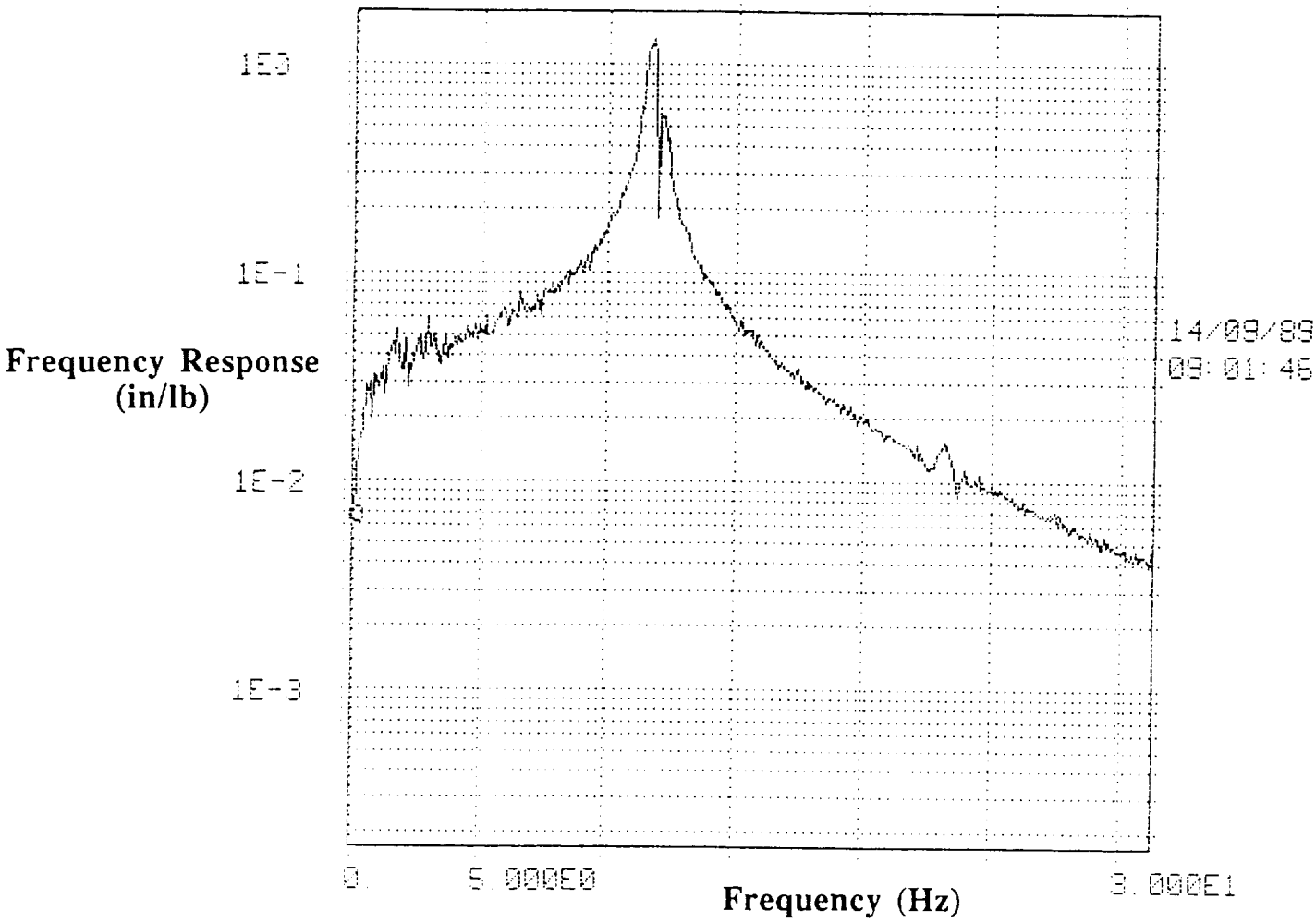

Diagonal test 11, horizontal direction

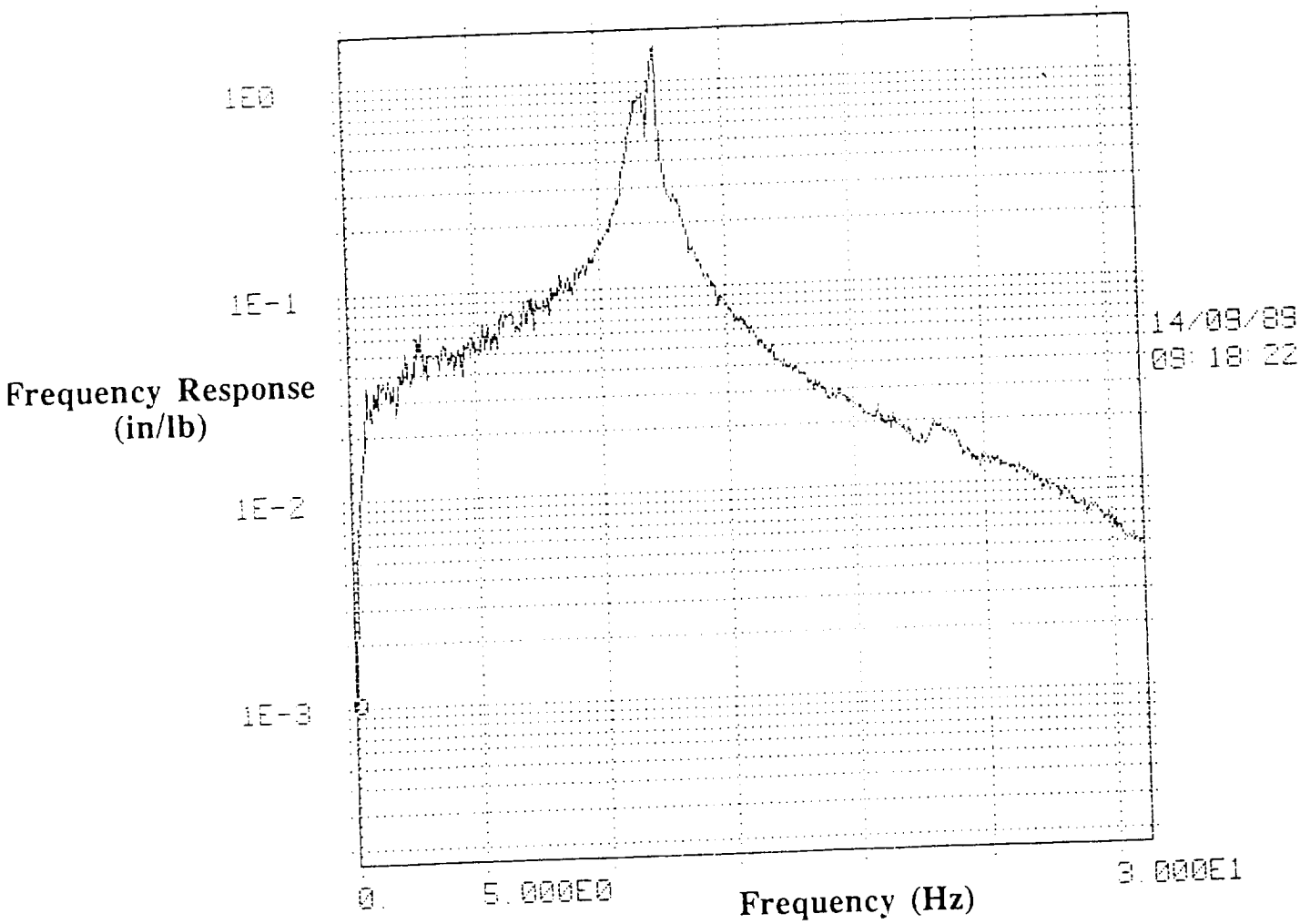

Diagonal test 11, vertical direction

Appendix B

(Taken from Ref. 4 pages 92-139)

PAGE 146 INTENTIONALLY BLANK

PRECEDING PAGE BLANK NOT FILMED

Appendix B
Mini-Mast Longeron Test Results

PRECEDING PAGE BLANK NOT FILMED

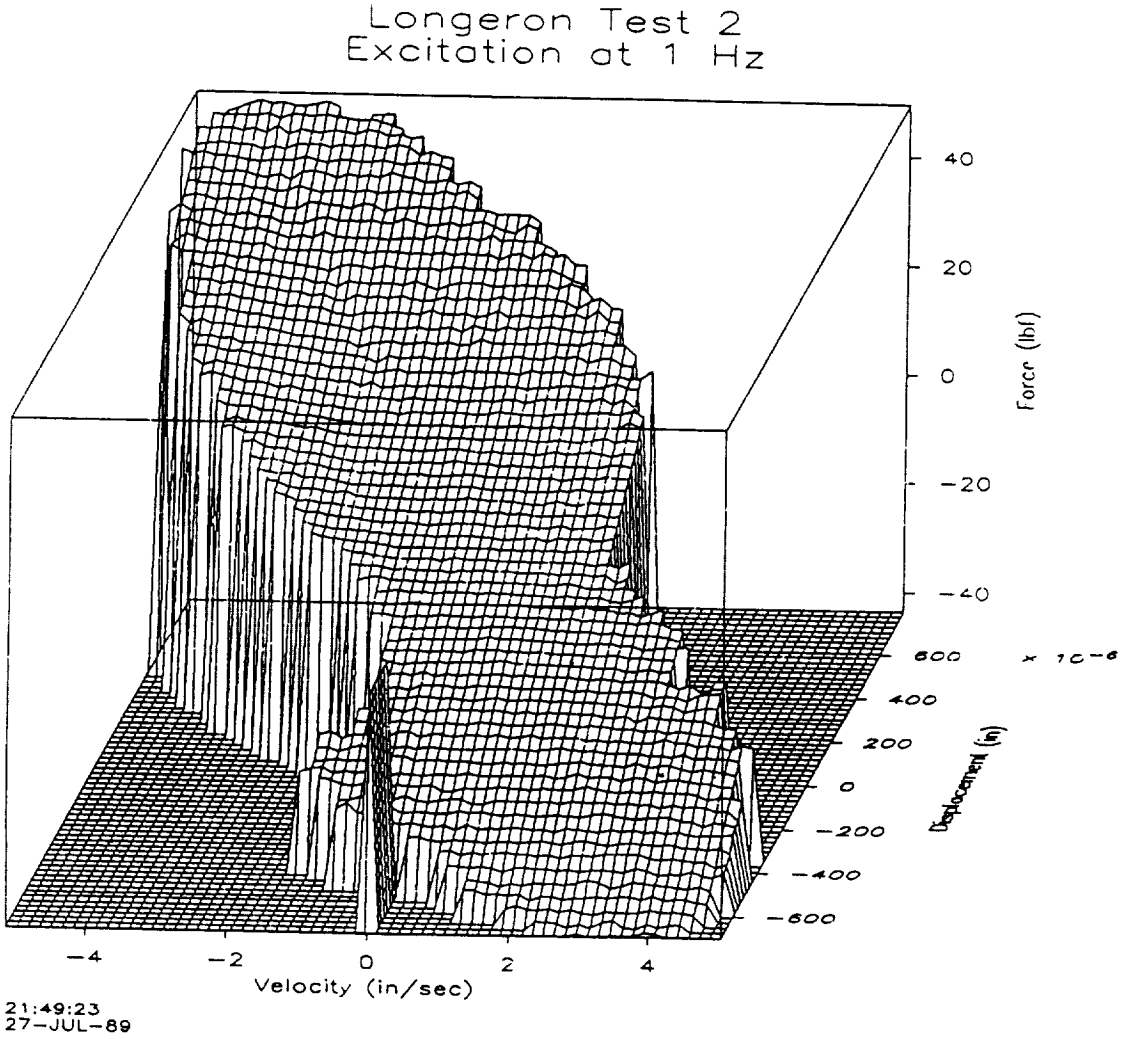
Longeron Test 2
Excitation at 1 Hz
40
20
0
-20
-40
Force (lbf)
600
400
200
0
-200
-400
-600
x 10-6
Displacement (in)
-4
-2
0
2
4
Velocity (in/sec)
21:49:23
27-JUL-89

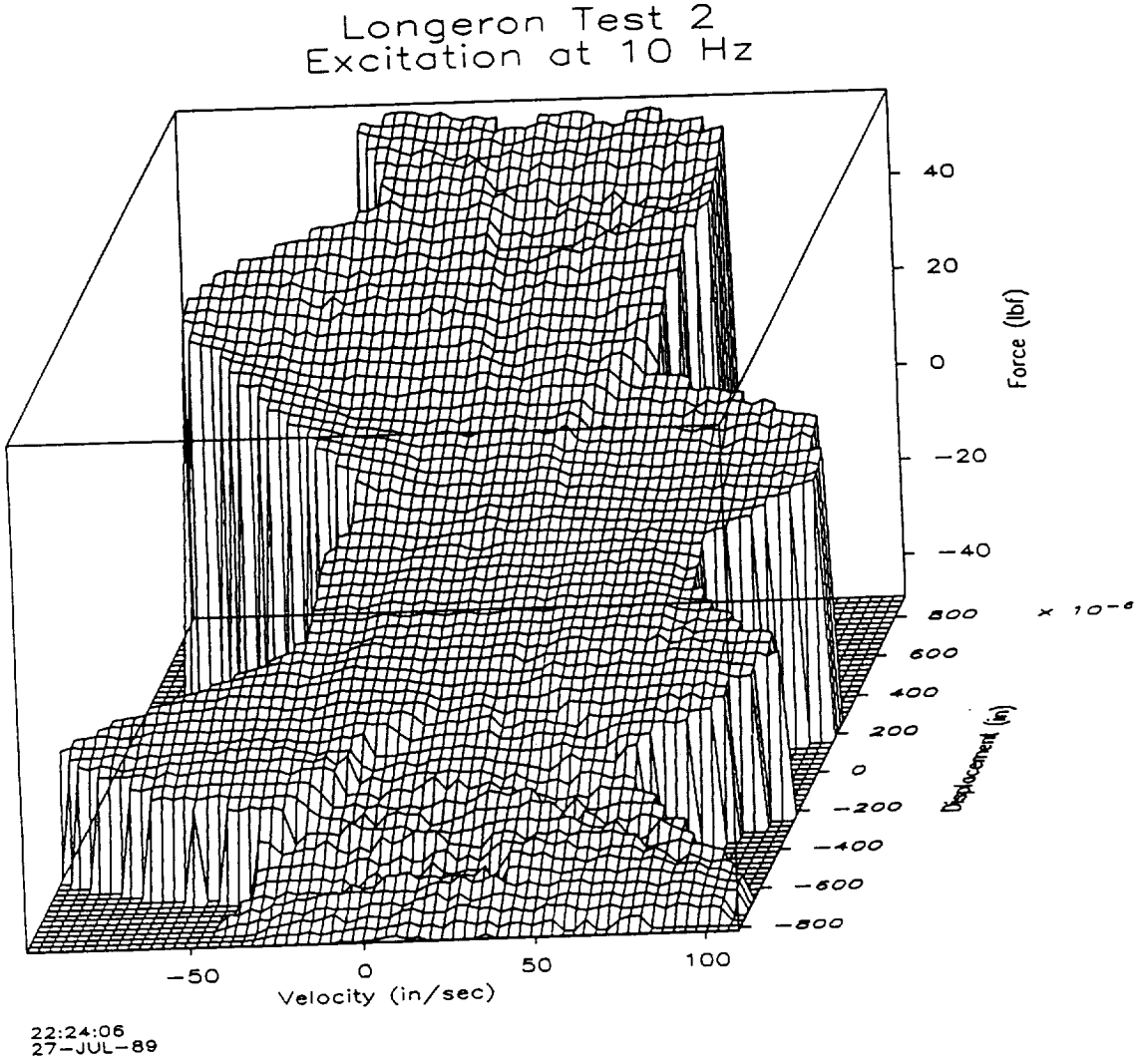
Longeron Test 2
Excitation at 10 Hz
40
20
0
−20
−40
Force (lbf)
800
600
400
200
0
−200
−400
−600
−800
x 10⁻⁶
Displacement (in)
−50
0
50
100
Velocity (in/sec)
22:24:06
27-JUL-89

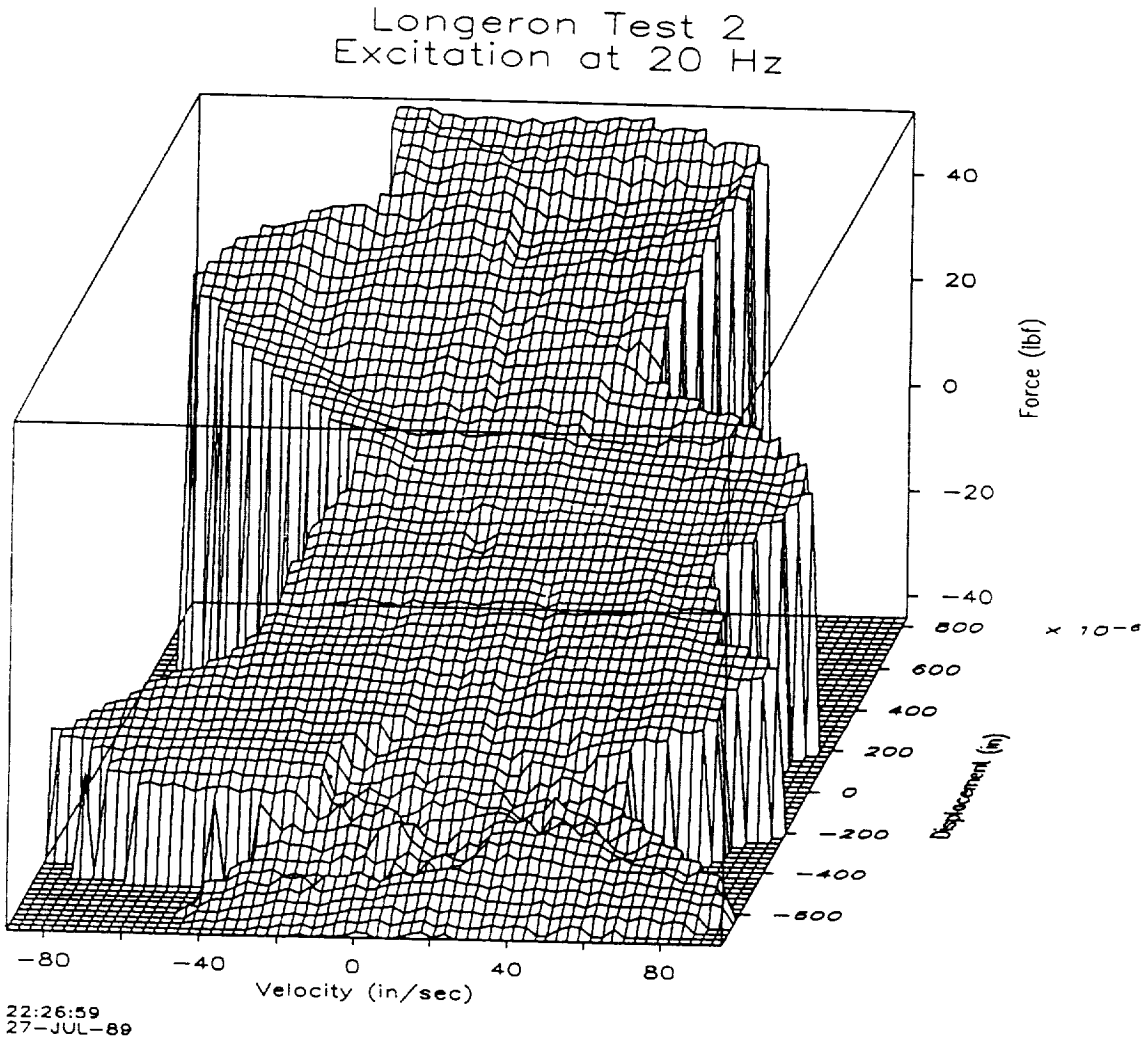
Longeron Test 2
Excitation at 20 Hz
40
20
0
−20
−40
Force (lbf)
800
600
400
200
0
−200
−400
−600
x 10−6
Displacement (in)
−80
−40
0
40
80
Velocity (in/sec)
22:26:59
27−JUL−89

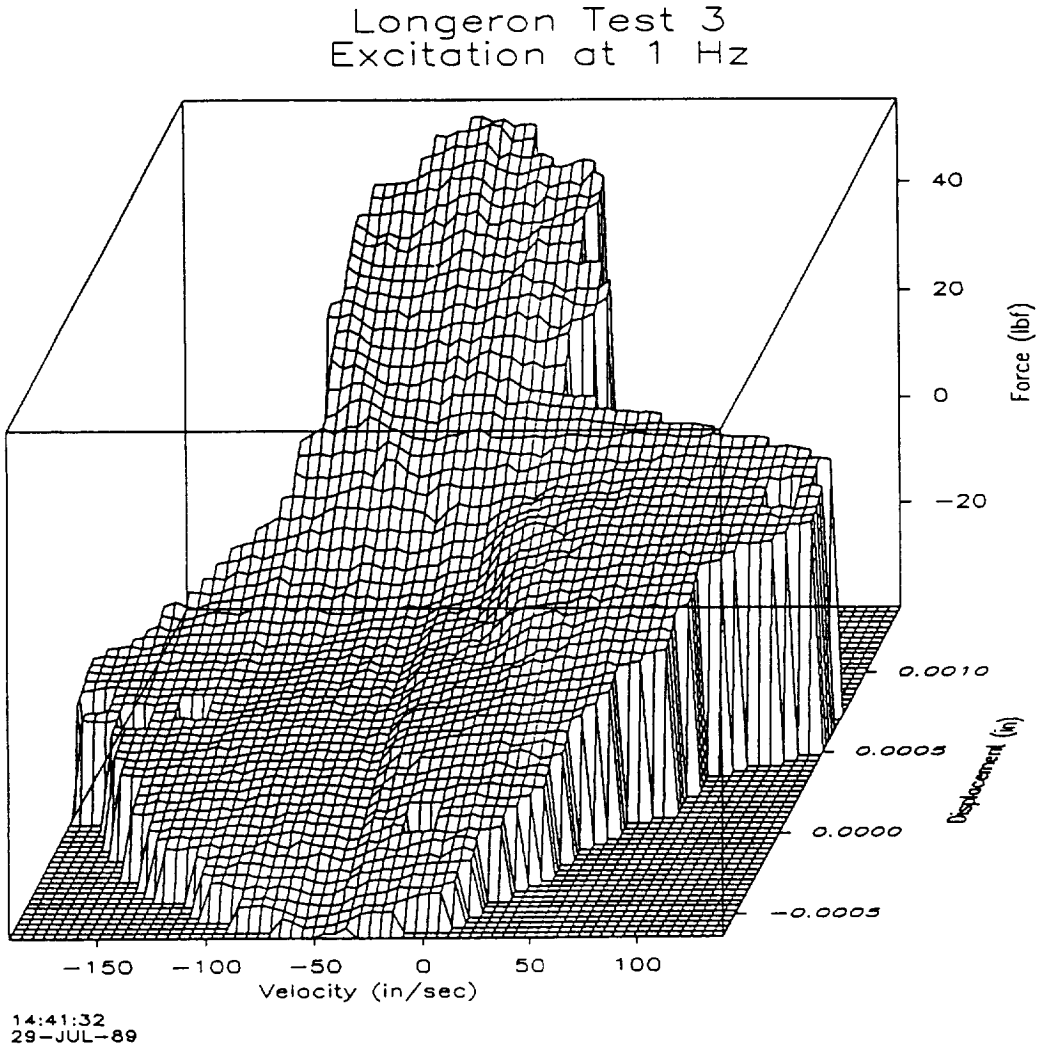
Longeron Test 3
Excitation at 1 Hz
40
20
0
−20
Force (lbf)
0.0010
0.0005
0.0000
−0.0005
Displacement (in)
−150
−100
−50
0
50
100
Velocity (in/sec)
14:41:32
29−JUL−89

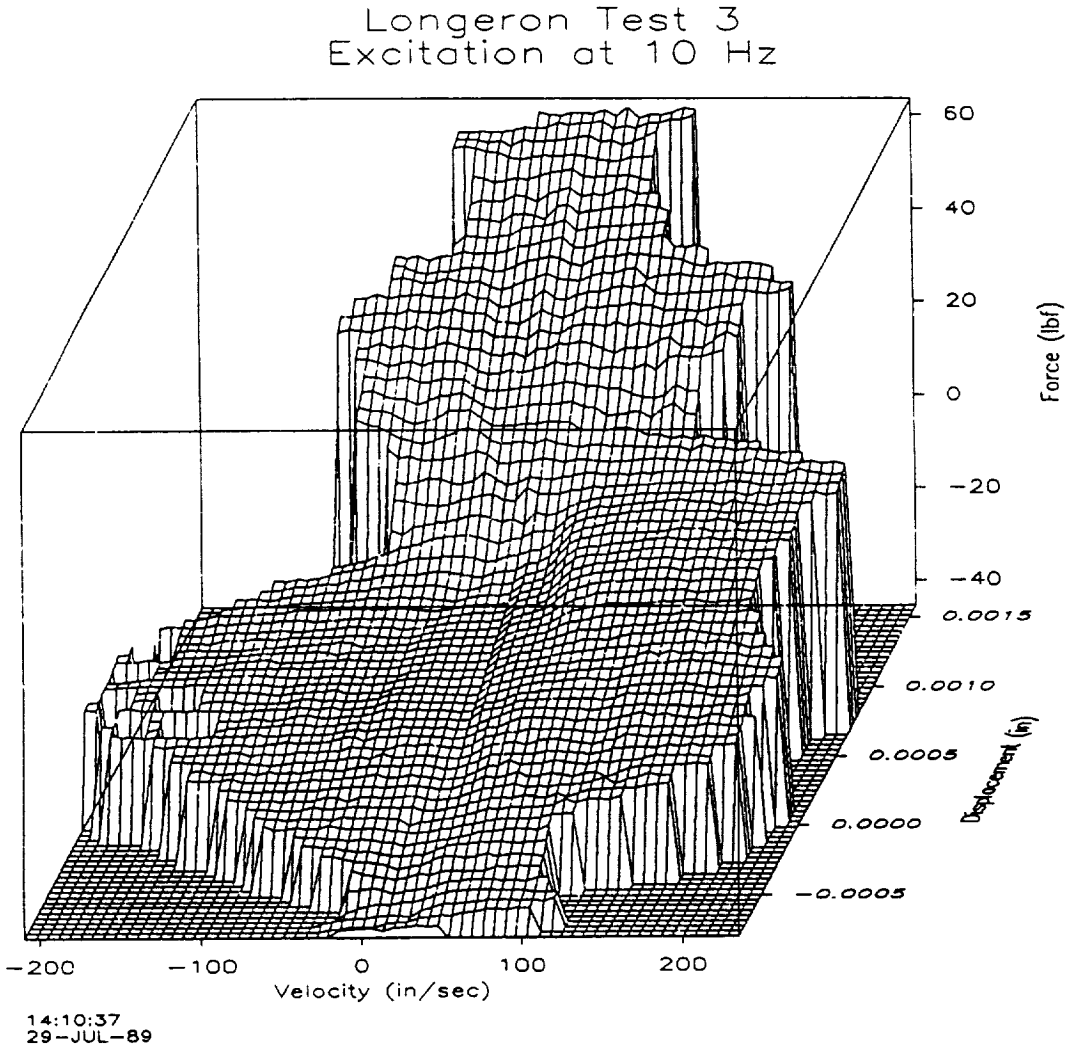
Longeron Test 3
Excitation at 10 Hz
60
40
20
0
−20
−40
Force (lbf)
0.0015
0.0010
0.0005
0.0000
−0.0005
Displacement (in)
−200
−100
0
100
200
Velocity (in/sec)
14:10:37
29−JUL−89

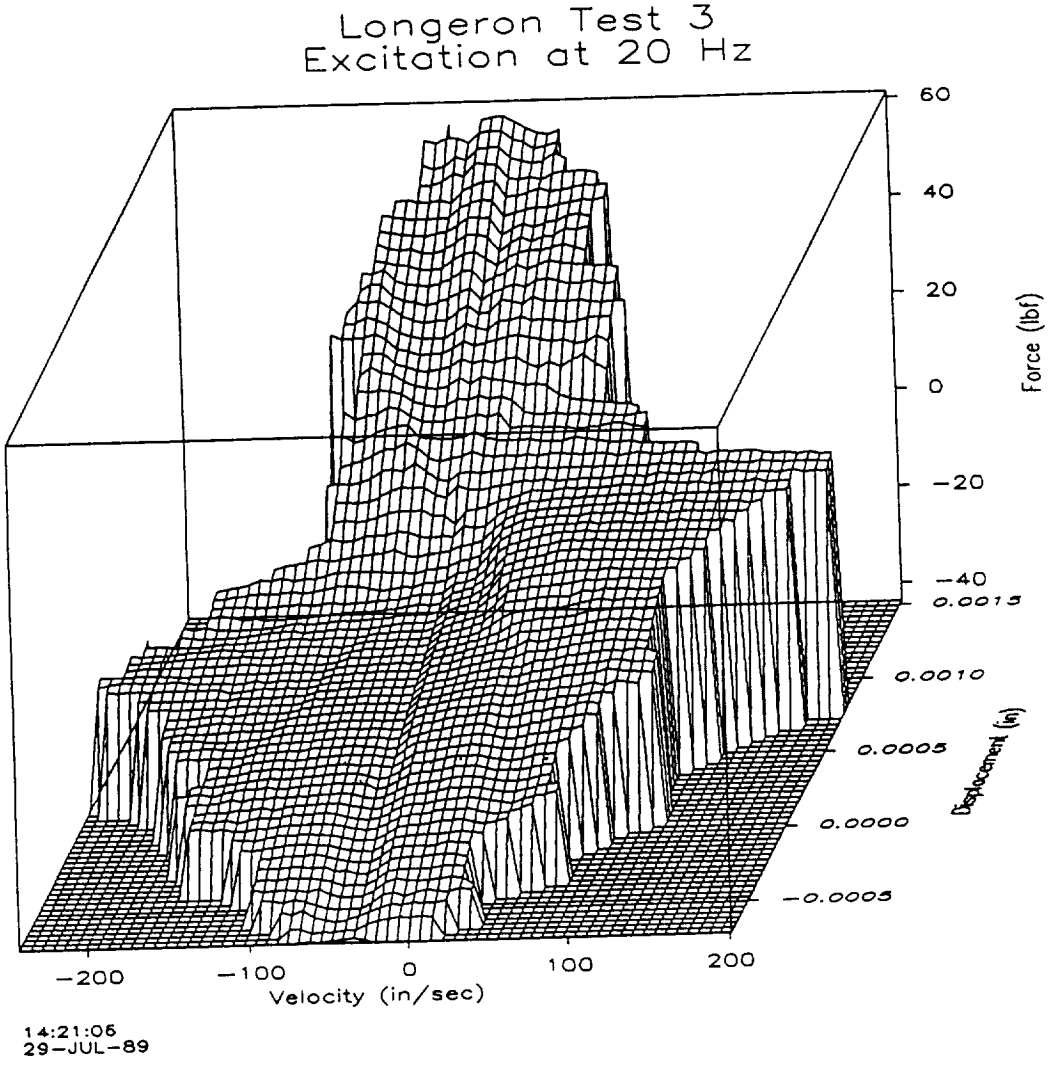
Longeron Test 3
Excitation at 20 Hz
60
40
20
0
−20
−40
Force (lbf)
0.0015
0.0010
0.0005
0.0000
−0.0005
Displacement (in)
−200
−100
0
100
200
Velocity (in/sec)
14:21:06
29−JUL−89

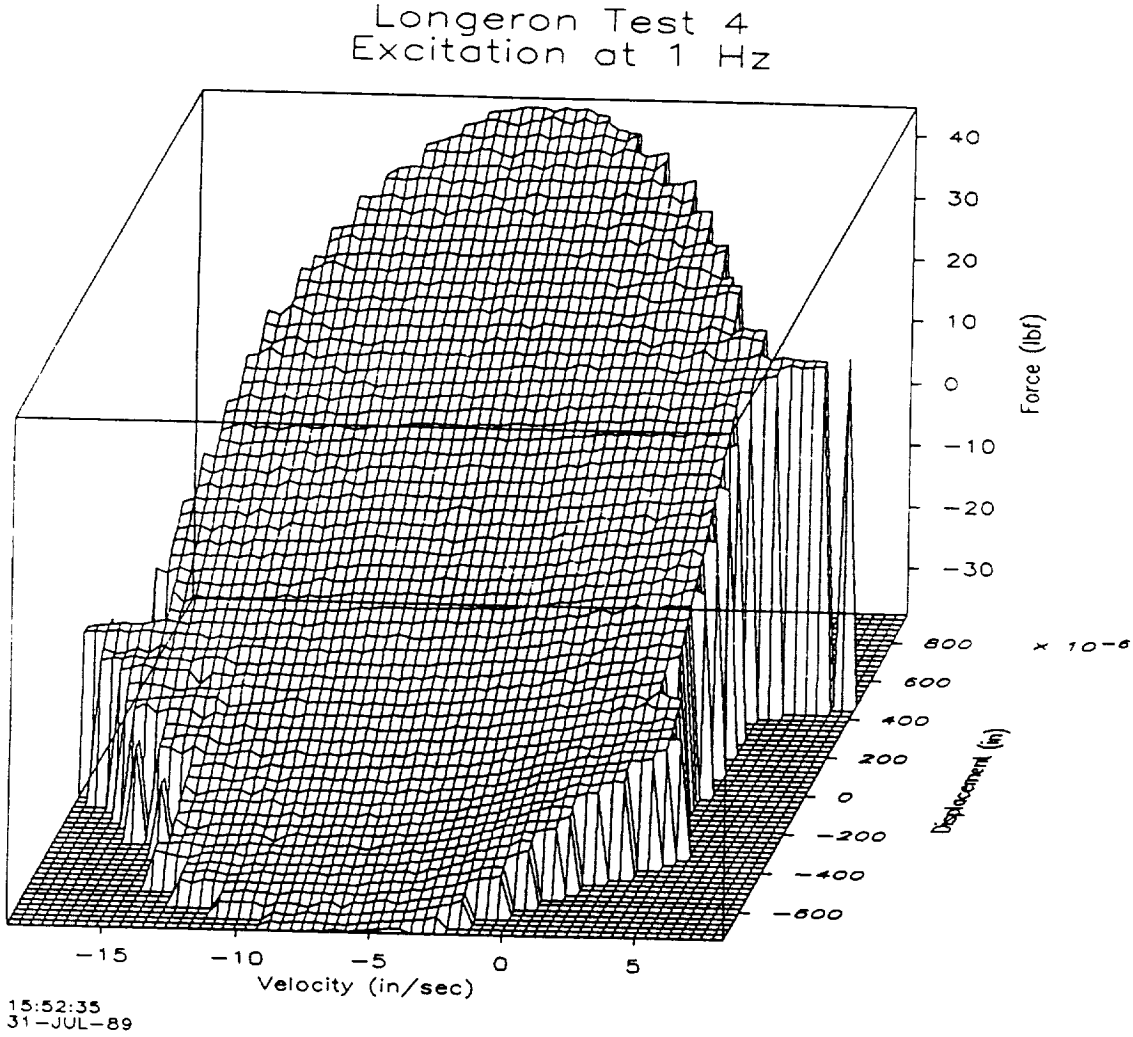
Longeron Test 4
Excitation at 1 Hz
40
30
20
10
0
−10
−20
−30
Force (lbf)
800
600
400
200
0
−200
−400
−600
x 10−6
Displacement (in)
−15
−10
−5
0
5
Velocity (in/sec)
15:52:35
31−JUL−89

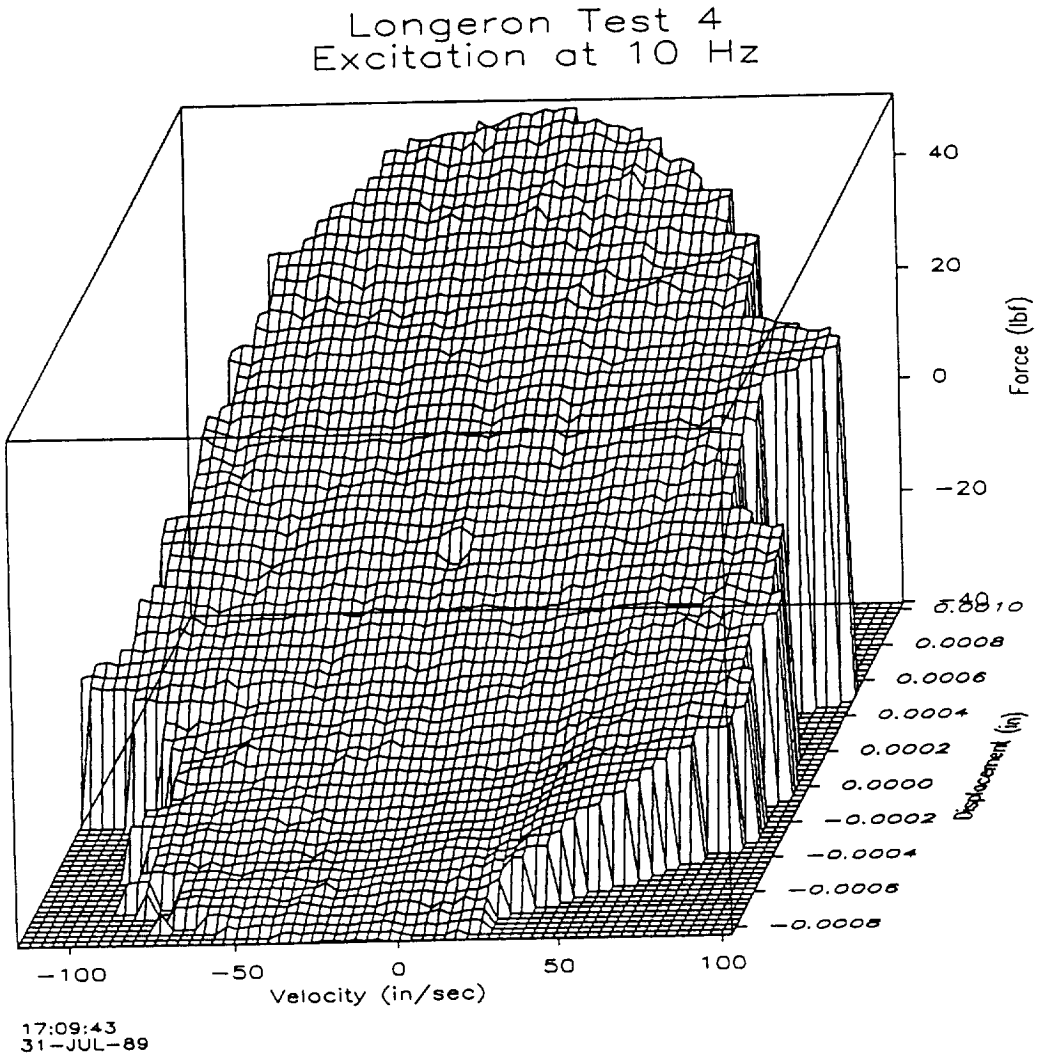
Longeron Test 4
Excitation at 10 Hz
40
20
0
−20
Force (lbf)
0.0010
0.0008
0.0006
0.0004
0.0002
0.0000
−0.0002
−0.0004
−0.0006
−0.0008
Displacement (in)
−100
−50
0
50
100
Velocity (in/sec)
17:09:43
31−JUL−89

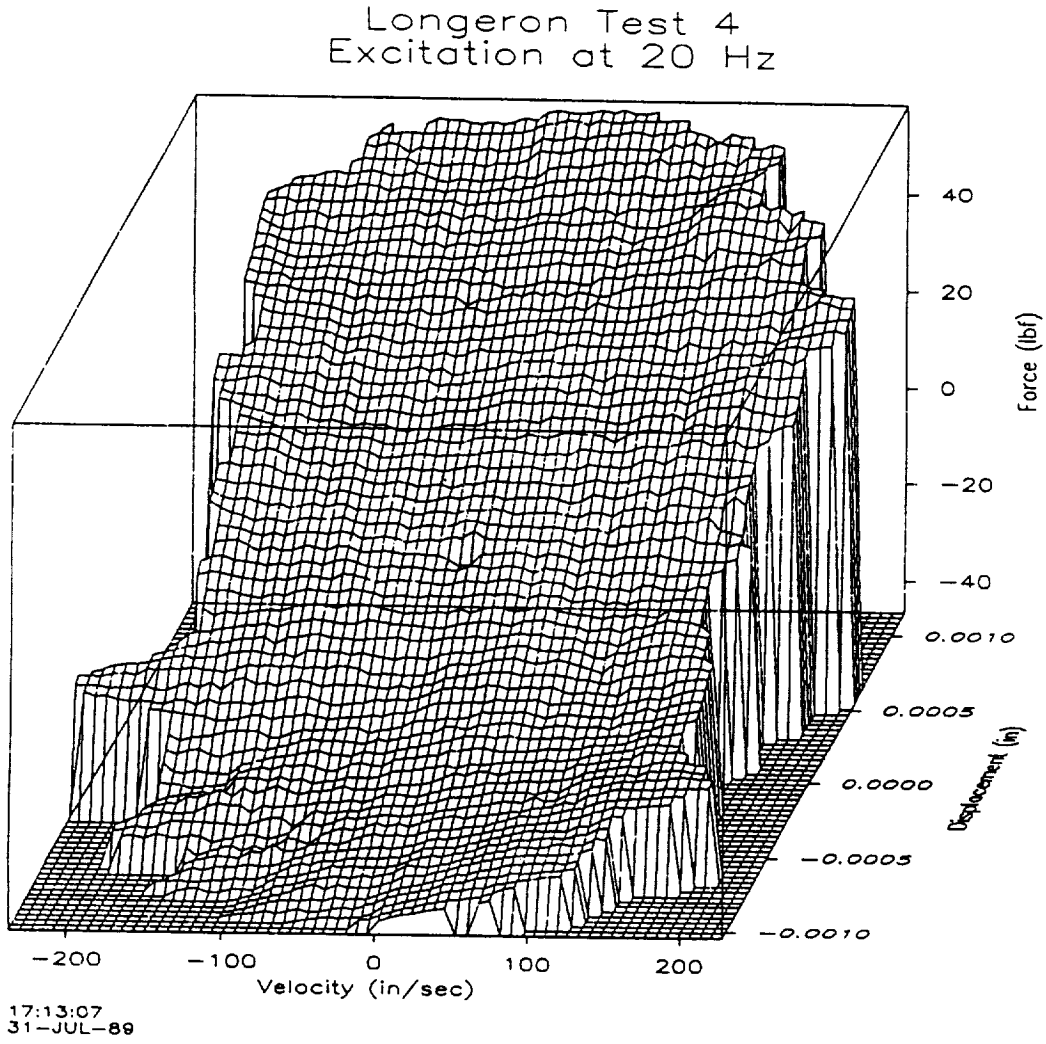
Longeron Test 4
Excitation at 20 Hz
40
20
0
−20
−40
Force (lbf)
0.0010
0.0005
0.0000
−0.0005
−0.0010
Displacement (in)
−200
−100
0
100
200
Velocity (in/sec)
17:13:07
31−JUL−89

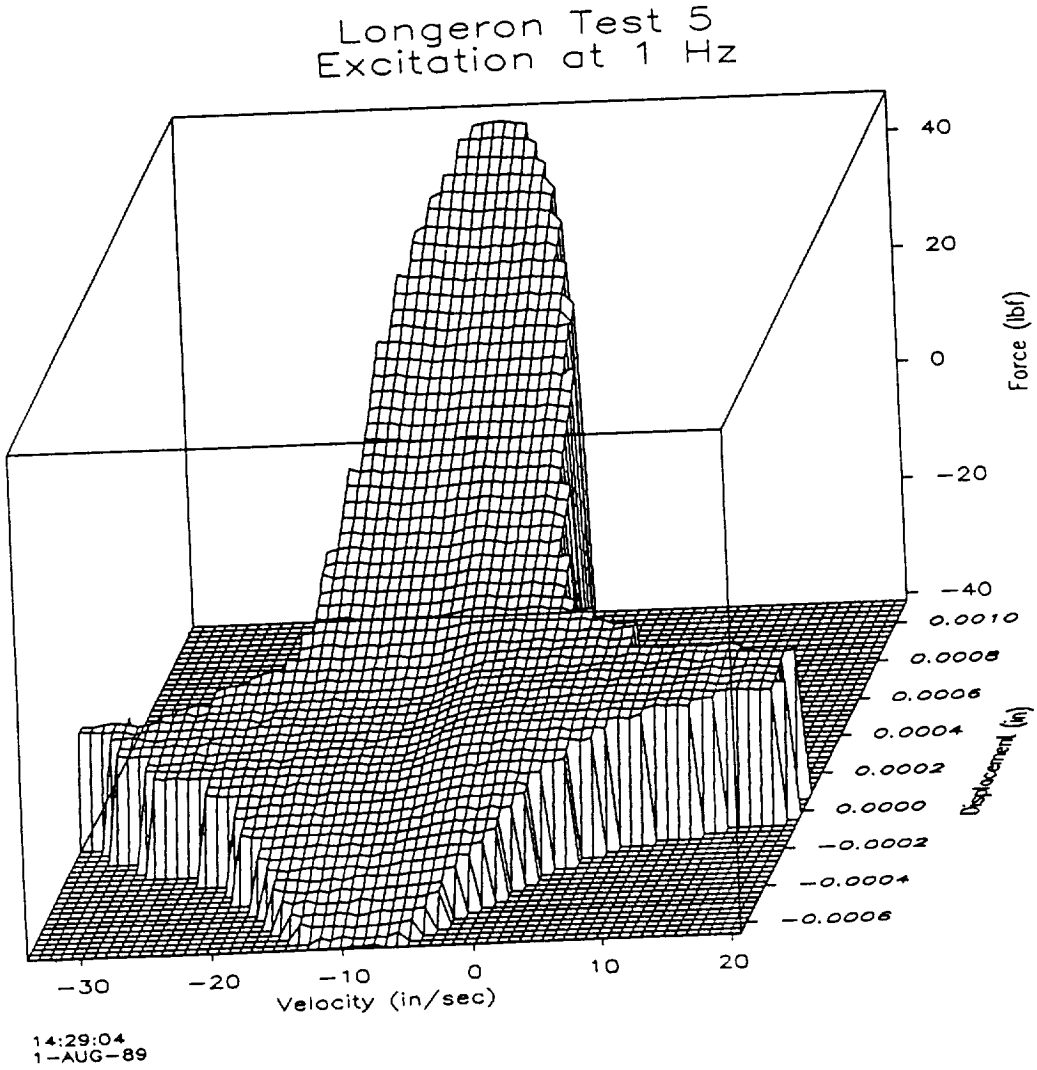
Longeron Test 5
Excitation at 1 Hz
40
20
0
−20
−40
Force (lbf)
0.0010
0.0008
0.0006
0.0004
0.0002
0.0000
−0.0002
−0.0004
−0.0006
Displacement (in)
−30
−20
−10
0
10
20
Velocity (in/sec)
14:29:04
1−AUG−89

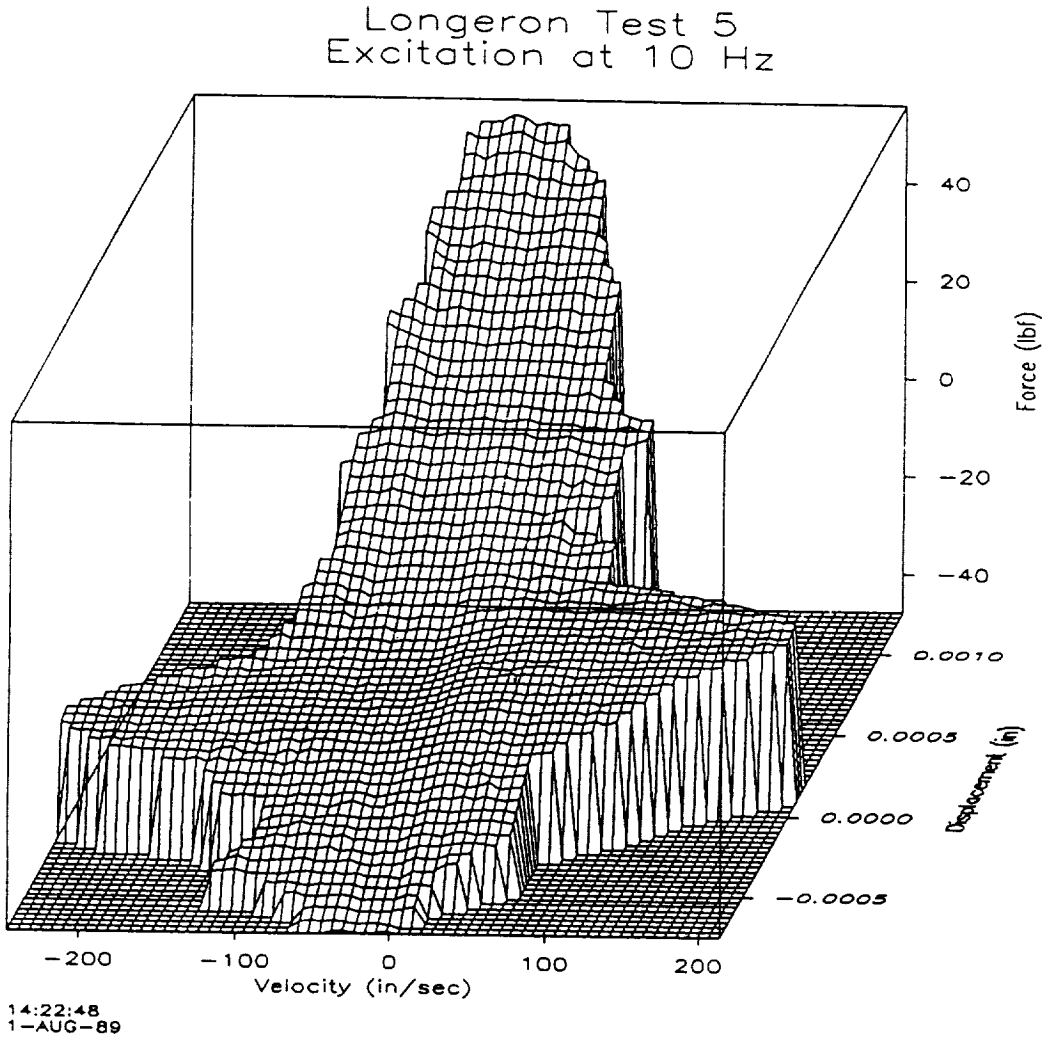
Longeron Test 5
Excitation at 10 Hz
40
20
0
−20
−40
Force (lbf)
0.0010
0.0005
0.0000
−0.0005
Displacement (in)
−200
−100
0
100
200
Velocity (in/sec)
14:22:48
1−AUG−89

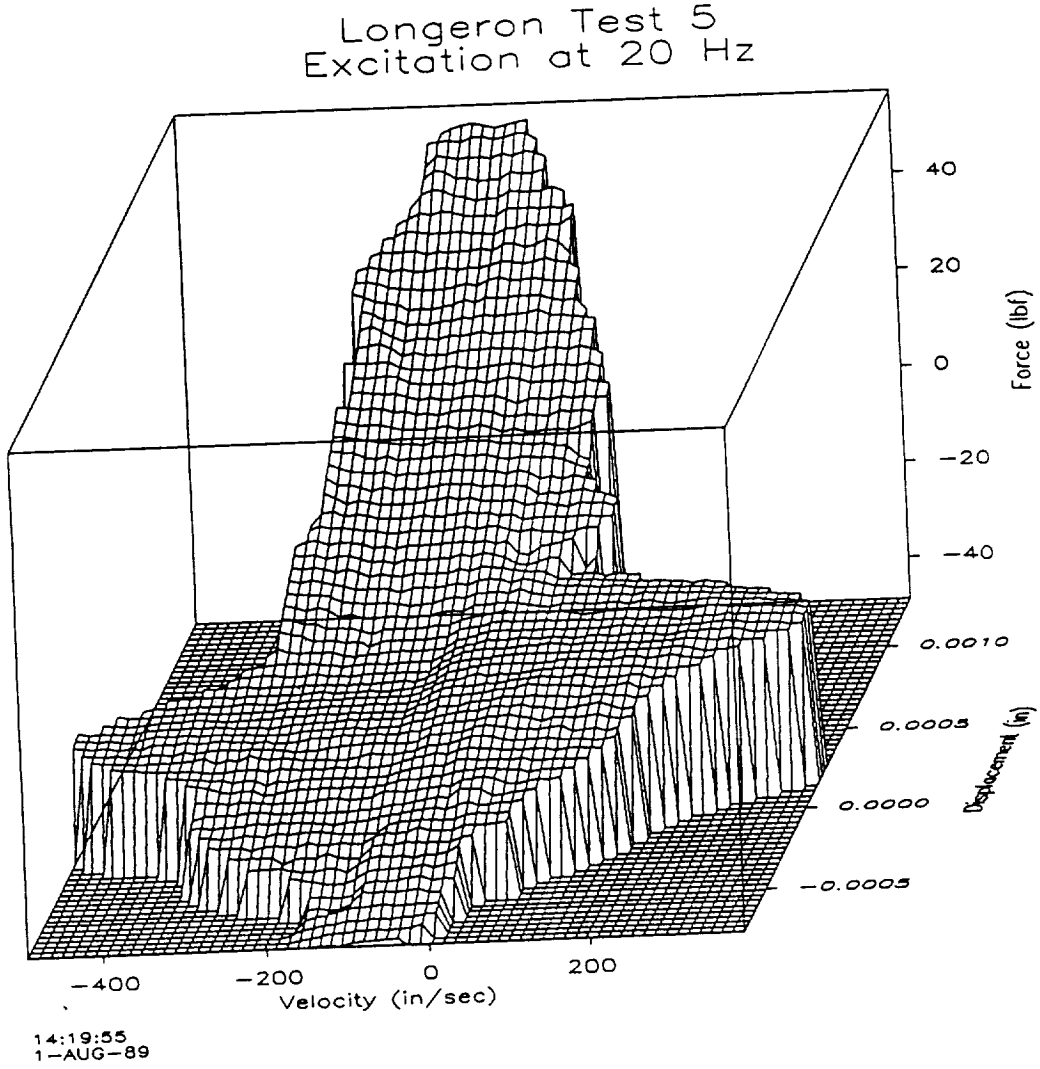
Longeron Test 5
Excitation at 20 Hz
40
20
0
−20
−40
Force (lbf)
0.0010
0.0005
0.0000
−0.0005
Displacement (in)
−400
−200
0
200
Velocity (in/sec)
14:19:55
1−AUG−89

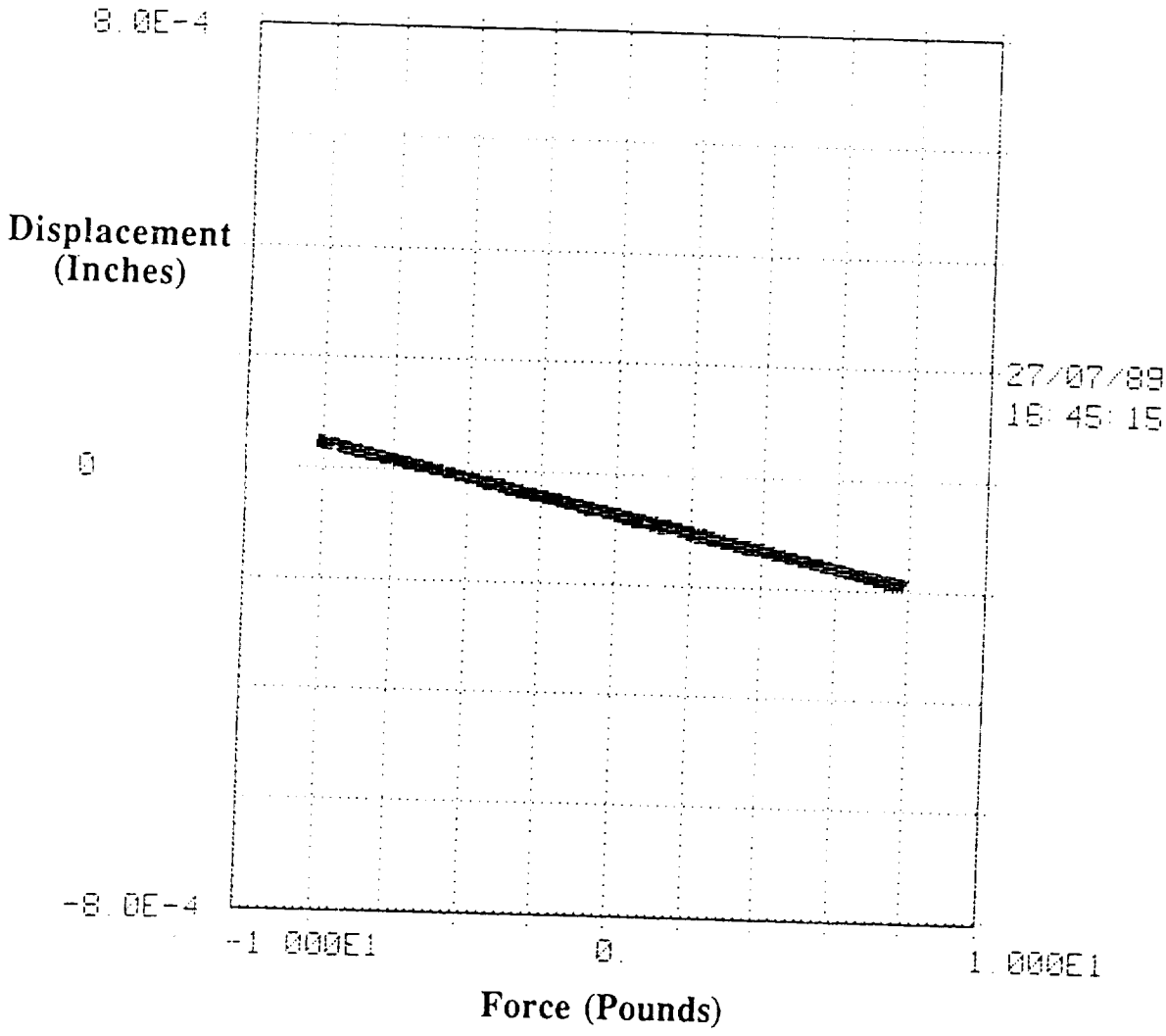

Longeron test 2, excitation at 10 Hz

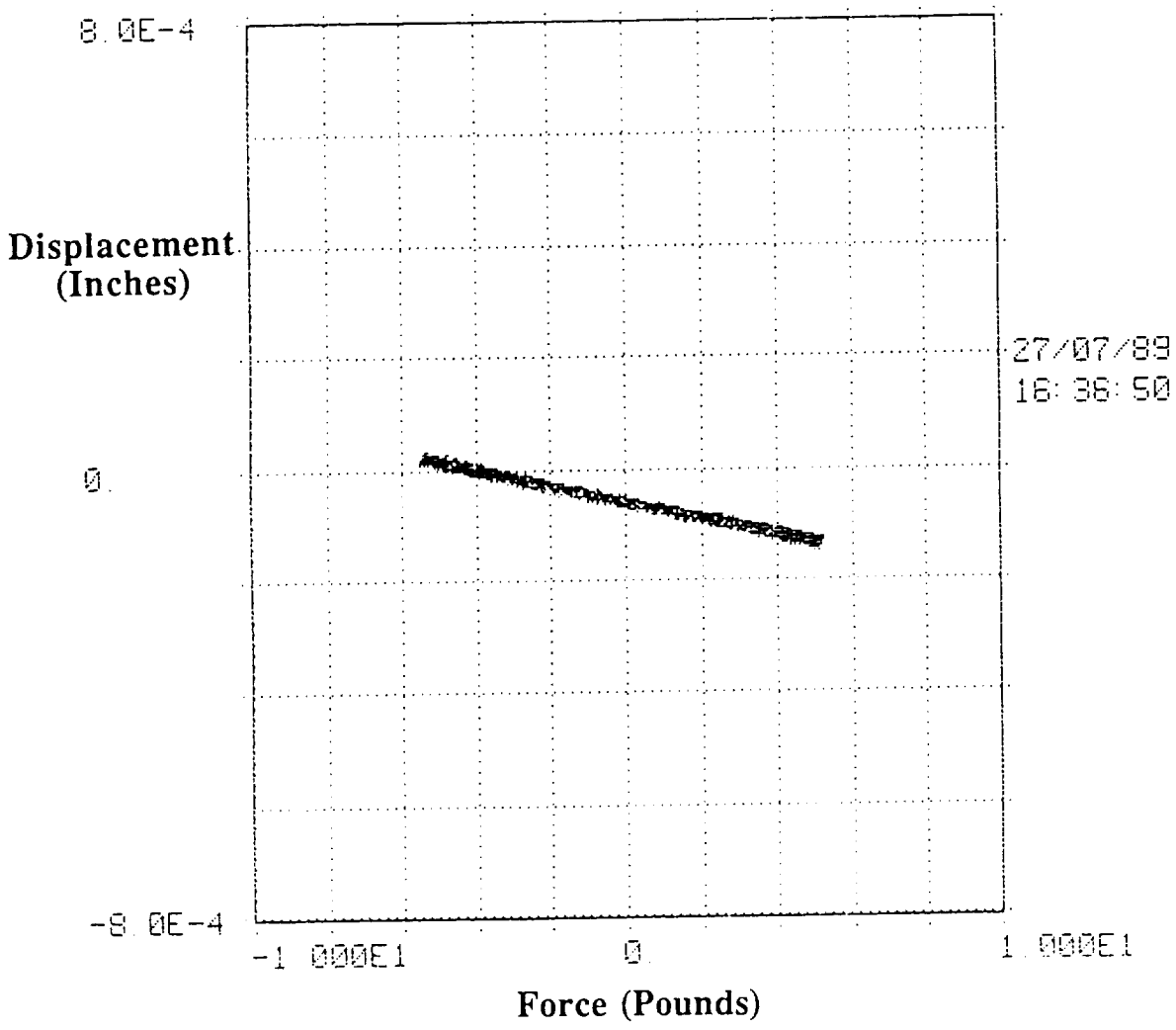

Longeron test 2, excitation at 1 Hz

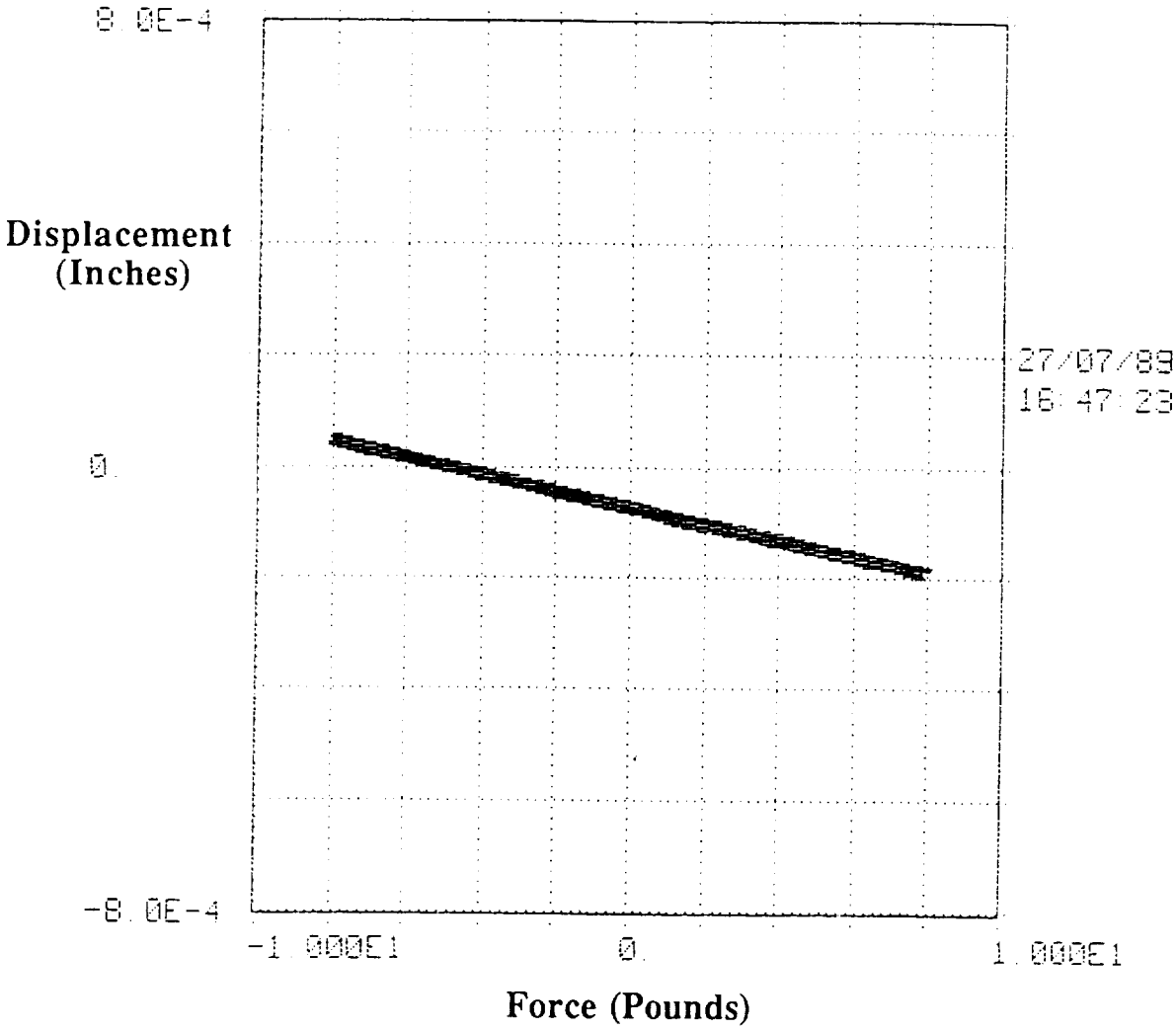

Longeron test 2, excitation at 20 Hz

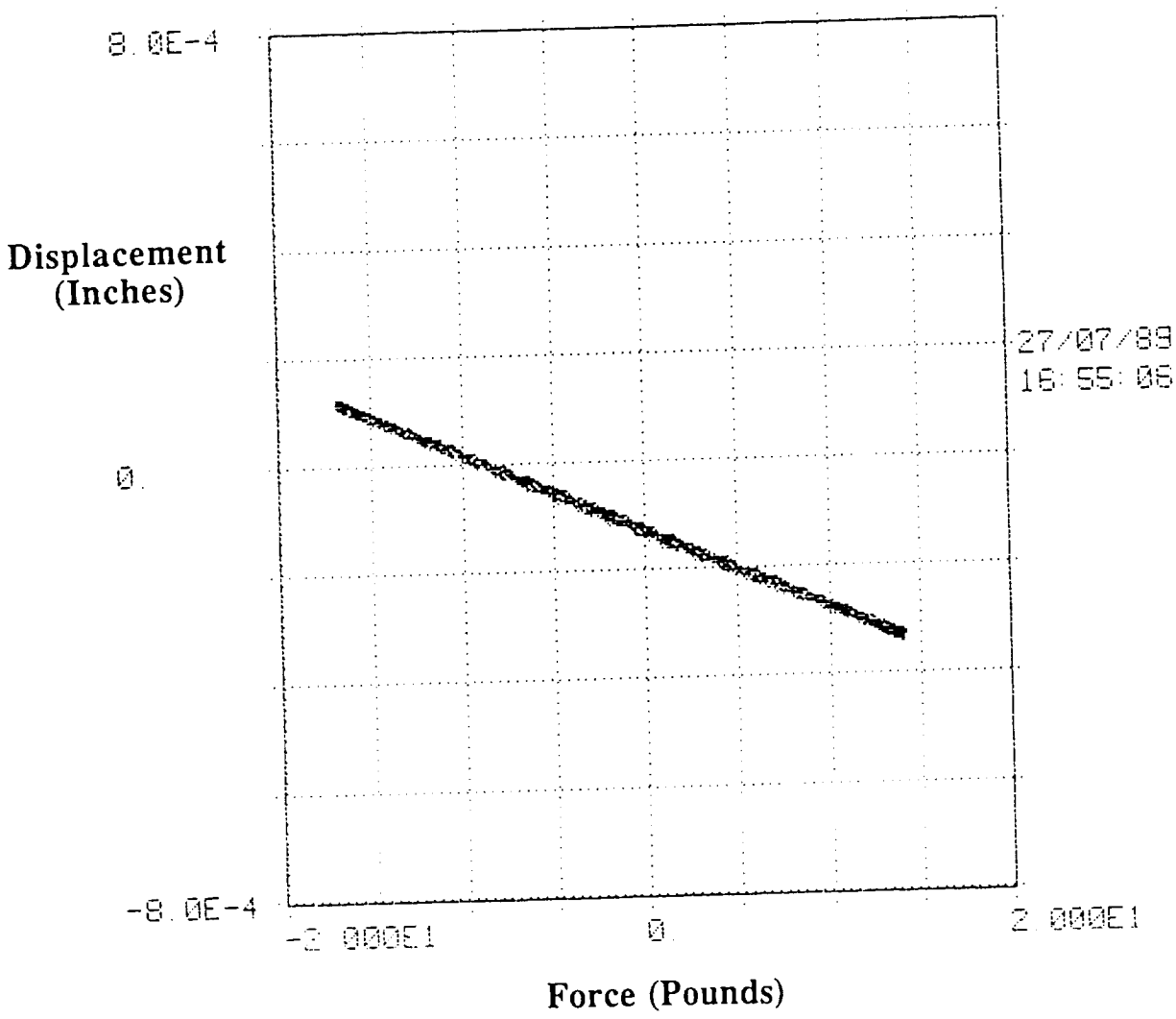

Longeron test 2, excitation at 1 Hz

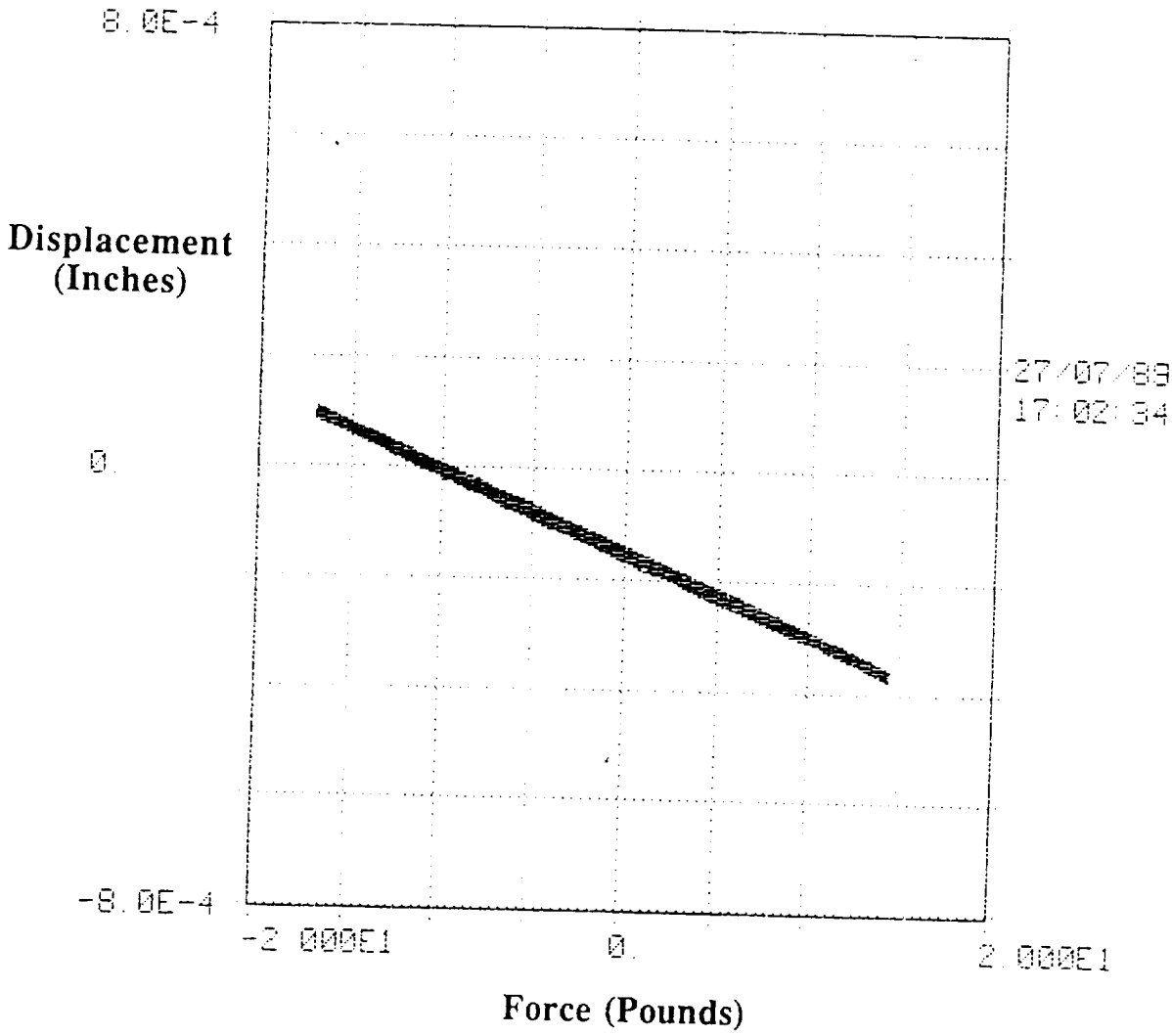

Longeron test 2, excitation at 10 Hz

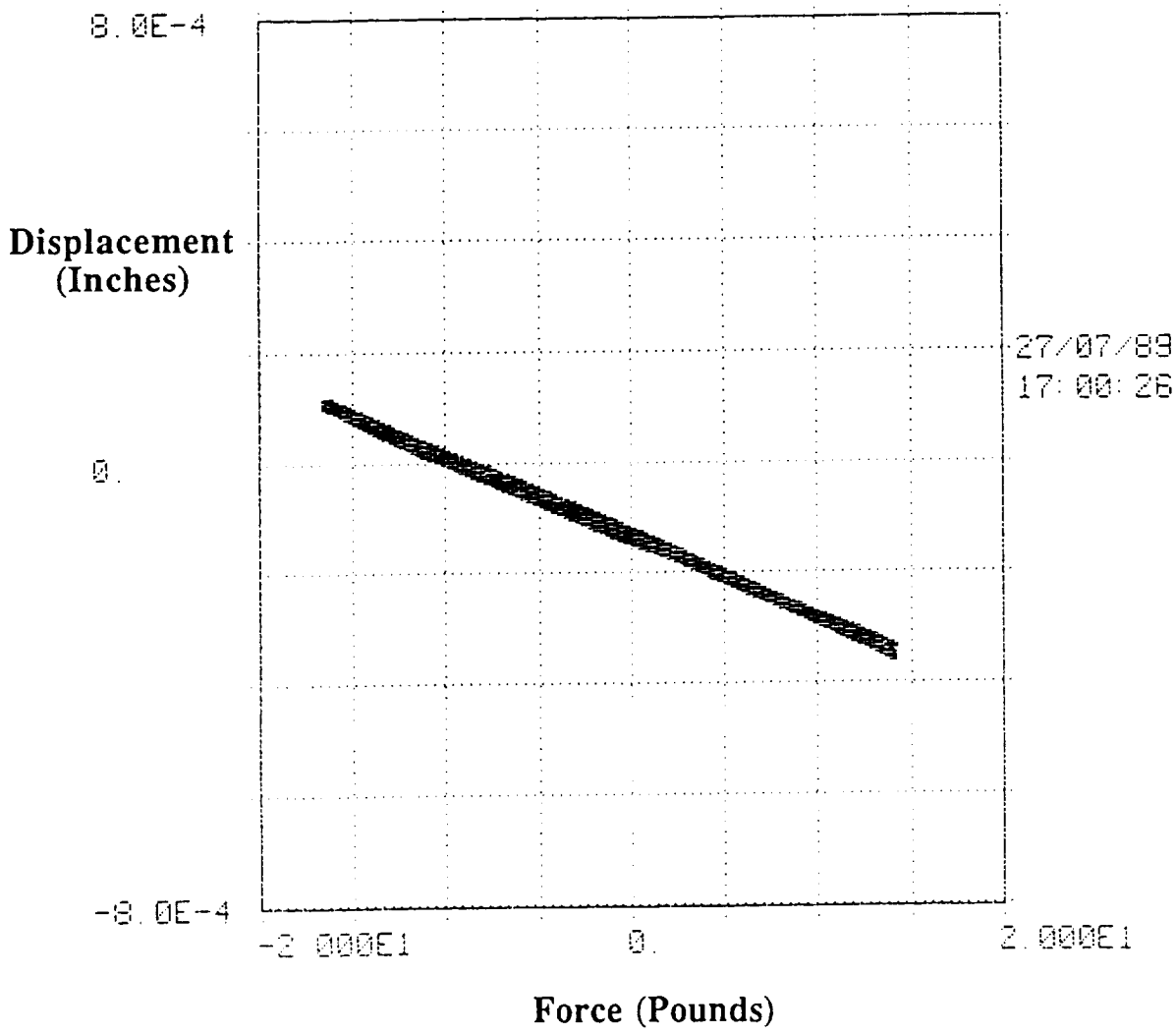

Longeron test 2, excitation at 20 Hz

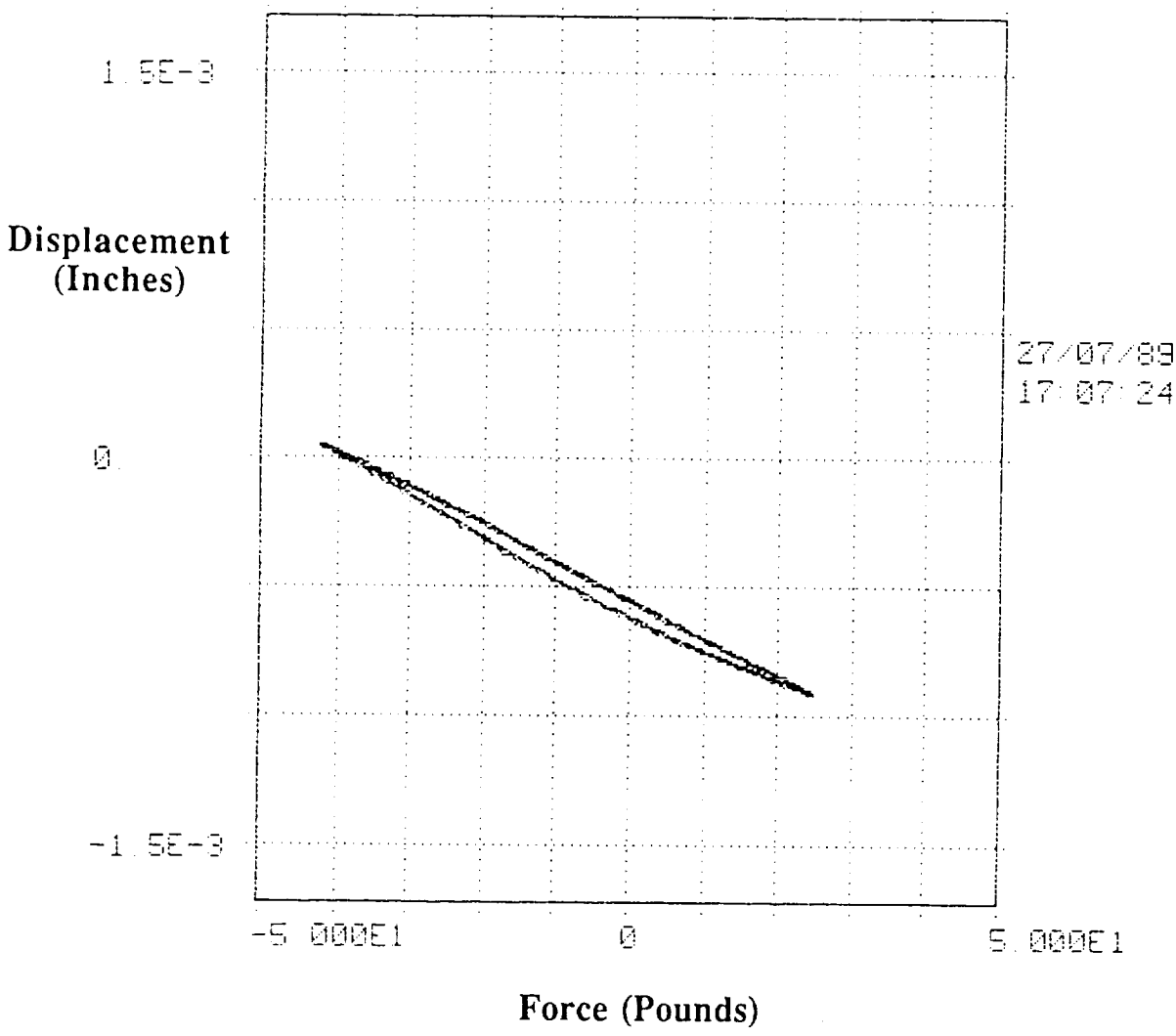

Longeron test 2, excitation at 1 Hz

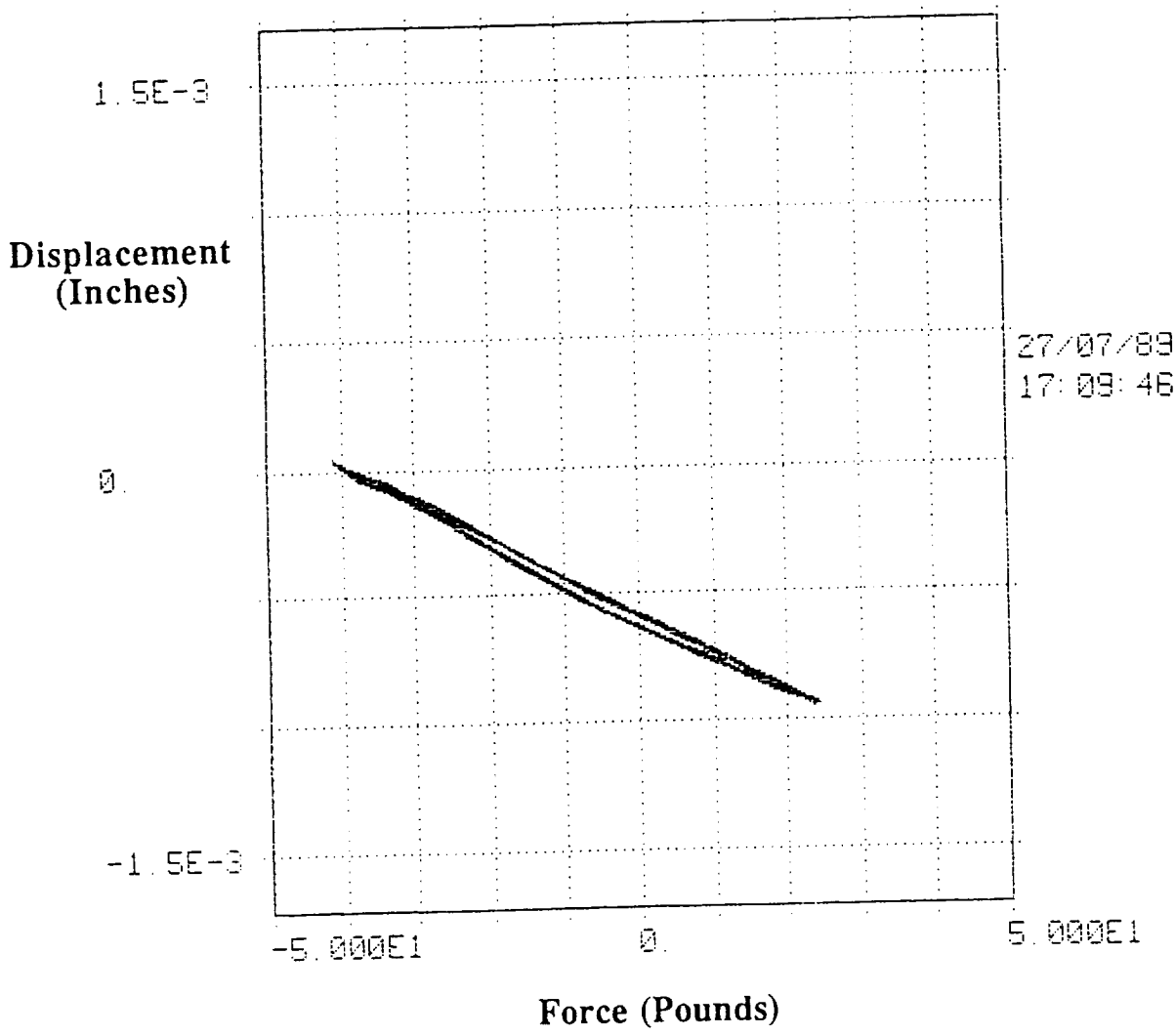

Longeron test 2, excitation at 10 Hz

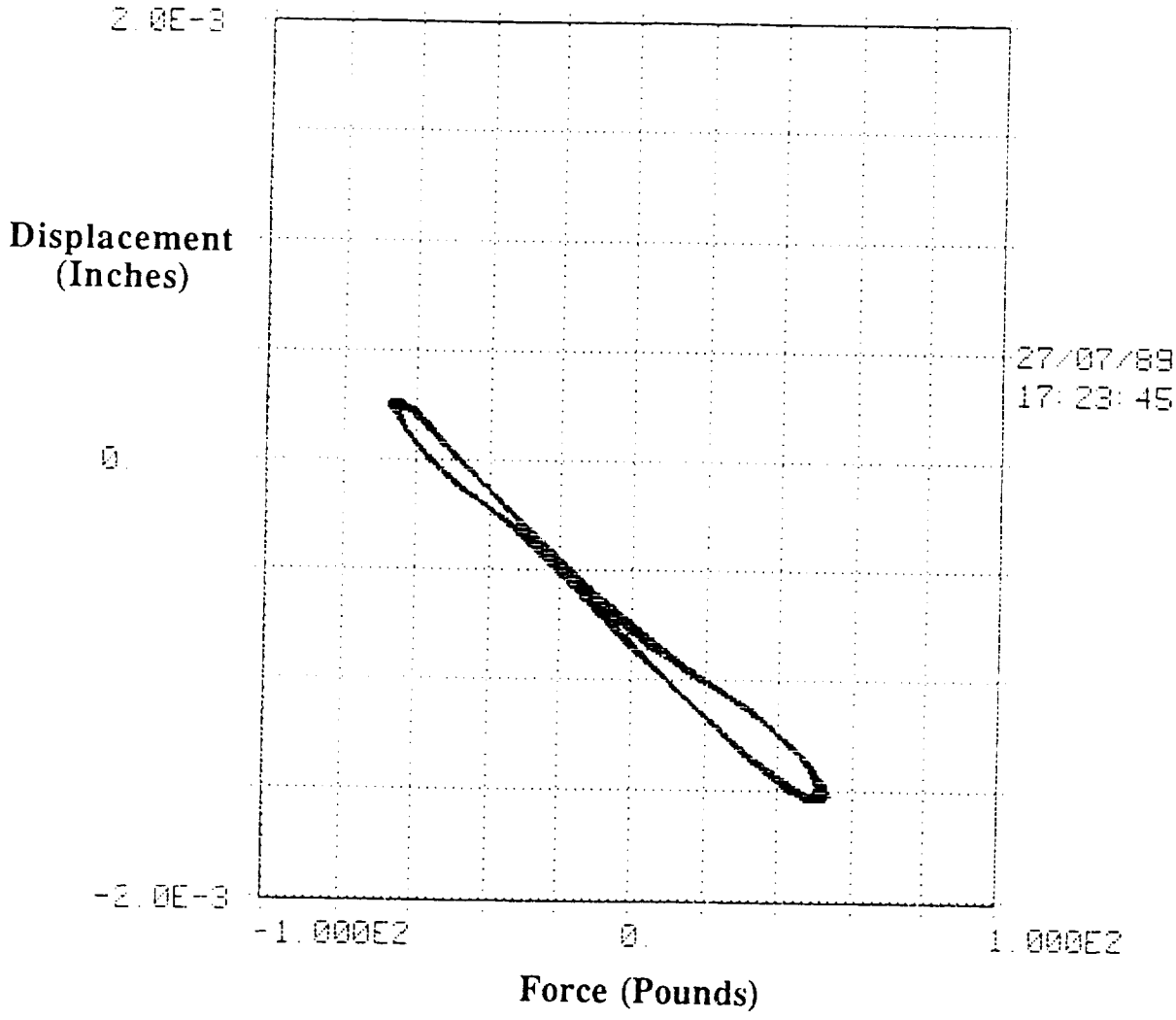

Longeron test 2, excitation at 20 Hz

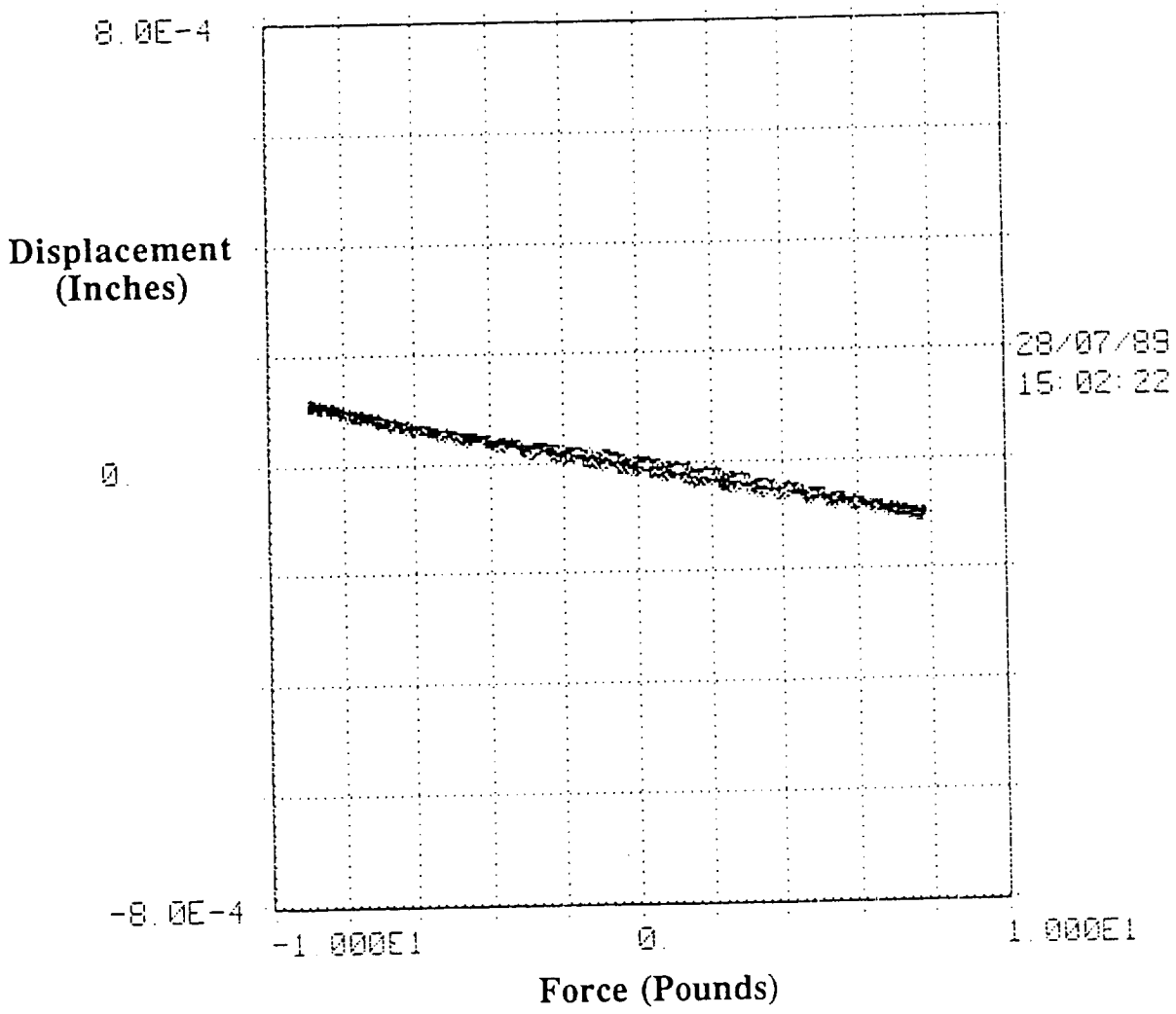

Longeron test 3, excitation at 1 Hz

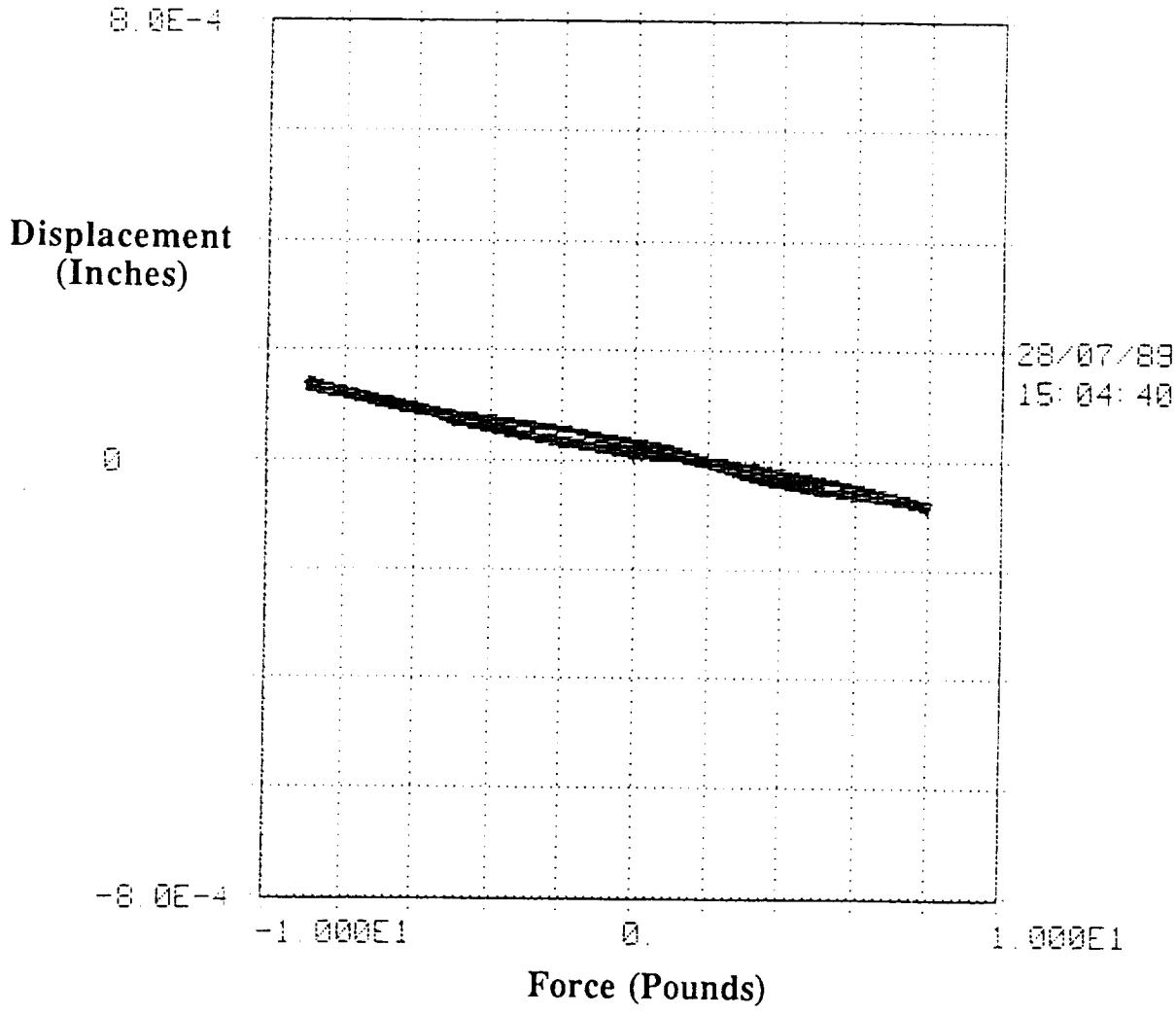

Longeron test 3, excitation at 10 Hz

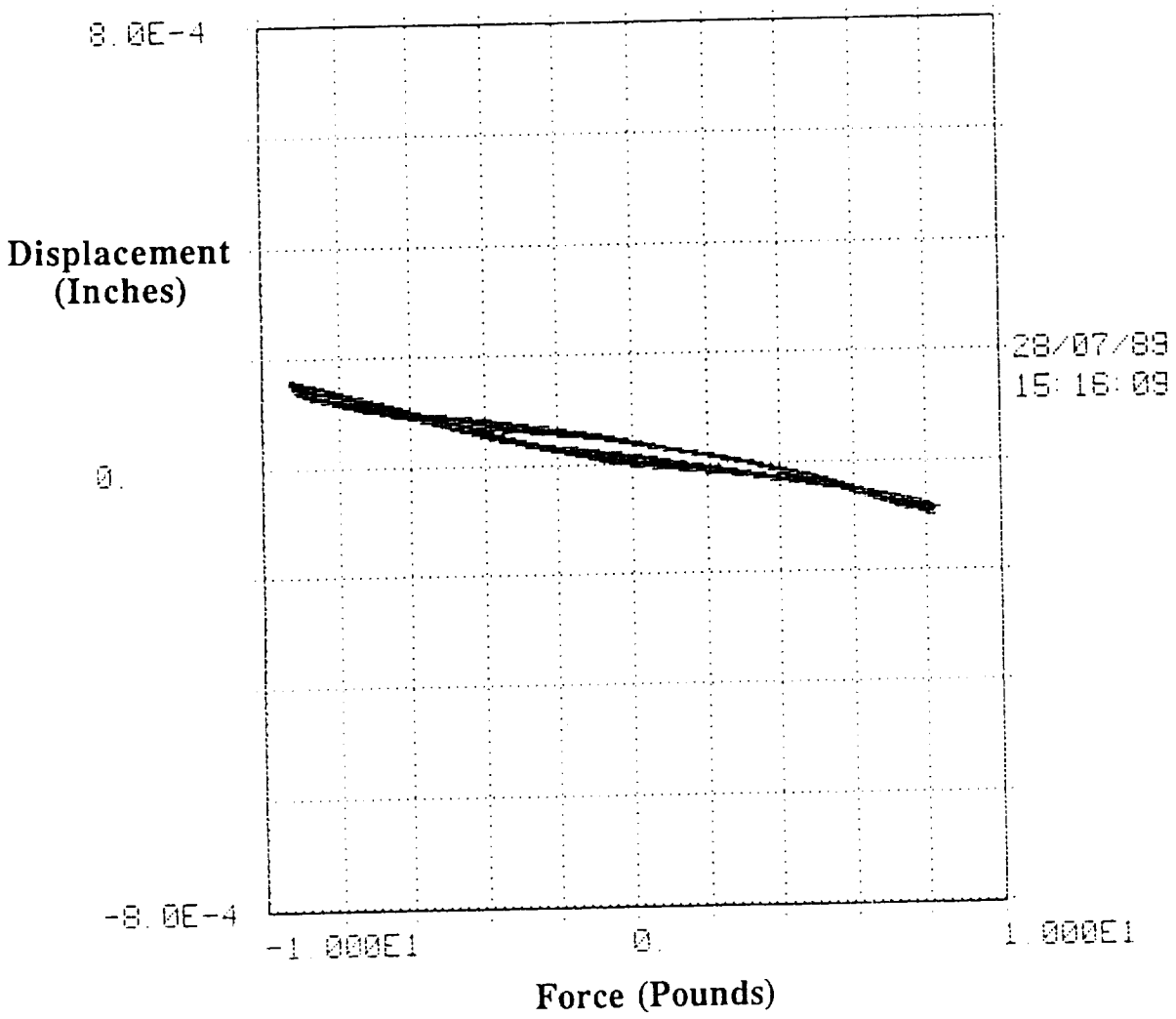

Longeron test 3, excitation at 20 Hz

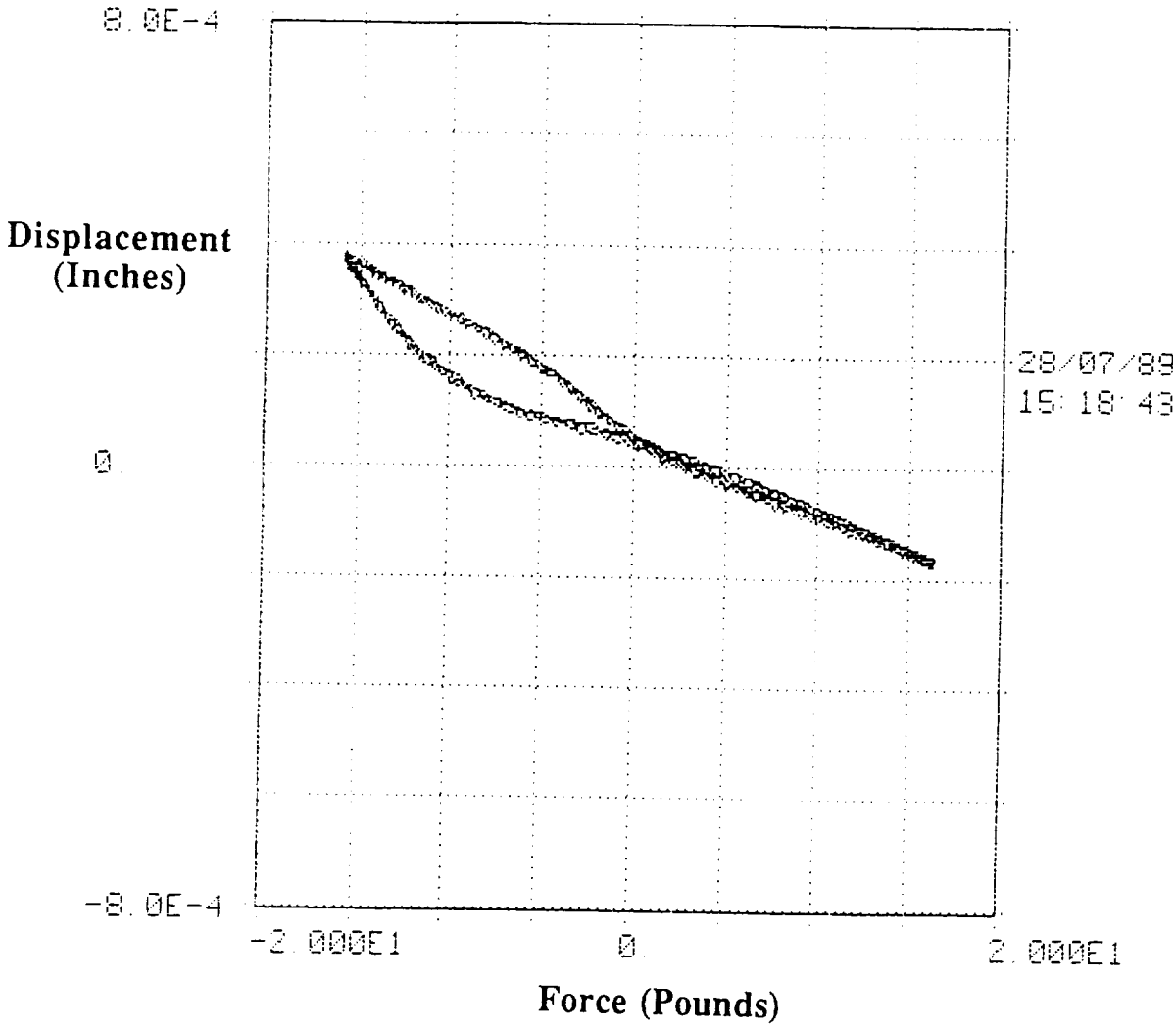

Longeron test 3, excitation at 1 Hz

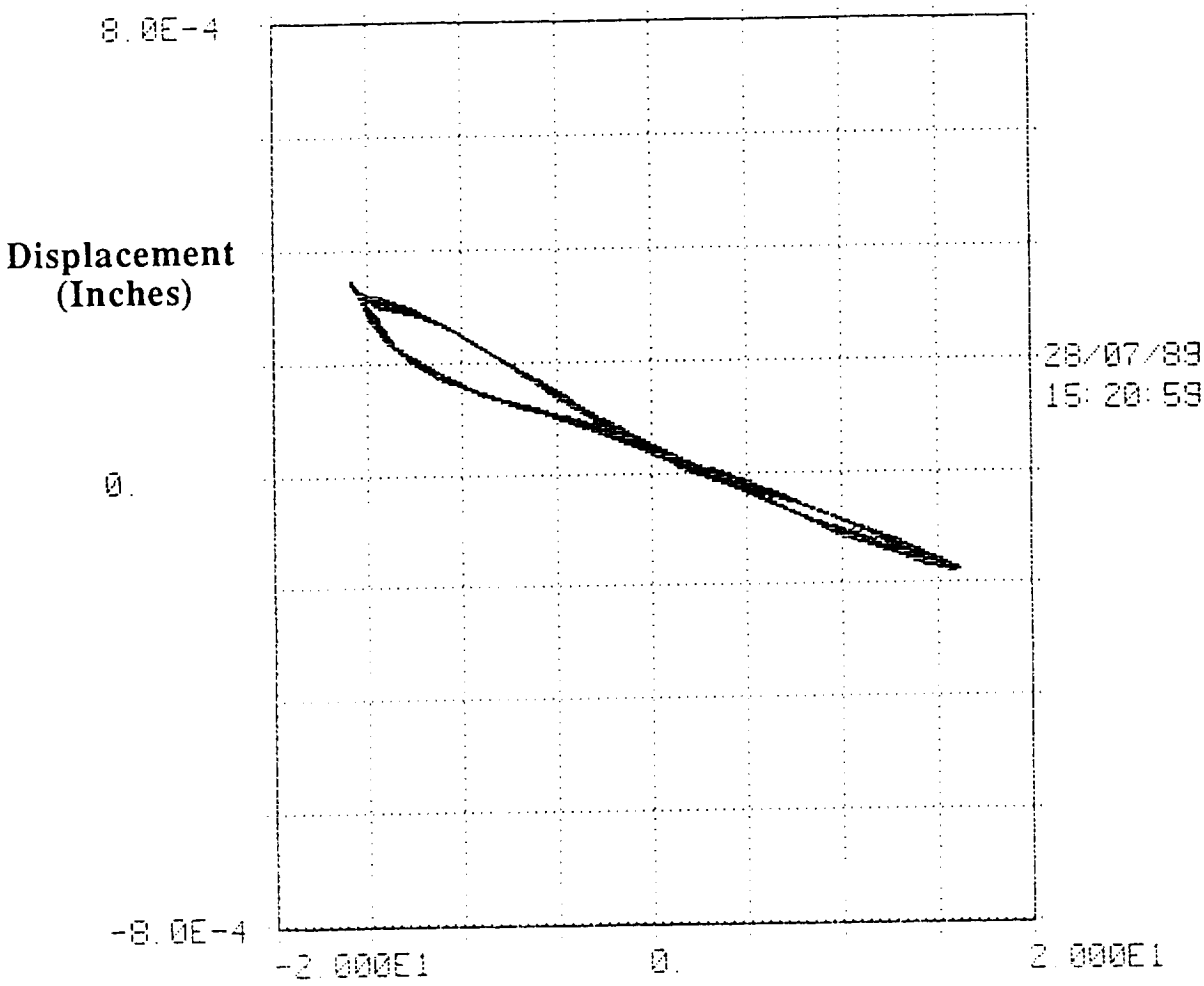

Longeron test 3, excitation at 10 Hz

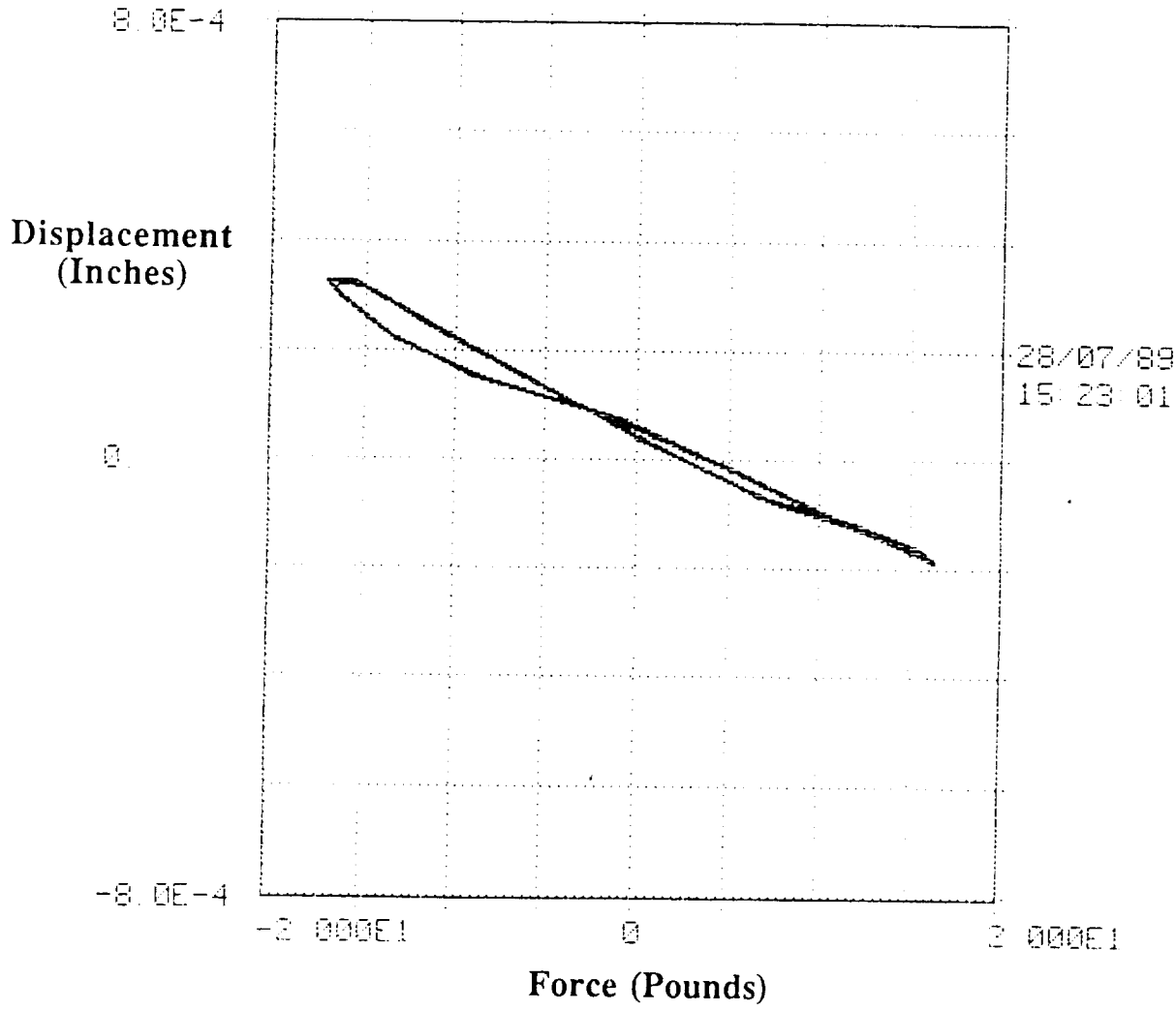

Longeron test 3, excitation at 20 Hz

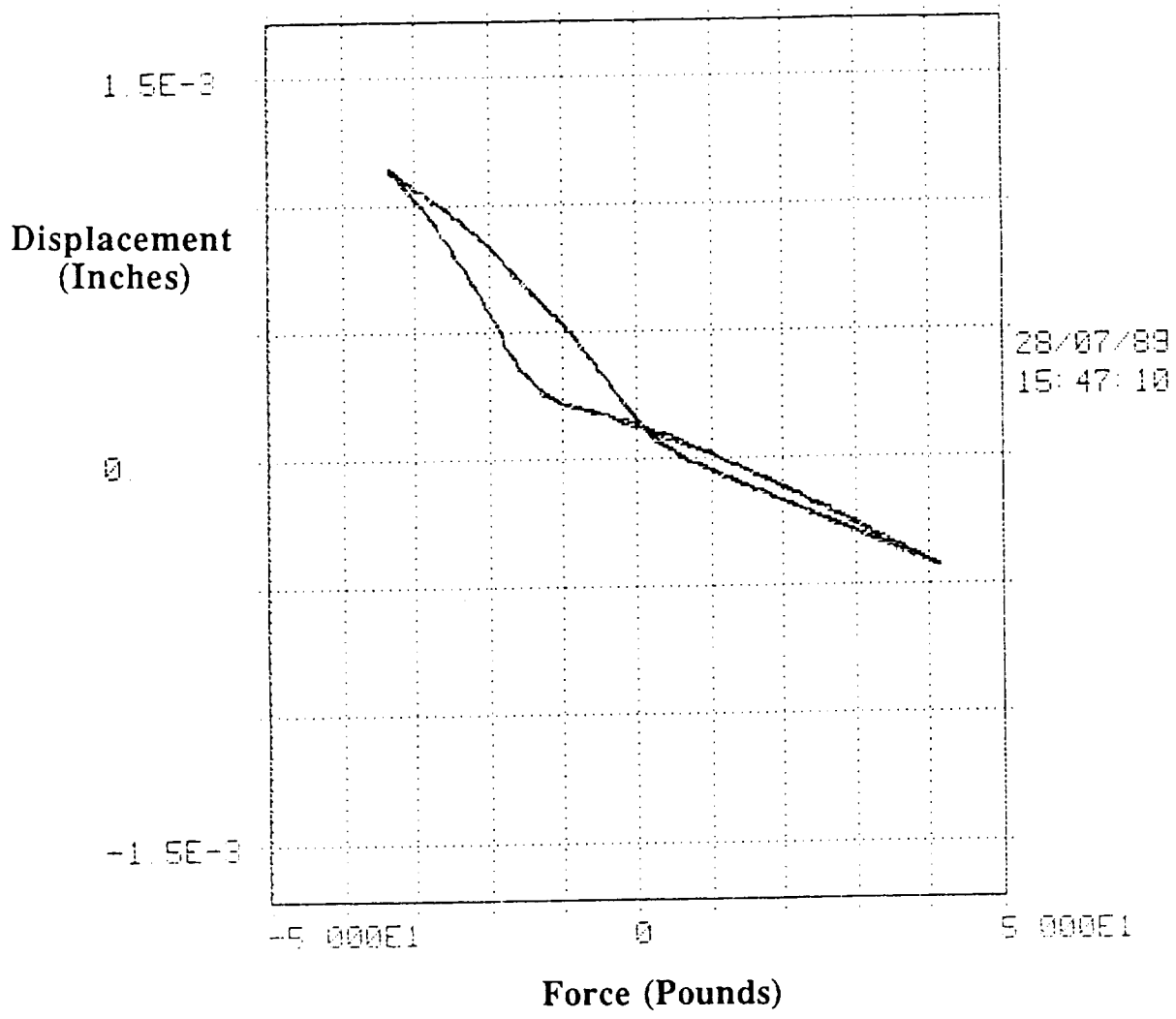

Longeron test 3, excitation at 1 Hz

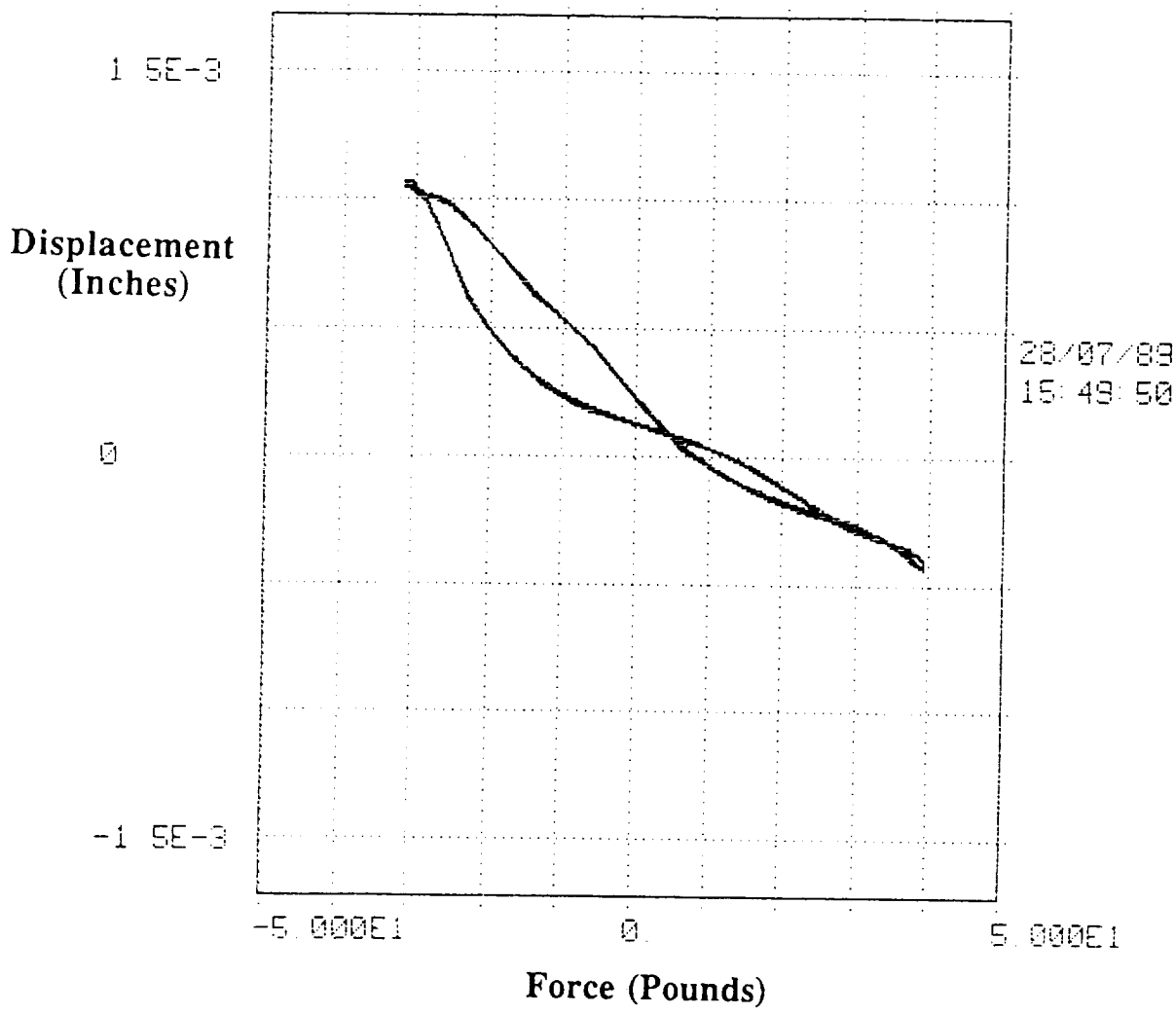

Longeron test 3, excitation at 10 Hz

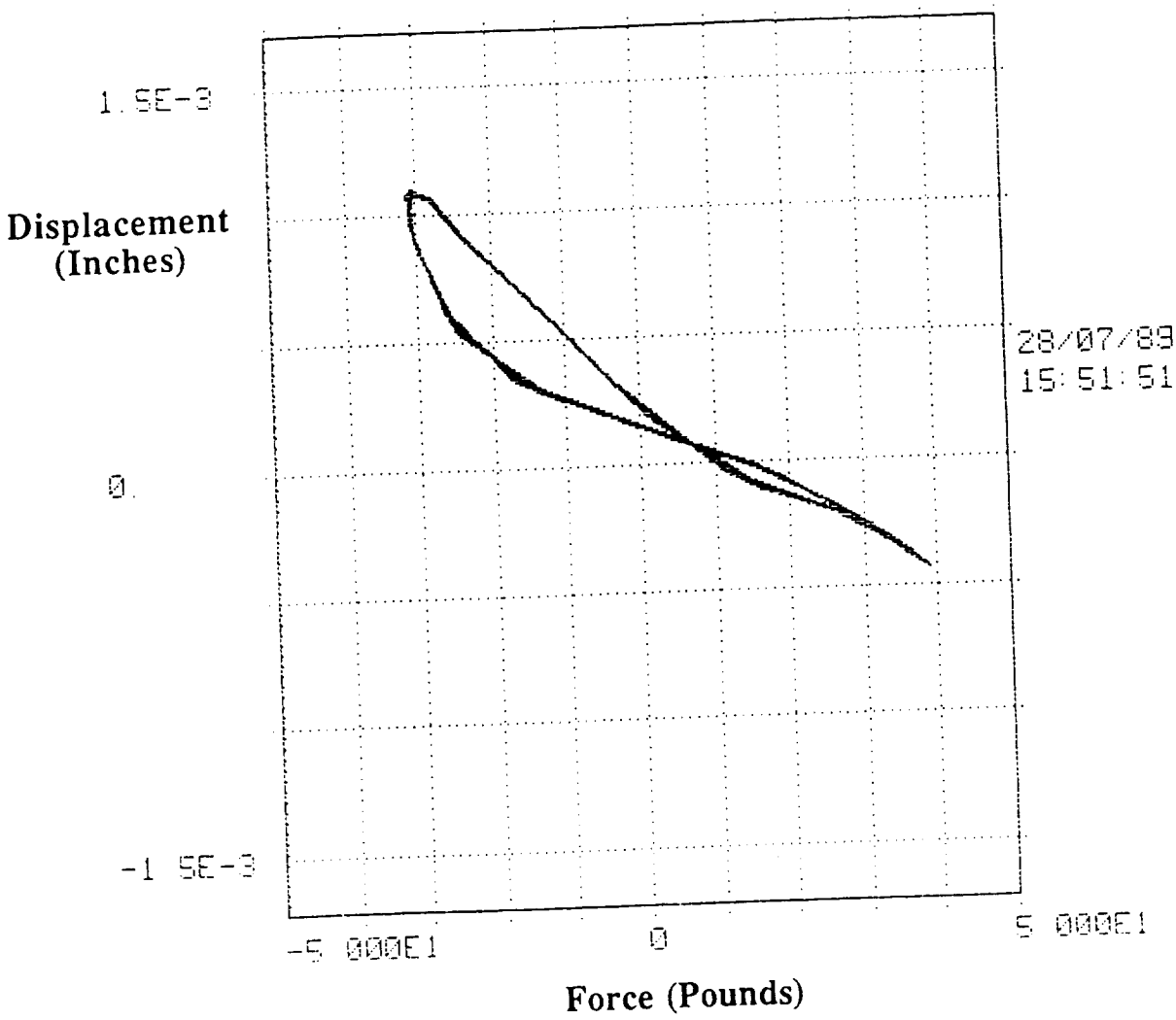

Longeron test 3, excitation at 20 Hz

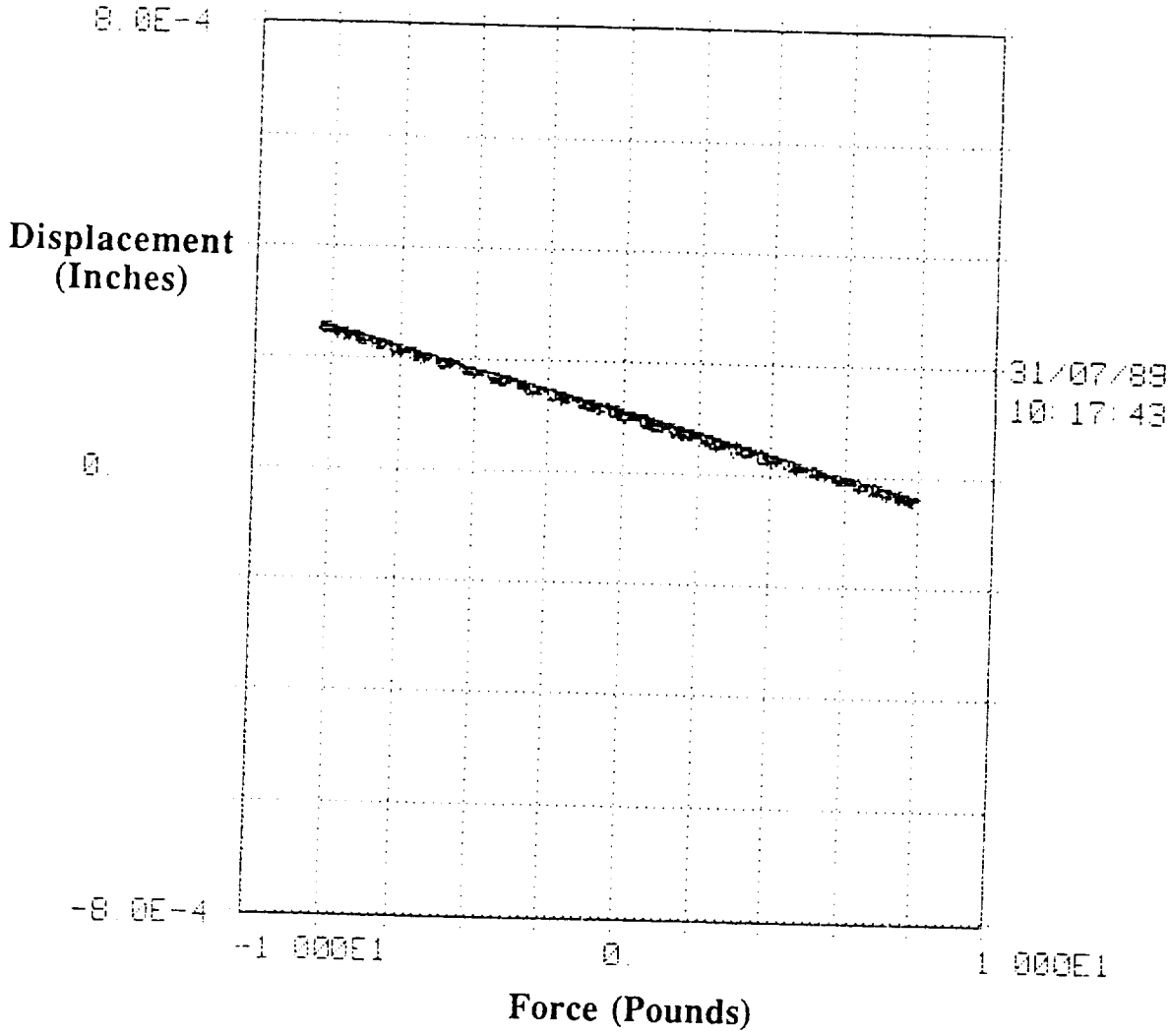

Longeron test 4, excitation at 1 Hz

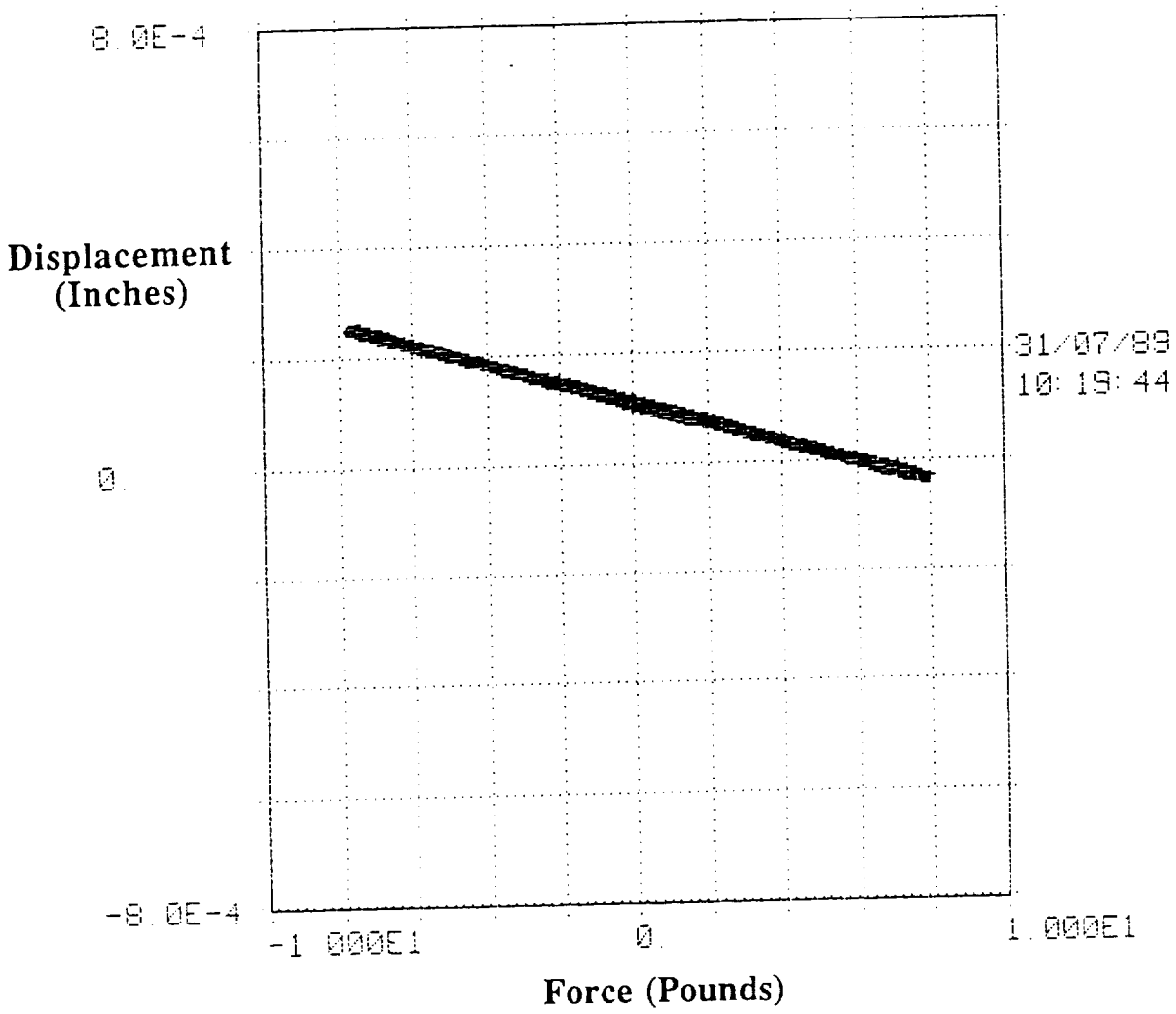

Longeron test 4, excitation at 10 Hz

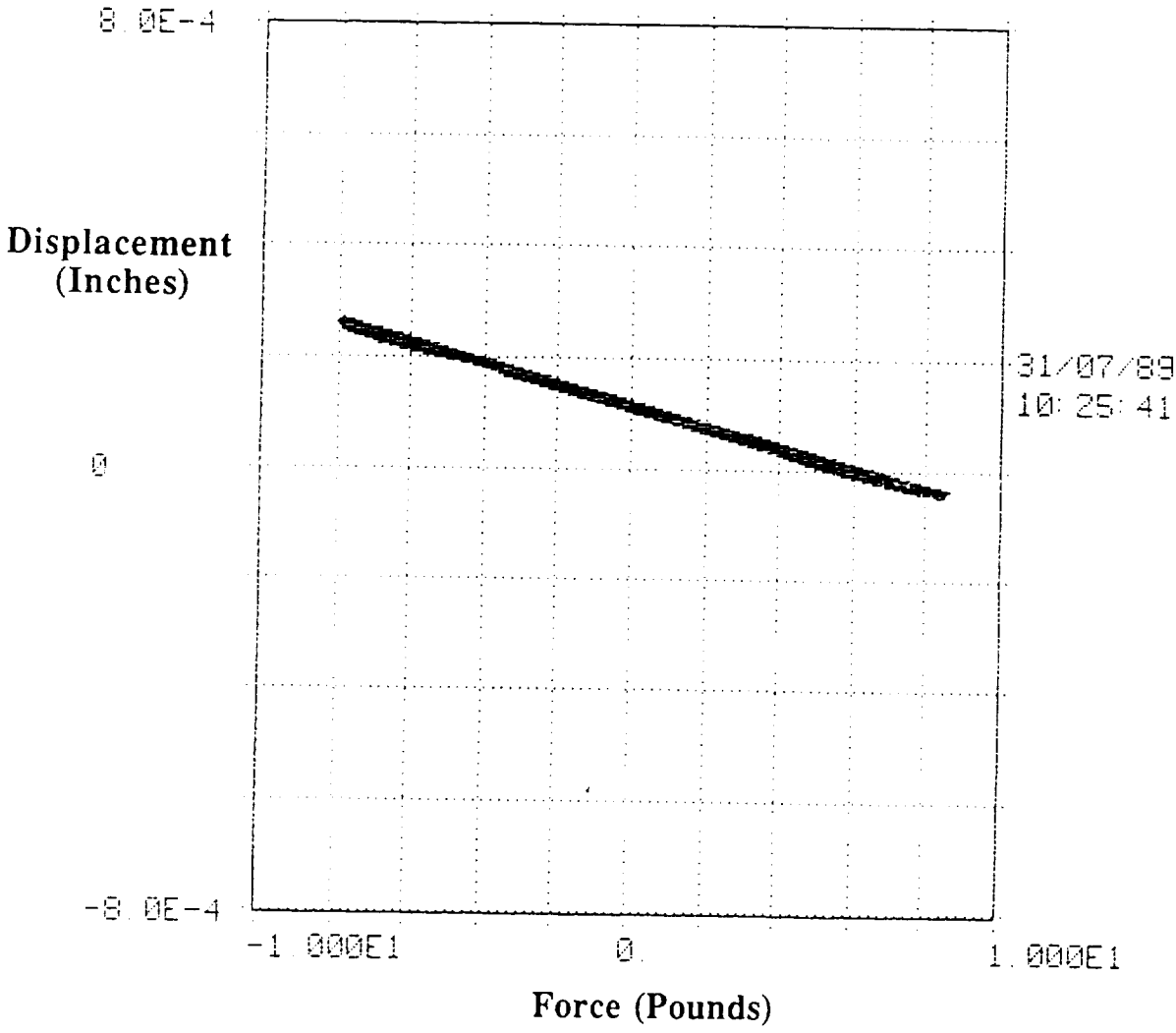

Longeron test 4, excitation at 20 Hz

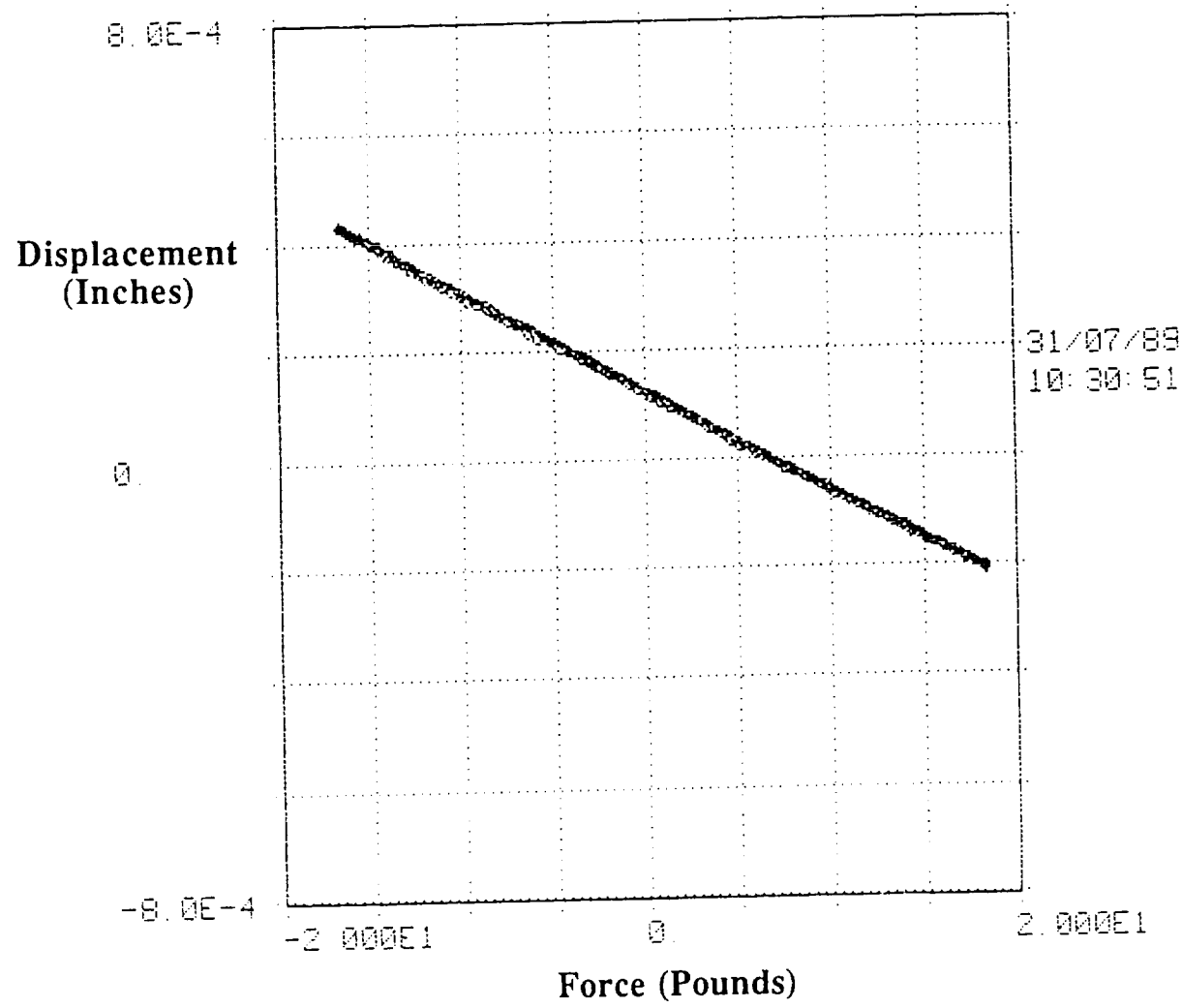

Longeron test 4, excitation at 1 Hz

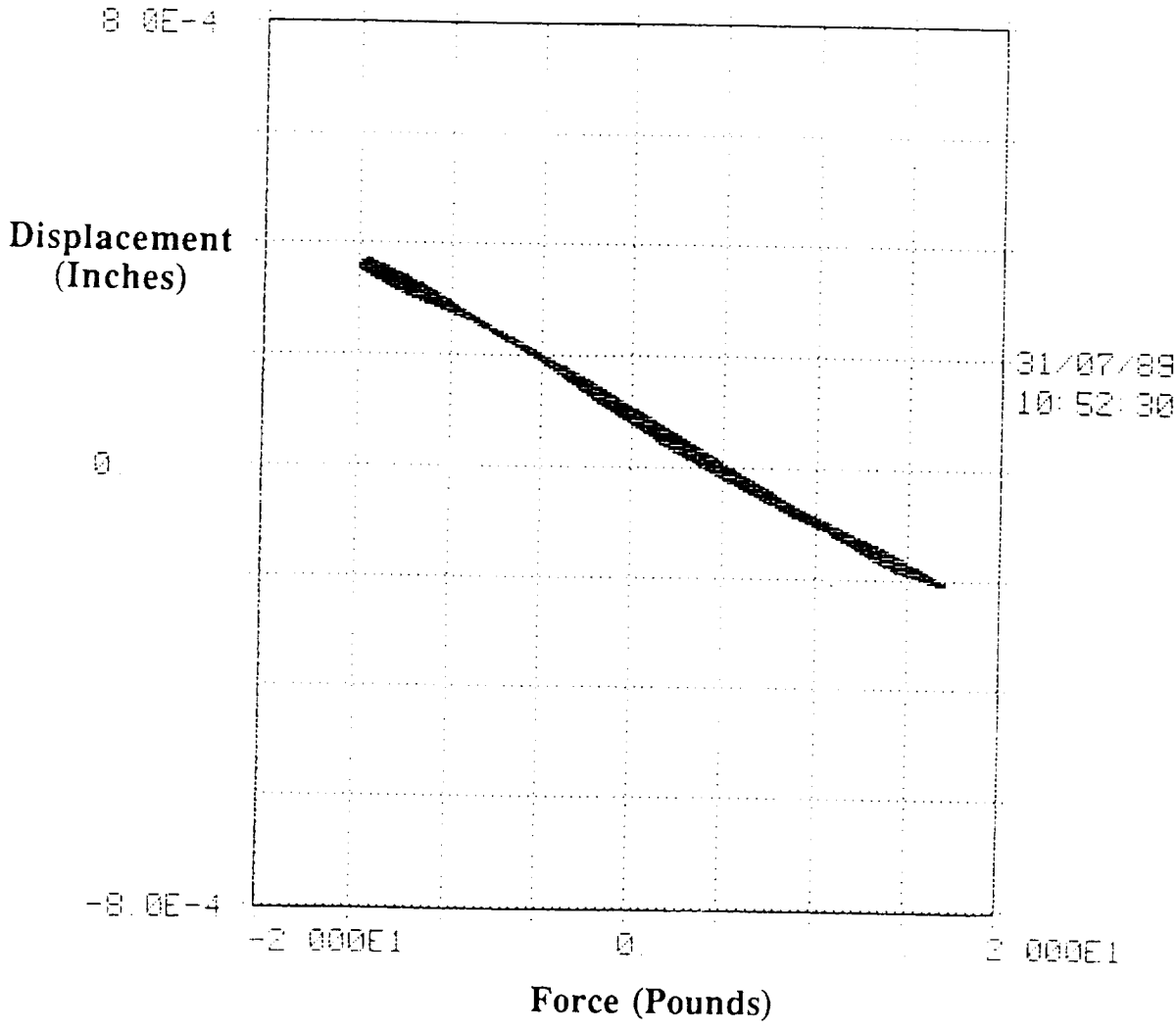

Longeron test 4, excitation at 20 Hz

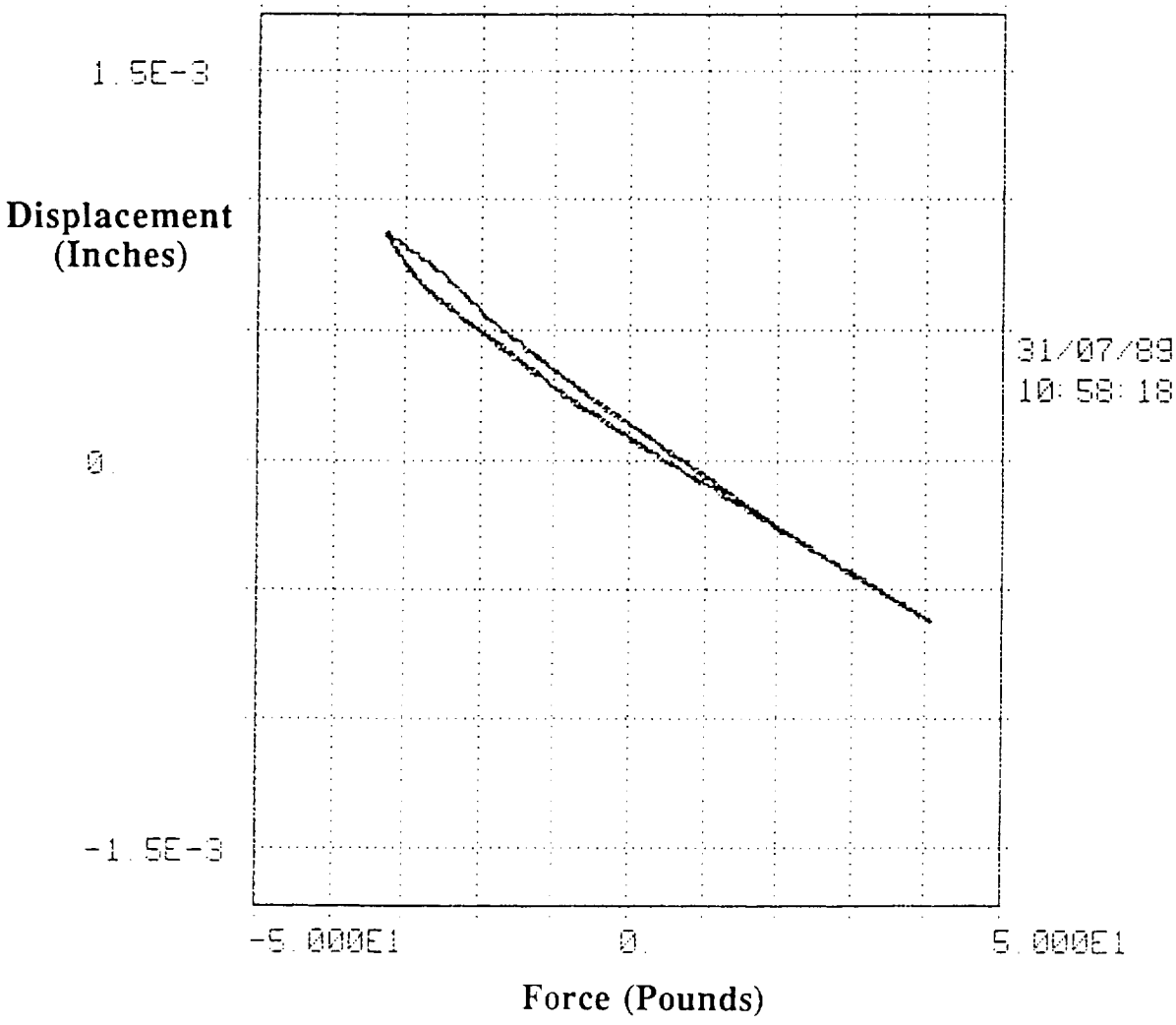

Longeron test 4, excitation at 1 Hz

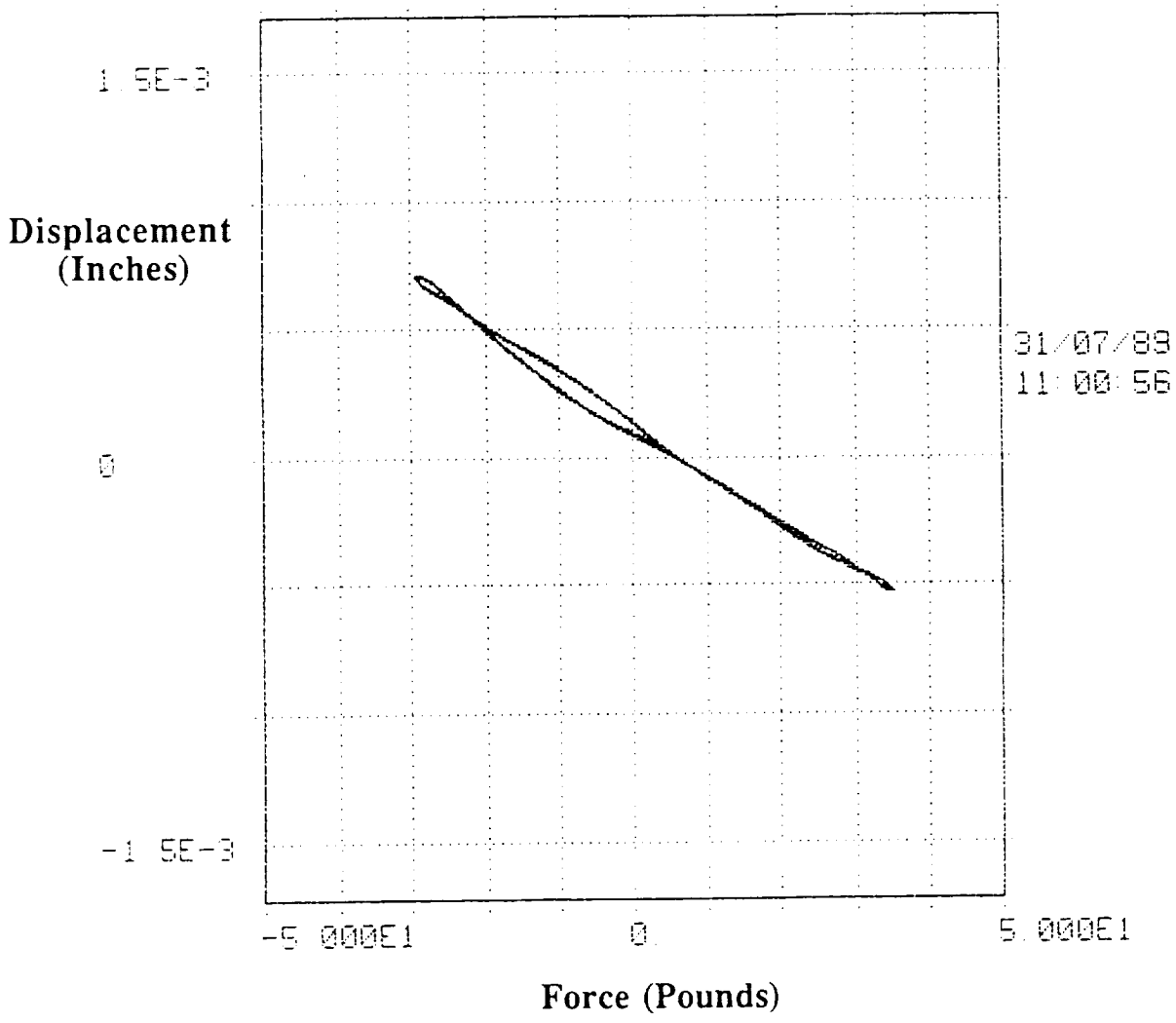

Longeron test 4, excitation at 10 Hz

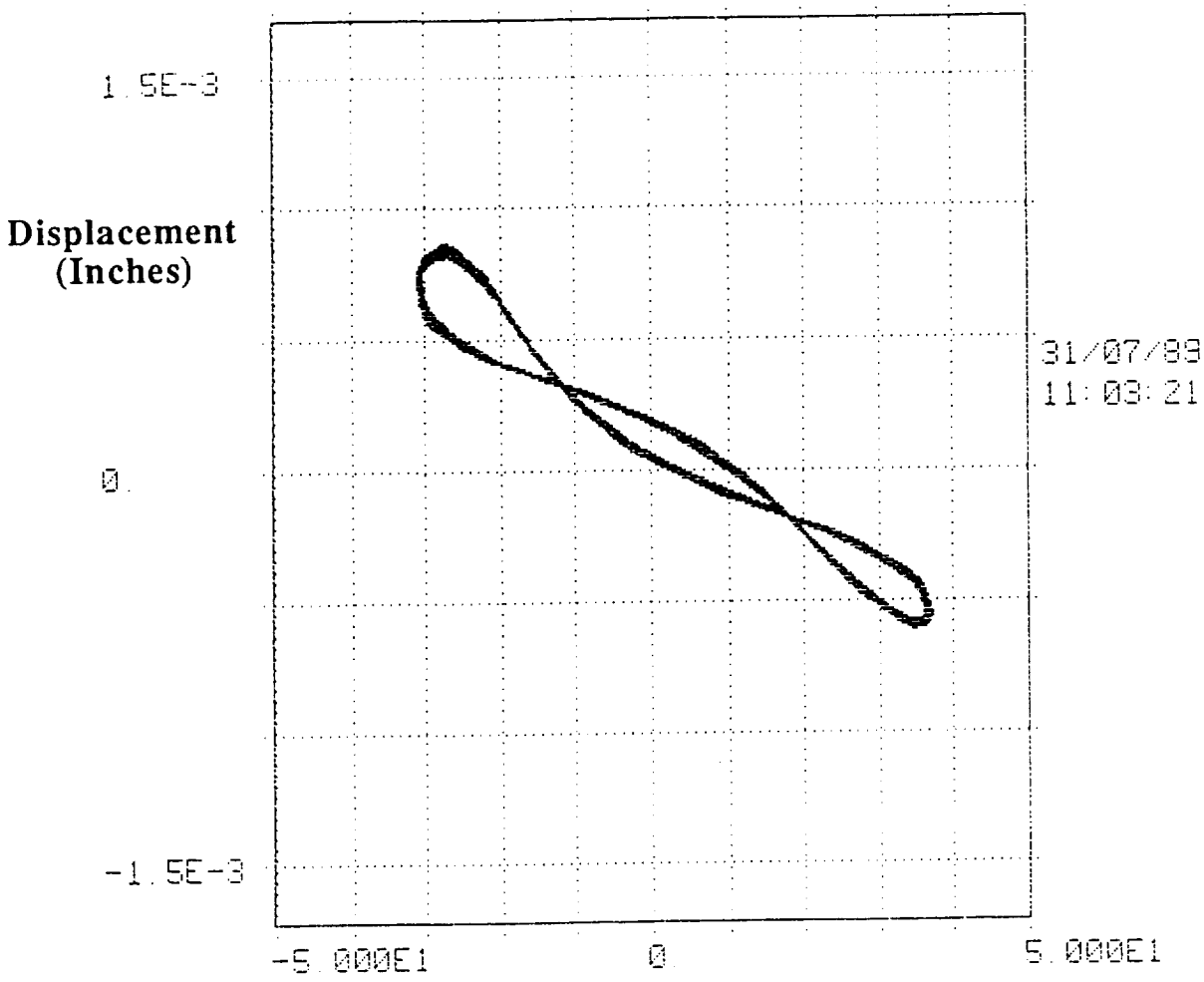

Longeron test 4, excitation at 20 Hz

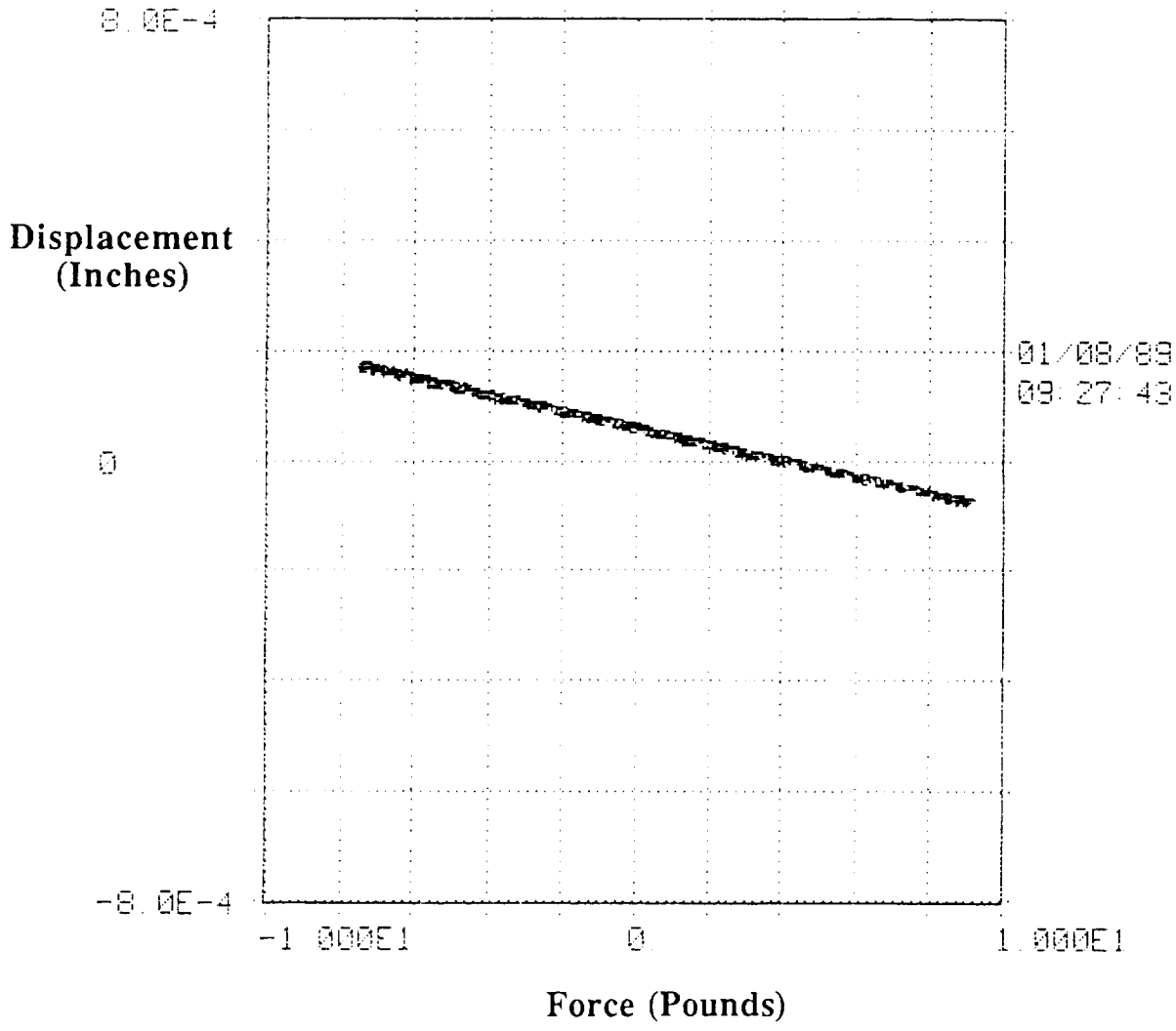

Longeron test 5, excitation at 1 Hz

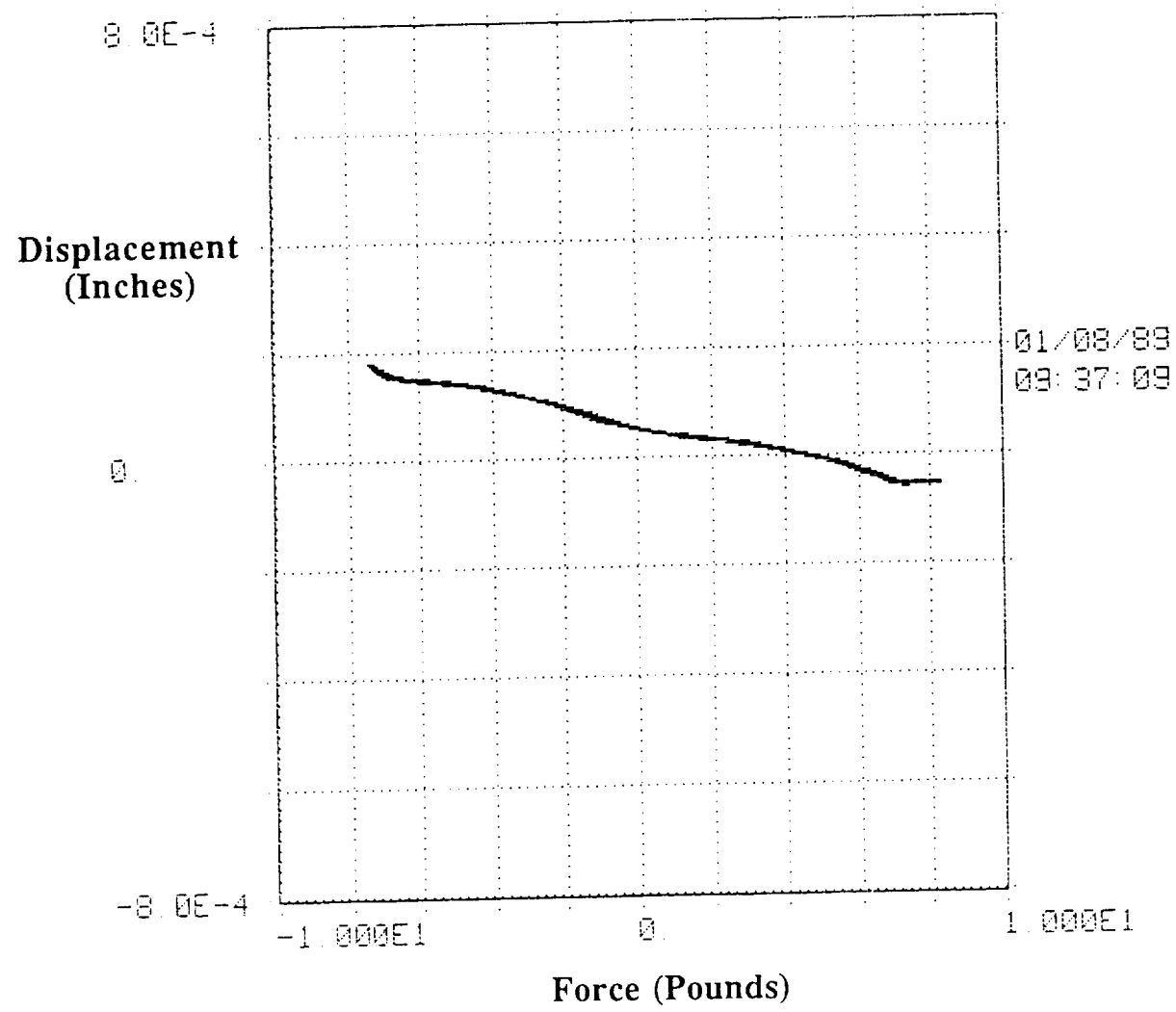

Longeron test 5, excitation at 10 Hz

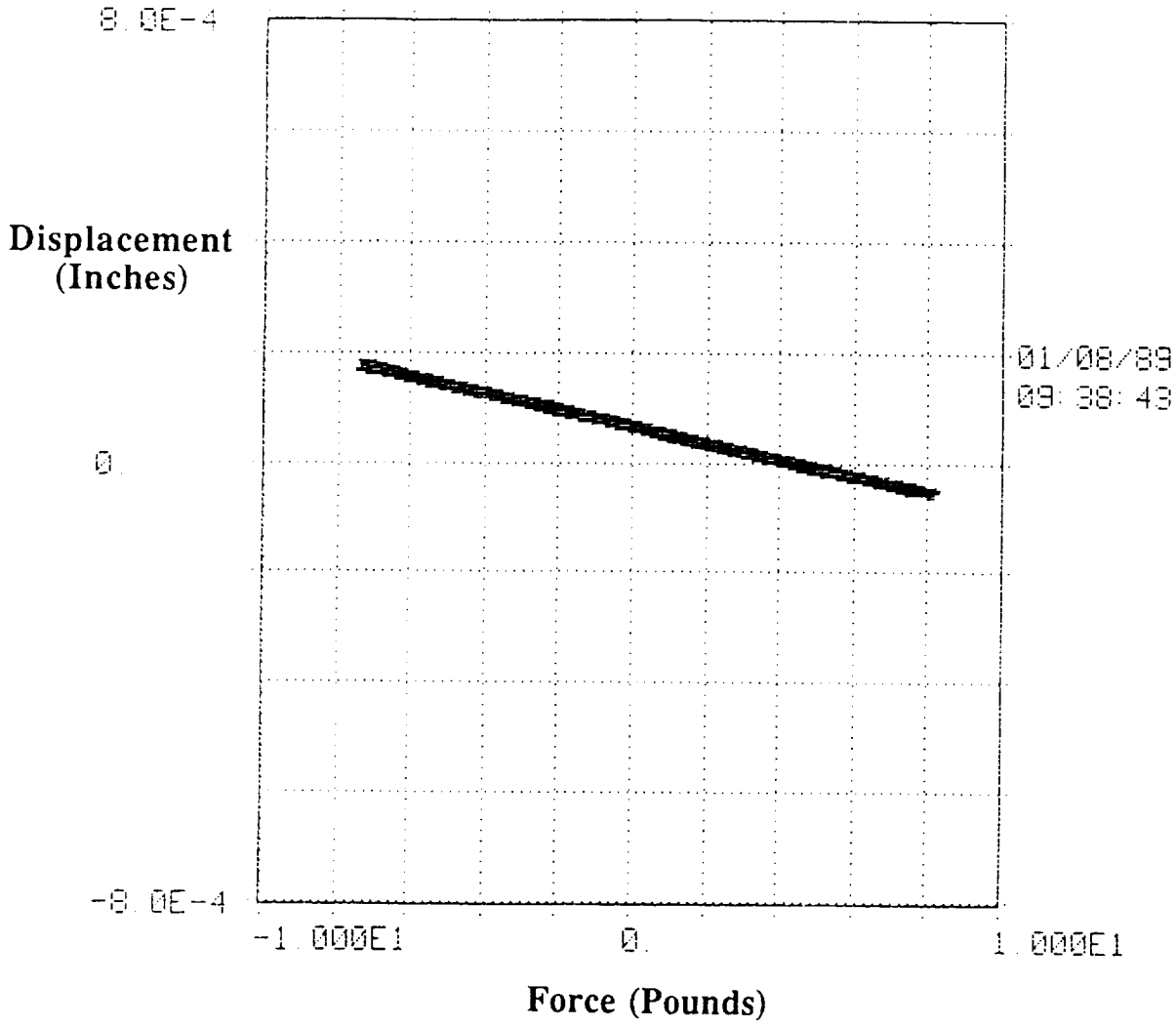

Longeron test 5, excitation at 20 Hz

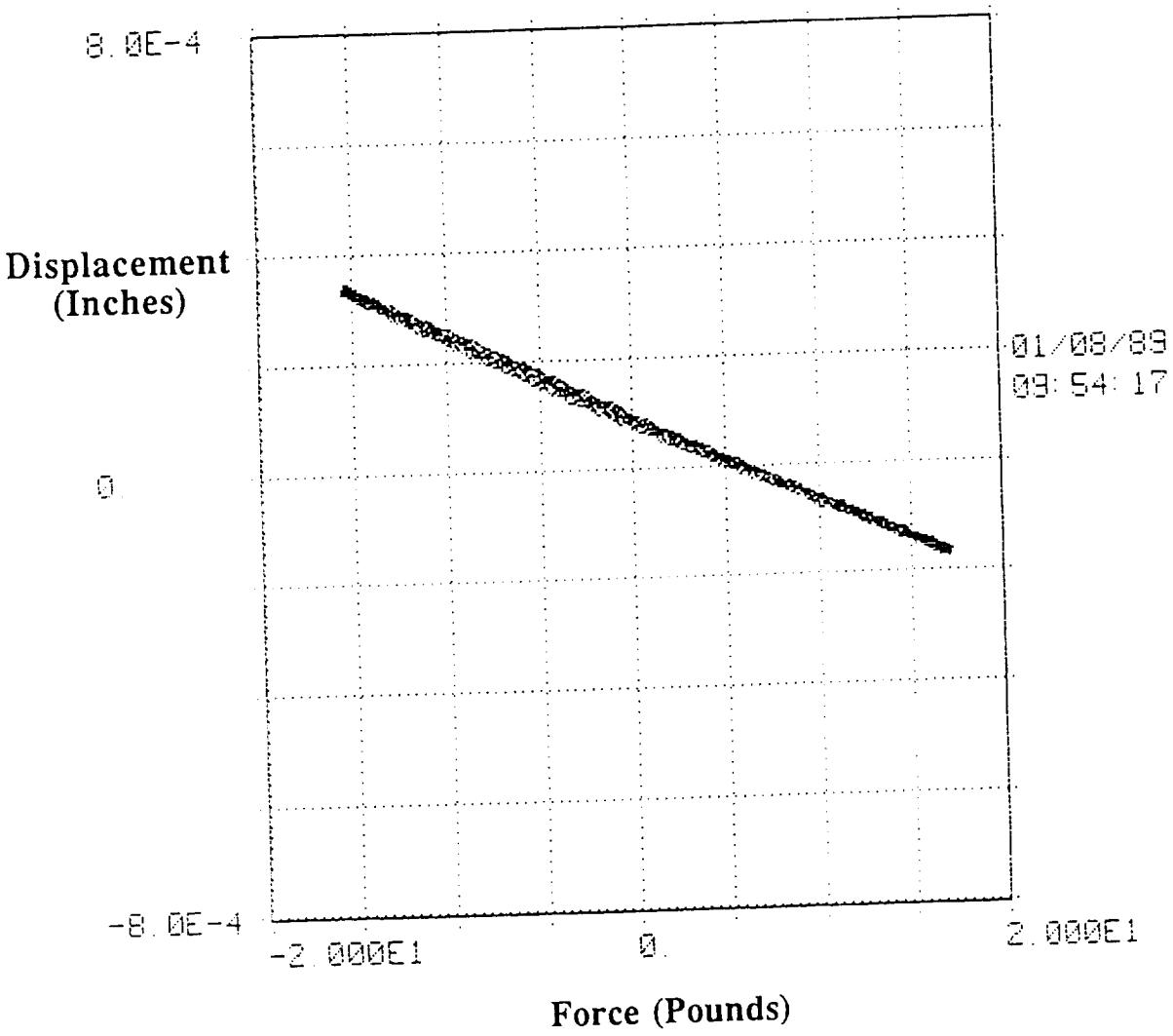

Longeron test 5, excitation at 1 Hz

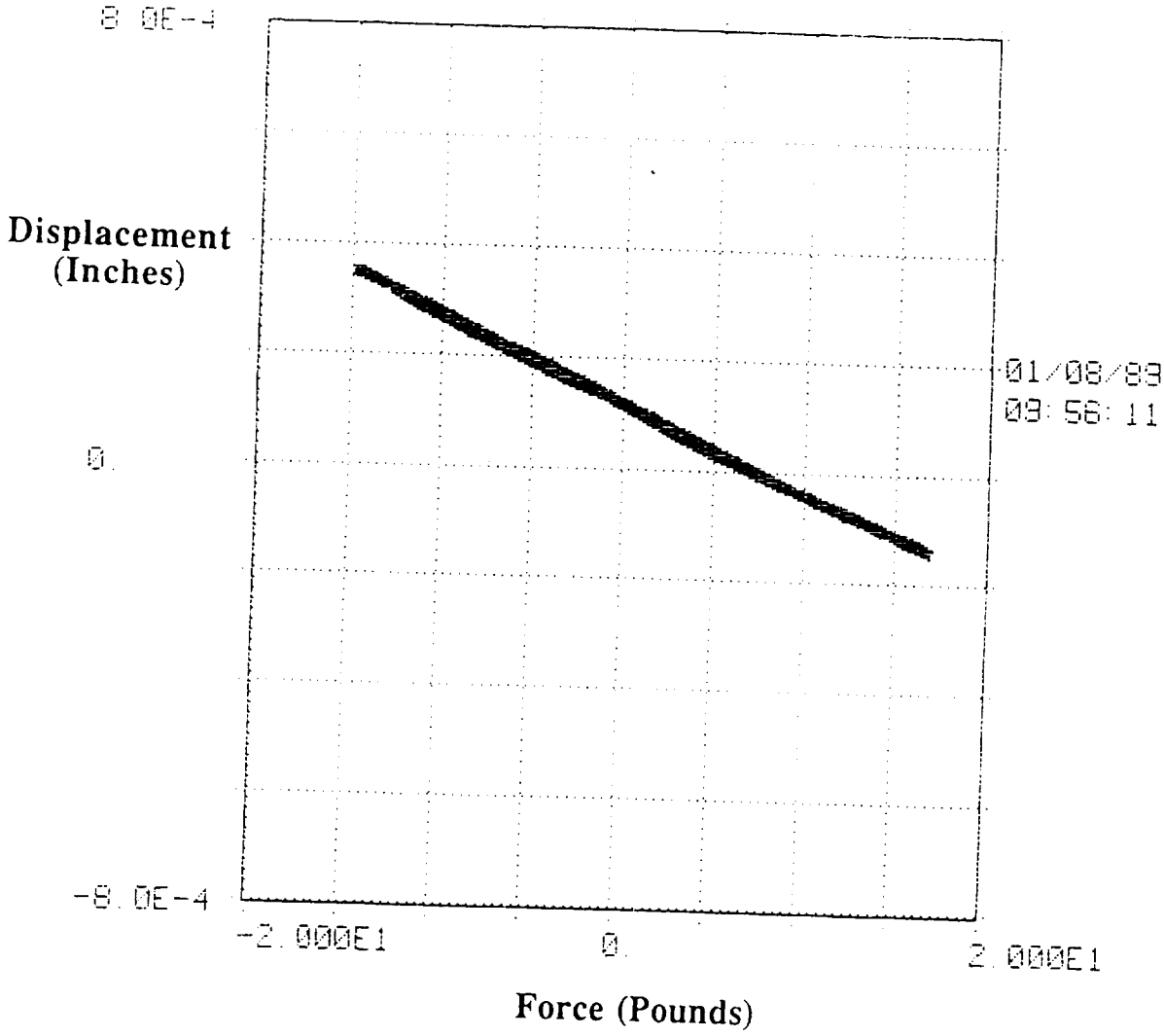

Longeron test 5, excitation at 10 Hz

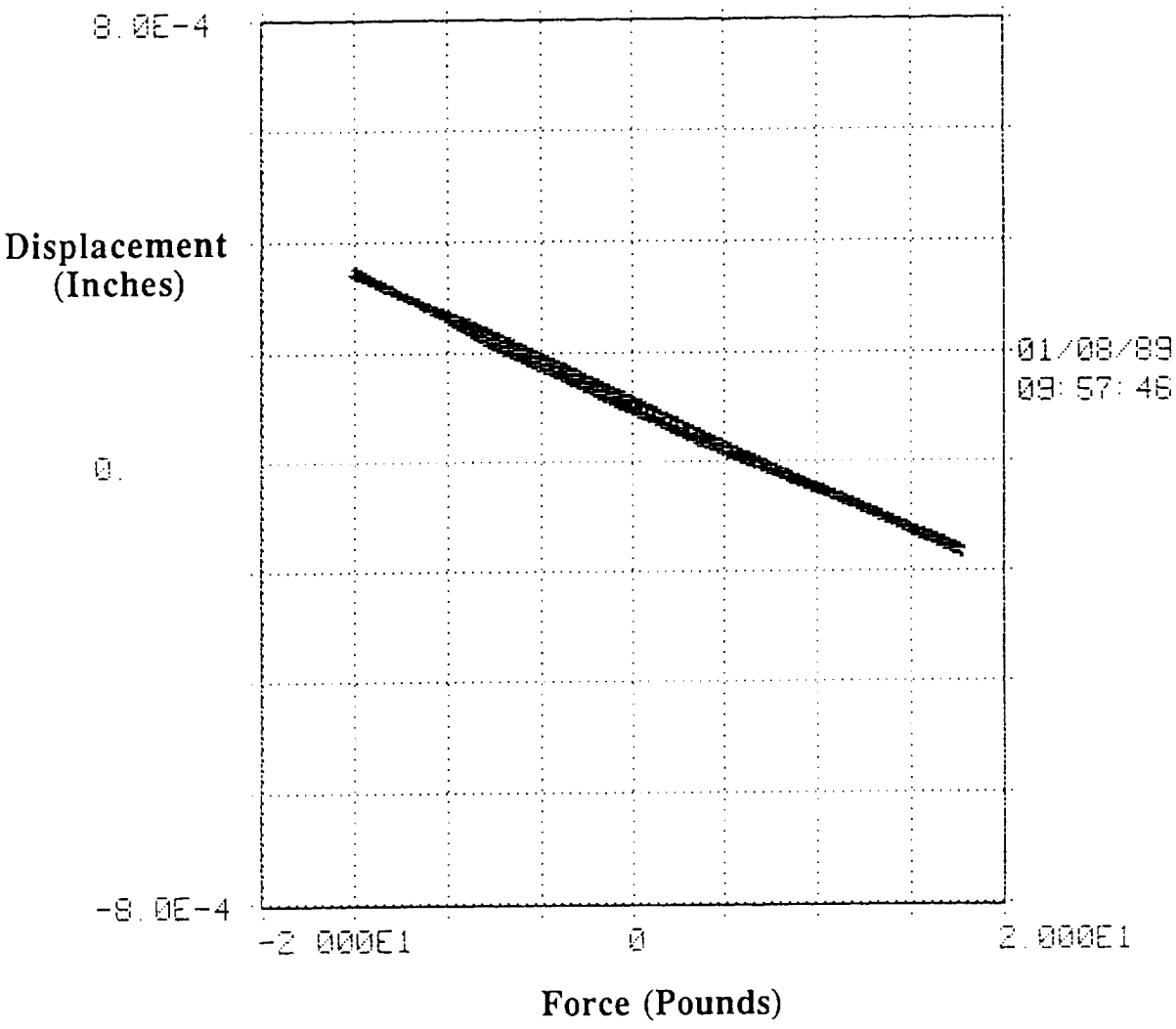

Longeron test 5, excitation at 20 Hz

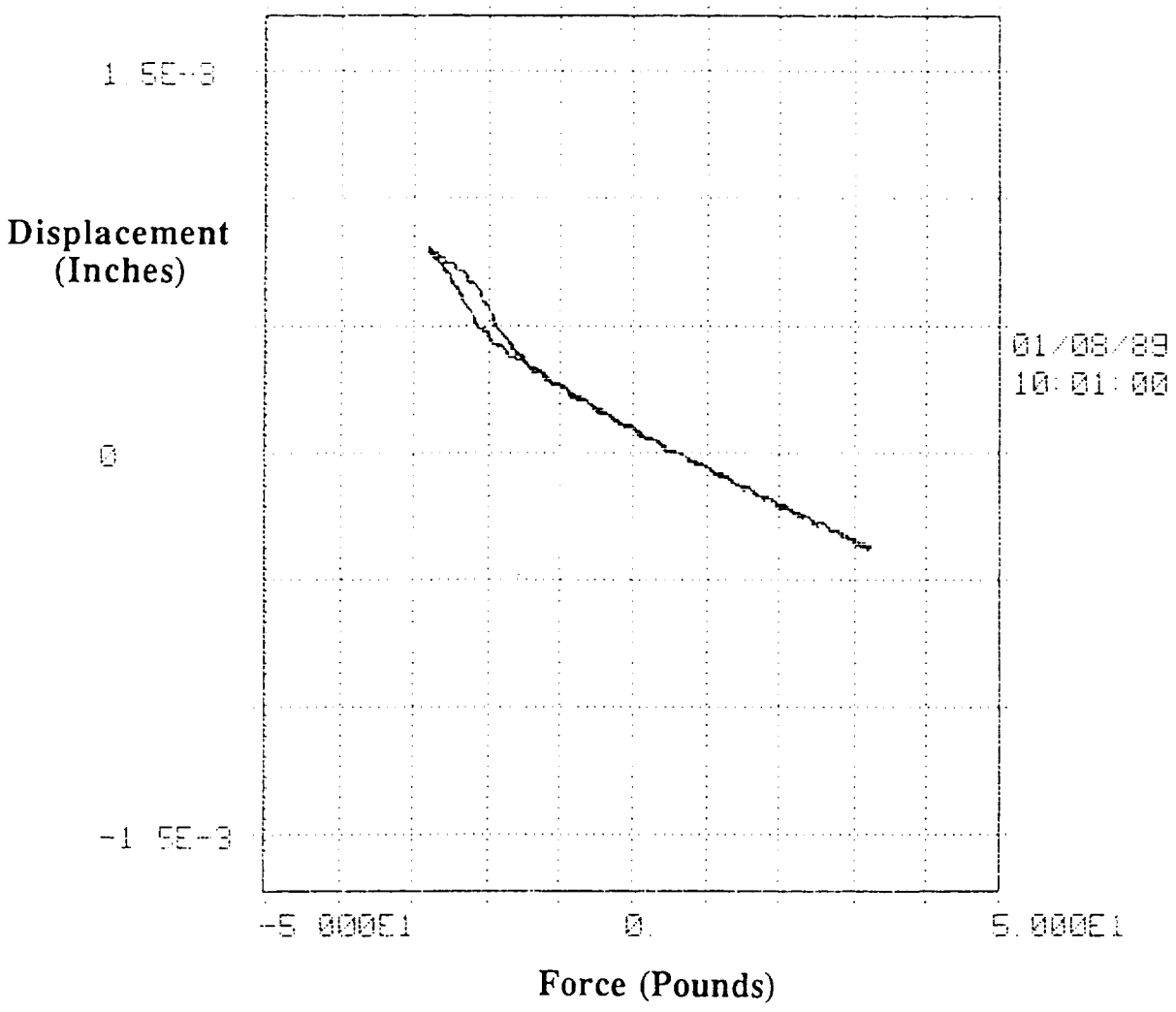

Longeron test 5, excitation at 1 Hz

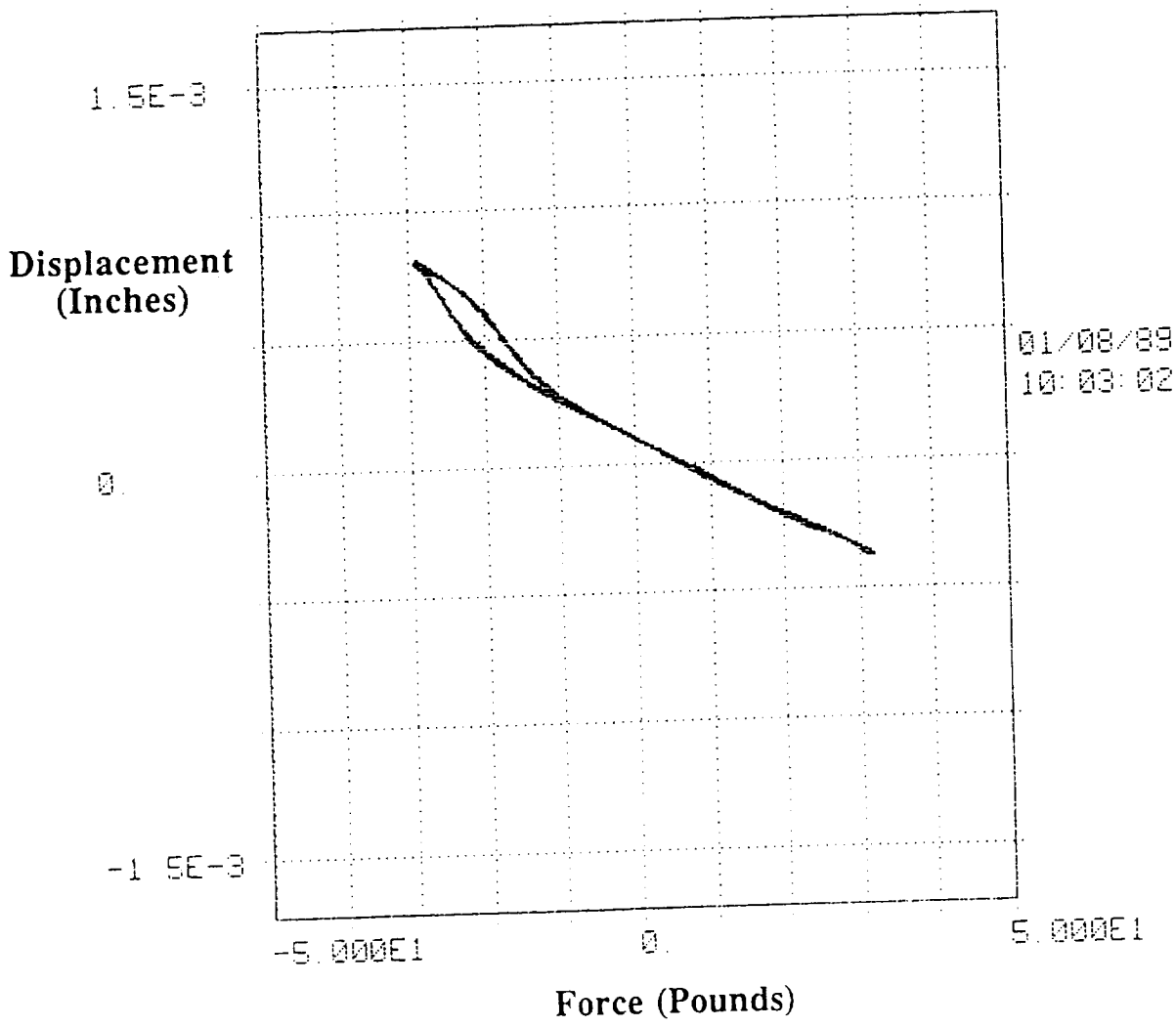

Longeron test 5, excitation at 10 Hz

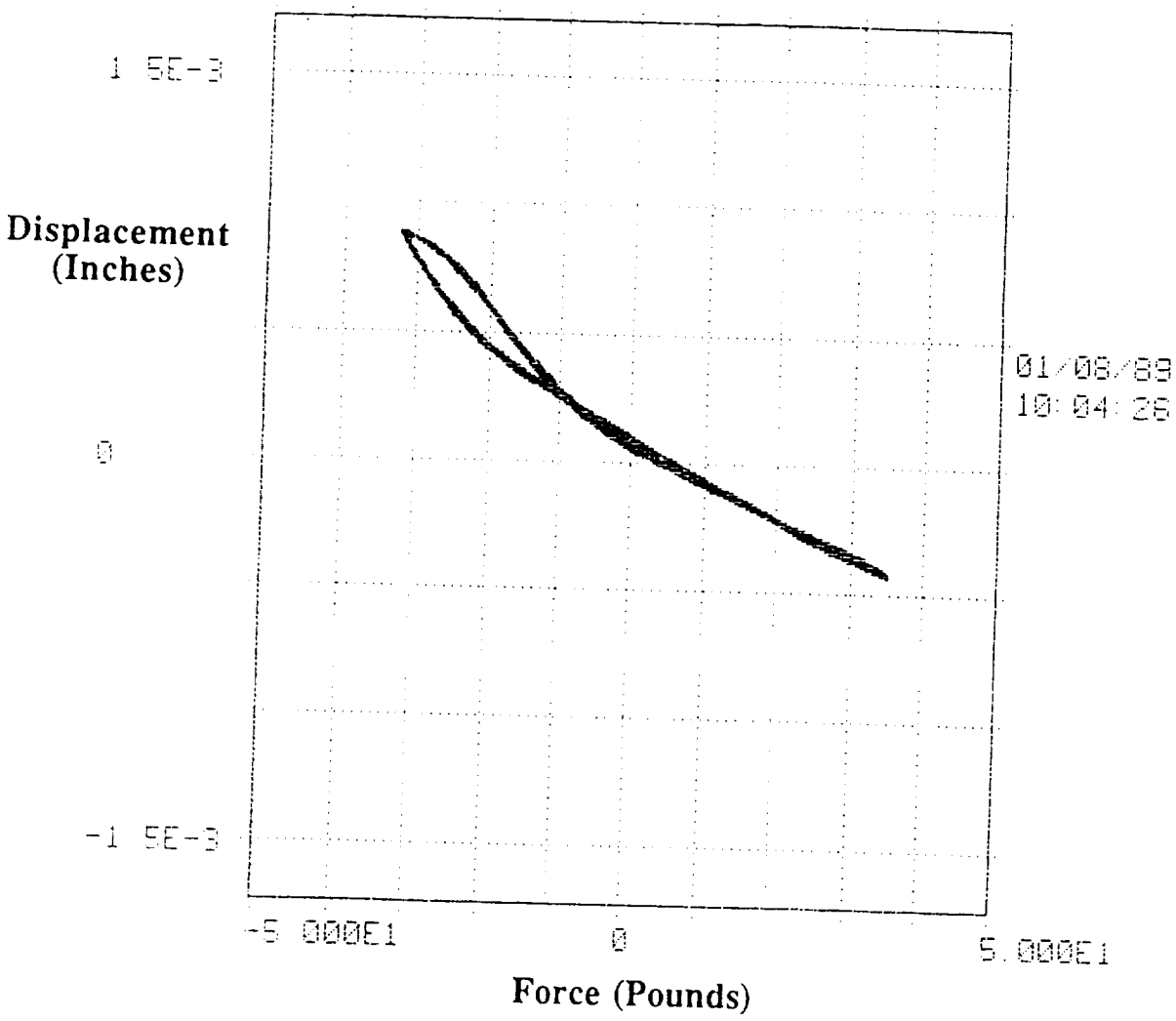

Longeron test 5, excitation at 20 Hz

Appendix C

(Taken from Ref. 1)

87-0892 NONLINEAR TRANSIENT ANALYSIS OF JOINT DOMINATED STRUCTURES

J. M. Chapman*, F. H. Shaw**, and W. C. Russell***
Boeing Aerospace Company
Seattle, Washington

Abstract

A residual force technique is presented than can perform the transient analyses of large, flexible, and joint dominated structures. The technique permits substantial size reduction in the number of degrees of freedom describing the nonlinear structural models and can account for such nonlinear joint phenomena as free-play and hysteresis. In general, joints can have arbitrary force-state map representations but these are used in the form of residual force maps. One essential feature of the technique is to replace the arbitrary force-state maps describing the nonlinear joints with residual force maps describing the truss links. The main advantage of this replacement is that the incrementally small relative displacements and velocities across a joint are not monitored directly thereby avoiding numerical difficulties. Instead, very small and "soft" residual forces are defined giving a numerically attractive form for the equations of motion and thereby permitting numerically stable integration algorithms. The technique was successfully applied to the transient analyses of a large 58 bay, 60 meter truss having nonlinear joints. A method to perform link testing is also presented.

1.0 Introduction

Current structural research has been devoted to the analysis of large erectable and deployable space structures. The impetus for such research is to establish the flight ready technology necessary for accurate shape control, vibration suppression, and control of these large and flexible space structures. One such structure is the proposed Space Station having long beamlike lattices forming its primary support structure as shown in Fig. 1. Another is the deployable truss to be used in NASA's Control of Flexible Structures (COFS) program (Ref. 1) and is shown in Fig. 2.

Two basic methods for lattice construction are under evaluation by NASA. The first uses erectable lattice members requiring astronaut EVA for construction while the second uses a pre-assembled but deployable truss requiring little EVA activity. One major disadvantage of deployable trusses is, however, the inherently nonlinear joints used in such structures. Usual analysis and testing techniques therefore become insufficient. The objective of this paper is to present an analysis technique that can perform the nonlinear static and dynamic analyses of a structure having nonlinear

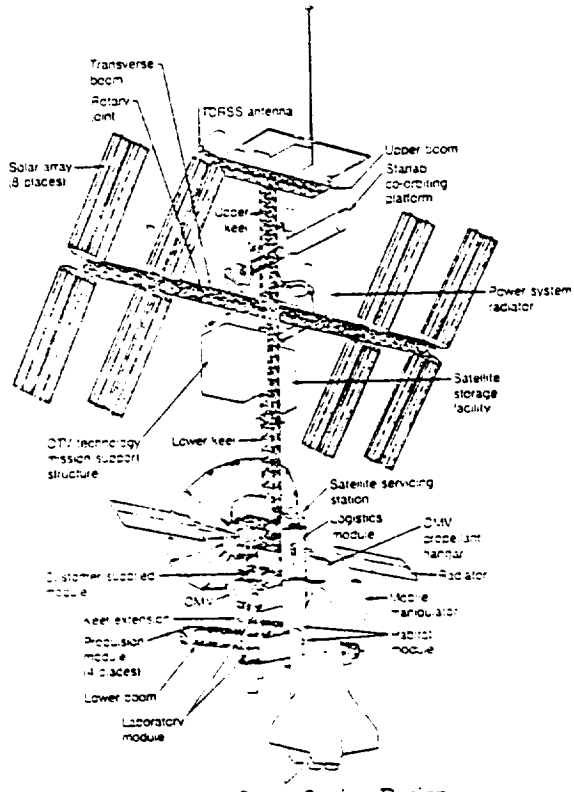

Fig. 1 A Space Station Design.

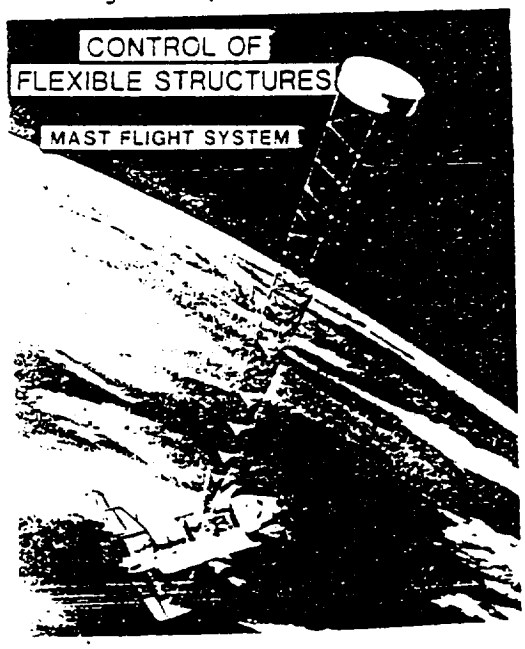

Fig. 2 COFS MAST Flight System.

* Principal Engineer
** Senior Engineer
*** Senior Engineer

Copyright © American Institute of Aeronautics and Astronautics, Inc., 1987. All rights reserved.

ORIGINAL PAGE IS
OF POOR QUALITY

PAGE 198 INTENTIONALLY BLANK

PRECEDING PAGE BLANK NOT FILMED

joints. Validation of the technique with test results still remains to be demonstrated.

One of the primary objectives of the COFS program is to establish and demonstrate the required Controls/Structure Interaction (CSI) technology necessary for the control and dynamic analysis of large space structures. The MAST truss which is one of the primary structures of the COFS experiments is a deployable, joint dominated truss structure which will probably exhibit nonlinear behavior. Accurate modeling and analysis techniques predicting the structural dynamic characteristics of this joint dominated structure is therefore required for the development and verification of the COFS CSI technology. The analytical technique presented in this paper may be applied to the COFS deployable trusses and then evaluated using results from the flight and ground experiments.

The analytical technique presented in this paper and in Ref. 2 is coined the Residual Force Technique (RFT) and can accommodate nonlinear joints typical to deployable or erectable trusses. The deformation of such structures are typically assumed to be governed primarily by axial contraction or elongation in the truss members and the analysis technique is designed to take advantage of this assumption. Specifically, the axial force transmitted through a joint is taken to be an arbitrary function of the axial displacement and velocity across the joint (Ref 3). Empirical data showing this force transmission dependency can be obtained using the methods from Ref. 3 or Ref. 4 and can be shown graphically in the the form of "force-state" maps. Force-state maps of typical deployable joints are shown in Figures 3 and 4. A force-state map of a typical Space Station erectable joint is shown in Fig. 5. Force-state maps for these joints were obtained using sinusoidal loadings and the frequency independence of the resulting force-state maps was then used to verify the assumed functional dependence of the joints.

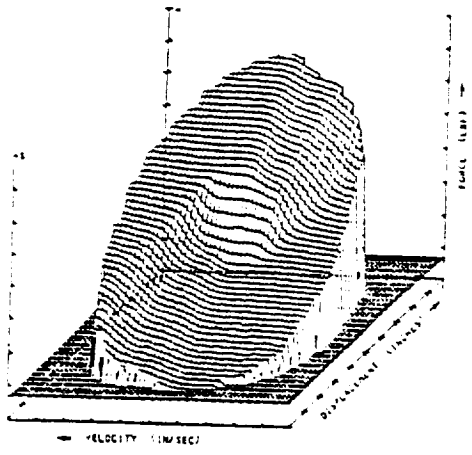

Fig. 3 Force-State Mapping of a pinned joint.

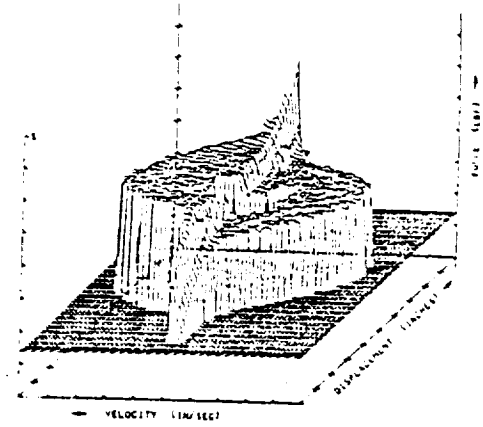

Fig. 4 Force-State Mapping of an pinned joint having an undersized pin.

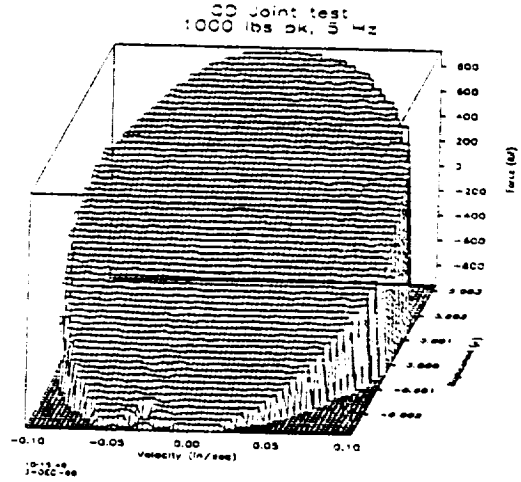

Fig. 5 Force-State Mapping of an erectable Space Station joint.

Direct monitoring of the joint's extremely small relative displacements and velocities during a transient analysis was found in Ref. 2 to be impractical however, and the concept of a link was introduced to remedy the situation. A link is defined as the composite series of joints and tubular members existing between two truss verticies. Numerical difficulties were then avoided by monitoring the displacements and forces of the relatively soft links in lieu of the incremental displacements and velocities of the extremely stiff joints.

The link concept introduced in Ref. 2 ultimately proved to have four basic advantages. First, stable integration of the equations of motion could be obtained when the nonlinearities were defined in terms of the links instead of the joints. Second, substantial size reduction of the equations of motion were obtained even before modal extraction. Third, direct tests on the links could be performed to validate the analytical description of

ORIGINAL PAGE IS
OF POOR QUALITY

the link. And fourth, direct testing of the links could identify link behavior not predictable from joint testing alone (Ref. 4). These four advantages of the link concept then motivated link testing in addition to the joint tests. A proposed link testing procedure will be presented in this paper.

Link testing may not only be sufficient but also necessary for certain deployable hinge joints having complex load paths varying from tension to compression. Specifically, the hinge joints of the deployable truss in Ref. 4 were shown to invalidate the assumed axial dependency of the joint and the axial force-state maps of the isolated hinge joints were insufficient to predict the link behavior. The hinge joints within the Ref.4 truss frame actually "buckled" laterally causing the links containing the hinge joints to be much softer axially than predicted. Eccentricities in the joint's manufacture and assembly were identified as the primary cause for this lateral buckling behavior. Since the joint tests were designed to measure the axial force in the joint as a function of its axial displacement and velocity and the test fixturing was designed to prevent any lateral movement of the hinge, the lateral buckling behavior of the joint was restricted. Such lateral restraint did not exist in the truss however, depicting the need for a simple definitive test that could directly measure the joint's properties as it would behave within the truss structure. Link testing should satisfy this requirement.

Link testing as proposed in this paper should provide the composite description of the link's stiffness and damping as required by the analytical simulation. However, joint testing on isolated joints should still be performed to better understand the total behavior of the link.

The basic approach to deriving an accurate nonlinear structural model of a large, flexible, joint dominated structure is to first obtain empirical data describing the nonlinear behavior of the joints and/or links, incorporate this data into a structural model using the residual force technique, and then compare the predicted response with the empirical response obtained from static and modal survey ground tests. Model update may then be necessary.

A review of the residual force technique will be given here followed by selected applications on a 10 bay deployable truss and a 60 meter COFS deployable truss. Various joint nonlinearities will be examined. Finally, a procedure to directly measure the stiffness and damping properties of the composite link will be presented.

2.0 Residual Force Technique

The residual force technique was introduced in Ref. 2. The primary objective of the technique was to account for such nonlinear joint phenomena as free-play and hysteresis during the transient analysis of a large, flexible, and joint dominated structure. Another objective of the technique was to permit substantial size reduction in the number of degrees of freedom describing the nonlinear structural model since otherwise the model would be prohibitively large. The technique was shown to compute simple (two degree of freedom) problems an order of magnitude faster than standard nonlinear techniques and to successfully complete transient analyses of large problems (500 nonlinear degrees of freedom) where standard techniques failed to converge.

In the residual force technique, the linear and nonlinear characteristics of the truss are separately identified and placed on the left and right hand sides of the equations of motion, respectively. The "residual" forces appearing on the right hand side represent the nonlinear corrections that must be applied to a linear structure in order to replicate the nonlinear response. The nonlinear properties of the joints can be obtained empirically in the form of force-state maps. While the nonlinear behavior of the joints may be characterized using force-state maps, the study in Ref. 2 showed that the practical inclusion of these nonlinear effects in a nonlinear structural model is to first generate, either analytically or empirically, force-state maps for the truss links. Residual force maps are then generated to account for the small nonlinear corrections in the link's structural behavior.

The equations of motion governing the dynamic response of a large, flexible, and joint dominated structure are derived below. This derivation necessarily entails a discussion of the assumptions used to model the nonlinear structure. With these assumptions, the idea of "residual force maps" will be introduced and discussed for some simple joint nonlinearities. The general equations of motion for nonlinear joint dominated structures will then be presented along with the selected applications.

2.1 Modeling Assumptions

The modeling assumptions used by the residual force technique in the analysis of a typical deployable or erectable structure are shown in Fig. 6. As shown, the longerons and lacing members have two or three nonlinear joints that can be characterized using force-state maps. Note that the battens are shown not to have nonlinear joints. This is because stable behavior of trusses (or beamlike lattice structures) generally require that all battens be rigidly attached to the lattice vertices. If the battens were pinned instead of rigidly attached, geometric nonlinearities due to the finite size of the joint must be considered. Moreover, low frequency joint rotation modes would exist unnecessarily complicating the dynamic behavior of the

ORIGINAL PAGE IS
OF POOR QUALITY

structure. Deployable trusses should therefore avoid pinned battens if at all possible.

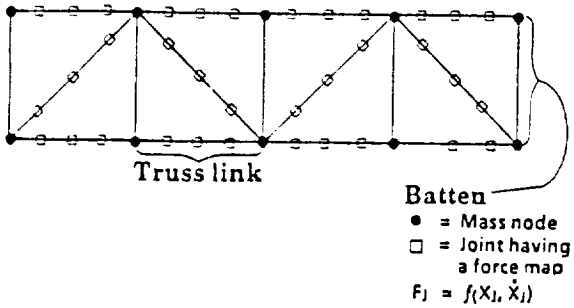

Fig. 6 Residual Force Technique Modeling Assumptions.
- o Battens are not pinned
- o Truss Links are axial members only
- o Joints have Force-State Maps
- o Mass lumped at verticies

Another modeling assumption required in the residual force technique is that the mass of the truss can be lumped at nodes. This approximation is usually valid for low frequency excitation as is generally the case for the Space Station or other large space structures. It remains to be seen if damping effects can be accurately calculated when using the lumped mass approach.

The concept of a truss link is also pictorially shown in Figure 6. A truss link is defined here as the composite series of joints and tubular members that represent the truss structure between two truss verticies. Truss links are ideally considered as axial load carrying members only and are modeled as a series combination of nonlinear joints and linear springs.

The complete description of the truss link requires, in general, monitoring all the "internal" degrees of freedom of the link that describe the relative displacements of each joint and spring. In certain special instances however, a composite force map for a massless truss link can be derived. First, if all joint force maps depend only upon displacement then an equivalent force map for the link can be easily derived. Second, if the massless truss link has only two arbitrary but identical joints then a residual force map for the link can be derived. And finally, if the joint stiffness is large, the damping small, and the rates low for each joint, then the force map for the link can again be derived. This last special instance is generally the case for Space Station trusses and suggests that an equivalent force map for the link can be derived directly from testing. If none of the above three special instances apply to the truss being analyzed, then all interior degrees of freedom of the link must be monitored during the analysis. One easy way to accomplish this is to simply include additional mass freedoms along the truss link.

Special attention has been given to the modeling of the truss links because the success or failure of a transient analysis technique strongly depends upon the ability to accurately monitor the nonlinear stiffness and damping effects of the generally stiff joints. Direct monitoring of the extremely small relative displacements across the joints is impractical. Instead, the residual force method takes advantage of the fact that the joints are in series with a relatively soft spring and a residual force map for the link is derived. In essence, the forces in the joints are monitored instead of the relative displacements.

2.2 Residual Force Maps

The derivation of a residual force map for a joint in series with a soft spring will be given here (see Fig. 7).

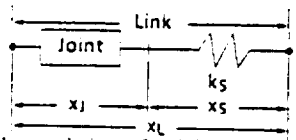

Fig. 7 Link consisting of a joint in series with a soft spring.

The force in the joint can be described by a force-state map $f_J(x_J, \dot{x}_J)$ giving the joint force as an arbitrary function of the relative displacement x_J and velocity $\dot{x}_J$ across the joint. This force must also equal the force in the soft spring, and both the spring force and the joint force are equal to the force F_L in the link. Therefore,

$$F_L = f_J(x_J, \dot{x}_J) = k_S x_S \qquad (1)$$

where k_S is the stiffness of the soft spring and x_S is the relative displacement across the spring. Define x_L as the total relative displacement across the link. Then

$$x_L = x_J + x_S \qquad (2)$$

The first step in generating the residual force map for the link is to transform the displacement axis of the joint force-state map so that the new force map is a function of the total link displacement and the joint's relative velocity. The force in the link can then be expressed as

$$F_L = f_J(x_L, \dot{x}_J) \qquad (3)$$

The second step in the residual force map construction uses the definition of the residual force as the difference between the linear "left hand side" force and the total nonlinear link force. Therefore,

$$F_R = k_S x_L - F_L \qquad (4)$$

The linear force in Eq. (4) is obtained by considering the joint to be infinitely stiff within the link.

Using Equations (1) and (2) to determine the relative displacement within the joint gives

$$x_J = x_L - F_L / k_S \qquad (5)$$

With the above definition for the residual force in Eq. (4), Eq. (5) can then be expressed as

$$x_J = F_R / k_S \tag{6}$$

Therefore, it is found that the joint's relative displacement is directly proportional to the residual force. Also, differentiating both sides of Eq. (6) gives

$$\dot{x}_J = \dot{F}_R / k_S \tag{7}$$

The joints relative velocity can therefore be expressed in terms of the first time derivative of the residual force.

Using Equations (3), (4) and (7) then gives

$$F_R = f_R(x_L, \dot{F}_R) \tag{8}$$

Eq. (8) is a first order nonlinear differential equation involving the residual force, its derivative, and the total relative displacement of the link. This expression can be thought of as a residual force map where the force axis of Eq. (3) has been transformed into a residual force axis using Eq. (4), and the joint's relative velocity axis has transformed to a new axis having the time derivative of the residual force as the independent variable.

The main advantage of the residual force map in Eq. (8) is that the incrementally small joint displacements and velocities have been "stretched out" offering a numerically more attractive description of the link. Moreover, the residual forces are generally small.

2.3 Residual Force Map Examples

The first example of a residual force map is that for a gap in series with a soft spring as shown in Fig. 8. The spring is grounded at one end and attached to a mass at the other so that all equations of motion for this one degree of freedom problem may be shown.

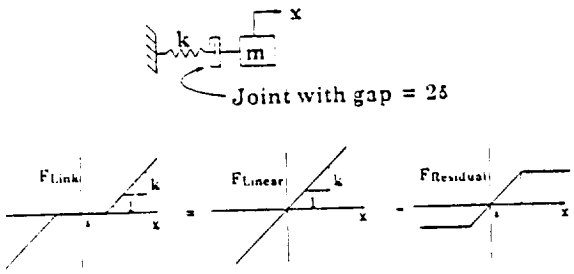

Fig. 8 A spring-mass system having a gap element.

This example gives the basic idea of a residual force and shows how the residual force can be expressed in terms of the total relative displacement across the link. This result will also be true for any number of joints in series with a soft spring so long as the force maps of the joints are independent of velocity.

The joint in the spring-mass system of Fig. 8 is a gap element having a total free-play of 2δ. The force vs. displacement curve for this system therefore has a flat spot with zero force while in the gap. This curve can also be reproduced by including a small residual force acting on a linear spring having no gap. The equations of motion then take the form

$$m \ddot{x}_L + k_S x_L = F_R \tag{9}$$

Note that the stiffness on the left hand side of Eq. (9) can be derived by considering the joint to be infinitely stiff. Also note that all nonlinear terms are on the right hand side of Eq. (9).

The second example to be considered is of two identical Voigt joints in series with a soft spring (see Fig. 9). This "truss link" is again grounded at one end and attached to a mass at the other to formulate a single degree of freedom problem so that all equations of motion may again be shown.

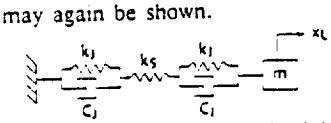

Fig. 9 A link with two Voigt joints.

Using the procedure of Section 2.2 for calculating the residual force, a linear first order differential equation for the residual force can be derived in the following form.

$$(C_J / (k_J + 2k_S))\ \dot{F}_R + F_R = (k_S - k_L)\ x_L \tag{10}$$

where k_L is the total stiffness of the link generated using the series rule and C_J is the damping coefficient.

The equations of motion for this link-mass system then become

$$m \ddot{x}_L + k_S x_L = F_R \tag{11}$$

Note again that the stiffness on the left hand side of Eq. (11) is derived by considering the Voigt joints to be infinitely stiff.

There are two interesting observations to be made about the first order differential equation for the residual force in Eq. (10). First, the derivative term is normally small suggesting a perturbation solution to the differential equation. And second, the nonhomogeneous term on the right hand side of the differential equation is always small for joints that are much stiffer than the "soft" link spring. Monitoring the residual force therefore appears to be much more numerically attractive than monitoring the incrementally small displacements and velocities across the Voigt joints.

The perturbation solution of the first order differential equation for the residual force in Eq. (10) can be expressed as

$$F_R = (k_S - k_L) (x_L - C_J \dot{x}_L /(k_J + 2k_S)) \quad (12)$$

The residual force is therefore seen to be a function of the link's relative displacement and velocity. This means that the residual force for the link is itself expressible in terms of a force-state map. This result will always be true whenever the joint stiffness is large, the joint damping is small, and the rates are low.

2.4 Equations of Motion of a Truss Having Nonlinear Joints

The equations of motion governing the free and forced dynamic response of a structure having nonlinear joints are derived here for the representative structure shown in Fig. 6 and modeled using the assumptions discussed in Section 2.1. The links are therefore assumed to be massless and axial load bearing members only.

Define x as the physical displacements at all mass freedoms, and define x_L as the relative displacements of the links. A matrix C then exists so that

$$x_L = C^T x \quad (13)$$

where C is determined from the coordinates and connectivity of the structure.

Let F_R represent the residual forces in the links derived according to Section 2.2. The nonlinear forces F_{nl} acting on the physical freedoms x then satisfy

$$F_{nl} = C F_R \quad (14)$$

The equations of motion for a joint dominated structure then becomes

$$M \ddot{x} + K x = F_{nl} + F_{external} \quad (15)$$

where M and K are the mass and linear stiffness of the structure, respectively. The linear stiffness is again derived by considering all the nonlinear joints to be infinitely stiff.

The equations of motion in Eq. (15) were derived using the residual force technique on a structure satisfying the assumptions in Section 2.1. One essential feature of this technique is to replace the arbitrary force maps describing the nonlinear joints with residual force maps describing the truss links. The main advantage of this replacement is that the incrementally small relative displacements and velocities across a joint are not monitored directly thereby avoiding numerical difficulties. Instead, very small and "soft" residual forces are defined giving a numerically attractive form for the equations of motion and thereby permitting numerically stable integration algorithms.

The only mass degrees of freedom shown in Fig. 6 are at the truss verticies but additional mass freedoms along each truss link may be required depending upon the nature of the joint nonlinearities as discussed in Section 2.1.

The total number of degrees of freedom defined by the nodal equations of motion shown in Fig. 6 can be on the order of 2000 or more degrees of freedom for large space structures and methods to reduce this large number are therefore desired. Using the system's modes is a natural choice for size reduction in that it takes advantage of the linearity of the left hand side of the nodal equations of motion. However, using a truncated set of structural modes generally has the disadvantage of decreasing the represented flexibility of the structure. This disadvantage can be offset by including the residual flexibility due to the neglected modes in all calculations affecting the dynamic response of the structure. However, for problems considered to date, the residual flexibility terms have not been required. The numerical accuracy of the results were determined simply by including most if not all of the system modes and comparing the results to the truncated solution.

3.0 Applications of the Residual Force Technique

In this section the Residual Force Technique will be applied to a 10 bay deployable truss and a 58 bay, 60 meter COFS deployable truss each having various joint nonlinearities.

3.1 Nonlinear Analysis of a 10 Bay deployable Truss

A nonlinear transient analysis is performed here for a ten bay deployable truss. Fig. 10 shows the first and second bending modes for this truss where each bending mode actually represents two orthogonal modes having identical frequencies. Gaps of 0.004 inches were included in all the longerons and lacing links. This gap value is reasonable in that each link has three deployable joints. The longeron links have two pin joints and one hinge joint, and the diagonal links have two pin joints and one telescoping joint.

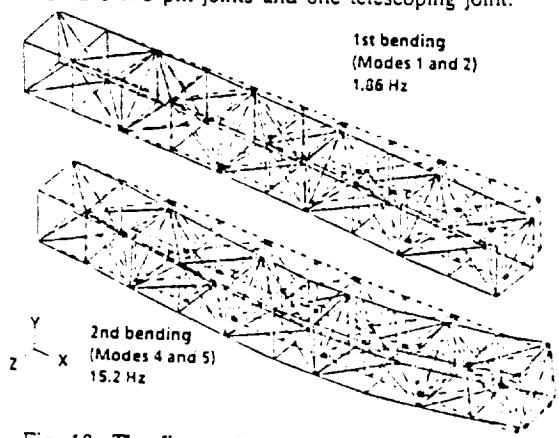

Fig. 10 The first and second bending modes of a cantilevered 10 bay deployable truss having a 780 pound tip mass.

The tip response of the gapped ten bay cantilevered truss having 1% modal damping subject to an initial impulse is shown in Fig. 11. The response of the linear gapless structure is also shown for comparison. Three observations can be made from Fig. 12. First and second, the amplitude and period of the nonlinear response is greater than those for the linear structure. The most interesting observation, however, is that the damping of the nonlinear structure appears to be greater than 1 percent. Evidently, energy is being transferred from the lower to the higher modes as a result of the nonlinear coupling between the modes. This phenomena was also seen in Ref. 2 for selected applications.

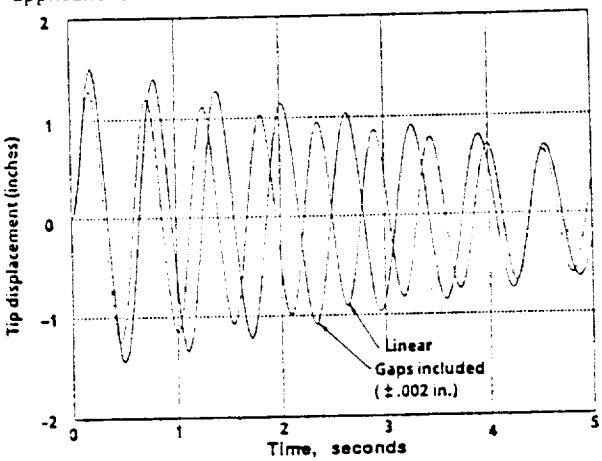

Fig. 11 Tip response of the ten bay truss having gap elements of 0.004 inches and one percent modal damping.

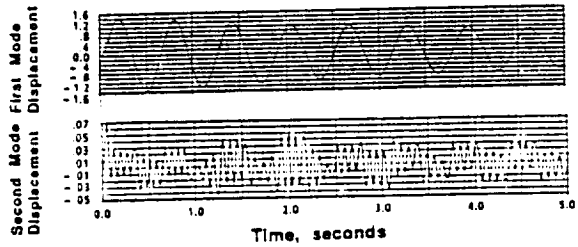

Fig. 12 Modal response of the first and second bending modes of the ten bay truss having gap elements and one percent modal damping.

The nonlinear coupling between the modes is clearly shown in Fig. 12. Nearly equal response in modes 1 and 2 as well as in modes 4 and 5 is due to the fact that the initial impulse excited these modes equally The decaying response of modes 1 and 2 again show the phenomena that the period increases as the amplitude decreases. The response of modes 4 and 5, however, does not appear to be decaying exponentially as expected for modal damping. A strong 2 hertz component in modes 4 and 5 indicates strong coupling with the first bending modes and offers an explanation why decay is not also occurring for the second bending modes. Modes 1 and 2 are evidently driving the response of modes 4 and 5 with sufficient intensity to overcome damping. A net energy drain from modes 1 and 2 to the higher modes will therefore result. This phenomena also explains why the modal damping of modes 1 and 2 seems to be larger than the allotted 1 percent, the difference being made up by the energy transferral to the higher modes having a greater energy dissipation potential.

Fig. 13 shows the linear and nonlinear responses for mode 4. Note that the maximum response occurs shortly after the initial impulse and that the magnitude of the nonlinear response is much greater than the magnitude of the linear response. Having gaps in the truss therefore permits greater modal participation for the applied tip loading impulse. Note also that if no coupling between the modes were to exist, then mode 4 would decay relatively quickly.

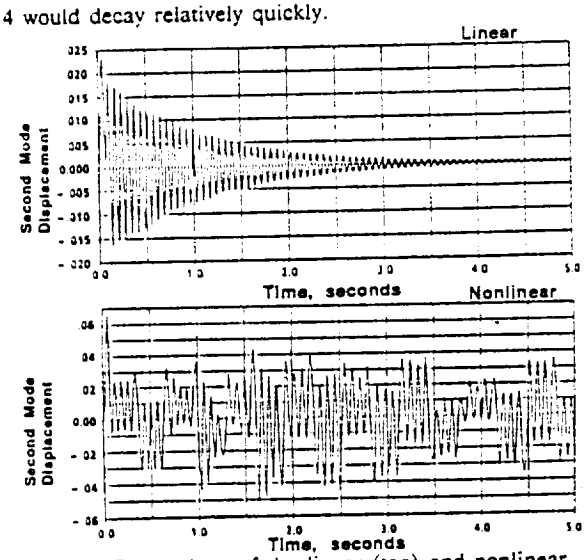

Fig. 13 Comparison of the linear (top) and nonlinear (bottom) response on the second bending mode of the ten bay truss (gap elements and 1% modal damping).

Fig. 14 shows the tip response when the joints have Voigt damping and Fig. 15 shows the tip response for joints that have bilinear stiffness. Joints having this nonlinear stiffness were considered because they exemplify the bilinear character of a Space Station erectable joint whose force-state map was shown in Fig. 5.

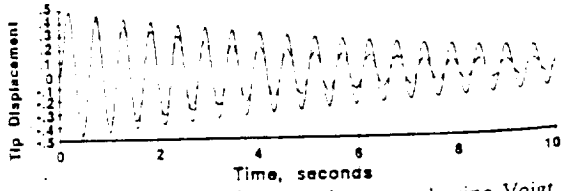

Fig. 14 Tip response of the ten bay truss having Voigt damping (dashed curve). Solid curve is linear case having 1% modal damping.

ORIGINAL PAGE IS OF POOR QUALITY

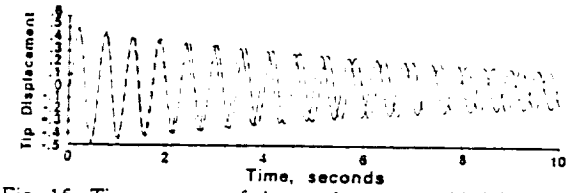

Fig. 15 Tip response of the ten bay truss with joints having a bilinear stiffness (10 % softer in compression) and 1% modal damping. Solid curve is linearcase having 1% modal damping.

3.2 Nonlinear Analysis of the 60 Meter COFS Truss

An investigation of the 58 bay, 60 meter COFS truss using the residual force technique shows that significant changes in the global response are possible when small nonlinearities exist within the joints or links. Three cases are examined in addition to the linear case having infinitely stiff joints. The three cases are joints with gaps, joints with Voigt damping, and links with Coulomb friction.

The COFS truss was cantilevered and subjected to a 100 Newton tip load for one second. The response after the impulse is examined. The results in Figures 16,17, and 18 show marked changes in the tip response when joint effects are included. Energy transferral to the higher modes was again demonstrated for this nonlinear joint dominated structure.

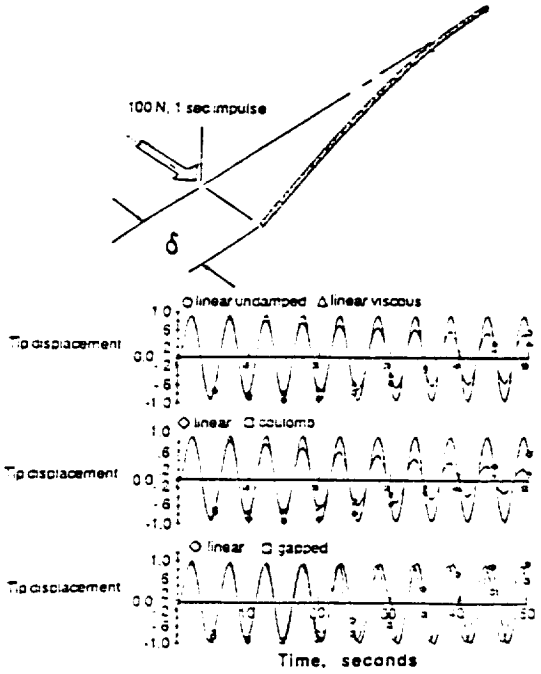

Fig. 16 Tip displacements of the 60 meter COFS truss having Voigt damping (top), Coulomb damping (center), and gap elements (bottom). All are compared to the linear undamped case.

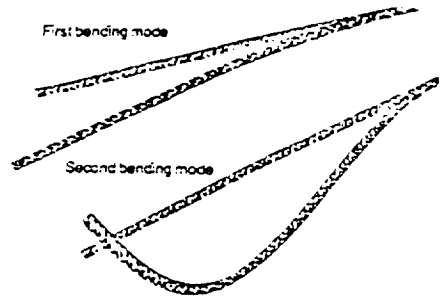

Fig. 17 First and second bending modes of the COFS truss.

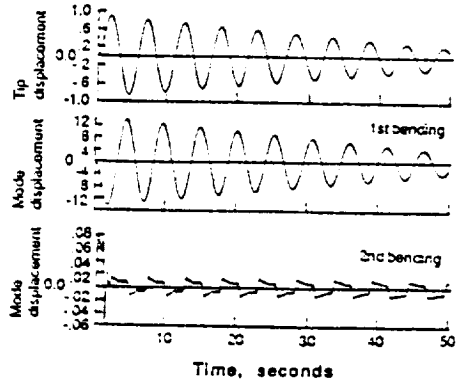

Fig. 18 Tip and modal displacements of the COFS truss having Coulomb damping.

4.0 Link Testing

References 3 and 4 describe the rationale, procedure, instrumentation, and data processing for force-state mapping of joints. Most of the instrumentation and software may be used in link testing. This section will describe those aspects of the testing procedure that are unique to link testing. Testing of individual joints will still be possible with the proposed apparatus but may not be necessary.

Figure 19 shows the proposed apparatus with a diagonal link of a COFS MAST truss (Ref.1) installed for testing. Figure 20 shows the instrumentation. The machine base must be essentially rigid and approximately 90" in length to accommodate either the longeron or diagonal links of the COFS truss.

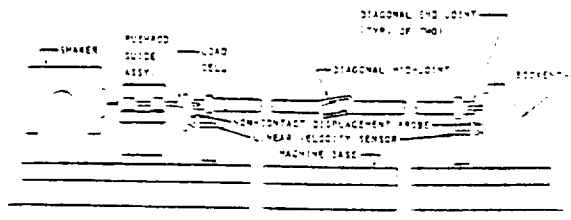

Fig. 19 Force-State Mapping of multi-joint links.

ORIGINAL PAGE IS
OF POOR QUALITY

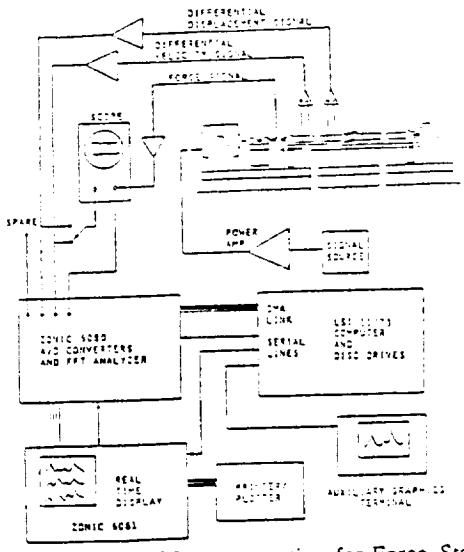

Fig. 20 Schematic of Instrumentation for Force-State Mapping Test of links.

The shaker pushrod is guided by a linear bearing assembly. This will react any moment produced by an eccentric joint and will insure that the input force direction is well controlled.

Relative motion between the ends of the link, both displacement and velocity, is measured indirectly. The motion of each end is sensed relative to ground and transducer outputs are differenced electronically to produce signals proportional to link deformation. The need for an absolutely rigid "bookend" fixture and rigid connection to it is thus eliminated. It was considered impractical to fixture a single sensor, either displacement or velocity, to span the entire 65-inch length of the link. Further, the differential sensing will allow testing of links of different lengths and of individual joints without the need for intricate, specialized fixturing.

Displacement sensing will be performed by non-contact eddy current probes rather than by linear variable displacement transformers (LVDT's) as were used in the earlier joint tests. Eddy current probes have the advantages of zero friction, better range/resolution, and, most importantly, have virtually no phase lag within the frequency band of interest. This last feature will be particularly significant because of its relevance to damping measurement and because it is likely that data will be required at higher frequencies than in previous force-state map tests.

The arrangement of the apparatus and the use of differential sensing will allow force-state maps of individual joints to be determined (if necessary) with only minor additional fixturing. The velocity and displacement sensing pairs will simply be moved to pick up motion on either side of the joint in question. As long as the drive frequency is well below the first resonance of the apparatus, the force will not vary along the link. The signal conditioning, data acquisition, and processing for characterizing a single joint will then be exactly as for the entire link.

Data derived from the link tests may also be correlated with constrained individual joint data.

5.0 Summary

The transient analysis of structures having nonlinear joints can be accomplished using the residual force technique. The current technique assumes that the structural members are axial load carrying members only and that the joints have arbitrary force-state map characterizations. The technique introduced a link concept which has four basic advantages. First, stable integration of the equations of motion could be obtained when the nonlinearities were defined in terms of the links instead of the joints. Second, substantial size reduction of the equations of motion were obtained even before modal extraction. Third, direct tests on the links could be performed to validate the analytical description of the link. And fourth, direct testing of the links could identify link behavior not predictable from joint testing alone. These four advantages of the link concept then motivated link testing in addition to the joint tests. A proposed link testing procedure was presented in this paper.

The residual force technique was applied to a ten bay deployable truss and a 58 bay 60 meter COFS deployable truss. Nonlinear analyses were performed for these trusses having nonlinear gap joints, linear Voigt joints, joints with bilinear stiffness, or links having Coulomb friction. Results from the nonlinear gap analyses generally indicate that coupling between the modes can display some interesting effects during free vibration. One particularly interesting effect was that the damping of the structure appeared to be higher than could be accounted for from modal damping alone. Energy transferral from the lower to the higher modes was found to exist as a result of the modal coupling. The apparently increased damping was due to the fact that the energy transferred to the higher modes is inherently dissipated more quickly. Another interesting phenomenon was that the lower modes could drive the higher modes even during free vibration and that these modes could display a rather large quasi-steady state behavior even when modal damping was present. Gaps were also found to increase the amplitude and period of the free vibration response as expected.

Future work will further examine the effects of modal truncation that was used in the transient analyses of the deployable trusses examined in this paper. Also, other joint nonlinearities will be studied and their

ORIGINAL PAGE IS
OF POOR QUALITY

effects on the free and forced response of a joint dominated structure determined. Comparison of the analysis predictions with test results also needs to be performed before the residual force technique and truss modeling assumptions can be substantiated.

6.0 Acknowledgments

This was performed under the NASA/MSFC contract NAS 8-36420, "Development of Structural Dynamic Analysis Tools." The authors wish to acknowledge Combined Systems Analysis (CSA) Engineering for their support in joint and link testing.

7.0 References

1. NASA, "*Control of Flexible Structures (COFS) Technology Program*," Office of Aeronautics and Space Technology Notice, Feb. 7, 1986.

2. J.M.Chapman, F.H. Shaw, and W.C. Russell, "*Dynamics of Trusses Having Nonlinear Joints*," presented at the Workshop on Structural Dynamics and Control Interaction of Flexible Structures, April 22-24, 1986, Marshall Space Flight Center.

3. E.F. Crawley and A.C. Aubert, "*Identification of Nonlinear Structural Elements by Force-State Mapping*," AIAA paper 84-0992 presented at the 1984 SDM meeting.

4. R. Ikegami, S.M. Church, D.A. Kienholz, and B.L. Fowler, "*Experimental Characterization of Deployable Trusses and Joints*," presented at the Workshop on Structural Dynamics and Control Interaction of Flexible Structures, April 22-24, 1986, Marshall Space Flight Center.

ORIGINAL PAGE IS
OF POOR QUALITY

Appendix D

(Taken from Ref. 3)

Transient Analysis of Dynamic Events

The diagonalized equations of motion governing the transient response of the Orbiter/payload system subject to both linear and nonlinear forces are given by[6]:

$$\ddot{Q} + c\dot{Q} + \omega^2 Q = \phi^T F_L + \phi^T F_{NL}(Q, \dot{Q}, \ddot{Q}) \qquad 6.1$$

where $Q, \dot{Q}, \ddot{Q}$ = system generalized coordinated displacement, velocity and acceleration at each time point

c, ω^2 = system modal damping and eigenvalues

ϕ^T = system eigenvectors (transposed)

F_L = linear force time history (forcing function)

F_{NL} = nonlinear force time history (typically a function of Q, $\dot{Q}$, $\ddot{Q}$)

The initial conditions for Q and $\dot{Q}$ at time $t = 0$ are given by:

$$Q(0) = \begin{cases} 0 & \text{for rigid body modes} \\ \omega^{-2}\ \phi^T\ (F_L + F_{NL}) & \text{for flexible modes} \end{cases} \qquad 6.2$$

$$\dot{Q}(0) = 0$$

The nonlinear terms are accounted for in the transient analysis by treating them as "nonlinear forces on the right-hand-side of the generalized equations of motion."

Solving the generalized equations of motion at each time point yields a time history of the response quantities Q, $\dot{Q}$ and $\ddot{Q}$ which includes the effects of the nonlinear forces as well as the linear forces. The solution technique of treating the nonlinear forces as prescribed forces on the right hand side of the equation is necessarily an iterative predictor-corrector type technique, and as such, requires convergence checks on the nonlinear forces and response quantities at each time point. A detailed discussion of the predictor-corrector technique is given below.

The predictor-corrector integration algorithm assumes the force time history varies linearly in time over a time increment. The integration step size must therefore be chosen so that the frequency content of the forcing function is adequately described. For usual Shuttle/payload liftoff and abort landing events, the time increment chosen to represent the linear forcing function is 2 to 4 milliseconds since this increment should adequately describe any forcing function up to 40 Hz. The time increment chosen to account for the nonlinear forces in the transient analysis is 1 millisec for the frictionless cases and 0.5 millisecs for the friction cases. However for the friction cases, the step size is reduced to 0.1 millisecs whenever the relative velocities of the sliding surfaces approaches zero. Once the surfaces are determined to be stuck or to be sliding in the opposite direction, the step size is then increased back to 0.5 millisecs. The importance of decreasing the step size during the region where the friction forces could exhibit step function like behavior is evident in that this is a region where the friction force has a high frequency content.

PAGE 210 INTENTIONALLY BLANK

PRECEDING PAGE BLANK NOT FILMED

Predictor–Corrector Method

Given the differential equation.

$$\ddot{Q} + 2\xi\omega\dot{Q} + \omega^2 Q = F(t) \qquad 6.3$$

where the "dots" represent differentiation with respect to time, the exact solution for $Q(t)$ can be written as:

$$Q = Q_o \cos(\omega t + \theta) + \frac{1}{\omega^2}\int_o^t \sin\omega(t-\tau)F(\tau)d\tau \qquad when\ \xi = 0$$

The constants Q_o and θ are chosen depending upon the initial conditions. A similar solution can be written for ξ not equal to zero.

Assume the force F varies linearly in time between time t_1 and t_2; then knowing all t_1 quantities, the solution at t_2 can be expressed as:

$$Q_2 = aQ_1 + b\dot{Q}_1 + cF_1 + dF_2 \qquad 6.4.1$$

Also

$$\dot{Q}_2 = AQ_1 + B\dot{Q}_1 + CF_1 + DF_2 \qquad 6.4.2$$

$$\ddot{Q}_2 = \alpha Q_1 + \beta\dot{Q}_1 + \zeta F_1 + \delta F_2 \qquad 6.4.3$$

The subscripts 2 and 1 designate quantities at t_2 and t_1 respectively. The constants (a, b, c, d, A, B, C, D, α, β, ζ, δ) depend upon ω and ξ and the step size ($t_2 - t_1$).

In order to calculate (Q_2, $\dot{Q}_2$, $\ddot{Q}_2$) using equation 6.4, the force F_2 must be prescribed. This is impossible however, when F_2 depends upon (Q_2, $\dot{Q}_2$, $\ddot{Q}_2$) in some nonlinear way; e.g., velocity squared damping, sliding friction, etc. Fortunately, a predictor–corrector technique can be implemented to numerically obtain an approximate solution. The technique is an iterative procedure and proceeds as follows:

1. Let $F_2^{(1)} = F_{L_2} + F_{NL_1}$; i.e., the first guess for F_2 is simply the linear force at time t_2 plus the nonlinear force at time t_1.
2. Calculate $[Q_2^{(1)}, \dot{Q}_2^{(1)}, \ddot{Q}_2^{(1)}]$ using Eq. 6.4 with F_2 replaced by $F_2^{(1)}$.
3. Calculate $F_2^{(2)}$ using $[Q_2^{(1)}, \dot{Q}_2^{(1)}, \ddot{Q}_2^{(1)}]$.
4. Calculate $[Q_2^{(2)}, \dot{Q}_2^{(2)}, \ddot{Q}_2^{(2)}]$ using $F_2^{(2)}$.
5. Etc.

The iterative process is continued until a covergence criteria is met; i.e., the change in $F_2^{(k)}$ is small.

The above process may also be used when Coulomb friction forces are included in the generalized force F. The technique of calculating say $F_2^{(2)}$ (Step 3) is straight forward except in the case when Coulomb friction causes two or more "sliding" surfaces to lock up. Step 3 then proceeds as follows:

a) Use

$$\ddot{X}_2 = \phi\ddot{Q}_2 = \phi\{\alpha Q_1 + \beta\dot{Q}_1 + \zeta F_1 + \delta F_2\} \qquad 6.5$$

Where $\ddot{X}_2$ represents the relative acceleration between the "stuck" surfaces at time t_2 and ϕ is the matrix of eigenvectors relating the physical X freedoms to the generalized Q freedoms. Eq. 6.5 can also be expressed as:

$$\ddot{X}_2 = \ddot{X}_2^{(1)} + \phi\delta\left(F_2 - F_2^{(1)}\right) \qquad 6.6$$

where

$$\ddot{X}_2^{(1)} = \phi\left\{\alpha Q_1 + \beta\dot{Q}_1 + \zeta F_1 + \delta F_2^{(1)}\right\}$$

and

$$F_2^{(1)} = F_{L_2} + F_{NL_1}$$

b) Use the following equation to identify that portion of F_2 that is due to the forces between the stuck surfaces;

$$F_2 = \phi^T f_2 + R_2 \qquad 6.7$$

where f_2 is defined as the force in physical coordinates between all stuck surfaces and R_2 are all remaining generalized forces. Note that R_2 contains the Coulomb friction forces for surfaces that are sliding and not stuck.

Combining equations (6.5 - 6.7) then gives:

$$\ddot{X}_2 = \ddot{X}_2^{(1)} + \left\{\phi\delta\phi^T\right\}\left\{f_2 - f_2^{(1)}\right\} + \phi\delta\left\{R_2 - R_2^{(1)}\right\}$$

c) Calculate $R_2^{(2)}$ using $[Q_2^{(1)}, \dot{Q}_2^{(1)}, \ddot{Q}_2^{(1)}]$ quantities in the normal manner.

d) Calculate $f_2^{(2)}$ by requiring $\ddot{X}_2^{(2)} = 0$. Thus,

$$f_2^{(2)} = f_2^{(1)} - G^{-1}\left\{X_2^{(1)} + \phi\delta\left(R_2^{(2)} - R_2^{(1)}\right)\right\} \qquad 6.8$$

Where $G = \phi\delta\phi^T$

e) If any of the friction forces $f_2^{(2)}$ are greater than that allowed by the static coefficient of friction, then that force is set to the force due to sliding friction (same sign retained however since the relative velocity is zero) and steps (1) through (e) are repeated.

f) All sliding surfaces are checked for possible stiction whenever the relative velocity between the surface changes sign. This is accomplished simply by assuming the surfaces to be stuck when the relative velocity first changes sign and then calculating the stuck forces using steps (1) through (e). Note that this surface will be automatically released and allowed to slide if the proper tests are satisfied in step (e).

NASA
National Aeronautics and Space Administration

Report Documentation Page

1. Report No.	2. Government Accession No.	3. Recipient's Catalog No.
NASA CR-4324		

4. Title and Subtitle
Nonlinear Modeling of Joint Dominated Structures

5. Report Date
September 1990

6. Performing Organization Code

7. Author(s)
J. M. Chapman

8. Performing Organization Report No.

9. Performing Organization Name and Address
Boeing Aerospace
Engineering Technology Organization
P. O. Box 3999, MS 82-97
Seattle, WA 98124

10. Work Unit No.
585-01-91-01

11. Contract or Grant No.
NAS1-18864

12. Sponsoring Agency Name and Address
National Aeronautics and Space Administration
Langley Research Center
Hampton, VA 23665-5225

13. Type of Report and Period Covered
Contractor Report - Final

14. Sponsoring Agency Code

15. Supplementary Notes
Technical Monitor - Rudeen Smith-Taylor, Langley Research Center

16. Abstract

The report describes the development and verification of an accurate structural model of the non-linear joint-dominated NASA Langley Mini-Mast truss under the CSI Guest Investigator Program. The approach is to characterize the structural behavior of the Mini-Mast joints and struts using a test configuration that can directly measure the struts' overall stiffness and damping properties, incorporate this data into the structural model using the residual force technique, and then compare the predicted response with empirical data taken by NASA/LaRC during the modal survey test of the Mini-Mast. A new testing technique, referred to as "link" testing, was developed and used to test prototype struts of the Mini-Mast. Appreciable nonlinearities including free-play and hysteresis were demonstrated. Since static and dynamic tests performed on the Mini-Mast also exhibited behavior consistent with joints having free-play and hysteresis, nonlinear models of the Mini-Mast were constructed and analyzed. The Residual Force Technique was used to analyze the nonlinear structural model of the Mini-Mast having joint free-play and hysteresis.

17. Key Words (Suggested by Author(s))	18. Distribution Statement
Link Testing, Residual Force Technique, Coulomb Friction, Joints and Struts, ERA	unclassified - unlimited subject category - 18

19. Security Classif. (of this report)	20. Security Classif. (of this page)	21. No. of pages	22. Price
unclassified	unclassified	584	A25

NASA FORM 1626 OCT 86 For sale by the National Technical Information Service, Springfield, VA 22161-2171

NASA-Langley, 1990

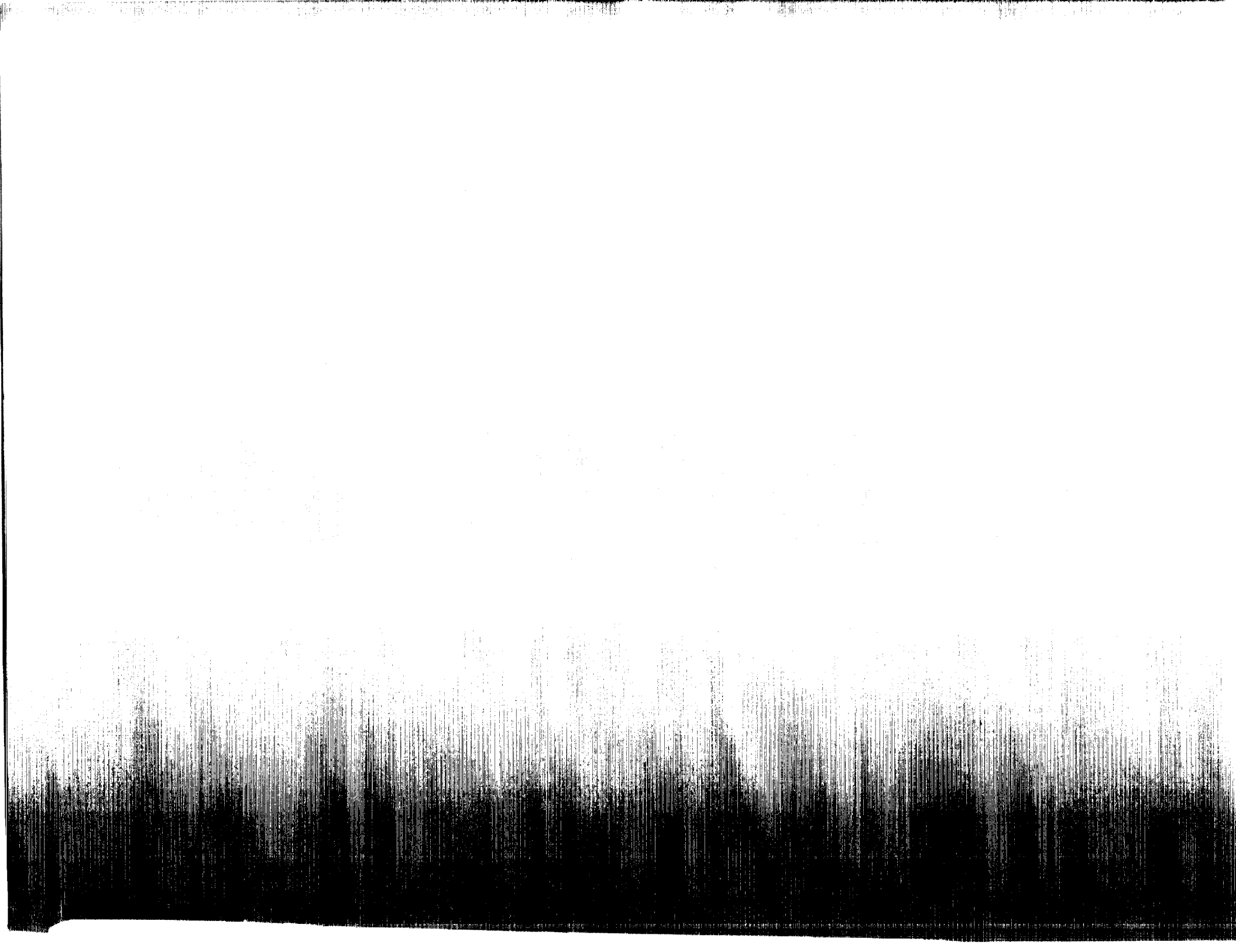

National Aeronautics and
Space Administration
Code NTT-4

Washington, D.C.
20546-0001

Official Business
Penalty for Private Use, $300

NASA

NASA

National Aeronautics and
Space Administration

Washington, D.C.
20546

SPECIAL FOURTH CLASS MAIL
BOOK

Postage an Fees Paid
National Aeronautics and
Space Administration
NASA-451

Official Business
Penalty for Private Use $300

U.S. MAIL

[illegible]
NASA
[illegible]
[illegible]
[illegible]
[illegible]